Targeting the cell cycle : A novel therapeutic strategy against ATIP3- deficient breast cancer

Maria Haykal

THESE DE DOCTORAT

NNT : 2023UPASL109

université PARIS-SACLAY

Targeting the cell cycle:

A novel therapeutic strategy against ATIP3-deficient breast cancer

Cibler le cycle cellulaire : une nouvelle stratégie thérapeutique contre les cancers du sein déficients en ATIP3

Thèse de doctorat de l'université Paris-Saclay

École doctorale n° 582 CBMS Cancérologie : biologie – médecine - santé
Spécialité de doctorat : Sciences du Cancer
Graduate School: Life sciences and health
Référent : Faculté de médecine

Thèse préparée dans l'unité de recherche Prédicteurs moléculaires et nouvelles cibles en oncologie (INSERM, Université Paris Saclay), sous la direction du Dr Clara NAHMIAS, directrice de recherche CNRS

Thèse soutenue à Paris-Saclay, le 23 Novembre 2023, par

Maria HAYKAL

Composition du Jury

Dr Laurence LAFANECHÈRE Directrice de recherche, Institut Albert Bonniot (UMR 5309)	Présidente
Dr Daniele FACHINETTI Directeur de recherche, Institut Curie (UMR 144)	Rapporteur & Examinateur
Dr Susana GODINHO Principal investigator, Barts Cancer Institute	Rapporteur & Examinatrice
Dr Olivier GAVET MCU, Sorbonne Université	Examinateur
Dr Valeria NAIM Chargée de recherche, Institut Gustave Roussy (UMR 9019)	Examinatrice

« Je vais me mettre au travail pour oublier le tragique moment où nous vivons tous. […] Je suis à un point extrêmement important pour ma route pour lequel je ne puis distraire aucune force. L'avenir ? Je l'attends – quoiqu'il arrive je ne bougerai pas. »
Henri Matisse, 1940

Acknowledgments

I would like to express my deepest appreciation to the members of my thesis jury: my reviewers Dr Daniele Fachinetti and Dr Susana Godinho, and examinators Drs Laurence Lafanechère, Olivier Gavet and Valeria Naim, for their valuable time and insightful feedback on this manuscript. Their expertise and guidance have played a crucial role in shaping the research and enriching the quality of this work.

Switch bien nécessaire en Français !

Un ENORME merci à ma directrice de thèse, Clara. Merci pour ton soutien, ta présence et pour tout ce que tu m'as apporté pendant ces 4 dernières années. Merci pour toutes les discussions scientifiques (ou pas !) enrichissantes. Merci pour la confiance que tu m'as accordée pour mener à bien ce projet qui me tient tant à cœur.

Merci à la fondation Janssen Horizon, à la Ligue nationale contre le cancer et à Prolific d'avoir financé ce travail. Merci également aux ingénieurs des plateformes d'imagerie et d'évaluation clinique. Tudor, merci pour tout le temps passé avec moi aux microscopes (divers et variés). Je peux dire que je suis une fan inégalée de l'imagerie maintenant ! Merci à Mélanie pour ta patience et pour le temps passé avec moi à l'animalerie.

Mes années de thèse auraient été beaucoup beaucoup plus durs sans le soutien de mon équipe. La microtubule dream team. Merci non seulement d'être des collègues exceptionnelles mais aussi des amies exceptionnelles. Finalement, le plus dur de cette thèse va être de vous quitter (mais chaque chose en son temps !).

Sylvie, c'est en grande partie grâce à toi que ce travail a abouti. Merci d'avoir répondu à toutes mes questions (il y en avait toujours beaucoup trop), merci de m'avoir appris la simplicité et l'efficacité, ça m'a rendu la vie au labo tellement plus simple ! Merci pour tes conseils toujours pertinents. Merci pour la bonne ambiance au quotidien. Tu es le pilier de la pièce :). Cynthia, princesse ? caillou ? chanteuse ? (non) danseuse ? (pas trop non plus) toquée (certes), mais surtout douée. Merci pour ton aide et pour toutes les fois où tu m'as dépanné. Merci pour ta joie de vivre et ton humour. Hadia, ex-pièce 130 et actuelle voisine. Merci pour ta bonne humeur et pour les moments de rires. Merci pour les moments de détente (chez toi à jouer, en Italie sous la pluie, ou à Paris pour manger encore et encore). Morgane, un merci tout particulier pour ton soutien pendant ces derniers mois, merci d'être la personne que tu es. Merci d'être toujours aussi radieuse, souriante et drôle. Merci pour les moments délires (les bâillonnements, l'électricité et ta mâchoire qui vient d'un autre monde !!). Laure, merci pour ton soutien au quotidien. Merci d'avoir rendu mon aventure (oui la thèse est une aventure) aussi belle. Merci de m'avoir fait rire au moins une fois par jour, pour ta folie et ton humour toujours au rendez-vous, bref ! pour la personne exceptionnelle que tu es ! Merci également à Audrey et Elisa de l'équipe Gynéco pour la bonne ambiance et votre bienveillance ; ça va être très dur de retrouver une tortilla aussi bonne (clin d'œil à Elisa).

Merci à mes collègues et amis de l'U981. La bonne ambiance était toujours au rendez-vous. Merci pour les très bons moments passés dans les couloirs du B2M mais aussi à l'extérieur du labo, pour les apéros et les soirées !

Mille mercis (très particuliers) à Océane (ma future chef, je l'espère). Merci de m'avoir tant apporté et guidé pendant ces dernières années autant scientifiquement que personnellement. Merci d'avoir été disponible et l'écoute à chaque fois que j'ai eu besoin de toi. Merci de m'avoir donné l'opportunité de collaborer avec toi sur tes différents projets. Merci de la belle personne que tu incarnes et que j'espère pouvoir devenir un jour.

Merci à mes meilleurs amis Bruna et Ralph. Merci également à mes amis de longue date, de Bordeaux, de Paris, et du Liban pour votre soutien et pour votre amitié. Merci d'être toujours là, malgré mon insociabilité ces derniers temps. Je saurai vous remercier autrement !!

Merci à mes parents pour leur soutien pendant mes longues années d'études. Merci de m'avoir donné les moyens de réussir et merci de votre amour.

Enfin, merci à Guillaume. Merci de m'avoir supporté tous les jours, de m'avoir encouragé, et de m'avoir soutenue dans tous mes choix.

Cette thèse est dédiée à mon Papa d'amour.

Table of contents

List of figures

List of abbreviations

53BP1	p53-binding protein 1
ADC	Antibody-Drug Conjugate
ADP	Adenosine Diphosphate
AKT	Protein Kinase B (PKB)
APC/C	Anaphase-Promoting Complex/Cyclosome
ATM	Ataxia Telangiectasia Mutated
ATR	Ataxia Telangiectasia and Rad3-related
ATRIP	ATR-interacting protein
AURKB	Aurora kinase B
BL1/BL2	Basal-Like 1/Basal-Like 2
BLM	Bloom Syndrome Protein
BRCA1/BRCA2	Breast Cancer Gene 1/2
BUB1/BUB3	Budding Uninhibited by Benzimidazoles 1/3
CAN	Copy Number Alteration
CCAN	Constitutive Centromere-Associated Network
CDC20	Cell Division Cycle 20
CDC25A/B/C	Cell Division Cycle 25A/B/C
CDC34	Cell Division Cycle 34
CDC45	Cell Division Cycle 45
CDC6	Cell Division Cycle 6
CDC7	Cell Division Cycle 7
CDK	Cyclin-Dependent Kinase
CDKN1A	Cyclin-Dependent Kinase Inhibitor 1A (p21)
CDT1	Chromatin Licensing and DNA Replication Factor 1
CENPA/B/C/E/T	Centromere Proteins A/B/C/E/T
CHK1/CHK2	Checkpoint Kinase 1/2
CIN	Chromosomal Instability
CK1	Casein Kinase 1
CMG	Cdc45-MCM-GINS
CRBN	Cereblon
CRISPR	Clustered Regularly Interspaced Short Palindromic Repeats
CTIP	CtBP-interacting protein
DBF4	Dumbbell Former 4
DCIS	Ductal Carcinoma In Situ
DDK	Dbf4-dependent kinase
DDT	DNA Damage Tolerance
DNA	Deoxyribonucleic Acid
DNA2	DNA replication ATP-dependent helicase/nuclease 2
DNTP	Deoxynucleotide Triphosphate
DSB	Double-Strand Break
E2F	Transcription Factor E2F
EGFR	Epidermal Growth Factor Receptor
EMA	European Medicines Agency
EME1	Essential Meiotic Structure-Specific Endonuclease 1
ER	Estrogen Receptor
ERCC1	Excision Repair Cross-Complementation Group 1

EXO1	Exonuclease 1
FANCA/B	Fanconi Anemia Group A/B
FANCD2	Fanconi Anemia Group D2
FCP1	RNA Polymerase II C-terminal Domain Phosphatase
FDA	U.S. Food and Drug Administration
FGFR1	Fibroblast Growth Factor Receptor 1
FOXM1	Forkhead Box M1
FRET	Förster Resonance Energy Transfer
GINS	Go-Ichi-Ni-San
H2AX/H2B	Histone H2A Variant X/B
HER2/ERBB2	Human Epidermal Growth Factor Receptor 2
HIRA	Histone Regulator A
HLTF	Helicase-Like Transcription Factor
HR	Homologous Recombination
HRD	Homologous Recombination Deficiency
HRR	Homologous Recombination Repair
HSP90	Heat Shock Protein 90
IDC	Invasive Ductal Carcinoma
ILC	Invasive Lobular Carcinoma
ITH	Intra-Tumoral Heterogeneity
KIF2B/KIF2C	Kinesin Family Member 2B/2C
KIFC1 (HSET)	Kinesin Family Member C1 (Highway Set)
K-MT	Kinetochore-Microtubule
LAR	Luminal Androgen Receptor
LCIS	Lobular Carcinoma In Situ
MAD1/MAD2	Mitotic Arrest Deficient 1/2
MAP	Microtubule-Associated Protein
MAP4/MAP7	Microtubule-Associated Protein 4/7
MCM2-7	Mini-Chromosome Maintenance Proteins 2-7
MDC1	Mediator of DNA Damage Checkpoint 1
MiDAS	Mitotic DNA Synthesis
MPS1	Monopolar Spindle 1
MRE11	Meiotic Recombination 11
MRN	MRE11-RAD50-NBS1 Complex
MSH2-6	MutS Homolog 2-6
MTD	Maximum Tolerated Dose
MVA	Multivariegated Aneuploidy
NLS	Nuclear Localization Signal
NPAT	Nuclear Protein, Ataxia-Telangiectasia Locus
ORC	Origin Recognition Complex
OS	Overall Survival
PALB2	Partner and Localizer of BRCA2
PARP	Poly(ADP-ribose) Polymerase
PCNA	Proliferating Cell Nuclear Antigen
pCR	Pathological Complete Response
PDGFRB	Platelet-Derived Growth Factor Receptor Beta
PDX	Patient-Derived Xenograft
PFS	Progression-Free Survival

PI3K/PIK3CA/PIK3R1	Phosphoinositide 3-Kinase/Catalytic Subunit Alpha/Regulatory Subunit 1
PLA	Proximity Ligation Assay
PLK1	Polo-Like Kinase 1
POLD3	DNA Polymerase Delta 3
PR	Progesterone Receptor
Pre-RC	Pre-Replicative Complex
PROTAC	Proteolysis-Targeting Chimeras
PTEN	Phosphatase and Tensin Homolog
RAD50	DNA Repair Protein RAD50
RAD51	DNA Repair Protein RAD51
RB	Retinoblastoma Protein
RIF1	Rap1 Interacting Factor 1
RNA	Ribonucleic Acid
RNAseq	RNA Sequencing
ROS	Reactive Oxygen Species
RPA	Replication Protein A
RRM2	Ribonucleotide Reductase Subunit M2
SAC	Spindle Assembly Checkpoint
SCF	SKP, Cullin, F-box-containing complex
SKP1	S-Phase Kinase-Associated Protein 1
SLX4	Structure-Specific Endonuclease Subunit SLX4
SMARCAL1	SWI/SNF-related, Matrix-associated, Actin-dependent Regulator of Chromatin, Subfamily A-like 1
SMC2/SMC4	Structural Maintenance of Chromosomes 2/4
SSB	Single-Strand Break
ssDNA	Single-Stranded DNA
STAG2	Stromal Antigen 2
STK11	Serine/Threonine Kinase 11
T-DXd	Trastuzumab Deruxtecan
TNBC	Triple-Negative Breast Cancer
TOME-1	Trigger Of Mitosis Entry 1
TOPIIA	Topoisomerase II Alpha
TP53	Tumor Protein 53 (p53)
TRCP	F-box/WD repeat-containing protein 1A
TROP2	Tumor-Associated Calcium Signal Transducer 2
USP44	Ubiquitin-Specific Peptidase 44
WRN	Werner Syndrome ATP-dependent Helicase
ZRANB3	Zinc Finger RANBP2-Type Containing 3

I. INTRODUCTION

In 1914, Boveri wrote, "It is conceivable that for any one cell type there is one particular abnormal combination of chromosomes that endows the cell with the properties of malignancy". This insight anticipated cancer as a multifaceted process.

Fast forwarding to the year 2000, Douglas Hanahan and Robert Weinberg summarized the essential concepts of cancer as the "hallmarks of cancer" which have been evolving ever since[1,2]. The now well-known hallmarks include the capacity for sustaining proliferative signaling, evading growth suppressors, resisting cell death, replicative immortality, angiogenesis, invasion and metastasis, reprogramming cellular metabolism, avoiding immune destruction, tumor-promoting inflammation, and genome instability (Figure 1).

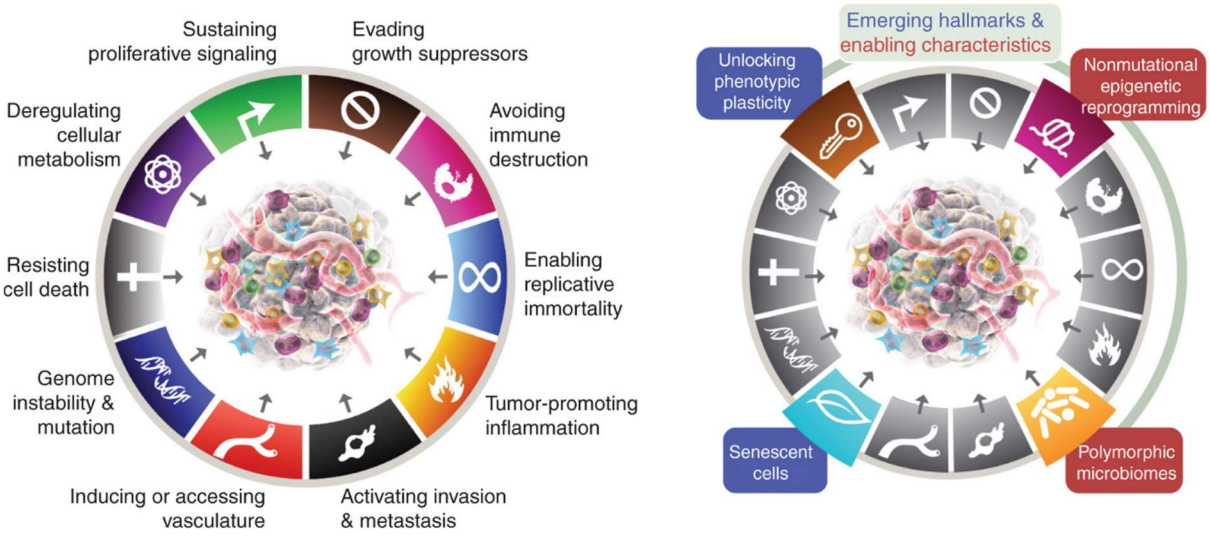

Figure 1: Hallmarks of cancer
(from [3])

1 BREAST CANCER – ONE-SIZE DOES NOT FIT ALL

1.1 EPIDEMIOLOGY

1.1.1 Demographics, incidence and mortality

Breast cancer took the lead as the most frequently diagnosed cancer worldwide in 2020. During that year, there were over 2.26 million new cases of breast cancer, and nearly 685,000 deaths were attributed to this disease globally. Breast cancer is the leading cause of cancer-related deaths among women, and it stands as the fifth most common cause of cancer-related deaths overall[4].

Australia/New Zealand, Western Europe, North America, and Northern Europe exhibited the highest breast cancer incidence rates, surpassing 80 cases per 100,000 females. In contrast, Central America, Eastern and Middle Africa, and South-Central Asia reported the lowest incidence rates, with fewer than 40 cases per 100,000 females (Figure 2). Regarding breast cancer mortality rates, Melanesia, Western Africa, and Micronesia/Polynesia showed the highest rates, exceeding 20 deaths per 100,000 people. In contrast, most other regions across the world had mortality rates ranging between 10 and 15 deaths per 100,000 individuals (Figure 3).

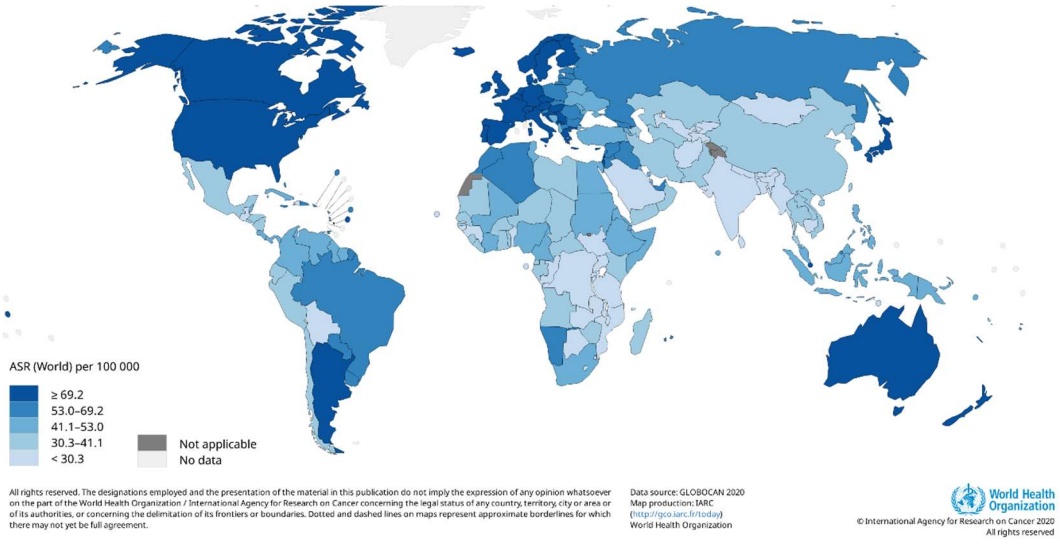

Figure 2: Estimated age-standardized incidence rates (World) in 2020
(From https://gco.iarc.fr/)

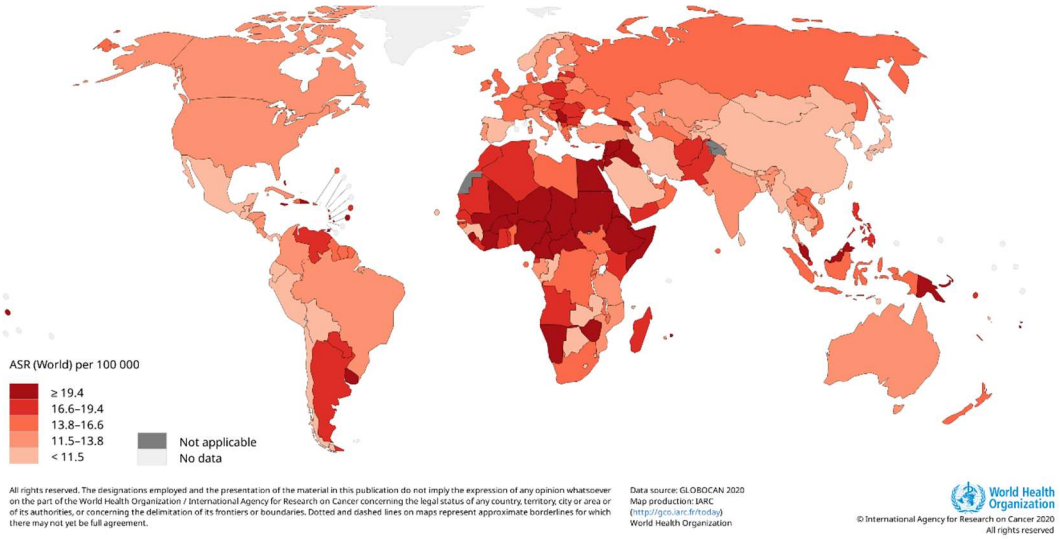

Figure 3: Estimated age-standardized mortality rates (ASR) (World) in 2020
(From https://gco.iarc.fr/)

In various high-income countries across North America, Europe, and Oceania, there has been a notable increase in breast cancer incidence rates[5]. This rise can largely be attributed to the improved detection of early-stage tumors with well-established screening programs. As a result, more cases with very favorable prognoses are being identified, contributing to the overall increase in the reported breast cancer incidence and decreasing mortality rates.

Distinct patterns have emerged in the transitioning countries in South America, Africa, and Asia. Historically, these regions have experienced low incidence rates of breast cancer. However, recently, there has been a rapid rise in breast cancer cases in these areas linked to behavioral changes (obesity, inactivity), reproductive health, increased life expectancy, and sociocultural environments.

Breast cancer mortality rates have risen in sub-Saharan Africa, ranking among the world's highest. In most high-income countries, 5-year survival rates exceed 90%, but in 12 sub-Saharan African countries, the figure is only 66%[6]. The primary reasons for this higher mortality rate are late-stage diagnosis and limited access to quality healthcare.

1.1.2 Genetic predisposition

Approximately 10% of breast cancers have an inherited component and are linked to a family history, but this proportion varies significantly based on ethnicity and country[7].

Mutations in two high-penetrance tumor suppressor genes, *BRCA1* (17q21) and *BRCA2* (13q13), affect the proteins involved in homologous DNA repair mechanisms[8]. These mutations follow an autosomal dominant inheritance pattern, leading to loss-of-function or missense changes. Individuals with *BRCA1* mutations have an average cumulative risk of 72% to develop breast cancer by the age of 80 years, whereas those with *BRCA2* mutations have a slightly lower risk of 69%[9].

Various syndromes associated with germline mutations in genes responsible for DNA repair and the maintenance of genomic integrity have been found to contribute to the inherited risk of breast cancer. The advent of next-generation sequencing has facilitated the screening of gene panels beyond *BRCA1* and *BRCA2*, allowing for the assessment of inherited breast cancer risk. These panels include genes such as *ATM*, *CHEK2*, *PALB2*, *PTEN*, *STK11*, and *TP53*, which play a role in determining the susceptibility to breast cancer[10].

1.1.3 Risk factors

Numerous cases of breast cancer can be linked to factors related to pregnancy, hormonal therapy, and lifestyle choices (alcohol consumption, obesity, smoking, and inactivity). For instance, every 10 g of alcohol consumed daily by an adult woman may lead to a 10% increase in breast cancer risk[11]. Central obesity has also been extensively studied, indicating a strong adverse effect on the risk of breast cancer and survival in women[12]. The association between oral hormonal contraceptives and breast cancer risk remains debatable, with the absolute risk being small and not associated with increased mortality[13]. However, menopausal hormone therapy has been conclusively linked to an increased risk of breast cancer in women[14].

1.2 CLASSIFICATION

Through decades of observation and research, it has become evident that breast cancer, similar to other cancer types, displays heterogeneity. Three primary types of heterogeneity have been identified[15]: (1) Population heterogeneity refers to differences among tumors from different patients. (2) Intratumor heterogeneity relates to spatial variations within a single tumor mass. (3) Temporal heterogeneity involves variability over time during tumor growth and development or in response to treatment.

1.2.1 Histological classification

The histopathological classification of breast carcinoma relies on analysis of the diverse morphological features of the tumors. It encompasses approximately 20 major tumor types and 18 minor subtypes[16]. However, a significant limitation of this classification is that approximately 80% of all breast cancers eventually fall into only two major histopathological classes: preinvasive *in situ* carcinomas and invasive carcinomas (Figure 4).

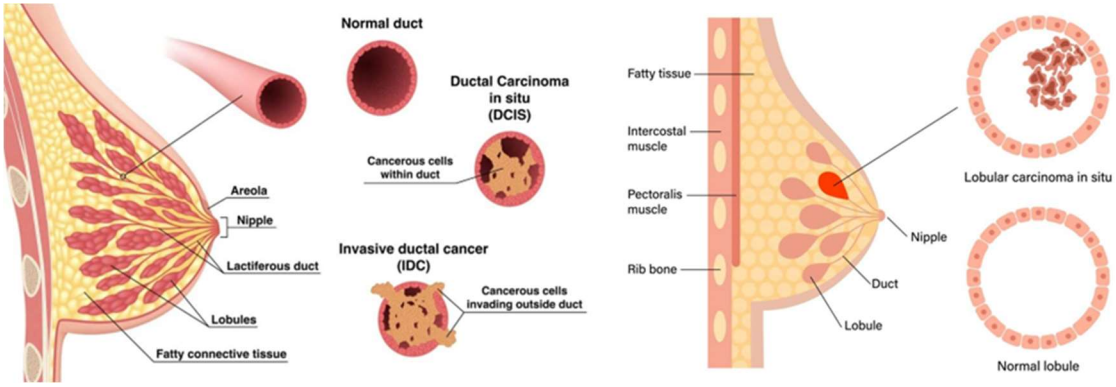

Figure 4: Histological types of breast cancers
(Adapted from https://teachmesurgery.com/breast/malignant-disease/breast-carcinoma-in-situ/)

All breast cancers arise in the terminal lobular units of the collecting duct[17]. *In situ* carcinomas do not spread to surrounding tissues. Cancer cells remain confined to the lobular-duct system, giving rise to ductal carcinoma *in situ* (DCIS) or lobular carcinoma *in situ* (LCIS). Invasive carcinomas are defined by the invasion of cancer cells into the surrounding tissues. If the tumor is derived from DCIS, it leads to invasive ductal carcinoma (IDC); more rarely, if it arises from LCIS, it becomes invasive lobular

carcinoma (ILC). This histological classification fails to fully capture the broader heterogeneity of breast cancer because it groups tumors with distinct biological and clinical profiles within the same class. As a result, histopathological classification offers limited prognostic and predictive implications and its clinical utility remains modest. Regarding the clinical management of breast cancer patients, histologic grading is more significant than morphologic type. The most widely used system is Bloom and Richardson's histologic grade[18], which was later modified by Elston and Ellis[19]. This grading system evaluates three key features: proportion of tubule formation, mitotic count, and degree of nuclear pleomorphism. The tumor grade reflects the potential aggressiveness of breast cancer and is a strong prognostic factor.

Breast cancer can also be classified according to the expression of molecular markers assessed by immunohistochemistry following biopsy of the tumor mass. Over 75% of breast cancers express the estrogen receptor (ER) and/or progesterone receptor (PR)[20], while 10% to 15% overexpress the receptor protein HER2 (ERBB2), which is involved in regulating cellular growth as a receptor tyrosine kinase[21]. These markers hold both prognostic and predictive value, making them essential for determining treatment approaches.

1.2.2 Molecular subtypes

The concept of intrinsic subtypes in breast cancer was introduced over two decades ago by Perou and Sorlie[22,23] through the gene expression analysis of breast cancer samples. They applied hierarchical clustering based on similar gene expression patterns across all samples, leading to the identification of two main clusters stratified according to the ER expression status. Within these clusters, six subtypes known as intrinsic subtypes emerged.

The largest cluster mainly consists of ER+ tumors and is further divided into three subgroups, characterized by the expression of genes typically found in luminal breast epithelial cells, referred to as luminal breast cancers. The other main cluster consists predominantly of ER tumors and has three subgroups. One comprises ER-, PR-, and

HER2-negative tumors, known as triple-negative breast carcinoma (TNBC), showing gene expression patterns typical of myoepithelial/basal epithelial cells and are hence referred to as basal-like tumors. The second subgroup displays high expression of HER2-related genes and is named the HER2-enriched group. A third group of tumors has gene expression patterns similar to those found in normal breast tissue samples, and is referred to as normal-like (Figure 5).

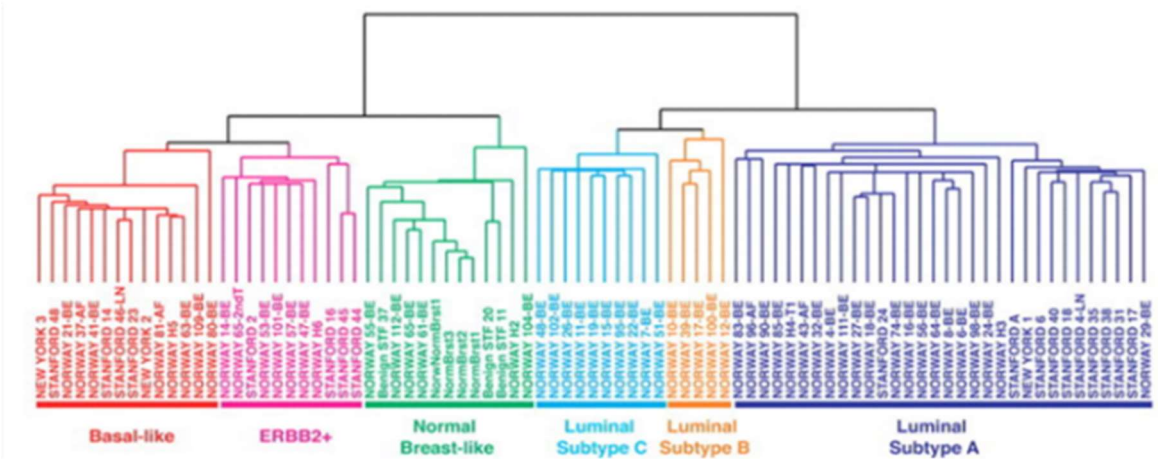

Figure 5: Breast cancer's intrinsic molecular subtypes
(from[23])

The six intrinsic subtypes of breast cancer are distinguished by both clinical and biological features. However, it is essential to note that considerable variation exists within each group. Among these subtypes, basal-like tumors stand out as they share the fewest similarities with other groups, but exhibit the greatest intrinsic diversity. Patients with basal-like tumors tend to have a poor prognosis, with nearly 40% experiencing relapse within five years of diagnosis.

Lehmann et al. 24, 25 identified four distinct subtypes of TNBC tumors through gene expression pattern analysis. They include two basal-like subtypes (BL1/BL2), mesenchymal (M), and luminal androgen receptor (LAR). Each subtype displays unique biology and differentially responds to standard-of-care chemotherapy[26].

1.3 TREATMENTS

The identification of molecular subclasses in breast cancer highlights the biological diversity that requires individualized approaches to therapy, rather than a one-size-fits-

all approach. Our current understanding of breast cancer biology offers initial clues for treatment decisions: luminal cancers, typically hormone receptor-positive, are suitable for endocrine therapy, whereas HER2+/ER− subtypes are driven by HER2 and can benefit from targeted therapies, such as trastuzumab (anti-HER2 antibody). However, chemotherapy remains the primary systemic treatment for TNBC patients. Owing to the absence of targeted therapies and the unfavorable prognosis associated with TNBC, there is a significant focus on identifying actionable molecular targets.

1.3.1 Chemotherapy

Studies over the past two decades have consistently demonstrated the significant benefits of the administration of both anthracyclines and taxanes in neoadjuvant (before surgery), adjuvant (after surgery), and metastatic settings[27]. Despite the absence of known targetable biomarkers and an overall poor prognosis, TNBC patients display a heightened response to chemotherapy compared to other breast cancer types, leading to what is termed the "TNBC paradox"[28]. Neoadjuvant chemotherapy has consistently revealed superior response rates in TNBC patients compared with non-TNBC patients. Around 30-40% of patients with early stage TNBC treated with standard neoadjuvant anthracycline and taxane-based chemotherapy regimens achieve a pathologic complete response (pCR) after treatment[29].

Even with the administration of optimal systemic chemotherapy, the survival rate for women with metastatic breast cancer is less than 30% at the five-year mark after diagnosis, and virtually all women with metastatic TNBC succumb to the disease[30]. This highlights the urgent need for ongoing research to develop more effective targeted therapies specifically tailored for patients with TNBC.

1.3.2 Targeted therapies

Due to the significant heterogeneity of TNBC, personalized treatment strategies that target molecular tumor-specific alterations are deemed the most appropriate approach to treat–60-70% of patients who do not achieve pCR. The majority of persistent TNBC cases after chemotherapy display alterations in pathways that can be targeted by

agents currently undergoing clinical investigation (Figure 6).

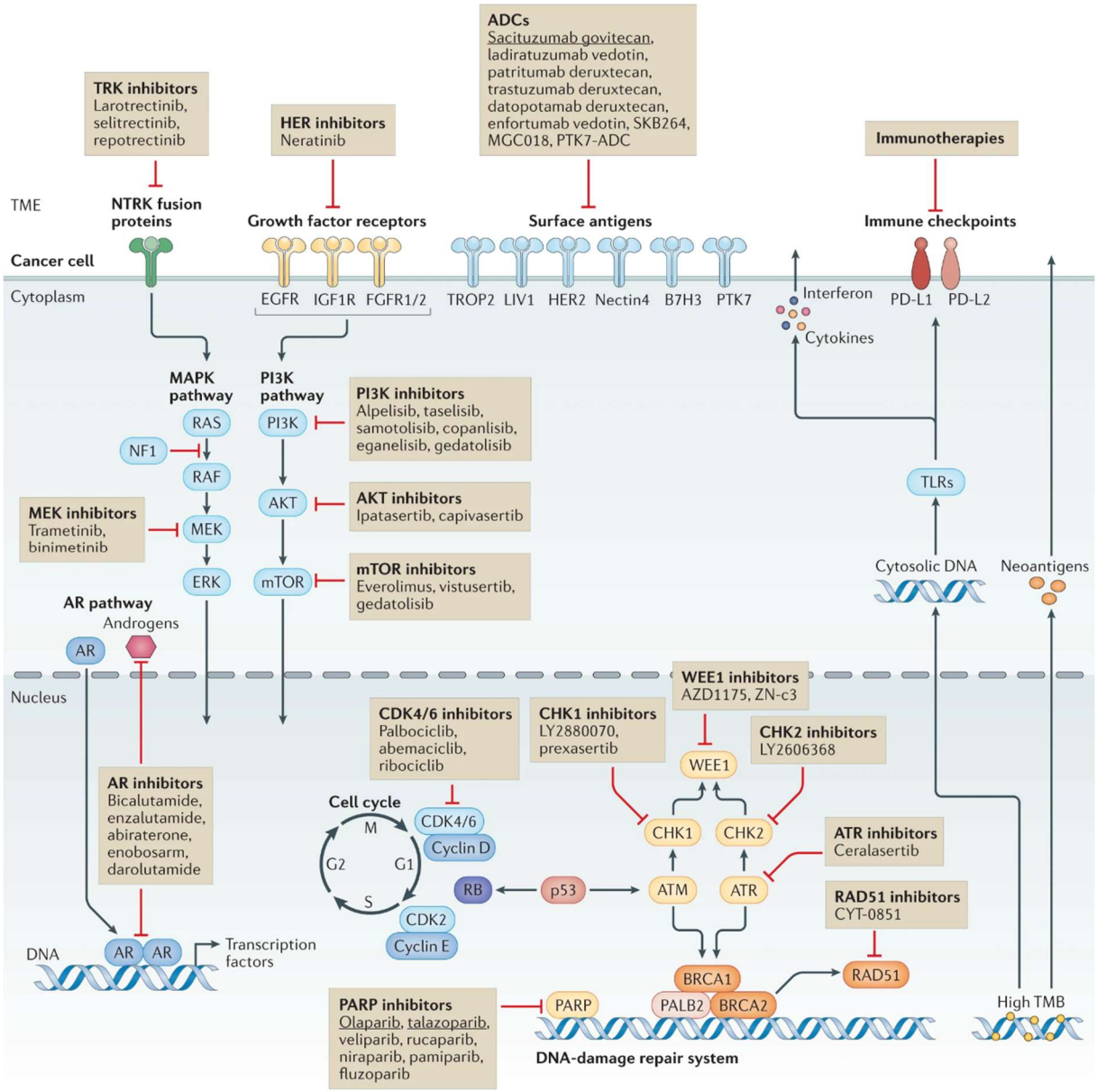

Figure 6: Targeted therapy strategies in TNBC

(approved drugs for TNBC are underlined, the others are under clinical investigation; from[31])

1.3.2.1 PARP inhibitors

The homologous recombination repair (HRR) pathway plays a crucial role in DNA double-strand break repair. Homologous recombination deficiency (HRD) can result from various molecular alterations, including germline or somatic mutations in *BRCA1/2*, and promoter methylation of *BRCA1*[32]. Germline *BRCA1/2* mutations are well-established biomarkers that indicate sensitivity to poly(ADP-ribose) polymerase

(PARP) inhibitors[33]. PARPs are enzymes involved in the detection of DNA strand breaks and in facilitating DNA repair[34]. By inhibiting PARP, double-strand breaks occur during cell replication[35]. In cells with intact *BRCA1*/2 function, these breaks are repaired via the HRR. However, in the context of HRD, particularly in cases of biallelic loss of *BRCA1*/2, cancer cells rely on PARP-mediated DNA repair for survival, rendering them susceptible to PARP inhibitor-induced synthetic lethality[35,36]. The FDA and EMA have approved the use of PARP inhibitors olaparib and talazoparib for treating patients with germline *BRCA1/2*-mutated HER2- metastatic breast cancer. This approval was based on positive results from the phase III OlympiAD and EMBRACA trials. Patients treated with PARP inhibitors experience significantly longer median progression-free survival (PFS) than those receiving other treatment options[37,38]. However, it's worth noting that these trials did not show statistically significant improvements in overall survival (OS)[39,40]. Nonetheless, the phase III OlympiA trial showed significant benefits of adjuvant olaparib in high-risk HER2- breast cancer with BRCA1/2 mutations[41]. It reduces the risk of invasive disease and distant recurrence, supporting the use of PARP inhibitors in early stage breast cancer. ASCO issued guidelines recommending adjuvant olaparib for high-risk, early-stage HER2- BRCA-mutated breast cancer, pending FDA approval[42].

1.3.2.2 Antibody-drug conjugates

Antibody-drug conjugates (ADCs) represent an innovative approach for cancer treatment. They consist of monoclonal antibodies joined to cytotoxic agents, or "cytotoxic payload," through a cleavable or non-cleavable linker[43]. This novel strategy allows for targeted delivery of cytotoxic payloads specifically to cancer cells expressing the antigen while reducing toxic effects on non-malignant tissues.

Trastuzumab deruxtecan (T-DXd) is a HER2-targeted antibody linked to a topoisomerase I inhibitor. The FDA granted accelerated approval for T-DXd in patients with advanced metastatic HER2+ breast cancer based on impressive results from the phase II DESTINY-Breast01 trial[44]. Notably, T-DXd also shows promising antitumor activity in metastatic HER2^{low} breast cancers, including TNBC, although the mechanisms

underlying such activity are unknown, and antitumor response can be due to bystander effects[45].

Sacituzumab govitecan combines a monoclonal antibody targeting TROP2 (trophoblast cell-surface antigen 2) with the DNA topoisomerase I inhibitor SN-38. TROP2 is overexpressed in all breast cancer subtypes; however, it is more elevated in TNBC than in ER+ or HER2+ tumors[46]. The phase III ASCENT trial confirmed a significant improvement in PFS and OS in all TNBC patients receiving this ADC compared to those receiving standard treatment[47], granting it FDA approval for the treatment of TNBC.

1.3.2.3 PI3K-AKT pathway inhibitors

The PI3K-AKT signaling pathway is frequently aberrantly activated in cancer, leading to the disruption of cell growth, survival, and metabolic regulation from external growth signals[48]. Activating mutations in *PIK3CA* or *AKT1* as well as inactivating mutations or loss of *PTEN* or *PIK3R1* can lead to activation of the PI3K pathway. Overall, approximately 50% of TNBC cases experience deregulation of some PI3K pathway component[49]. These alterations have been linked to the sensitivity to PI3K pathway inhibitors. When used in combination with nab-paclitaxel, the PI3K-selective inhibitor alpelisib demonstrates beneficial antitumor effects in patients with HER2-advanced breast cancer, particularly in those with activating PIK3CA mutations[50]. Two highly selective oral pan-AKT inhibitors, ipatasertib and capivasertib, were investigated in phase II studies LOTUS and PAKT alongside paclitaxel for the treatment of metastatic TNBC, and they significantly improved PFS in patients with mutations in *PIK3CA*, *AKT1*, and *PTEN*. However, the phase III IPATunity130 study of upfront paclitaxel with ipatasertib or placebo in patients with metastatic TNBC bearing such alterations failed to show an improvement in PFS.

1.3.2.4 Emerging druggable molecular targets

Randomized phase III trials have shown CDK4/6 inhibitors (which block cell cycling) to be effective and have become the preferred treatment option in combination with endocrine therapy for ER+/HER2- metastatic breast cancer[51]. CDK4/6 inhibitors are still

under clinical investigation for the treatment of TNBC. In addition, several inhibitors of key proteins involved in DNA damage response and DNA repair, such as ATR, ATM, CHK1/2, and WEE1, are currently being investigated in combination with chemotherapy or PARP inhibitors. Another emerging strategy is the use of androgen receptors (AR) inhibitors. The LAR TNBC subtype (see section 1.1.2.2), characterized by luminal-like gene expression and elevated AR levels, can be specifically targeted with AR inhibitors such as bicalutamide, enzalutamide, and abiraterone. Current evidence shows a small benefit of AR inhibitors in prolonging PFS; however, no significant antitumor activity has been observed in patients with AR-positive metastatic TNBC.

1.3.3 Immunotherapy: the future gold standard?

Breast cancer subtypes differ not only in their expression of targetable receptors, but also exhibit unique immune profiles. These profiles encompass variations in the quantity and composition of tumor-infiltrating lymphocytes (TILs), PD-L1 expression, tumor-associated antigens, and tumor mutational burden (TMB)[52–54]. Despite its slower start compared to other solid tumors, the investigation of immunotherapy for breast cancer has witnessed exponential growth over the past few years[55]. This surge in trials exploring immunotherapeutic agents has marked significant advancement in breast cancer research and treatment. Immune checkpoint inhibitors (ICIs) that target PD-1 or PD-L1, such as pembrolizumab and atezolizumab, have shown some early promise in the treatment of breast cancer, but overall response rates are still disappointing when taken alone[56,57]; although this could be due to the fact that ICIs were administered to patients with disease progression after chemotherapy and have a more immunosuppressed status. However, in the randomized phase III study KEYNOTE-522, pembrolizumab was combined with neoadjuvant chemotherapy in the early stages. Regardless of PD-L1 expression, the addition of pembrolizumab to neoadjuvant chemotherapy significantly enhanced the pCR rate and more crucially decreased the probability of recurrence in all patients[58]. In addition to the combination of ICIs with chemotherapy, combinations with the most promising results include those involving PARP inhibitors[59] or ADCs[60].A significant unmet need in the effort to realize precision

immunotherapy is the identification of predictive biomarkers of immunotherapy response, particularly in the case of TNBC. One of the intrinsic characteristics of cancer cells associated with the efficacy of ICIs in TNBC is the tumor mutational burden (TMB), which increases neoantigen load and tumor foreignness. However, only 8–10% of TNBCs have high TMB levels, and pembrolizumab monotherapy has stronger but still lower efficacy in these tumors[61]. Combining TMB with additional mutational signatures or genetic changes, such as APOBEC signature[62], may increase its predictive usefulness. Numerous studies have demonstrated that the effectiveness of ICIs in treating TNBC is linked to modifications in immune-related characteristics, such as lymphocyte infiltration patterns or gene expression-based markers. There is a potential for improvement because such biomarkers are strongly correlated, mostly redundant, and do not consider single-cell properties or spatial distribution[63,64]. Multiple lines of therapy and prior chemotherapy exposure are two of the most significant variables that can have a detrimental impact on the effectiveness of ICIs[65]. Clinical characteristics related to the overall tumor-host immunological fitness can also be associated with a reduced degree of benefit from ICIs. High neutrophil-to-lymphocyte ratios[66], unfavorable microbiome[67], and unique germline genetics[68] are other examples of these variables.

The combination of these characteristics and the establishment of a subtyping system inside the TNBC ecosystem could help in identifying the dominant mechanisms of resistance and sensitivity to immunotherapies.

2 ATIP3 – AN EMERGING TARGET FOR PERSONALIZED MEDICINE IN BREAST CANCER

The microtubule-associated tumor suppressor (*MTUS1*) gene, initially named *MTSG1*, was discovered in 2003[69]. It is located at chromosomal position 8p22, a region commonly lost in various solid tumors including breast cancer[70,71]. Seibold *et al.* identified the *MTSG1* transcript using a differential display RT-PCR approach and observed its upregulation in 3-dimensional cultures of quiescent compared to differentiated human endothelial cells[69]. The *MTSG1* gene encodes a 436 amino-acid polypeptide (48 KDa) that localizes to mitochondria and was found to be downregulated in pancreatic cancer, where its expression inhibited cell proliferation. In a separate study published a few months later, the same polypeptide was identified through a yeast two-hybrid system as an intracellular interacting partner of the human angiotensin II AT2 receptor and was named ATIP1[72]. The angiotensin II AT2 receptor is a unique example of a seven-transmembrane receptor that controls cell proliferation through intracellular pathways that do not involve typical G-protein signaling. ATIP1 was identified as a scaffold protein responsible for mediating the anti-proliferative effects of AT2 receptor signaling in a constitutive manner, even in the absence of receptor stimulation[72,73].

2.1 THE ATIP FAMILY OF PROTEINS

ATIP1 is part of the AT2-interacting protein (ATIP) family, which also includes ATIP3 and ATIP4. All ATIPs share a common C-terminal amino acid sequence of 396 residues, containing the AT2 receptor binding site and several coiled-coil motifs that facilitate homo- and hetero-dimerization. ATIP1, ATIP3, and ATIP4 are generated from alternative splicing and different promoter usage of the *MTUS1* gene, which has 17 coding exons[74]. *MTUS1* encodes two splice variants of ATIP3, known as ATIP3a and ATIP3b, differing by a single in-phase exon encoding a 60-amino-acid sequence at the N-terminal portion of the proteins. Although both variants share high sequence homology, no functional difference has been reported between them. In rodents, the

orthologous *mtus1* gene comprises 15 coding exons that are also alternatively spliced, leading to the generation of three different ATIP isoforms, named ATBP50, ATBP135, and ATBP60 in mice, exhibiting structural homology to human ATIP1, ATIP3, and ATIP4, respectively[75]. Additionally, the xenopus *MTUS1* gene ortholog encodes the ICIS protein that shares structural similarities with the mammalian ATIP3 isoform (Figure 7).

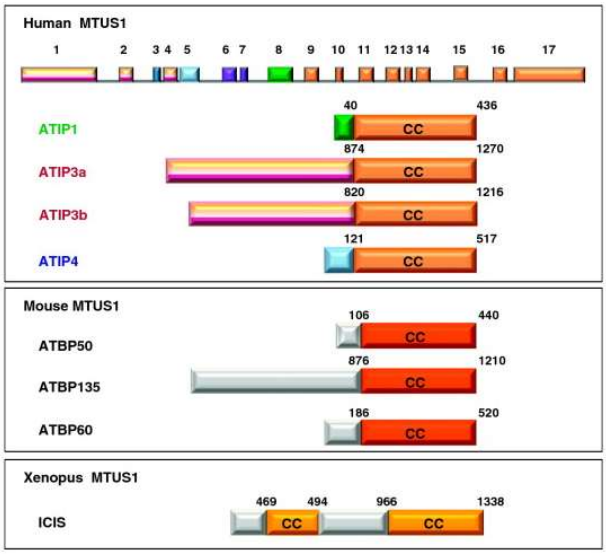

Figure 7: Structural organization of ATIPs and ATIP-related proteins

(Adapted from[76])

ATIP1 is primarily found in central nervous system tissues, female reproductive tissues thyroid, and heart. ATIP3 is the predominant transcript expressed in nearly all tissues except the brain. ATIP4 is exclusively detected in the brain. These expression patterns suggest specific roles and functions for each ATIP isoform in various tissues and organs.

2.2 ATIP3: A MULTIFUNCTIONAL ANTICANCER PROTEIN

MTUS1 knock-out mice developed B-cell lymphoproliferative disease, which is consistent with the first research that suggested *MTUS1* may be a potential tumor suppressor gene[77]. There have been several reports of *MTUS1* downregulation in many different cancers (Table 1). Only a small number of studies attempted to distinguish between various ATIP isoforms, and they all identified ATIP3 as the primary *MTUS1* isoform that was altered in human malignancies.

Cancer type	*MTUS1* isoform	Detection method	Expression level
Bladder cancer	N.D.	IHC	Underexpressed
	N.D.	RT-qPCR	Underexpressed
Breast cancer	N.D.	Microarray	Underexpressed
	ATIP3	Microarray	
	ATIP3	Microarray/IHC	
	ATIP3	Microarray/IHC	
Colorectal cancer	N.D.	RNA-seq	Underexpressed
	N.D.	IHC	
	N.D.	RT-qPCR/WB	
	N.D.	RT-qPCR	
Gallbladder carcinoma	N.D.	Microarray/IHC	Underexpressed
Gastric cancer	N.D.	RT-qPCR	Underexpressed
Lung cancer	N.D.	Microarray	Underexpressed
Oral cancers	N.D.	RT-qPCR	Underexpressed
	ATIP3	IHC	
	N.D.	Microarray/IHC	
Renal cancer	N.D.	IHC	Underexpressed
Uveal melanoma	N.D.	Microarray	Underexpressed

Table 1: MTUS1 gene status in various cancers

(Adapted from[78])

2.2.1 ATIP3 is a prognostic biomarker in breast cancer

In an effort to discover novel biomarkers in breast cancer, the expression levels of the *MTUS1* gene were examined in 151 breast tumors and compared to normal breast tissue, revealing for the first time a significant downregulation of *MTUS1* in 50% of all breast cancers and 70% of TNBC cases. Additional real-time RT-PCR analyses showed that ATIP3 is the primary transcript present in normal mammary gland tissue and downregulated in breast tumors[79]. Interestingly, ectopic expression of ATIP3 in breast cancer cells reduces in tumor growth and metastasis in preclinical models[80].

The mechanisms leading to the downregulation of ATIP3 in breast cancer are unknown. However, the ATIP3 promoter contains many CpG islands, which may indicate a regulation through promoter methylation at these sites[81]. Other potential mechanisms contributing to this downregulation include the influence of RNA binding proteins[82], long non-coding RNAs or miRNAs[83,84] on the stability of *MTUS1* mRNA.

Investigation into the prognostic value of ATIP3 across multiple patient cohorts indicated a strong correlation between low levels of ATIP3 and aggressive breast cancer subtypes, such as TNBC[24,25], high-grade tumors and metastatic breast cancers[80]. Low ATIP3 levels are associated with reduced overall survival rates, making it a prognostic biomarker for breast cancer patient survival (Figure 8).

The prognostic significance of ATIP3 was also evaluated when considered alongside its interacting partner, End-Binding Protein 1 (EB1), which has been observed to be more abundant in aggressive breast tumors. The fact that ATIP3 counteracts the effects of EB1 on microtubule dynamics (see section 2.2.2), suggests that tumors with low ATIP3 and high EB1 levels might be linked to increased malignancy and a poorer prognosis compared to other breast tumors. Studies conducted on five separate groups of breast cancer patients confirmed that the combined expression of ATIP3 and EB1 had greater prognostic value than either biomarker alone[85,86].

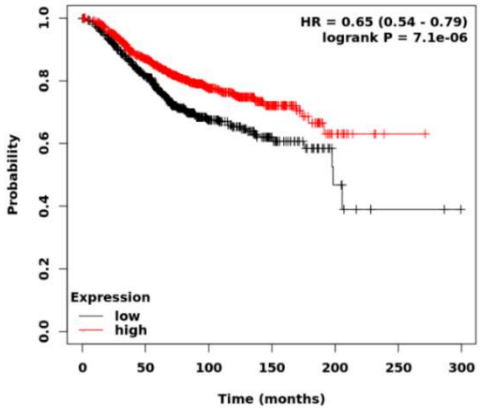

Figure 8: Kaplan-Meier overall survival curves of breast cancer patients with high or low ATIP3 expression levels
(generated using KMplot.com[87])

2.2.2 ATIP3 is a microtubule-associated protein

ATIP3 is a polypeptide of 1270 amino acids organized into a coiled-coil C-terminal region and an unstructured 874 amino acid N-terminal region[74]. Initial investigations into ATIP3's intracellular localization made it clear that it decorates the centrosome and the microtubule cytoskeleton in interphase and localizes to the mitotic spindle during all phases of mitosis (Figure 9). ATIP3 was found to bind onto stable microtubules – rather than soluble tubulin – through a positively charged, central region of the protein (D2)[79,80]. These basic residues are thought to interact with the acidic charges on tubulin tails, as it is the case for other microtubule-associated proteins (MAPs).

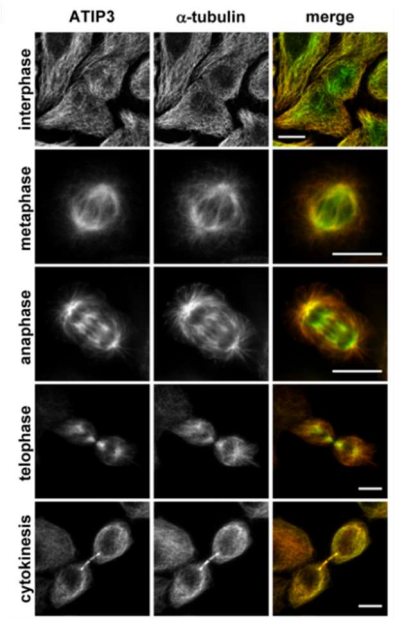

Figure 9: ATIP3 localization in different cell cycle stages
(from[79])

The microtubule cytoskeleton is crucial for maintaining cell homeostasis. Microtubules are polarized, highly dynamic structures that form by the GTP-dependent assembly of α/β tubulin dimers at their growing (+) ends. Continuous transition of microtubule ends between phases of polymerization and depolymerization interrupted by pauses, otherwise known as dynamic instability, is necessary to enable the cytoskeleton's quick adaptability to cellular changes[88]. Structural MAPs that locate along the microtubule lattice as well as microtubule plus ends-tracking proteins (+TIPs) that decorate the rapidly growing (+) ends, control microtubule assembly and dynamics[89]. ATIP3 is a structural MAP present along the microtubule lattice and is a powerful microtubule stabilizer[79]. Surprisingly, ATIP3 lowers microtubule dynamics at plus ends despite not binding to this site[80]. ATIP3 interacts with EB1 – an important member of the +TIP family – in the cytosol, reducing free EB1 turnover at its preferential site at the plus ends[90]. Cytosolic ATIP3/EB1 complexes govern the rate of microtubule development and shrinking by inhibiting EB1 accumulation at (+) ends, consequently controlling microtubule targeting to the cell cortex and consequent cell polarity and migration.

2.2.3 ATIP3 regulates mitotic spindle size

ATIP3 interacts with 145 proteins, out of which 9 are related to the microtubule cytoskeleton and/or mitosis[91]. Notably, ATIP3 interacts with KIF2A, a kinesin of the kinesin-13 family responsible for microtubule depolymerization[92], and its regulator Dda3, *via* a specific sequence of 112 amino acids located in the central basic region of ATIP3[91]. The complex formed by ATIP3, KIF2A, and Dda3 prevents the accumulation of KIF2A at the poles of the mitotic spindle (Figure 10). The stability of this complex depends on phosphorylation by Aurora A, a mitotic kinase localized at the spindle poles where it phosphorylates KIF2A, reducing its activity. ATIP3 maintains an active pool of Aurora A at the spindle poles, thereby controlling the activity of KIF2A and ensuring the integrity of the mitotic spindle[91]. When ATIP3 is depleted in cells, a shortening of the mitotic spindle occurs. This abnormality likely leads to significant problems in the proper segregation of chromosomes during cell division.

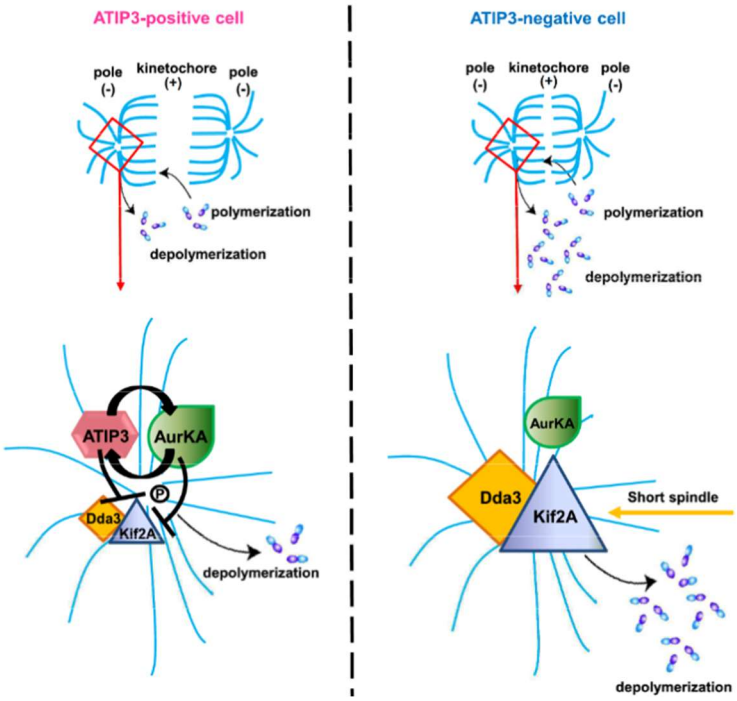

Figure 10: Mechanism of metaphase spindle size regulation by ATIP3
(Adapted from[91])

2.2.4 ATIP3 is a predictive biomarker of breast cancer sensitivity to taxanes

Taxanes (paclitaxel and docetaxel) are the most used chemotherapeutic agents for breast cancer treatment (see section 1.1.3.1). These drugs are also known as spindle poisons, because they bind to microtubules at the "taxane site," blocking microtubule dynamics. Through the stabilization of spindle microtubules during mitosis, taxanes induce mitotic arrest eventually leading to cell death. At extremely low concentrations, in the nanomolar range, taxanes induce the formation of multipolar spindles and other abnormalities during mitosis, ultimately resulting in aneuploidy[93] (see section 5.2.3). Taxanes provide significant benefits for only 15-20% of breast cancer patients, making crucial the identification of biomarkers that can accurately predict patient response. Cohort analysis of breast cancer patients who underwent neoadjuvant treatment with taxanes allowed the identification of 17 genes encoding microtubule regulating proteins differentially expressed in chemoresistant breast tumors[94]. Among these genes, *MTUS1* stands out as one of the most significantly deregulated. ATIP3 expression is found to be markedly reduced in taxane-sensitive tumors that achieved pathological complete response (pCR), including in the BL1 subtype of TNBC. In

addition, lymph node metastases are less frequent among tumors expressing low levels of ATIP3 following treatment with paclitaxel compared to tumors expressing high ATIP3 levels. This is counterintuitive as ATIP3 deficiency is associated with heightened microtubule dynamics, which is opposite to the stabilizing effect that taxanes like paclitaxel have on microtubules. So, how does ATIP3 deficiency sensitize to taxanes?

At the molecular level, the depletion of ATIP3 leads to an increased accumulation of paclitaxel along the microtubule structure, explaining the heightened sensitivity to low doses of chemotherapy[95]. Importantly, during mitosis, ATIP3 deficiency triggers centrosome amplification and the formation of multipolar spindles, both of which lead to aneuploidy. In the presence of low doses of taxanes, these mitotic abnormalities accumulate to a level that exceeds tolerance and leads to significant cell death[94]. Thus, ATIP3 deficiency induces aneuploidy, paradoxically rendering cancer cells more sensitive to taxanes[96] (see section 5.2.3). Consistent with these molecular findings, human breast tumors with low *MTUS1* levels display high levels of aneuploidy and chromosome instability[94]. In summary, ATIP3 deficiency, by boosting microtubule dynamics at the growing plus ends, not only enhances paclitaxel binding to microtubules during interphase but also encourages the formation of multipolar spindles during cell division (Figure 11). The potent impact of taxanes in ATIP3-deficient breast tumors likely results from a combination of these two mechanisms.

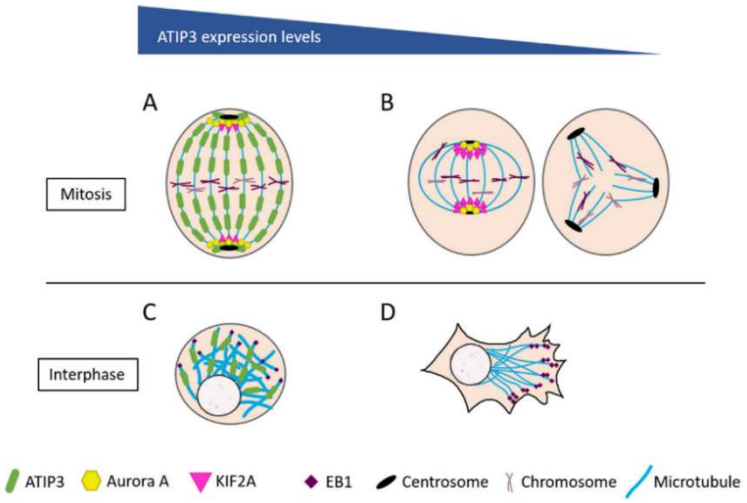

Figure 11: Consequences of ATIP3 downregulation (from[78])

3 THE CELL CYCLE – AN INTRICATE CHOREOGRAPHY

Cell division is rigorously managed through an intricate system of regulatory processes, safeguards, and checks. This elaborate system ensures that a cell must meet specific criteria before it is permitted to proceed through the cell cycle and divide, thereby ensuring the generation of two cells that are genetically identical. The key aspects of cell cycle control are primarily centered around the replication of the cell's DNA and its distribution to the daughter cells.

3.1 OVERVIEW OF THE CELL CYCLE

In 1953, Alma Howard and Stephen Pelc introduced the concept of defined time frames for cell division, identifying two main distinct phases of the cell cycle: interphase and the M phase[97]. Interphase, in turn, can be further divided into three subphases: the S-phase, which involves DNA replication; the G1 phase, occurring before the S-phase; and the G2 phase, which takes place before the M phase (Figure 12).

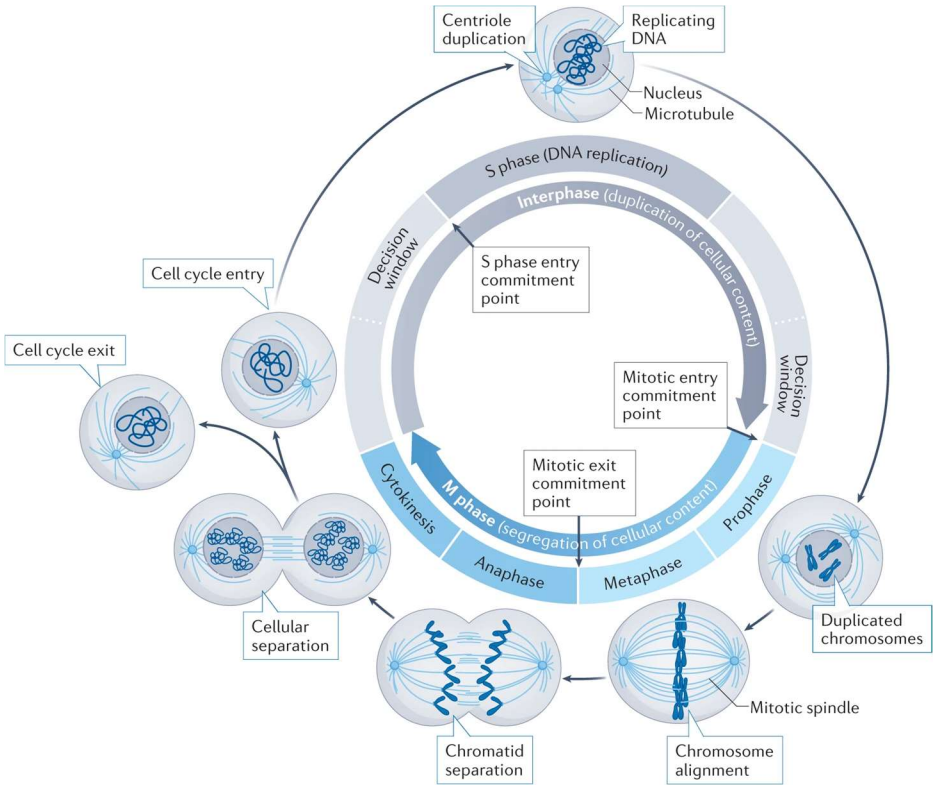

Figure 12: Overview of the cell cycle
(from[98])

In the G1 phase, cells face a first decision window: enter into the cell cycle and initiate DNA replication, remain in G1 or exit the cell cycle and enter a non-proliferative state known as quiescence or G0. Subsequently, after DNA replication, another decision point arises during the G2 phase. Cells can progress into the M phase, which serves a dual function of accurately segregating duplicated DNA (mitosis) and dividing the entire cellular content into two new daughter cells (cytokinesis).

The cell cycle is governed by the oscillating functions of Cyclin-Dependent Kinases (CDKs). The activity of CDKs is induced by mitogenic signals and can be inhibited by the activation of cell cycle checkpoints. Cells rely on these checkpoints to monitor DNA damage during interphase, as well as loss of DNA replication fork integrity during S phase and errors in spindle assembly during M phase (Figure 13). Checkpoint sensors identify errors in the aforementioned mechanisms and activate specific effectors to induce cell cycle arrest and activate the relevant repair pathways.

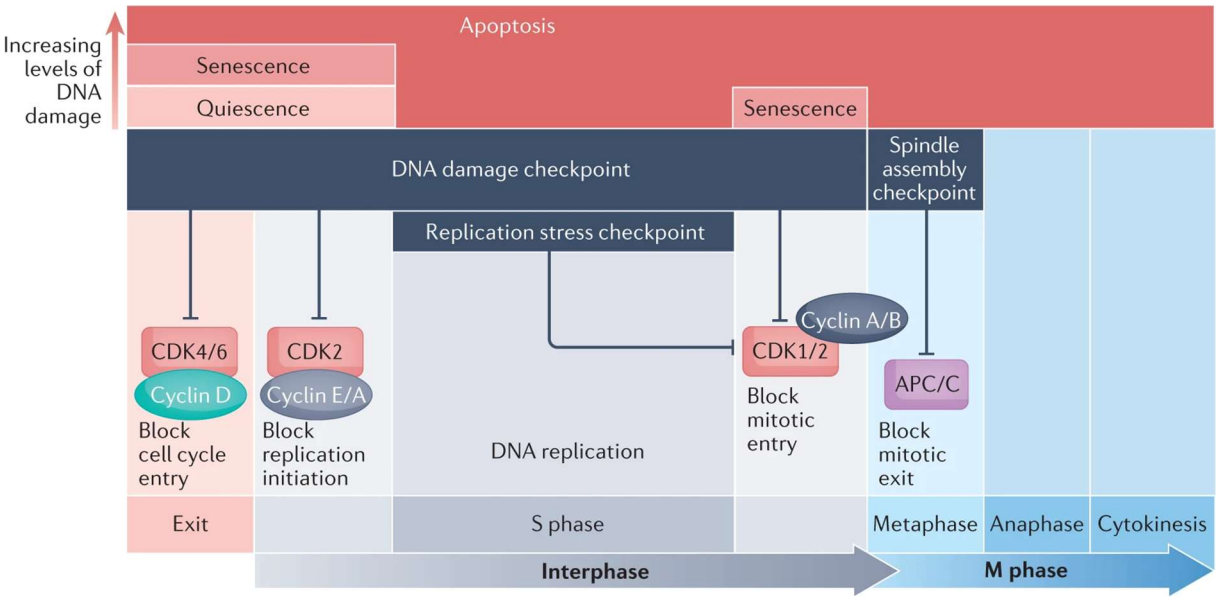

Figure 13: The cell cycle checkpoints
(Adapted from[98])

Cancer cells override their cell cycle checkpoints through mutations of CDKs or their inhibitors, dysregulation of signaling pathways, and defective DNA repair mechanisms, allowing uncontrolled cell division despite DNA damage or abnormalities.

3.2 CELL CYCLE CONTROL IN CANCER

Although often depicted as simple stop signs, checkpoints actually encompass sophisticated functions: surveillance, engagement, arrest, repair, and release. These functions are composed of numerous molecular-level steps that come into play. Intriguingly, checkpoints achieve something remarkable: they transform a relatively minimal amount of molecular information, such as a single DNA lesion or a misaligned chromosome, into a regulatory process that pauses the cell-cycle machinery.

3.2.1 G1 phase: crossing the point of no return

3.2.1.1 The restriction point

During the G1 phase of the cell cycle, cells decide whether to enter the cell cycle, initiate DNA replication, and divide or to exit the cell cycle and enter quiescence. Cells commit to either quiescence or future S phase entry at the 'restriction point'[99]. This decision is based on the presence of mitogenic signals that trigger the activation of D-type cyclins - CDK4/6 complexes. These complexes phosphorylate the retinoblastoma protein (RB) weakening its growth-suppressive functions and resulting in the activation of members of the E2F family, stimulating the expression of a set of hundreds of genes that promote DNA replication[100]. Components of the CDK4/6–RB pathway are commonly mutated in cancer cells[101]. Type D cyclins and CDK4/6 constitutive activation or amplification, and deletion of RB, confer cancer cell the ability to proliferate independently of mitogenic signals therefore overriding the restriction point.

Beyond the restriction point, origin licensing, the initial step in the process of DNA replication, takes place. During licensing, specific proteins called origin recognition complexes (ORCs) bind to potential replication origins on the DNA, marking them as sites where replication can potentially initiate. Following licensing, multiple proteins such as CDC6, CDT1 and MCM2-7 proteins come together at DNA replication origins and create pre-replication complexes (pre-RCs)[102]. These complexes remain in a waiting state until they receive a signal, mediated mainly by CDK2, to start the process of origin firing at the beginning of S phase (Figure 14).

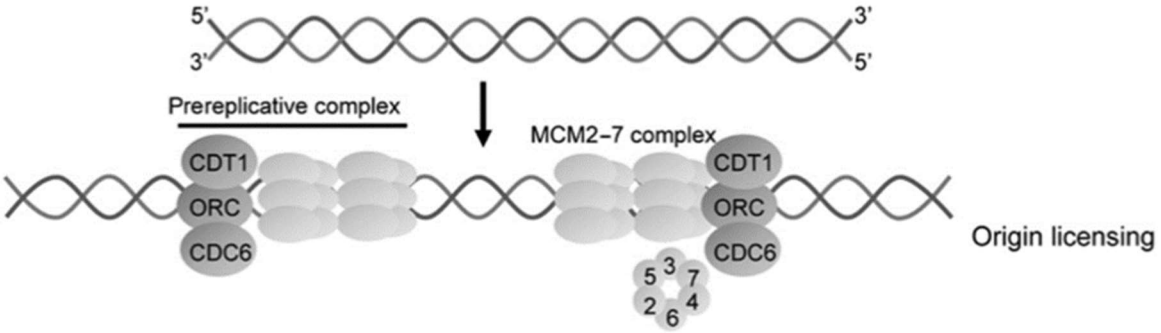

Figure 14: Assembly of the pre-replication complexes
(Adapted from[103])

3.2.1.2 The G1 DNA damage checkpoint

Throughout the cell cycle, DNA is constantly exposed to endogenous and exogenous sources of damage. On a daily basis, each cell experiences approximately 55,000 single strand breaks (SSBs) and around 25,000 double strand breaks (DSBs)[104]. One of the primary sources of internal DNA damage is oxidative phosphorylation, which generates reactive oxygen species (ROS)[105]. External factors also contribute to DNA damage, including exposure to ultraviolet light and various chemo/radio-therapies[106]. These DSBs pose a direct threat to genome stability; therefore, a series of intricate mechanisms of repair take place to prevent the buildup and spread of genetic mistakes during cell division[107].

During the G1 phase, DSBs require repair before the onset of replication. If the primary DNA lesions are left unattended during replication, they can impede the DNA replication process or transform into other forms of DNA damage causing hazardous consequences for the cell. The occurrence of DSBs initiates a swift signaling process relying on the checkpoint protein kinase known as ataxia telangiectasia mutated (ATM)[108]. This response leads to alterations in ongoing transcription rates, activation of DNA repair mechanisms, and interaction with cell cycle regulators, ultimately causing a deceleration or halt in progression through the cell cycle.

The DNA damage sensor complex MRN (MRE11, RAD50, and NBS1) triggers the phosphorylation of ATM[109]. ATM then phosphorylates S139 on the histone variant H2AX, resulting in the formation of γH2AX on the DNA which leads to chromatin

changes around the DSB[110]. This mark serves as a signal recognized by mediator proteins, which then amplify local ATM activity and recruit repair factors to the damaged site such as 53BP1, BRCA1 and MDC1[111,112]. Concurrently, ATM activates the checkpoint kinase 2 (CHK2) kinase, which emanates from the DSB location and contributes to the DNA damage response (DDR)[113]. In the context of a DSB occurring during G1 phase, both ATM and CHK2 are essential for stabilizing the p53 protein. This stabilization of p53 leads to the activation of an array of transcriptional targets, including the CDK inhibitor protein p21 (also known as CDKN1A), effectively halting the progression of the cell cycle[114,115]. Complementing this transcriptional reaction, ATM and CHK2 engage in pathways that prevent the entry into S-phase[116,117]. These pathways promote the degradation of cyclin D and the CDC25A phosphatase that reverse inhibitory phosphorylations on CDK2[118,119] (Figure 15). Unsurprisingly, loss of p53, one of the most frequently mutated proteins in cancer cells, results in the complete abrogation of the G1 checkpoint.

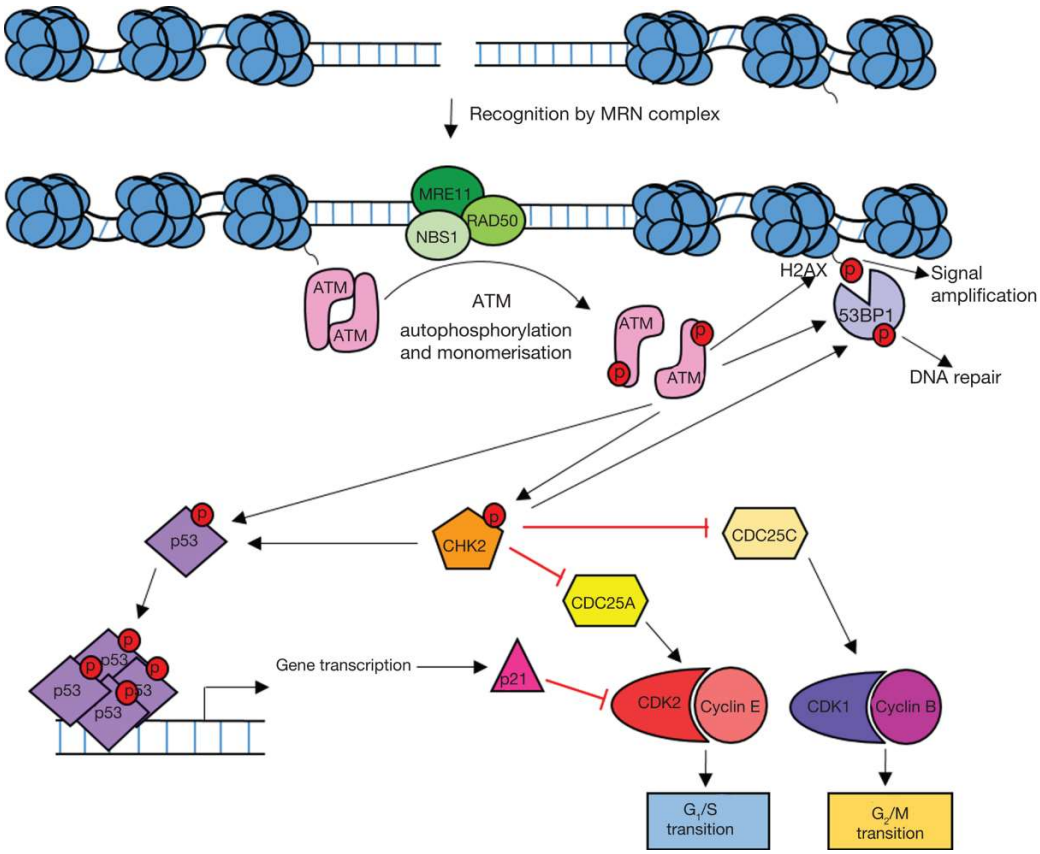

Figure 15: The DNA Damage checkpoint
(Adapted from[120])

Bypassing the restriction point and the G1 DNA damage checkpoint, whether due to p53 or RB mutations, overexpression of cyclins and CDKs or alterations in checkpoint signaling, releases cells into S phase where DNA replication takes place, despite the potential presence of unrepaired DNA damage.

3.2.2 S phase: DNA replication

Preserving DNA integrity during replication is a highly complex task demanding the coordination of DNA fork progression, an adequate supply of deoxyribonucleotides, functional DNA repair mechanisms and intact checkpoints.

The initiation of DNA replication marks the entry into the S phase. DNA replication commences bidirectionally from numerous distinct locations scattered throughout the genome, referred to as 'replication origins'[121]. This distribution ensures the timely replication of the entire genome. Maintaining genome integrity requires that DNA replication occurs only once during the cell cycle. Preventing the re-initiation of replication from an origin that has already been utilized is crucial, as even a single instance of re-replication from an origin could induce DNA damage[122,123]. To avert such re-initiation, the replication process is divided into two sequential stages: origin licensing during the G1 phase, succeeded by replication initiation, referred to as 'origin firing,' in the S phase[124]. During an unperturbed S-phase, not all licensed origins necessarily fire and some origins may be held in a "dormant" state during certain parts of the S-phase to prevent excessive DNA replication[125]. These dormant origins can act as backup in case of replication slow down or failure[126]. Origins are often organized into clusters whose firing occurs in a coordinated and timely fashion giving rise to early-replicating and late-replicating origins[102].

Origin firing is orchestrated by DBF4-Dependent CDC7 kinase (DDK), working in conjunction with cyclin E–CDK2 to phosphorylate the pre-RCs[127,128]. This facilitates the binding of CDC45 and GINS complex to MCM2–7, activating the DNA helicase (called the CMG complex)[129]. As a result, the double-stranded DNA unwinds, DNA polymerase is recruited, and DNA synthesis is initiated (Figure 16).

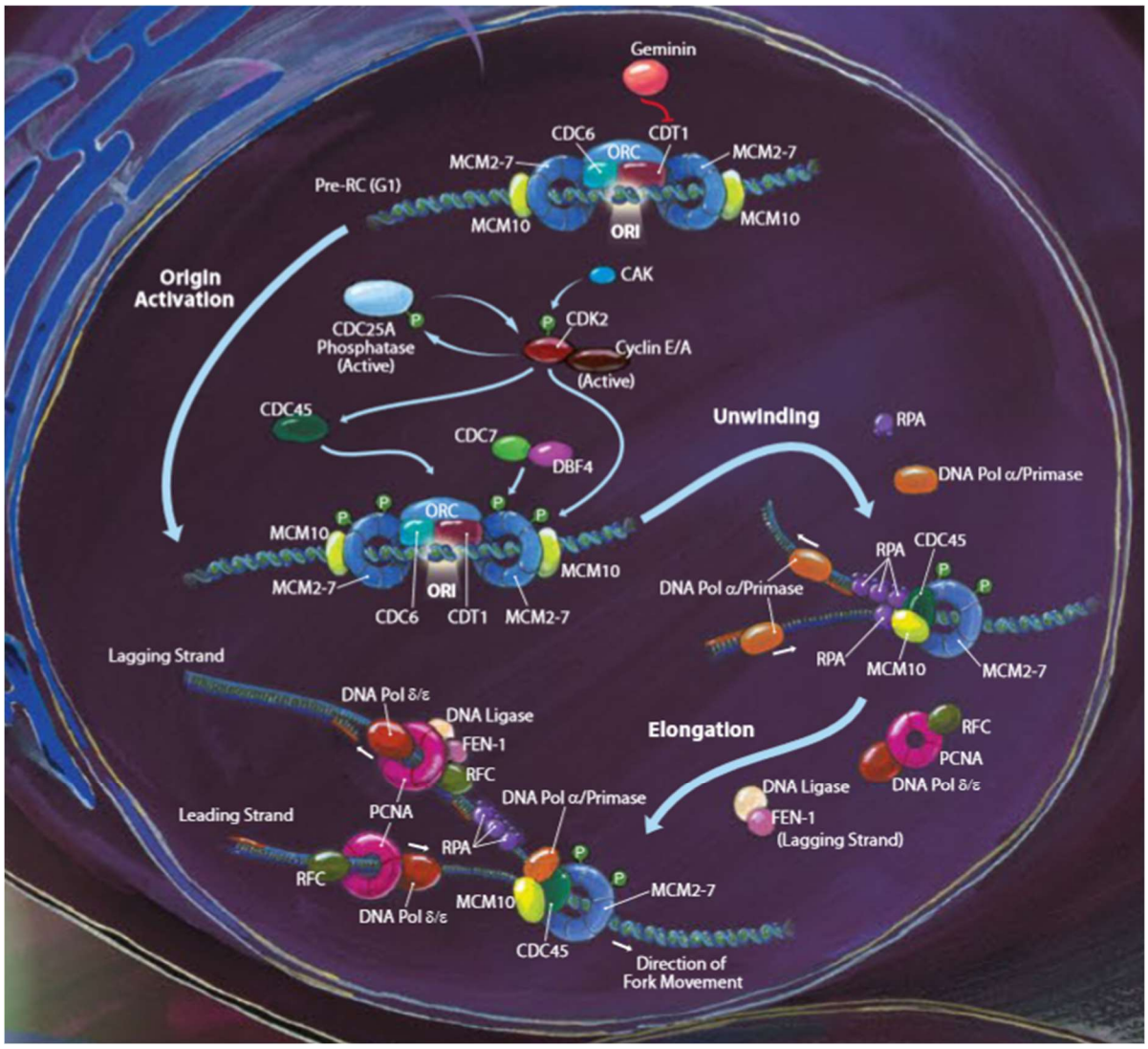

Figure 16: The DNA replication machinery

(adapted from https://www.rndsystems.com/resources/posters/regulation-cell-cycle-dna-damage-induced-checkpoint-activation)

3.2.2.1 Replication stress

After origins initiate and the process of DNA replication begins, cells must effectively manage a balance between accuracy, speed, and the consumption and allocation of resources like nucleotides and replication factors. This ensures the completion of replication in an optimal manner. Although the DNA replication machinery is highly accurate, it is often challenged by endogenous or exogenous stresses causing the slowing or stalling of replication fork progression and/or DNA synthesis otherwise known as **replication stress**[130].

3.2.2.1.1 Sources of replication stress

Replication stress originates from many distinct factors, of which: physical barriers to fork progression such as DNA lesions and secondary DNA structures; challenges like conflicts between transcription and replication machineries; intermediates or products of specific DNA repair processes; nucleotide imbalances and dysregulated origin firing (Figure 17).

DNA lesions can directly block the movement of the replication fork, which is the site where DNA replication occurs. DNA polymerases encounter the lesion and cannot bypass it, leading to the **stalling** of the replication fork. In some cases, if the replication fork encounters a particularly severe or complex lesion, it may **collapse**, leading to the formation of a DSB[131]. In addition, aside from the typical right-handed double helix, the DNA molecule has the capacity to take on various alternative structures known as non-B or secondary DNA structures. These alternate forms can readily manifest within the genome, particularly in specific repetitive DNA sequences. These unique structures pose a distinct obstacle to the smooth advancement of replication forks[132]. Several specialized helicases and nucleases are essential for unraveling these structures and promoting replication fork progression, with the absence or malfunction of these enzymes being associated with a wide range of disorders characterized by genetic instability[133,134].

Transcription-replication conflicts arise when the processes of transcription and DNA replication occur simultaneously on the same DNA strand, leading to potential collisions and structural conflicts. One notable example is the formation of R-loops, where the nascent RNA molecule hybridizes with the template DNA strand, creating a three-stranded structure. This can impede the progression of the replication fork, as it encounters the R-loop structure during replication[135]. Beyond secondary configurations and R-loops within the template DNA, condensed chromatin could also present an obstacle for both DNA replication and repair. Heterochromatin regions, like centromeres, peri-centromeres, and telomeres, inherently pose challenges for

replication due to their compact nature, necessitating specialized mechanisms of chromatin alteration to guarantee the smooth advancement of replication forks[136,137].

Perturbations in the cellular nucleotide pools are another important source of replication stress. High deoxyribonucleotide triphosphate (dNTP) levels undermine the accuracy of DNA replication by diminishing the proofreading effectiveness of polymerases[138]. Conversely, reduced dNTP levels induce replication stress by compromising polymerase functions[139]. Also, the quality of dNTP pools and the balance among individual dNTPs are critical[140]. Inadequate control of replication initiation can contribute to replication stress, where excessive origin activation can exhaust nucleotide pools and slow replication forks, while insufficient origins can result in incomplete replication and the potential loss of genetic material.

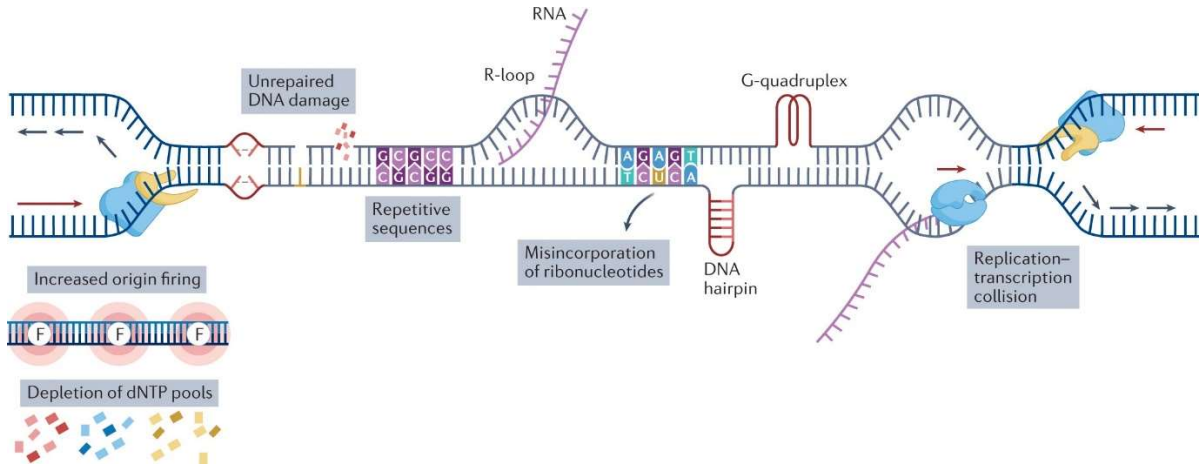

Figure 17: The sources of replication stress
(from[141])

3.2.2.1.2 The replication stress response

Replication stress results in the formation of stretches of single-stranded DNA (ssDNA), a result of the uncoupling of the polymerase from the helicase that continues to unwind the parental DNA after polymerase has stalled[142]. This causes the activation of the replication stress response (Figure 18). Replication stress is not DNA damage, and the main function of the DNA replication checkpoint response is to prevent replication stress-induced DNA damage.

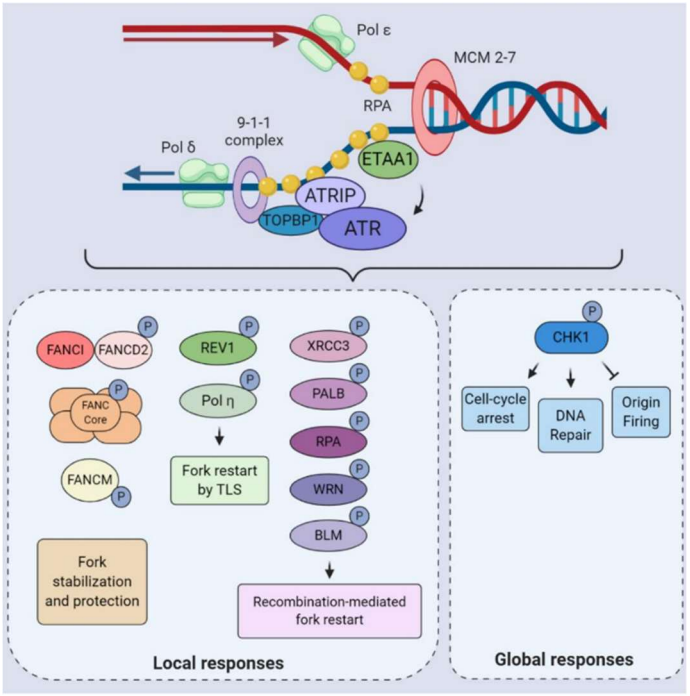

Figure 18: The DNA replication stress response

(Adapted from[143])

Replication protein A (RPA) exhibits a strong binding affinity for ssDNA, serving as a foundational platform for the recruitment of a multitude of sensor proteins. These include ataxia telangiectasia and Rad3-related (ATR)-interacting protein (ATRIP), the 9-1-1 DNA clamp complex (RAD9-RAD1-HUS1), topoisomerase II binding protein 1 (TOPBP1), and Ewing tumor-associated antigen 1 (ETAA1)[144–147]. This assembly of proteins collaborates to initiate the activation of the central replication stress response kinase ATR. Once activated, ATR coordinates a multifaceted reaction at stalled replication forks, phosphorylating several downstream targets, with its primary effector kinase being checkpoint kinase 1 (CHK1). This ATR-CHK1 signaling cascade orchestrates the replication stress response locally by stabilizing stalled replication forks, promoting fork repair and restart and globally by suppressing origin firing and arresting the cell cycle. This response serves as a temporary resolution, as extended stalling of a replication fork can result in its collapse. This involves the dissociation of replisome components from the DNA, which in turn leads to the formation of DSBs. When this occurs, the DNA damage checkpoint response is triggered to initiate the repair of the resulting damage.

3.2.2.1.3 Local effects at stalled replication forks

Replication forks can bypass the DNA lesions that block replication and continue DNA synthesis using different mechanisms: Template switching may allow the fork to bypass an obstacle by switching from the original template strand to a nearby intact strand, allowing DNA synthesis to continue in a different direction[148]. In scenarios involving unrepaired DNA lesions, where the fork cannot be restarted directly, dormant replication origins in proximity to the stalled site can be activated to rescue replication forks[125] (Figure 19a). The fork restart may also involve repriming downstream of the lesion leaving behind a ssDNA gap[149]. These ssDNA gaps are then addressed through the translesion synthesis, a DNA damage tolerance (DDT) mechanism enabling the cell to 'tolerate' the presence of the DNA lesion[150] (Figure 19b). If the obstacles present are not tolerated or bypassed, the forks face stalling or collapse.

1. Fork stabilization

The replication stress response stabilizes stalled forks and promotes their recovery. The stability of the replication fork has been regarded as a response orchestrated by CHK1 in the face of replication stress to shield the fork from harmful nucleolytic degradation. However, this view has been challenged by evidence showing that fork stability is maintained in the absence of CHK1[151] and that ATR protects the fork against collapse[152]. **Fork reversal** represents a mechanism of fork stabilization, where DNA replication fork temporarily changes its direction, regressing back along the parental DNA strands. This process involves the unwinding of the fork's DNA helix, leading to the formation of a four-way junction or "chicken-foot" structure[153]. Fork reversal is mediated by DNA processing enzymes such as the DNA recombinase RAD51[154] or DNA translocases like the SWI/SNF subfamily A-like 1 (SMARCAL1), zinc finger RANBP2-type containing 3 (ZRANB3), and helicase like transcription factor (HLTF)[155–157]. Reversed forks are protected from extensive nucleolytic cleavage by the action of many proteins including but not restricted to BRCA1/2[158], FANCA/B and FANCD2[159]. In the absence of such protection factors, reversed forks become susceptible to the extensive degradation mediated by the activity of nucleases like MRE11[158], DNA2[160], EXO1[161]

(Figure 19c).

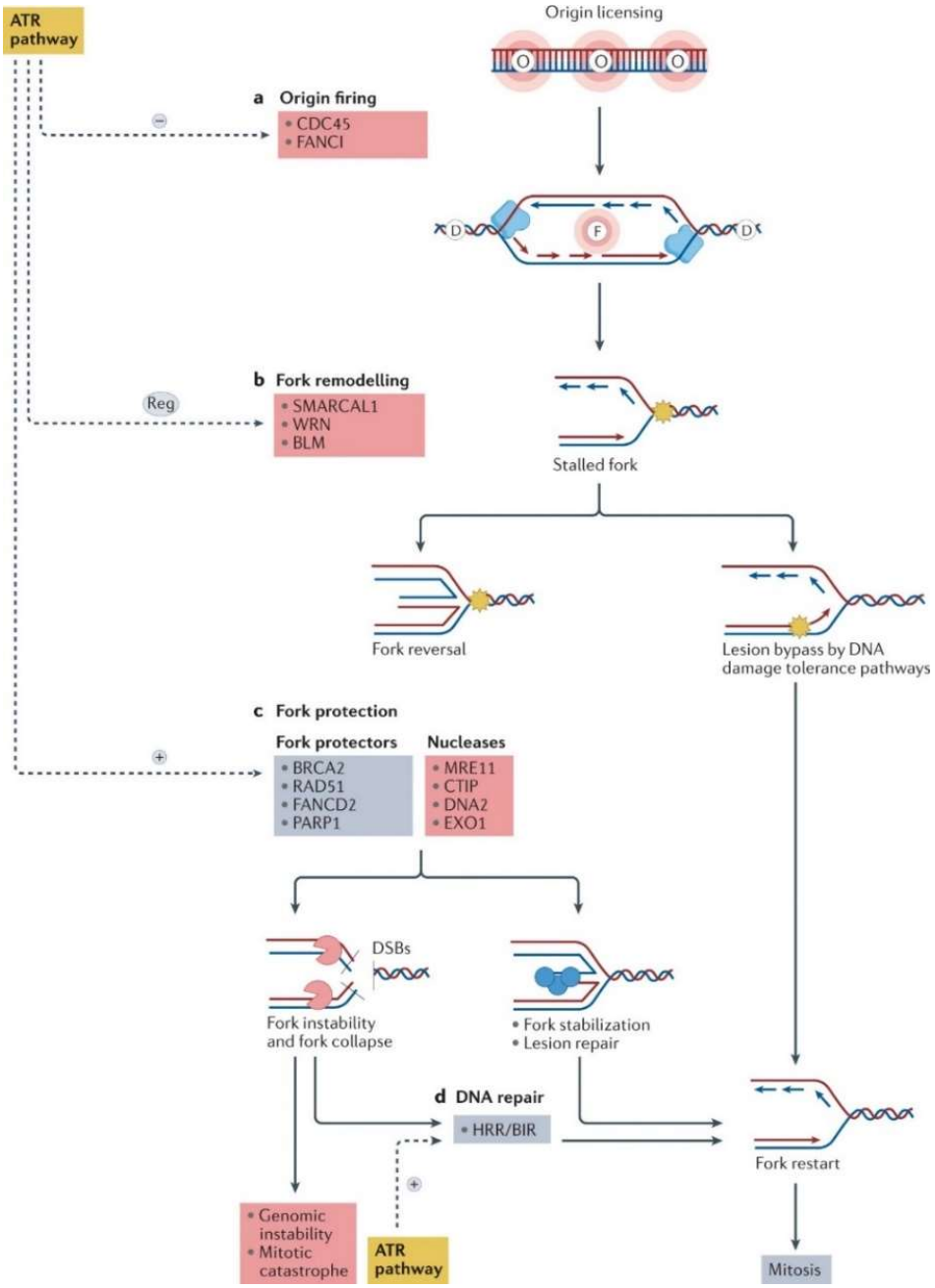

Figure 19: The replication stress response consequences on replication forks (Adapted from[141])

2. Fork Restart and repair

If fork stalling is sustained, efficient fork restart is required to resume fork progression and prevent fork collapse into DSBs. Many remodeling factors are recruited to the stalled fork site, including helicases, polymerases, and DNA repair proteins that collaborate to unwind any secondary structures, remove DNA lesions, and prepare the fork for restart. The DNA2 nuclease and WRN helicase cooperate to resect reversed

forks to restart replication[160]. DNA2 degrades reversed forks with a 5′-to-3′ polarity and WRN helicase assists in DNA2 degradation possibly by opening the reversed arm. Moreover, the structure-specific endonuclease complex of methyl methanesulphonate (MMS) and ultraviolet-sensitive 81 (MUS81) can restart replication fork after stalling by generating DSBs, that could be repaired through homologous recombination machinery[162–164]. Stalled fork restart can also occur via homologous recombination (HR). In this context, the nuclease MRE11 is recruited to the stalled forks to excise the lagging strand[36]. Additionally, CtIP, a factor involved in DNA resection, exerts a positive influence on the restart of the stalled fork[165].

The outcome of the nucleolytic processing of reversed forks is closely related to the checkpoint status in cancer cells. ATR-CHK1 pathway is required to prevent excessive nuclease-mediated cleavage of replication forks. Such nucleases are MRE11[155,166], the exonuclease EXO1, which is more active and counteracts fork reversal in checkpoint-deficient cells[161,167] and the endonucleases MUS81-EME1 and XPF-ERCC1[162,103]. The activities of MUS81-EME1 and XPF-ERCC1 are promoted by the key regulator SLX4[168]. SLX4 depletion or depletion of MUS81 and XPF together prevents DSB formation at forks stalled by gemcitabine[103]. MUS81 cleavage of stalled forks might aid fork restart through DSB induction but nuclease cleavage often disrupts restart when the checkpoint is inactive[164]. As a structure-specific endonuclease, MUS81 aberrantly attacks stalled forks as they resemble repair intermediates, but the S-phase checkpoint prevents this to avoid overwhelming DNA repair with complex DSBs (Figure 19d).

3.2.2.1.4 Global effects on origin firing and cell cycle arrest

During mild replication stress, ATR primarily halts the activation of new replication sites while permitting dormant origins to fire to minimize fork stalling[169]. However, during heightened replication stress ATR-CHK1 suppresses origin firing by multiple mechanisms such as blocking the loading of CDC45 and other pre-initiation complex factors at origins[170–172]. By inhibiting the initiation of replication origins, ATR limits the count of active replication forks. This prevents the overaccumulation of ssDNA and the

depletion of the nuclear RPA pool, thereby safeguarding against the occurrence of replication catastrophe, the widespread failure of the DNA replication[139,173].

ATR-CHK1 pathway halts the cell cycle progression to allow sufficient time for the cell to effect lesion repair and prevent premature entry into mitosis with under-replicated DNA. CHK1 phosphorylates the CDK activating phosphatases CDC25A/C[174], preventing their removal of inhibitory phosphorylations of CDK1/2[175]. The degradation of CDC25A[118] as opposed to nuclear export and cytoplasmic sequestration CDC25C triggers cell cycle arrest[176].

Although cell-cycle checkpoints have important functions, it's possible for DNA that hasn't been fully replicated (under-replicated DNA) and replication or repair structures that haven't been fully resolved to escape the attention of these checkpoints. These unresolved issues can persist into later phases of the cell cycle and even extend into the subsequent cell cycle[177].

3.2.3 Cell division

The objective of cell division is to evenly distribute the replicated genetic material into two daughter cells, ensuring they both possess identical genomes. In 1882, Walther Flemming, introduced the term "mitosis" to characterize this process, represented in Figure 20 through his stunning illustrations.

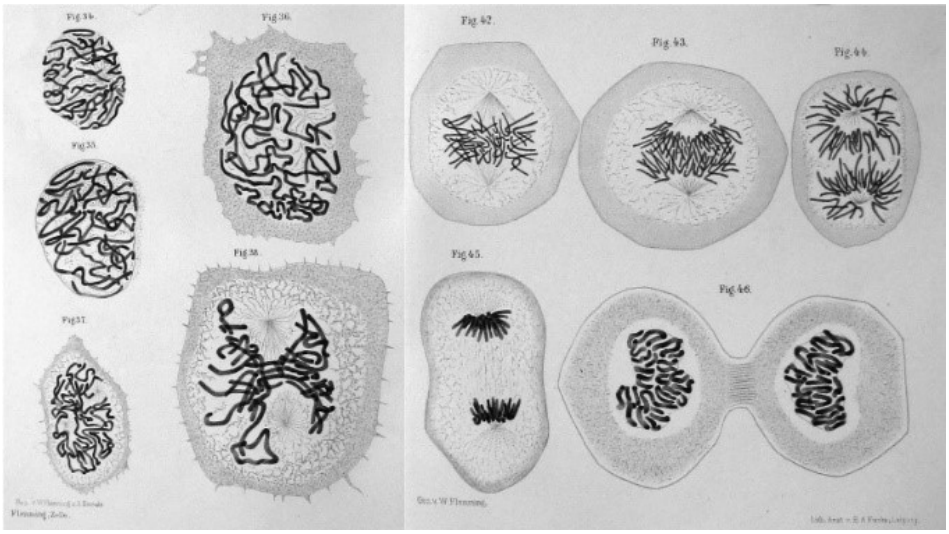

Figure 20: Drawings of mitosis in salamander cells found in Walther Flemming's book (From Zellsubstanz, Kern und Zelltheilung, published in1882)

The cell's decision of **when to enter mitosis** is critical. The timing of mitotic entry varies across species: in mammalian cells, the transition between S and M phases can take up to several hours and is known as G2 phase.

3.2.3.1 G2 Phase: the calm before the storm?

The G2 phase of the cell cycle orchestrates essential processes to establish an optimal environment for the subsequent entry into mitosis. Cells ensure the separation of DNA replication and cell division according to the following suggested models: (1) Gradual CDK activation coupled to different thresholds for starting DNA replication and mitosis[178], (2) different cyclin proteins appearing at specific times and cellular locations[179], (3) transcriptional oscillator networks[180], and (4) a checkpoint that delays mitosis before DNA replication is completed.

Although DNA replication and cell division temporally occur at distinct phases of the cell cycle, from a signaling perspective, they are closely linked. Mitotic kinases CDK1 and Polo-Like Kinase 1 (PLK1) exhibit activity before the onset of mitosis. Intriguingly, more than a 100 phosphorylation sites associated with mitosis (mostly substrates of CDK1 and PLK1) are phosphorylated at the S/G2 boundary[181,182] indicating the timing of mitotic entry could be linked to the level of DNA replication activity. When DNA synthesis is partially suppressed, S-phase is prolonged, leading to a delay in the onset of mitosis. Conversely, if DNA replication is completely halted, the initiation of mitosis could be accelerated[183]. This suggests that a threshold of replication activity exists, under which mitotic entry is not prevented.

Additionally, ATR plays a role in coordinating DNA replication with the start of the G2 phase. DNA replication in S-phase activates ATR/CHK1 signaling, which represses CDK1/PLK1 activity and prevents premature CDK1-mediated phosphorylation of FOXM1 (the transcription factor of the pro-mitotic network)[184]. Completion of DNA replication allows CDK1 and PLK1 activation, driving the onset of mitosis (Figure 21).

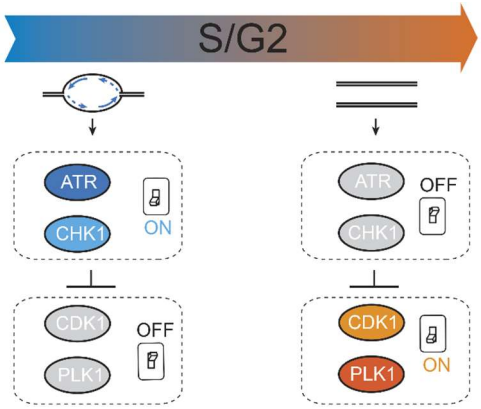

Figure 21: S/G2 transition is dictated by molecular switches
(Adapted from[185])

3.2.3.2 Control of the G2/M transition

The G2 phase functions as a "waiting room" in instances where cells encountered problems during the preceding S phase such as incompletely replicated loci or unrepaired DNA damage. Upon damage detection, the DNA damage checkpoint is engaged to inhibit the mitotic entry regulatory network therefore halting cell cycle progression until the DNA damage has been comprehensively repaired. The G2/M transition is a highly conserved pathway from fission yeast to humans. The master regulator of the G2/M transition is CDK1, whose activity is governed on its timely coupling with cyclin B. Following the initial assembly of the cyclin B-Cdk1 complex, its function is directly modulated in two ways: **negatively** by **WEE1/MYT1 kinases** that phosphorylate CDK1 (Tyr15/Thr14) to inhibit its activity, and **positively** by **CDC25 phosphatase**, which removes these phosphate groups from the sites targeted by WEE1/MYT1, thus promoting CDK1 activation (Figure 22)[186].

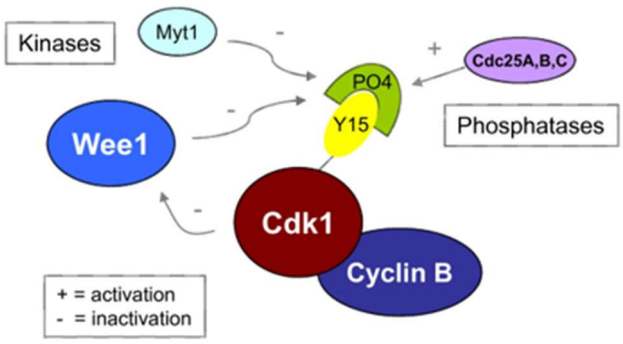

Figure 22: CDK1/cyclin B regulation during the G2/M transition
(Adapted from[186])

In response to DNA damage, the ATM and ATR signaling pathways are activated, which leads to the phosphorylation and activation of CHK1 and CHK2 respectively, the subsequent activating phosphorylation of CDC25, which prevents activation of cyclin B-CDK1 and results in G2 arrest.

Incomplete cell cycle checkpoint control in cancer cells could result in the subsequent transmission of DNA damage into mitosis or mitotic entry with under-replicated DNA, that can lead to catastrophic consequences.

3.2.3.3 Mitosis

Mitosis is probably the most dramatic stage in a cell's cycle. The initiation of mitotic entry triggers extensive modifications across the cellular compartments. Within a matter of minutes, cells assume a rounded morphology, duplicated centrosomes undergo separation while microtubule dynamics intensify, the nuclear envelope disintegrates, and chromosomes undergo condensation while being searched for and captured by microtubules at kinetochores.

As cells enter mitosis, a sequence of synchronized molecular processes exercises significant changes in the structure of previously replicated interphase chromatin. This transformation leads to the formation of condensed, cylindrical chromosomes that can be effectively separated and distributed to the daughter cells[187] (Figure 23).

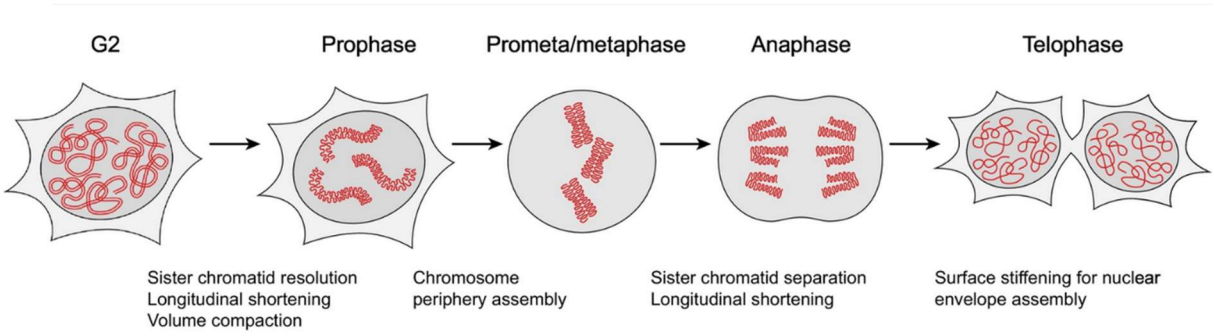

Figure 23: Chromosome reorganization during mitosis
(Adapted from[187])

3.2.3.3.1 From DNA to chromosomes

Prophase, the initial mitotic phase, involves **chromosome condensation**. Chromosome condensation is tightly linked to the successful progression of cell division and the cell cycle. Its failure can have significant consequences, including the formation of lagging chromosomes and aneuploidy. The necessity for proper chromosome condensation becomes even more apparent when considering the mechanical requirements during mitosis. To withstand the forces exerted by the mitotic spindle *via* kinetochore attachments at the centromere, mitotic chromosomes must exhibit high mechanical rigidity. This rigidity is achieved through condensin-mediated linkages of DNA loops. Condensin I confers rigidity to centromeric chromatin[188,189], while Condensin II contributes to rigidity along the chromatid axis[190] and confers elastic stiffness to chromosomes[191]. On the other hand, sister chromatids are held together by a ring-like structure known as the cohesin complex, which is established during S-phase. This complex maintains centromeric cohesion between chromatids until the onset of anaphase[192]. Cohesin is removed from chromosomes in two steps during cell division to enable the physical separation of sister chromatids. The majority of cohesin is removed from the chromosome arms during early mitosis. However, residual cohesin remains concentrated at centromeres, where it is protected from removal by shugoshin-1 (from the Japanese 'guardian spirit'), resulting in the classical X-shaped mitotic chromosome[193]. Once all chromosomes have aligned at the metaphase plate, the protease Separase removes centromeric cohesion and triggers anaphase onset. It is now established that the creation of a fully folded, cytogenetically normal metaphase chromosome relies on the coordinated completion of DNA replication and sister chromatid separation along with chromatin condensation[194–196]. Disruption of either of these processes can lead to abnormalities of chromosomes in mitosis.

3.2.3.3.2 Chromosomes engage with the spindle

3.2.3.3.2.1 Mitosis building blocks: centromeres and kinetochores

Centromeres play a pivotal role in ensuring faithful chromosome segregation during mitosis. Unlike the conventional understanding that specific DNA sequences are crucial

for centromere function, centromeres are primarily epigenetically specified. The hallmark feature of most eukaryotic centromeres is the presence of the histone H3 variant, CENP-A[197]. Centromeres typically consist of a central core housing CENP-A nucleosomes, organized in homogenous ordered repeats. Additionally, there is an outer heterochromatic domain known as the pericentromere, characterized by less ordered repeats (Figure 24). The structural foundation of centromeres is laid on arrays of a 171 bp monomer called α-satellite DNA, with monomers arranged head-to-tail to form higher-order repeats across the centromere core. For DNA sequences to confer centromere functions, they must be recognized by proteins that recruit the chromosome segregation machinery. Notably, CENP-B plays a critical role by directly interacting with and stabilizing both CENP-A nucleosomes and the kinetochore protein CENP-C, contributing significantly to centromere function[198–200].

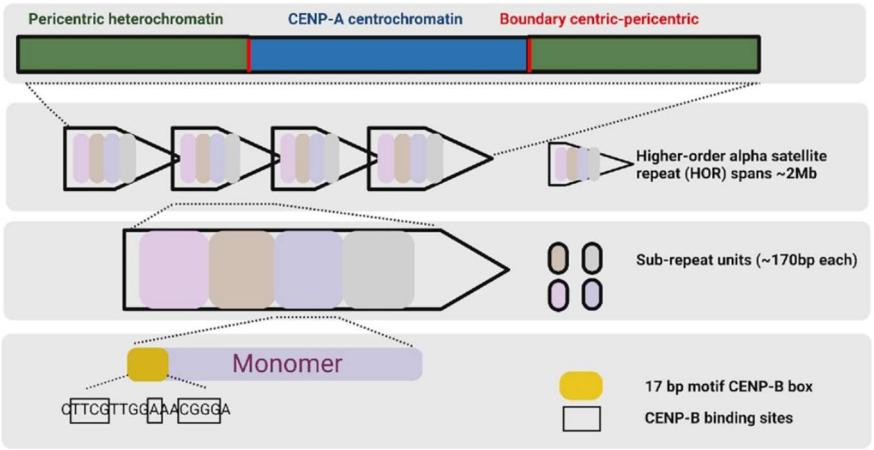

Figure 24: The structure of centromeric DNA
(Adapted from[201])

The kinetochore, a proteinaceous structure crucial for spindle attachment, is located on centromeric chromatin. Approximately 100 different proteins collaborate to construct the kinetochore on centromeric chromatin[202]. While kinetochores specifically assemble and function during mitosis, centromeric chromatin and the Constitutive Centromere-Associated Network (CCAN), comprising 16 associated proteins, persist throughout the cell cycle[203]. Once assembled on the centromere, the CCAN serves as a platform for the outer kinetochore assembly (Figure 25).

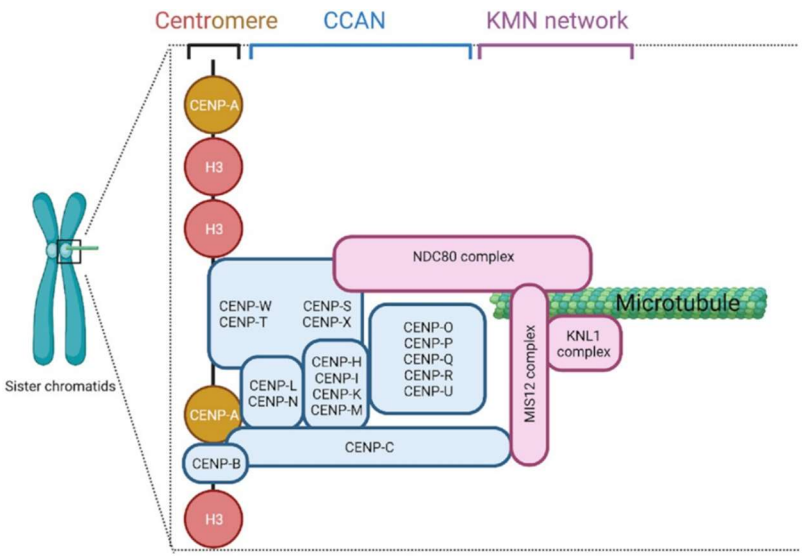

Figure 25: Kinetochore organization
(Adapted from[201])

Key proteins, including CENP-C and CENP-T, recruited by the CCAN, play a crucial role in recruiting microtubule-binding proteins of the kinetochore, forming the KNL1–MIS12–NDC80 (KMN) network[204,205]. These protein interactions are tightly regulated, with the CCAN recruiting a complete kinetochore exclusively during mitosis[206]. Notably, the NDC80 complex, crucial for microtubule binding, is sequestered outside the nucleus during interphase, only interacting with CENP-T during mitosis due to CDK phosphorylation[206].

In addition to microtubule binding, CCAN proteins contribute to resisting forces generated by spindle microtubules[207], controlling metaphase oscillations[208] and chromosome congression through the recruitment of the motor protein CENP-E[209,210]. Collectively, the orchestrated interplay between centromeres and kinetochores ensures the key function of centromeres - the segregation of corresponding chromosomes - during mitosis. This macromolecular coordination safeguards accurate chromosome segregation, making the centromere-kinetochore system a fundamental component of cell division processes.

3.2.3.3.2.2 The spindle assembly checkpoint

To ensure accurate chromosome segregation, a conserved signal transduction system called the spindle assembly checkpoint (SAC) delays the onset of anaphase until all

chromosomes make correct attachments to spindle microtubules[211,212]. The checkpoint signaling depends on kinetochore localization of the conserved checkpoint proteins MPS1, BUB1, BUB3, MAD1, and MAD2[213]. MPS1 is a protein kinase that interacts with NDC80, and is required for checkpoint activity and kinetochore localization of all other checkpoint proteins[214–216]. A biochemical cascade is initiated at unattached kinetochores, which inhibits a polyubiquitin ligase known as the "cyclosome" or anaphase-promoting complex (APC/C)[217]. Upon proper attachment of the last chromosome, this cascade is deactivated, likely influenced by both tension at the kinetochore and microtubule binding. Subsequently, the APC/C can polyubiquitinate crucial proteins, leading to their degradation by the proteasome. This, in turn, activates separase that degrades connections between sister kinetochores, facilitating the commencement of anaphase.

Following the successful alignment and attachment to the spindle, sister chromatids undergo separation, moving towards their respective spindle poles, which are organized by the centrosomes. In the subsequent telophase, a new nuclear membrane emerges around the now-separated sister chromatids, marking the preparation for cytokinesis, the final step in cell division.

3.2.4 Mitosis: dealing with unfinished business

Chromosome aberrations in mitosis can arise from unresolved DNA structures that originate during S-phase and persist beyond interphase, causing disruptions in the orderly process of chromosome segregation. Such structures include incompletely replicated loci, sister chromatids that are topologically intertwined, and DNA repair or recombination intermediates that remain incompletely resolved. These issues emerge due to inherent challenges in fully replicating and segregating specific regions of the genome (or to exogenous stresses).

3.2.4.1 The centromere: a source of problems?

The molecular architecture of centromeric chromatin undergoes intricate cell cycle-dependent structural changes, with centromeric DNA potentially forming higher order

looped structures through recombination between repetitive elements[218]. These alterations present challenges for DNA replication machinery, as centromeres are known hotspots for chromosome breakage and rearrangements in mammalian cells[219]. Defects in centromere assembly or maintenance contribute to the observed chromosomal aberrations in cancer cells[220]. Centromere breakage can directly lead to chromosomal rearrangements, lagging chromosomes, chromosomal bridges, aneuploidy, micronuclei formation, and chromothripsis[221–224].

Preventing DNA looping through CENP-B depletion triggers DNA decondensation and chromosome breakage during mitosis[225]. During replication, centromeres associate with various DNA repair factors, including mismatch repair factors MSH2–6[226] and the nuclease/helicase DNA2[227]. The smooth progression of the replication machinery across centromeric repeats may necessitate specific helicases like DNA2, an enzyme enriched at centromeric regions under unperturbed conditions[227]. DNA2 depletion leads to DNA replication defects, stalled forks, activation of the ATR kinase-mediated DNA damage checkpoint, and a high frequency of missegregation.

During mitosis, centromeric DNA strands intertwine due to DNA replication, resulting in the accumulation of catenanes at centromeric regions that must be resolved before sister chromatid disjunction in anaphase[228]. DNA Topoisomerase IIα (TOPOIIα) is the key player in this decatenation activity[229]. DNA catenanes persist in centromeric regions until late in mitosis, shielded from TOPOIIα-mediated decatenation by cohesin. Once the SAC is satisfied, the remaining cohesin proteins at centromeres are cleaved, allowing TOPOIIα access to centromeric regions and the resolution of persistent DNA catenanes[230].

3.2.4.2 Under-replicated DNA in mitosis: Breaking Chromosomes?

When cancer cells experience replication stress in S-phase, they can progress into mitosis with under-replicated DNA. These regions could break due to the mechanical forces arising from chromatin condensation[231]. So, how do cells deal with such under-replicated DNA during mitosis?

One solution involves DNA synthesis in mitosis (MiDAS)[232], primarily at genomic loci known to be the most challenging to replicate within the genome: chromosomal fragile sites, ribosomal DNA, centromeres, and telomeres[233,234]. Replication stress-induced MiDAS takes place to complete DNA replication and promote the proper segregation of sister chromatids in anaphase. MiDAS uses a form of break-induced replication that requires the MUS81–EME1 endonuclease, activated by CDK1 that phosphorylates EME1 at the onset of mitosis[235,236], and the DNA Polymerase δ non-catalytic subunit POLD3[237]. If this last attempt to complete DNA replication fails, or time is simply too short during mitosis to complete replication, unresolved replication intermediates can lead to chromatin bridges, lagging chromosomes, ultrafine anaphase bridges, and chromosome breaks[238,239]. After mitotic exit, these aberrations result in the formation of 53BP1 nuclear bodies within G1 cells[231,240]. 53BP1, a versatile reader of chromatin, can detect both the replication status and the existence of DNA damage. Utilizing its oligomerization domain, it forms large compartments around DNA lesions, called nuclear bodies. These nuclear bodies serve to facilitate repair processes and maintain the structural integrity of chromatin near DNA lesions[241]. Consequently, they act as a protective shield, safeguarding inherited DNA lesions from nucleolytic degradation and unintended repair activities (Figure 26).

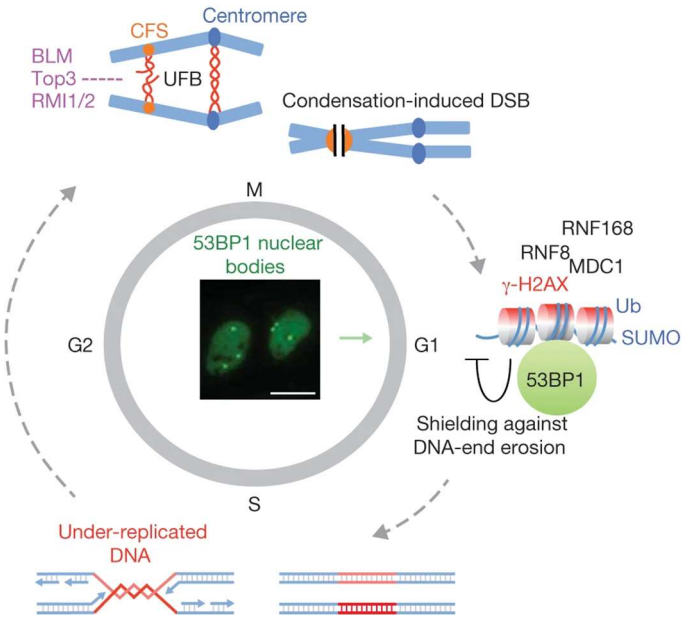

Figure 26: Dealing with unfinished business from S-phase during mitosis and beyond (Adapted from[242])

4 WEE1 KINASE – GUARDIAN OF GENOMIC INTEGRITY

The discovery of WEE1 dates back almost half a century, with Paul Nurse's work in 1975 identifying it in the fission yeast, *Schizosaccharomyces pombe*[243]. Research conducted in yeast uncovered a group of temperature-sensitive mutants that exhibited reduced cell division size, prompting the naming of the affected gene as "*wee1*"[244,245]. In subsequent investigations, WEE1 was found to be significantly active during the S and G2 phases of the human cell cycle[246]. Now, it is established that WEE1 is a crucial component of the G2/M cell cycle checkpoint that prevents entry into mitosis in the presence to cellular DNA damage (See section 3.2.3.2), though additional functions of WEE1 in S phase have been uncovered more recently. Almost all the roles attributed to WEE1 are due to its catalyzation of an inhibitory phosphorylation on Tyr15 of CDK1 and CDK2 rendering them inactive[247,248].

The WEE1 Ser/Thr protein kinase family includes two other kinases, MYT1 and WEE2. MYT1 functions as an essential component of an organelle-based cell cycle checkpoint to prevent CDK1-induced premature fragmentation of Golgi and the endoplasmic reticulum during G2 phase[249]. MYT1 negatively regulates CDK1 by inhibitory phosphorylation at Thr14 and by sequestering it within the cytoplasm[250,251]. On the other hand, WEE2 serves as an oocyte-specific kinase, playing a crucial role in regulating meiosis, where it prevents premature restart of oocyte meiosis prior to ovulation and permits metaphase II exit at fertilization[252].

4.1 WEE1 IS AN ATYPICAL TYROSINE KINASE

WEE1 is a 642-amino acid protein that consists of an N-terminal regulatory domain, a kinase domain, and a C-terminal domain (Figure 27). The N-terminal domain contains a nuclear localization signal (NLS) and phosphorylation sites at Ser53 and Ser123, which signal WEE1 for ubiquitination and degradation. Phosphorylation of the C-terminal tail allows binding to 14-3-3 peptides, influencing its localization and activity. WEE1 also has four cyclin binding motifs (RxL1, RxL2, RxL3, RxL4) for interaction with CDKs.

Although WEE1 structurally resembles a Ser/thr protein kinase, it functionally acts as a tyrosine kinase due to unique features in its activation site and a glycine-rich loop substitution[253,254].

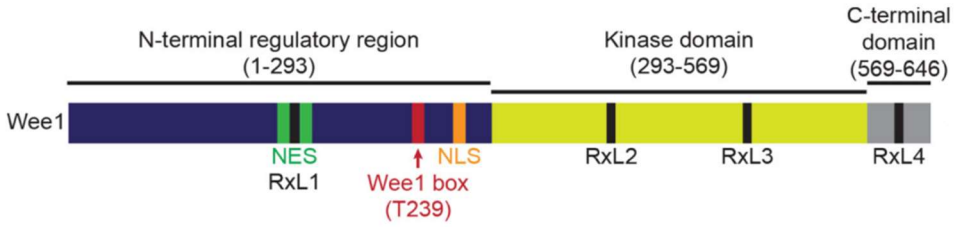

Figure 27: The structure of WEE1 kinase
(Adapted from[255])

4.2 WEE1 IS FINELY TUNED TO ENSURE CELL-CYCLE PROGRESSION

Following its synthesis in the cytoplasm, WEE1 rapidly binds to its chaperone, heat-shock protein 90 (HSP90), and phosphorylates HSP90 on its Tyr38. This interaction potentially contributes to the stabilization of WEE1 and facilitates its transport into the nucleus[256,257]. During interphase, CHK1 phosphorylates nuclear WEE1 at Thr642, facilitating the binding of 14-3-3β to the its C-terminal region. This not only enhances WEE1's activity but also likely aids in its retention within the nucleus[258,259].

At the onset of mitosis, WEE1 undergoes rapid inhibition to facilitate an increase in CDK1 activity and enable cell division (Figure 28). This inhibition is initiated through CDK1-dependent phosphorylation of Ser123, leading to nuclear export and destabilization of WEE1[260–263]. So, the primary shift from active to inactive WEE1 primarily hinges on CDK1 phosphorylation. The phosphorylated Ser123 residue serves as a docking site for PLK1 and casein kinase 1 (CK1). These two kinases phosphorylate WEE1 on Ser53 and Ser121 respectively, further enhancing its destabilization[261,262,264]. These phosphorylations create phosphodegrons, signaling WEE1 ubiquitination via ubiquitin-conjugating enzyme CDC34[265] and subsequent proteasome-dependent degradation, orchestrated by F-box proteins, beta-transducin-repeat-containing (β-TRCP)[262] and trigger-of-mitotic-entry 1 (TOME-1)[266]. Spatially, AKT-mediated phosphorylation of WEE1 at Ser642 generates a binding site for 14–3-3θ peptides, leading to the translocation of WEE1 from the nucleus to the cytoplasm[267].

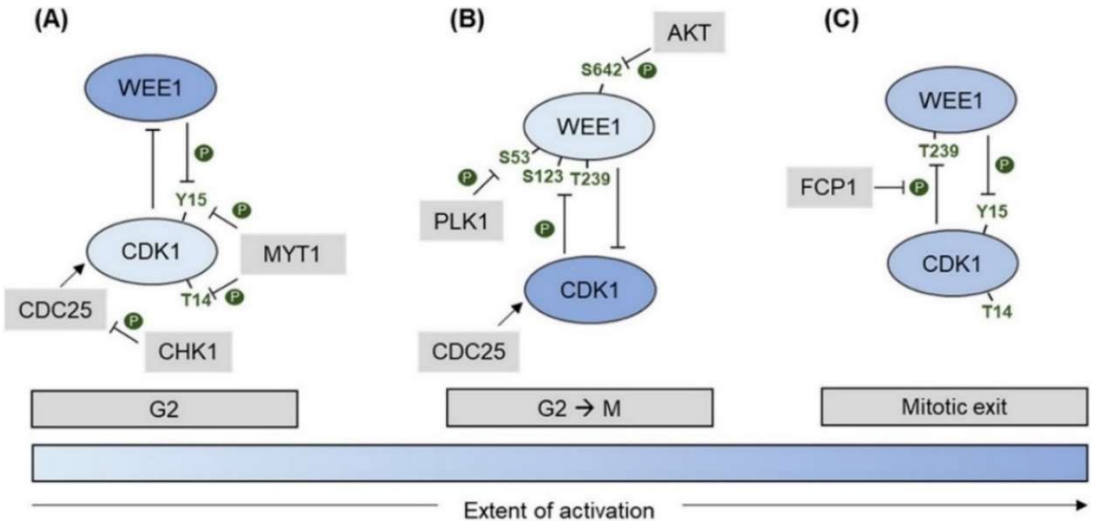

Figure 28: WEE1 regulates mitotic entry and exit
(Adapted from[268])

Importantly, WEE1's role doesn't cease with mitotic entry. During mitosis, interphase microtubules are disassembled to allow safe chromosomal movements through the actions of stabilizing and destabilizing MAPs. CDK1-cyclin B elevated levels significantly impact the restructuring of the cytoskeleton. For example, they inhibit microtubule growth-promoting MAP4 and MAP7[269,270]. However, certain MAPs are essential for spindle microtubule growth and spindle assembly. WEE1 plays a role in suppressing a subset of CDK1 localized at centrosomes and their nucleating microtubules[271]. This fraction of CDK1 remains inhibited by WEE1-mediated phosphorylation, contributing to spindle microtubule growth through further recruitment of WEE1[271,272]. As a result, microtubule-stabilizing MAPs are locally released from inhibitory phosphorylation, enabling spindle assembly.

In a broader context, mitotic phosphorylations work to inhibit WEE1 during mitosis to enforce the spindle assembly checkpoint, preventing premature CDK1 inactivation and anaphase onset. However, to return to interphase, these mitotic phosphorylations must be reversed by phosphatases at the end of mitosis (Figure 28)[273–276]. FCP1, an RNA polymerase II-carboxy-terminal domain phosphatase, targets WEE1 and dephosphorylates it at the inhibitory site T239, thereby constraining the CDK1 double-negative feedback loop[277]. FCP1 also acts on CDC20 (a coactivator of the ubiquitin ligase anaphase-promoting complex/cyclosome, APC/C) and USP44 (a

deubiquitinating peptidase opposing APC/C action), collectively promoting mitotic exit.

4.3 WEE1 SAFEGUARDS GENOMIC INTEGRITY BY KEEPING CDKS IN CHECK

In addition to its well-known role in regulating the G2/M checkpoint, WEE1 is implicated in the control of replication dynamics during an unperturbed S-phase (Figure 29 Left panel), and is an important actor of both the S and G2 DNA damage checkpoints (Figure 29 Middle and right panels).

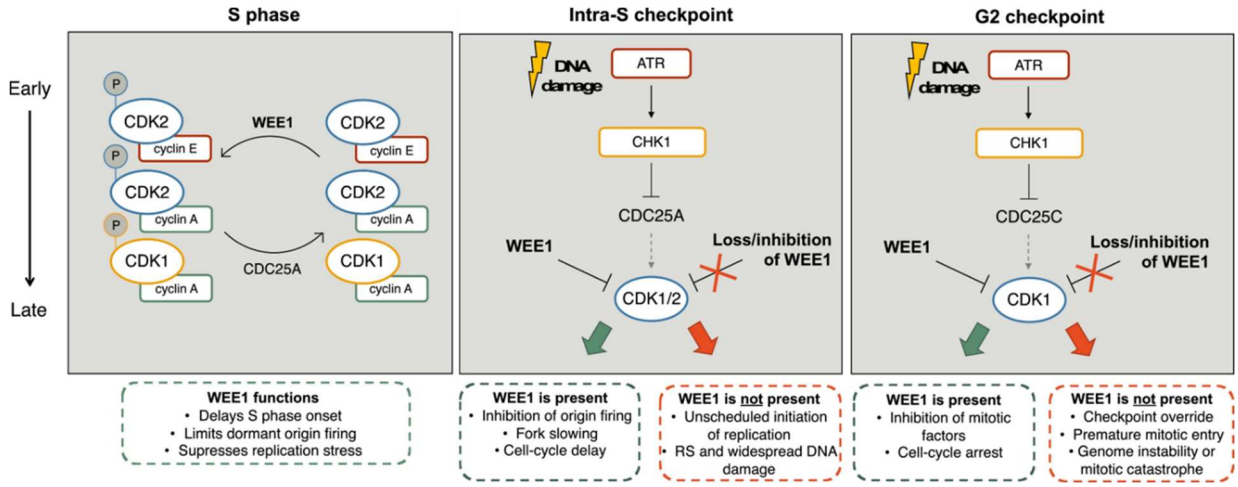

Figure 29: Roles of WEE1 in S-phase
(Adapted from[278])

WEE1 regulates DNA replication through the control of CDK-driven origin firing by maintaining an adequate pool of nucleotides. This regulated origin firing ensures that excessive generation of ssDNA is prevented. Upon loss of WEE1 activity, excessive origin firing and subsequent massive replication initiation result in exhaustion of nucleotide pools and replication fork stalling[279]. Furthermore, in the absence of WEE1, CDK1/2 phosphorylate the ribonucleotide reductase subunit RRM2[280], responsible for converting ribonucleotides to deoxyribonucleotides, leading to its unscheduled degradation via the CDK-SCF^{CyclinF} axis at times when dNTPs are still needed for DNA replication. This lack of DNA building blocks severely hampers DNA replication and causes replication stress (see section 3.2.2.1.1). In addition, WEE1 serves as a protector of replication forks against degradation by preventing the CDK1-dependent complex formation of the MUS81/SLX4 nuclease during S phase[281] that converts replication

forks into DSBs[282]. An alternative model of fork protection by WEE1 has recently emerged where WEE1 guards against the degradation of nascent DNA at stalled replication forks by DNA2[283].

The increase in CDK activity when WEE1 is inhibited has been shown to trigger hyperphosphorylation of proteins like 53BP1 and RIF1, both of which are involved in DNA repair regulation[284]. This hyperphosphorylation, notably in the C-terminal region of 53BP1, prevents its localization to damaged chromatin, inhibiting DNA repair. Under normal conditions, this mechanism primarily occurs during mitosis to prevent harmful sister telomere fusions[285]. However, WEE1 inhibition suppresses the recruitment of 53BP1 to chromatin after DNA damage during interphase, hindering DNA repair. Notably, 53BP1 and RIF1 protect stalled DNA replication forks from excessive DNA2-mediated degradation[286,287]. Therefore, WEE1, by limiting CDK-driven phosphorylation of 53BP1 and RIF1, may contribute to the protection of stalled forks from DNA2-driven degradation.

The vital roles of WEE1 and its ability to inhibit CDK activity become increasingly evident when cells encounter DNA damage. When WEE1 is active, it triggers the activation of the S-phase DNA damage checkpoint. This, in turn, leads to the inhibition of origin firing, a deceleration of replication forks, and ultimately results in a delay in the cell cycle. However, when WEE1 is either absent or inhibited, the lack of CDK inhibition causes an untimely initiation of replication, leading to increased replication stress that can result in extensive DNA damage. During the G2 DNA damage checkpoint, WEE1 plays a crucial role by inhibiting CDK1 and facilitating cell cycle arrest. This pause in the cell cycle allows sufficient time for DNA repair to occur before chromosome segregation. In contrast, when WEE1 activity is lacking, the checkpoint is overridden, leading to premature entry into mitosis with unrepaired DNA.

4.4 WEE1: AN EPIGENETIC MODIFIER?

Eukaryotic cells carefully maintain a precise histone-DNA stoichiometry, as imbalances between core histones and newly synthesized DNA pose a threat to chromosomal

integrity[288]. The regulation of histone transcription is actively suppressed during late S and G2 phases to prevent overproduction after DNA synthesis. *In vitro* kinase assays have shown that WEE1 directly phosphorylates core histone H2B at Tyr37 in late S-phase[289,290]. This phosphorylation prevents the binding of nuclear protein coactivator of histone transcription (NPAT) and RNA polymerase II. Additionally, histone regulatory homolog A (HIRA) is recruited following H2B Y37 deposition, acting as a transcriptional repressor to enforce gene silencing[289,290]. Additionally, WEE1's potential role in epigenetic regulation was suggested by studies of chromatin structural remodeling. The use of S-phase inhibitors in wild type *Drosophila* embryos causes significant delays in the initiation and rate of chromatin condensation, but these delays are abrogated in dWEE1-mutant embryos, indicating the role of WEE1 in regulating chromatin condensation timing[291]. This aligns with the role of CDK1/2 in chromatin remodeling during interphase and mitosis. CDK2, for example, is recruited to replication foci during S-phase, where it promotes the phosphorylation of H1 (linker histone) to facilitate chromatin decondensation and replication fork progression[292]. CDK1 predominantly handles H1 phosphorylation during mitosis that is required for structural rearrangement that induces metaphase chromatin condensation[293,294].

The interactions between WEE1 and histones, both direct and through CDKs, imply the possibility of WEE1 influencing chromatin synthesis by impacting chromatin accessibility (Figure 30). However, further research is needed to determine the full extent of WEE1's control over these mechanisms.

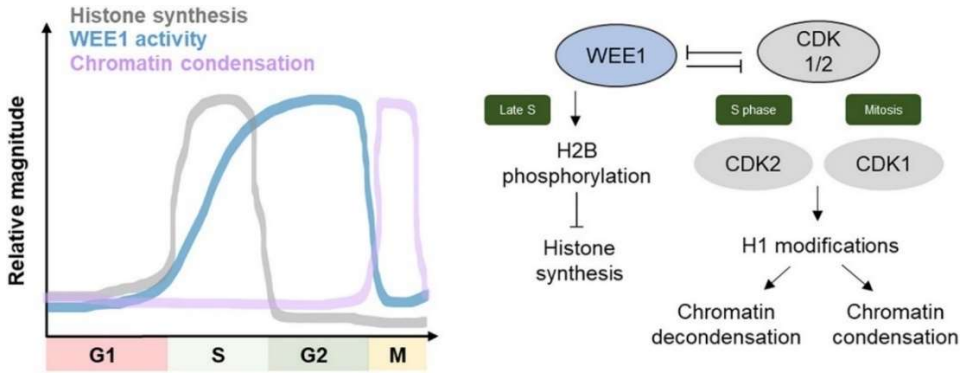

Figure 30: WEE1 roles in chromatin regulation
(Adapted from[268])

4.5 WEE1 IN CANCER

4.5.1 Is WEE1 an oncogene?

The precise biological role of WEE1 in cancer cells remains incompletely understood, but emerging evidence suggests that it acts more like an oncogene rather than a tumor suppressor. WEE1 somatic mutation in cancer is a rare genetic event, comprising less than 2% of the overall mutation frequency[295]. However, it is frequently found to be overexpressed in various types of tumors and associated with poor prognosis[296–300]. Additionally, a genome-wide CRISPR screen involving 563 cancer cell lines revealed that WEE1 is essential for the viability of nearly all cancer cell lines (https://depmap.org/portal/gene/WEE1?tab=dependency). Several mechanisms might underlie the dependency of cancer cells on WEE1 family proteins. Many cancer cells disable the p53 pathway, a key regulator of the G0/G1 and S phases. Consequently, these cells rely heavily on the G2/M checkpoint for cell cycle regulation. Additionally, cancer cells inherently possess higher genetic instability, making the overexpression of DNA damage response-related kinases crucial for maintaining tolerable levels of genomic instability.

Hence, it is plausible to speculate that once the process of malignant transformation is initiated, the upregulation of WEE1 could serve a pro-tumorigenic function by ensuring that cancer cells maintain an acceptable level of genomic instability, which is essential for their survival and proliferation.

4.5.2 WEE1 as target for cancer therapy

Although the full extent of WEE1's oncogenic role is yet to be completely understood, the idea of targeting WEE1 in cancer has garnered significant interest. The initial rationale for targeting WEE1 is based on the concept that inhibiting WEE1 leads to aberrant activation of CDK1, resulting in incomplete DNA replication, premature entry into mitosis, and eventual mitotic catastrophe[301]. These effects are especially pronounced when WEE1 inhibition is combined with DNA-damaging agents[302,303]. Now, it is becoming clear that the disruption of the DNA damage checkpoint in S-phase through WEE1 inhibition enhances response to different chemotherapies,

notably DNA-damaging agents[304,305]. Coupling the effects of DNA-damaging agents to those of WEE1 inhibition results in the failure to arrest the cell cycle while cells accumulate massive DNA damage until a point of no return. These insights endorse the sequential application of a WEE1 inhibitor subsequent to the administration of DNA-damaging agents[299]. This scheduling strategy is substantiated by a study indicating that the stepwise introduction of a WEE1 inhibitor alongside a PARP inhibitor selectively heightens sensitivity in tumor cells while sparing normal cells[306].

4.5.2.1 WEE1 inhibitors

While the idea of developing inhibitors against WEE1 is appealing, there have been relatively few such inhibitors created. The initial batch of small molecules identified as WEE1 inhibitors were somewhat nonspecific, affecting multiple other kinases along with WEE1. For example, PD0166285, one of the early drugs with inhibitory activity against WEE1[307], also targeted kinases like c-Src, EGFR, FGFR1, CHK1, and PDGFRb[308], which limited their progress into clinical trials. However, a more specific and potent WEE1 inhibitor, AZD1775 (Adavosertib, previously known as MK-1775), was discovered from a compound library[309]. AZD1775 still affected other kinases to some extent as it binds to the highly conserved ATP-binding site. It was initially thought to inhibit PLK1 with almost identical potency[310], but recent findings suggest that it doesn't significantly inhibit PLK1 at therapeutic concentrations *in cellulo*[311].

Proteolysis-Targeting Chimeras (PROTACs) are gaining interest because they can degrade the target protein using the cellular ubiquitin-proteasome system. A PROTAC for WEE1, ZNL-02-096, has been developed recently by conjugating AZD1775 to pomalidomide, which binds the ubiquitously expressed E3 ligase Cereblon (CRBN), inducing WEE1 degradation without affecting PLK1 levels[312]. So far, there haven't been published attempts to develop WEE1 inhibitors that work differently from targeting the ATP binding site, such as exploiting WEE1's structural properties. Interestingly, WEE1 lacks the classical HRD, DFG, and APE motifs present in kinases, presenting the opportunity to design and develop inhibitors for selective WEE1 targeting (Figure 31).

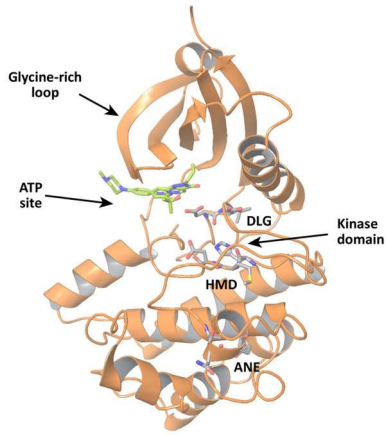

Figure 31: The 3-D structure of WEE1 kinase
(from[313])

4.5.2.2 WEE1 inhibitors in the clinic

The AZD1775 inhibitor has been evaluated in 58 clinical trials for different cancer types. Phase I trials demonstrated that AZD1775 is well-tolerated when used alone or in combination, with the maximum tolerated dose (MTD) ranging from 150 to 225 mg taken orally twice a day for 2.5 days every 2 weeks[314–316]. Additionally, correlative studies conducted on tumor biopsies confirmed its mechanism of action, as shown by reduced phosphorylation of CDK1 (Tyr15) and increased DNA damage (γH2AX) in cancer cells[314,316]. Phase II studies further supported the effectiveness of AZD1775 in sensitizing tumors to various chemotherapy agents. When combined with carboplatin, AZD1775 showed efficacy in TP53-mutated ovarian cancer patients who were refractory or resistant to first-line platinum-based chemotherapy[317]. Similar results were observed in platinum-resistant primary ovarian cancer patients when AZD1775 was combined with single chemotherapeutic agents (carboplatin, paclitaxel, gemcitabine, or pegylated liposomal doxorubicin)[318]. However, it's important to note that in some trials both single-agent and combination therapies with AZD1775 led to adverse effects of grade 3 or higher. These adverse effects are expected due to the essential role of WEE1 in normal cell proliferation, impacting tissues that undergo frequent cell divisions, such as the hematopoietic system and the gut. Therefore, efforts are underway to optimize the dosing and scheduling of AZD1775 to achieve a more favorable therapeutic balance[319].

Additionally, clinical candidate ZN-c3, which is more selective for WEE1,[320] is undergoing Phase I/II trials (NCT04158336, NCT04516447). Several other WEE1 inhibitors, including IMP7068 (NCT04768868), Debio0123 (NCT03968653), SDGR2, and NUV569, have either recently entered or are likely to enter clinical evaluation, highlighting the fact that WEE1 inhibition attractive and getting more attention.

4.5.2.3 What makes tumors sensitive to WEE1 inhibition?

Despite the significant number of clinical trials and studies using WEE1 inhibitors, few predictive biomarkers of response have been identified. Initially, sensitivity of cancer cells and tumors to WEE1 inhibition was thought to be due to p53 status. Some studies showed that p53-deficient cancer cells exhibit selective sensitization to AZD1775 when exposed to chemotherapy or radiotherapy [302,309]. Notably, in patient-derived pancreatic cancer models, AZD1775 synergizes preferentially with gemcitabine in xenografts with a p53-deficient background[303]. Clinical efficacy of AZD1775 has also been observed in a randomized clinical trial focusing specifically on RAS/TP53-mutant metastatic colorectal cancer patients[321]. However, other preclinical and clinical studies have demonstrated sensitivity of cancer cells and tumors to AZD1775 independently of p53 status[314,322–324]. Therefore, the role of p53 mutation as a predictive biomarker for WEE1 inhibition is complex, given potential contributions from genetic aberrations in other DNA damage response pathways. Currently, it is theorized that sensitivity to WEE1 is connected to increased levels of endogenous replication stress, notably oncogene-induced replication stress. This heightened susceptibility is thought to stem from the drug's capacity to magnify the replication stress burden through interference with the intra-S checkpoint.

As such, high levels of Cyclin E could be linked to a better response to AZD1775. Cyclin E levels have been linked to the efficacy of AZD1775 in breast cancer models[325] and in ovarian cancer PDXs[326], with cyclin E^{high} cells, that generally show elevated chromosome instability, being more sensitive compared with cyclin E^{low} ones. AZD1775 showed promising clinical activity in refractory low grade ovarian cancer harboring *CCNE1* gene

amplification[327]. On the other hand, high MYT1 levels could be indicative of resistance to AZD1775, indicating a compensatory effect between WEE1 and MYT1[300,328].

In conclusion, our current understanding lacks definitive information on predictive markers for the response to WEE1 inhibitors. To bridge this gap, extensive preclinical and clinical studies are imperative to pinpoint specific molecular contexts where the application of WEE1 inhibitors could be advantageous. Identifying these molecular vulnerabilities in cancer patients is pivotal, as it lays the foundation for designing innovative therapeutic protocols that leverage WEE1 inhibitors as a monotherapy in a synthetic lethality-based approach. Such endeavors hold the potential to reshape and enhance the precision of cancer treatment strategies.

5 ANEUPLOIDY – CANCER'S FRIEND OR FOE?

Normal human diploid cells typically contain 23 pairs of chromosomes, consisting of 44 autosomes and two sex chromosomes. However, under certain circumstances, the number of whole chromosomes can change, a condition known as **aneuploidy** (Figure 32). Interestingly, aneuploidy is a natural part of cellular development in some tissues, like the liver and brain. It appears to contribute to cellular diversity, which can be advantageous in responding to injuries. In the liver, for example, there is a dynamic process known as the "ploidy-conveyor" where cells can transition between diploidy and aneuploidy[329,330]. This mechanism helps generate aneuploid cells, which can be beneficial in resisting chronic liver injuries[331]. A similar phenomenon has been observed in the brain, where aneuploid neurons with functional activity have been found in both animal models and humans[332,333]. Conversely, aneuploidy is associated with aging and age-related disorders, notably neurodegeneration, in various tissues[334,335]. These discoveries indicate that a minimal occurrence of aneuploidy may be acceptable in certain circumstances within nonmalignant tissues[336]. On the contrary, elevated levels of aneuploidy can become detrimental in cases of neurodegenerative disorders and cancer.

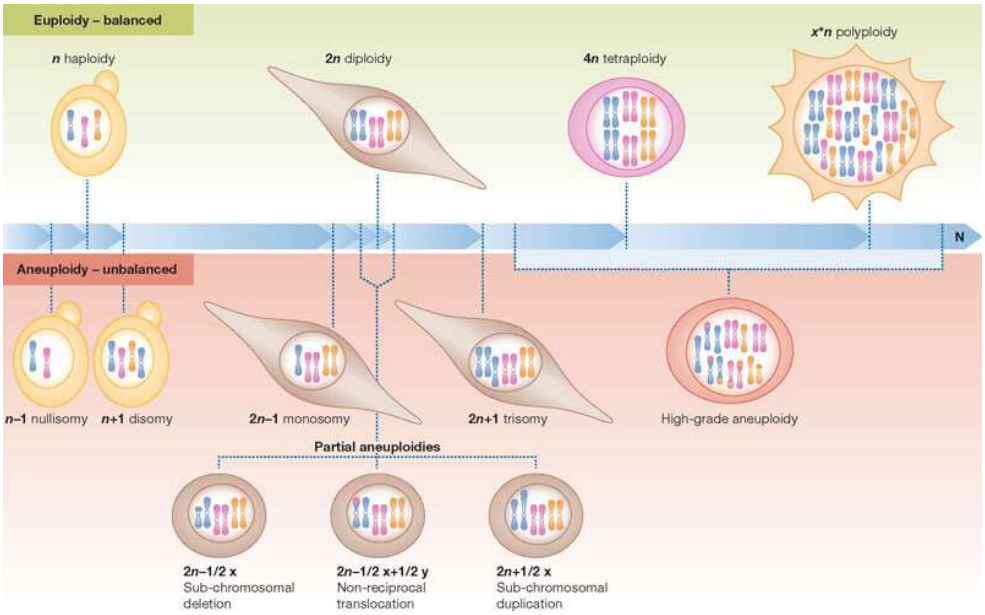

Figure 32: Definition of aneuploidy (Adapted from[337])

Aneuploidy typically arises from chromosome instability (CIN), a high rate of chromosome segregation errors, which occurs when the mitotic checkpoint fails. However, it's crucial to differentiate between aneuploidy, which refers to the 'state' of a cell's karyotype (chromosome number and structure), and CIN, which pertains to the 'rate' at which karyotypic changes occur[338]. While CIN does lead to aneuploidy by causing alterations in chromosome number and structure, it's worth noting that not all aneuploid cells display CIN. In fact, some aneuploid cells maintain a consistent and stable karyotype, a phenomenon that has received significantly less attention compared to the study of CIN.

5.1 ROUTES TO ANEUPLOIDY

Aneuploidy is the product of CIN, that can be reached by processes that reduce mitotic fidelity (Figure 33) or fueled by genomic instability.

5.1.1 Aneuploidy arises from mitotic defects

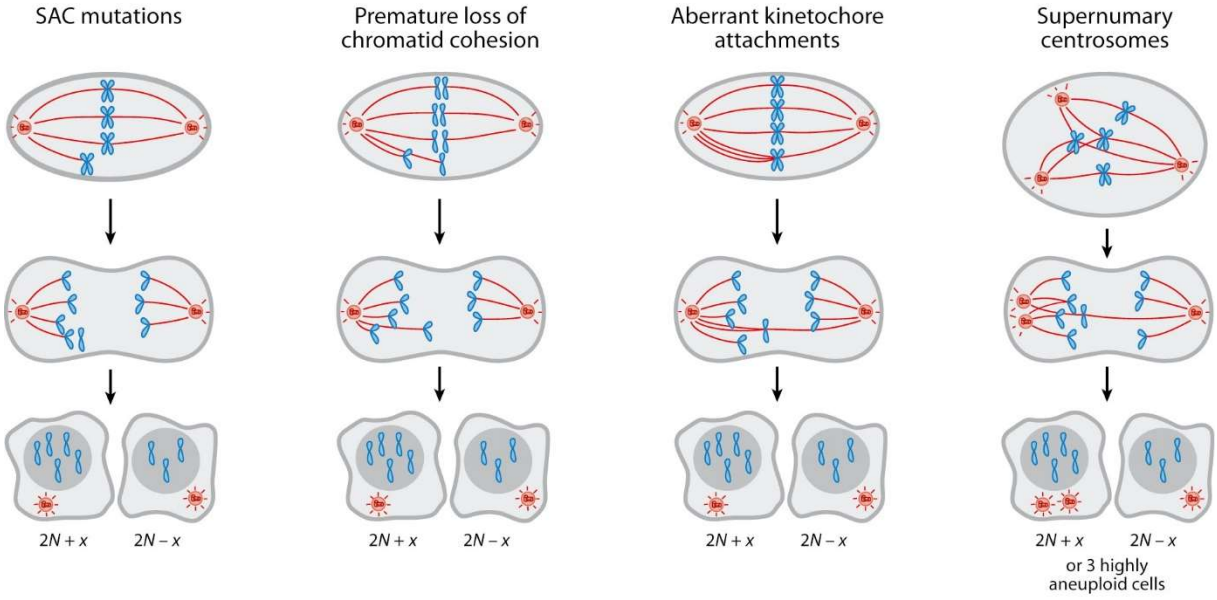

Figure 33: Mitotic causes of aneuploid

(Adapted from[339] N, haploid genomic content; x, any number of missegregated chromosomes)

5.1.1.1 Improper kinetochore-microtubule attachments

During metaphase, chromosomes gather at the mid-plane of the bipolar mitotic spindle, forming what's known as the metaphase plate. The back-to-back arrangement

of sister kinetochores on each chromosome favors the attachment of each chromatid to microtubules originating from opposite spindle poles (referred to as amphitelic attachments), ensuring proper chromosome alignment and segregation[340]. The accuracy of kinetochore-microtubule (k-MT) attachment is crucial for the faithful separation of chromosomes, with sister chromatid kinetochores needing to connect to opposite poles. Aurora kinase B (AURKB) at the inner centromere, aided by microtubule depolymerizing kinesins like KIF2B and KIF2C (MCAK), is central in establishing correct attachments. However, the inherent stochastic nature of k-MT attachments often leads to errors in chromosome attachment to the spindle, such as syntelic, monotelic, and merotelic attachments[341]. In healthy cells, these attachment defects occurring in early mitosis are typically detected and rectified before the onset of anaphase.

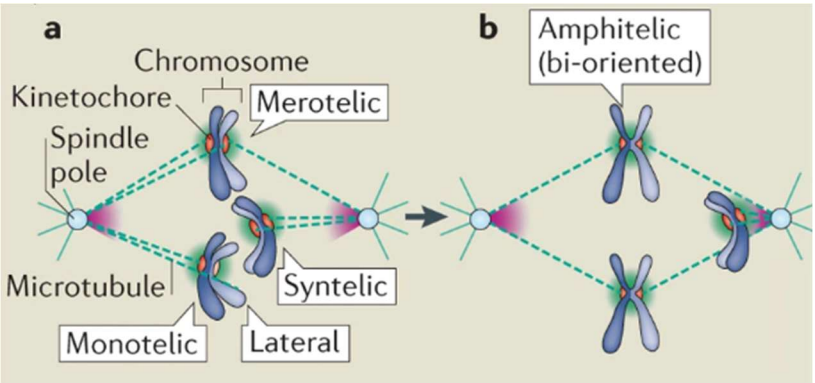

Figure 34: Types of kinetochore-microtubule attachments
(Adapted from[342])

This correction system involves tension-sensing factors like AURKB and MPS1, ensuring the accurate segregation of chromosomes[343]. Merotelic attachments arise when a single kinetochore attaches to microtubules emanating from both spindle poles. These merotelically oriented kinetochores are attached and under tension[344], and they do not activate the mitotic checkpoint signaling as they should. Consequently, they often remain uncorrected in cancer cells[345], leading to lagging chromosomes during anaphase.

The persistence of merotelic attachments in cancer cells can be attributed to two non-exclusive mechanisms: (i) a reduced rate of error correction and (ii) an increased rate of merotely. Additionally, some cancer cell lines exhibit heightened microtubule

assembly rates in early mitosis[345], resulting in microtubule hyperstabilization and errors in chromosome segregation. It's worth noting that defects in various centromere/kinetochore proteins have been observed to reduce chromosome segregation efficiency by increasing the occurrence of merotelic attachments and lagging chromosomes during anaphase[346,347]. However, mutations affecting these kinetochore proteins in cancer are rare, likely because they are essential for normal cellular function. Nevertheless, imbalances in the levels of these proteins might act in a dominant fashion[341]. Additionally, epigenetic abnormalities in centromeric chromatin, such as the loss of histone H3 lysine 4 dimethylation typically found at the core centromere interspersed with the centromere-specific histone H3 CENP-A, have been shown to lead to abnormal kinetochore protein levels, resulting in chromosome mis-segregation[348,349].

5.1.1.2 Mitotic checkpoint defects

A compromised SAC, which typically arrests cells with improper spindle kinetochore attachments, can lead to CIN and aneuploidy because cells can initiate anaphase before all of the chromosomes have established their proper spindle attachments. Heterozygous mice for SAC genes exhibit varying degrees of aneuploidy[350,351]. SAC impairment has been associated with increased aneuploidy and tumor development. Biallelic mutations in BUB1B are linked to mosaic variegated aneuploidy (MVA) syndrome[352]. However, it remains a subject of debate whether SAC defects are a common driver of CIN, as mutations in SAC genes are rarely found in cancer. Interestingly, some SAC proteins are frequently overexpressed in cancer, such as Mad2 (MAD2L1). MAD2 is an E2F transcriptional target that is abnormally expressed in cells with mutations in the Rb gene[353]. Transgenic mice overexpressing MAD2 develop aneuploid tumors, leading to the proposition that SAC hyperactivation could be causing CIN in this model[354,355]. However, MAD2 overexpression is associated with tetraploidization and hyperstabilization of kinetochore-microtubule (k-MT) attachments, which may explain its role in driving CIN[353,354,356]. Another SAC component, MAD1 (MAD1L1), is overexpressed in cancer but, in this case, produces a

dominant-negative effect that impairs SAC signaling[357]. It's important to note that many SAC proteins have functions outside of mitosis that may also contribute to tumorigenesis[358].

5.1.1.3 Supernumerary centrosomes and spindle defects

Centrosome amplification is a common occurrence in human tumors linked to CIN, contributing to tumorigenesis through various mechanisms[359,360]. This amplification can result from centriole overduplication or as an indirect consequence of genome doubling (tetraploidization). Initially, it was believed that extra centrosomes induced chromosome segregation errors by causing multipolar cell divisions[361]. However, recent research has shown that multipolar divisions are less frequent, and when they do occur, most progeny do not survive. Cancer cell lines with centrosome amplification tend to cluster these extra centrosomes during mitosis, allowing the formation of pseudo-bipolar spindles[362,363]. While centrosome clustering promotes cell survival, it increases the likelihood of merotelic attachments, and leads to frequent lagging chromosomes in cells with supernumerary centrosomes, resulting in chromosome segregation errors[363,364]. Tetraploid cells resulting from cytokinesis failure display CIN, while tetraploid cells that lose their extra centrosomes remain karyotypically stable[363,365]. Genome-doubling events are also common in cancer and seem to precede CIN development[366,367].

Failure to cluster extra centrosomes into two poles results in multipolar divisions, which can lead to severe karyotypic changes in daughter cells. Balanced multipolar divisions are typically lethal and unlikely to efficiently propagate CIN. Conversely, an unbalanced multipolar division could result in the missegregation or loss of a few chromosomes[364,368,369]. Knockdown of the kinesin KIFC1 (HSET) through siRNA prevents clustering and results in multipolar divisions and lethality, particularly in cells with multiple centrosomes. Notably, multipolarity can also occur without centrosome amplification or in acentrosomal spindles, as defects in mitotic spindle maintenance can lead to aberrant yet functional spindle poles[370].

5.1.1.4 *Defects in chromosome cohesion*

Prior to chromosome segregation, sister chromatids are held together by the cohesion complex until the onset of anaphase. When cohesion is compromised, leading to the premature separation of sister chromatids, individual sister chromatids can segregate independently as they attach to microtubules. This results in virtually random chromosome segregation because the connection between the sisters is crucial for ensuring that one sister attaches to each spindle pole. Both mutations and abnormal expression of genes related to the cohesin complex have been identified in various human cancers[371,372]. For instance, truncating mutations in the cohesin complex subunit STAG2 have been found in tumors. Introducing STAG2 inactivating mutations into a karyotypically stable cell line leads to defective sister chromatid cohesion and an increased rate of aneuploidy[373]. Hyperactivation of Separase can also induce aneuploidy[374].

5.1.2 Aneuploidy is fueled by genomic instability

As outlined in section 3.2.4, disruptions in DNA replication or repair processes occurring prior to mitosis can instigate anaphase segregation errors, culminating in aneuploidy. Replication stress induces chromosomal rearrangements and breakages during DNA repair[375]. This may yield acentric chromosome fragments that evade capture by the mitotic spindle or give rise to dicentric chromosomes, resulting in chromosome bridges during anaphase[376]. The interference with chromosome assembly preceding mitosis can also contribute to segregation errors. For instance, anomalies in chromosome condensation, sister chromatid cohesion, or the resolution of sister chromatid catenation can lead to the formation of anaphase bridges and lagging chromosomes, independently of improper kinetochore-microtubule attachment[373,377].

The reduction in the frequency of mitotic errors through the alleviation of replication stress via nucleoside complementation suggests their de novo formation during each phase of DNA replication[378]. Additionally, the transient induction of replication stress with aphidicolin has been shown to cause deviations in chromosome number.

Increased replication origin firing has also been shown to increase microtubule dynamics in mitosis, leading to chromosome missegregation[379]. Consequently, replication stress can lead to the missegregation of an entire, albeit likely damaged, chromosome. In precancerous lesions, the presence of replication stress may facilitate the onset of CIN in certain tumors[380].

5.2 ANEUPLOIDY IS A HALLMARK OF CANCER

While Theodor Boveri is credited with being the first researcher to suggest the potential link between aneuploidy and the development of cancer, laying the foundation for the "chromosome theory of cancer" over a century ago in 1914[381], observations made by David Hansemann as far back as the late 19th century also hinted at a connection between aneuploidy and cancer[382]. Nowadays, aneuploidy is recognized as a hallmark of cancer. Aneuploidy is a common characteristic found in most human cancers[383] and elevated levels of aneuploidy are associated with various aggressive features in cancer, including a poor prognosis, metastasis, and commonly with resistance to therapy[341,384].

5.2.1 The aneuploidy paradox in cancer

The deleterious effects of aneuploidy on cell fitness are well established, spanning from yeast to mammalian cells. The acquisition of an extra chromosome, or 'whole chromosome gains', generally hinders cell proliferation, disrupts metabolic processes, and triggers various stress responses[385–387]. Despite the detrimental consequences of aneuploidy on cellular fitness, changes in karyotype appear to confer proliferative advantages in specific scenarios. The fact that aneuploidy is a strikingly common feature in cancer creates a paradox in terms of its contribution to tumorigenesis, the so-called **'aneuploidy paradox'**[388].

While aneuploidy is generally selected against due to its impact on cellular fitness, this is not as clear-cut when it comes to cancer cells. It was suggested that the effects of CIN and derived aneuploidy on tumors may depend on the severity, timing, and duration of CIN (whether it's transient or chronic), the type of tissue involved[389], and

the tumor microenvironment, which can include the immune system's ability to eliminate aneuploid cells[390].

Aneuploidy can act both as both a tumor suppressor and a tumor initiator, depending on the context[391,392]. The role of aneuploidy in promoting tumorigenesis has been a subject of active research and debate. While it's noteworthy that mutations in genes regulating chromosome segregation are rare in cancers[393], and aneuploidy can inhibit proliferation, it is suggested that aneuploidy might be a consequence rather than a cause of tumorigenesis. Loss of tumor suppressors has been shown to also compromise centromere function, leading to CIN and aneuploidy[394]. However, accumulating evidence indicates that aneuploidy can indeed promote tumorigenesis through the loss of tumor suppressor genes and the gain of oncogenes[395].

Nonetheless, the analysis of specific aneuploid karyotypes and mouse models of CIN has revealed that aneuploidy can both promote and inhibit effects on tumorigenesis. For instance, the motor protein CENP-E serves as a prime example of this dual role. Mice with heterozygous CENP-E deletions have increased aneuploidy levels and are less likely to develop spontaneous liver tumors and DMBA-induced tumors. However, they exhibit a higher incidence of spleen lymphomas and lung adenomas. Many other mouse models of CIN have displayed varying effects on tumorigenesis, depending on cell type and genetic background[391].

Other studies revealed a perhaps general principle wherein aneuploidy can facilitate tumorigenesis. While increased CIN can aid in the evolution of advantageous karyotypes, it is more likely to generate disadvantageous ones. However, increasing chromosome mis-segregation in these mice by interfering with SAC function reduces tumor formation by increasing cell death[396]. These results suggest that a lower frequency of chromosome missegregation can actually promote tumorigenesis because it enhances the chances of creating a karyotype that supports tumor growth. However, when the rates of chromosome missegregation become excessively high, tumor cells tumor cells are unable to maintain these advantageous karyotypes. Instead,

they continuously produce cells with unviable karyotypes, which ultimately leads to cell death and, consequently, the suppression of tumor development.

5.2.2 The clinical value of aneuploidy

Aneuploidy can be reliably detected using various technologies, including conventional and molecular cytogenetic methods, single-nucleotide polymorphism arrays, comparative genomic hybridization arrays, genome-wide DNA and RNA sequencing[397,398]. Some of these methods are already employed in clinical settings, making aneuploidy an attractive biomarker for patient stratification, provided it holds prognostic or predictive value. Despite some complicating factors, exploring the diagnostic value of aneuploidy is worthwhile. Much like point mutations, aneuploidy can offer insights into prognosis, either by assessing overall aneuploidy burden or by examining specific recurrent alterations. Elevated aneuploidy levels have been linked to poorer clinical outcomes across various tumor types. In breast cancers, for instance, high aneuploidy levels are associated with reduced overall survival and recurrence-free survival[399–404].

A critical question that remains incompletely answered is why aneuploidy is generally connected with a worse prognosis. One reason is that aneuploid cancer cells often display reduced sensitivity to chemotherapy agents, making them more resistant to treatment[405]. This resistance is attributed to the diversity in tumor karyotypes. Additionally, aneuploidy induced by transient CIN can lead to resistance to the withdrawal of oncogenes in genetic mouse models[354,406]. It's important to note that the relationship between aneuploidy levels and drug resistance isn't a simple linear one; extreme levels of aneuploidy and/or CIN can render cells more sensitive, rather than resistant, to anticancer drugs[405,407–409], aligning with the concept of an optimal level of karyotypic heterogeneity and chromosome mis-segregation rate[410]. Nevertheless, in general, high aneuploidy levels are associated with chemotherapy resistance, giving aneuploidy not only prognostic but also predictive value. However, several factors can confound the prognostic value of aneuploidy[392]: First, aneuploidy is most prevalent in

the late stages of tumor development, potentially creating an apparent link between aneuploidy and clinical outcome simply because advanced tumors are both more aneuploid and more aggressive. Thus, interpreting the relationship between aneuploidy and patient prognosis requires controlling for factors like the timing of diagnosis and the rate of tumor growth. The association between aneuploidy levels and high degrees of CIN is a second complicating factor. Some cancer cells can exhibit high levels of aneuploidy while maintaining chromosomal stability[411]. For instance, CIN may be a temporary phenomenon that is counterbalanced during the evolution of tumors[412], but the resulting aneuploid karyotypes of cancer cells can persist long after CIN has been mitigated. Intratumor heterogeneity (ITH), which has become a prominent area of study thanks to advances in single-cell 'omics' technologies, is a third confounding factor. Numerical and structural CIN drive the development and maintenance of ITH more strongly than point mutations[405]. Furthermore, copy number alteration (CNA) heterogeneity, largely influenced by aneuploidy, is strongly associated with clinical outcomes[409]. Controlling for ITH when assessing the link between aneuploidy and clinical outcomes is thereby important.

Despite these complexities, both the degree of aneuploidy and specific aneuploidies have been convincingly associated with clinical outcomes, to the extent that they can inform clinical management in specific cases. Accounting for and controlling these confounding factors is expected to enhance our understanding of the prognostic and predictive value of cancer aneuploidy.

5.2.3 Exploiting aneuploidy as a therapeutic approach in cancer treatment

Although aneuploidy can promote tumor growth, it has been shown that the elevation of chromosome missegregation and the resulting aneuploidy beyond a certain level can be lethal to cancer cells[396,406,413,414]. Based on this rationale, key proteins and pathways involved in safeguarding the fidelity of chromosome segregation represent potential therapeutic targets for cancer treatment.

Increasing the rate of CIN/aneuploidy over a critical threshold (Figure 35) can be achieved by combining two factors that each cause low and tolerable levels of CIN, resulting in cell death and tumor suppression.

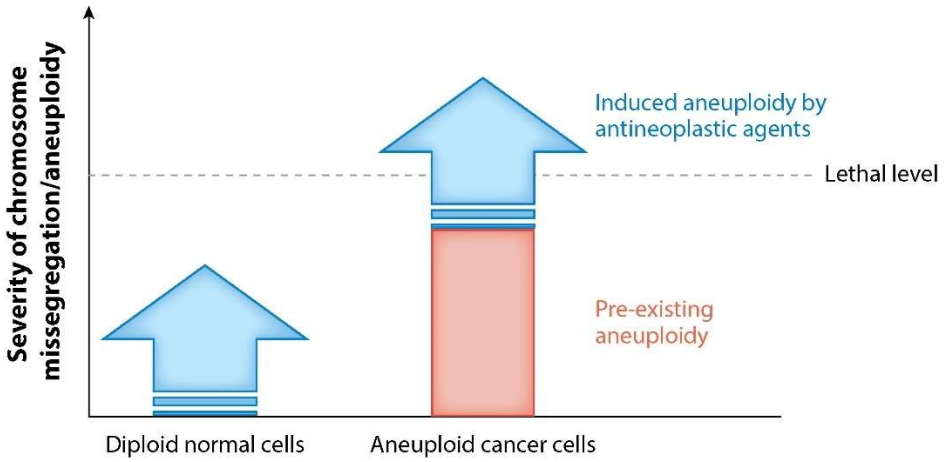

Figure 35: Threshold of CIN tolerability
(Adapted from[415])

Lethal levels of CIN can arise from a singular mechanism, such as the complete loss (as opposed to weakening) of the SAC signaling[416]. However, the combination of two insults, each individually causing a low, tolerable rate of CIN, can collectively exceed a maximally tolerated threshold, leading to cell death and tumor suppression[358]. Supporting this notion, both genetically and pharmacologically induced CIN have demonstrated efficacy in inducing cell death and suppressing tumors when combined[413,417]. Genetic modifications in various genes yield a tolerable CIN rate with a modest increase in spontaneous tumorigenesis, yet combining distinct genetic sources of CIN results in cells with elevated CIN rates, ultimately causing cell death and tumor suppression[396,406,414,418,419]. Conversely, reducing CIN levels, such as by overexpressing the microtubule depolymerase KIF2B in a mouse model of *KRAS*-induced lung cancer, promotes tumor growth[420], aligning with the idea that there exists an optimal rate of CIN for tumor growth, surpassing which inhibits tumor growth. Pharmacological treatments inducing CIN can synergize with genetic insults, surpassing the maximally tolerated threshold, thereby suppressing tumors. Notably, taxanes, widely used chemotherapeutics known to stabilize microtubules, induce

abnormal multipolar spindles and CIN at clinically relevant doses[421,422]. Combining genetically or pharmacologically induced CIN with low-dose taxane leads to higher rates of CIN and cell death[413,423]. Another instance involves the tumor suppressor p38α, which, when lost, increases CIN and aneuploidy. Inhibitors of p38α causing CIN enhance the effects of CIN-inducing drugs, including taxanes, requiring lower doses for cell death induction[424]. Downregulation of ATIP3 (see section 2.2.4) also support the idea that aneuploid tumor cells are more responsive to taxanes[94]. Overall, the evidence supports a model where a certain range of CIN weakly promotes tumors, but excessive rates of CIN induce cell death and tumor suppression.

II. OBJECTIVES

In the context of the central theme of the laboratory, which focuses on the study of microtubule-associated proteins and their regulation in breast cancer, my doctoral research has involved active participation in various projects. These efforts have resulted in the publication of two reviews of literature (Appendices 1 & 2) and two scientific article (Results & Appendice 3).

When I first arrived in the lab, the team had already established that ATIP3, a MAP (microtubule-associated protein), exhibited reduced expression levels in approximately 50% of breast cancer cases, a circumstance intricately linked to poor prognosis. Building on this foundation, they had recently made a pivotal discovery: breast cancer patients with lower levels of ATIP3 exhibited a notably improved response to taxane-based therapies. Intriguingly, tumors with diminished ATIP3 levels displayed a greater degree of aneuploidy and were associated with elevated levels of chromosomal instability (CIN). The underlying mechanism revealed that ATIP3 downregulation led to the formation of multipolar spindles during mitosis, driven by centrosome amplification. This phenomenon, combined with low doses of taxanes, synergistically sensitized cancer cells to taxanes, culminating in cell death. This mechanistic understanding provided a rationale for the improved responsiveness of aneuploid tumors to paclitaxel.

Given the substantial side effects of taxanes and their efficacy in only 30% of breast cancer patients, there emerged a pressing need for novel targeted therapies in breast cancer. Therefore, the central objective of my PhD thesis was to identify a therapeutic target for ATIP3-deficient cancers. I harnessed the distinctive features associated with ATIP3-deficient cancers as potential vulnerability. ATIP3 deficiency was tied to heightened CIN and aneuploidy. Therefore, the premise was that inducing exceptionally high levels of CIN and subsequent aneuploidy could push cancer cells past their viability threshold, resulting in cell death.

To address this, I initiated a screening of a panel of 28 cell cycle kinase inhibitors. The rationale behind this approach was that perturbations of the cell cycle regulators would induce defects in DNA repair or prompt CIN. When applied in an aneuploid context, this approach held the promise of better kill ATIP3-deficient cancer cells. In the course of this screening, the inhibition of WEE1 kinase emerged as particularly cytotoxic in aneuploid ATIP3-deficient cells. Subsequently, my efforts delved into characterizing the effects of WEE1 inhibition in ATIP3 cells and unraveling the mechanism through which aneuploidy heightened sensitivity to WEE1 inhibition. The culmination of this work is described in a scientific article that we have published on the 19th of September 2023 as a preprint on BioRxiv (DOI: https://doi.org/10.1101/2023.09.19.558475) and is presented in the results section.

In essence, my thesis explores the potential of WEE1 kinase inhibition as a targeted therapeutic strategy against aneuploid ATIP3-deficient breast cancers, presenting a promising avenue for advancing treatment modalities in breast cancer patients.

III. RESULTS

ARTICLE 1 – ANEUPLOIDY TRIGGERS VULNERABILITY TO WEE1 INHIBITION VIA SEVERE CHROMOSOME PULVERIZATION

In our investigation of potential therapeutic avenues for highly aneuploid breast cancers, characterized by a ATIP3 deficiency, we uncovered their vulnerability to WEE1 kinase inhibition.

Using ATIP3 depletion as a model to induce high levels of aneuploidy, we performed a chemical synthetic lethality screen of 28 cell cycle kinase inhibitors. Among the inhibitors tested, AZD1775, a WEE1 kinase inhibitor, exhibited heightened potency in highly aneuploid breast cancer cells, as indicated by reduced IC50 values. Importantly, this sensitivity was specific to cancer cells, sparing transformed non-cancer cells. Moving to *in vivo* models, xenografts of MDA-MB-468 breast cancer cells with ATIP3 depletion demonstrated increased tumor growth. However, treatment with AZD1775 not only prevented tumor growth but had a more pronounced effect on ATIP3-depleted tumors.

Further delving into the molecular mechanisms, we uncovered that WEE1 inhibition led to accelerated mitotic entry in aneuploid cells, a process driven by premature activation of CDK1. Live cell microscopy revealed that ATIP3-depleted cells entered mitosis an hour earlier than control cells. Remarkably, this acceleration was associated with an extension of the time spent in mitosis, resulting in aberrant mitotic phenotypes.

WEE1 inhibition induced a peculiar mitotic phenotype characterized by the detachment of centromere proteins from DNA and chromosome pulverization. Notably, this abnormal mitosis was linked to events occurring in S-phase, where WEE1 inhibition induced replication stress and DNA damage. We also examine the intricate interplay between replication stress induced by WEE1 inhibition and the subsequent manifestation of mitotic abnormalities. Specifically, we found that pre-existing replication stress, linked to ATIP3 depletion, substantially contributed to heightened

DNA damage levels during mitosis in response to WEE1 inhibition. The rescue of the mitotic phenotypes observed with nucleoside supplementation underscored the dysregulation of DNA replication as a driving force behind mitotic aberrations induced by WEE1 inhibition.

Mechanistically, we showed that MUS81 was responsible for some of the DNA damage in S-phase but not for the mitotic phenotypes; and that chromosome pulverization is orchestrated by the DNA2 helicase/nuclease. Depletion of DNA2 prevented abnormal mitotic phenotypes and chromosome pulverization.

Finally, we demonstrated that inducing aneuploidy in non-transformed or diploid cells using reversine rendered them vulnerable to WEE1 inhibition, leading to chromosome pulverization and cell death. This highlights the significant relationship between aneuploidy and cell sensitivity to WEE1 inhibition.

In conclusion, our study unveils a nuanced vulnerability of highly aneuploid breast cancers to WEE1 inhibition and provide a basis for potential clinical applications of WEE1-targeted therapies in aneuploid breast cancers, offering new avenues for improved patient stratification and treatment outcomes.

Increased vulnerability of aneuploid cancer cells to WEE1 inhibition involves severe chromosome pulverization

Maria M. HAYKAL[1,2], Sylvie RODRIGUES-FERREIRA[1,2,3] and Clara NAHMIAS[1,2*]

[1]Institut Gustave Roussy, Inserm U981, Biomarqueurs prédictifs et nouvelles stratégies thérapeutiques en oncologie, 94800, Villejuif, France.

[2]Université Paris-Saclay, 91400, Orsay, France.

[3]Inovarion, 75005 Paris, France

Correspondence: clara.nahmias@inserm.fr

Abstract

Aneuploidy, a hallmark of cancer, is a prominent feature in breast cancer. Here, we screened a panel of cell cycle kinase inhibitors to identify novel targets for highly aneuploid breast cancers. We show that increasing aneuploidy in breast cancer cells sensitizes to the inhibition of WEE1 kinase. Upon exposure to WEE1 inhibitor, aneuploid cells exhibit aberrant mitosis characterized by the detachment of centromere proteins from centromeric DNA and pulverization of chromosomes. The occurrence of such phenotype is driven by excessive levels of replication stress and DNA damage during S-phase combined with premature entry into mitosis. We show that DNA2 helicase/nuclease is the key player responsible for chromosome pulverization in mitosis. The heightened vulnerability of aneuploid cells to WEE1 inhibition, coupled with underlying molecular mechanisms, provides a rationale for clinical exploration of WEE1-targeted therapies against aneuploid breast cancers.

Introduction

Cellular DNA content is carefully controlled by cell cycle checkpoints, which monitor and regulate DNA replication and subsequent cell division, preventing genomic abnormalities[1]. Chromosomal instability (CIN), a condition of persistent chromosome missegregation, is a significant hallmark of human cancers[2]. Changes in mitotic spindle assembly checkpoint function, centrosome duplication, kinetochore function, and microtubule stability have all been linked to CIN[3]. Aneuploidy, an inevitable consequence of CIN, refers to the condition in which cells contain an atypical quantity of chromosomes. Aneuploidy can either designate the addition or removal of entire chromosomes (whole-chromosome aneuploidy) or specific chromosome parts (structural aneuploidy). Aneuploidy is detected in 90% of solid tumors[4]. The occurrence of aneuploidy generally reduces a cell's proliferative ability owing to the detrimental effects of proteotoxic stress and induction of DNA damage[5–7]. However, in tumors, high levels of aneuploidy are strongly associated with poor patient outcomes, suggesting that they may confer a growth advantage and contribute to some aspects of cancer[8].

Breast cancer is a heterogeneous disease affecting women worldwide. It is the most frequently diagnosed cancer and a leading cause of cancer-related deaths[9]. Breast cancer genomes are often aneuploid and display intricate numerical and structural chromosomal rearrangements[10–12]. Importantly, high levels of aneuploidy are associated with a poor prognosis in the majority of breast cancer cases[13–15]. Given the unfavorable prognosis associated with aneuploidy levels in breast cancer, there is an urgent need to design adapted therapies for these tumors[16,17].

ATIP3, a microtubule-stabilizing protein, is a prognostic biomarker for breast cancer patient survival[18,19]. Recent work has shown that depletion of ATIP3 induces centrosome amplification and the formation of multipolar mitotic spindles, thereby increasing aneuploidy. Interestingly, ATIP3 deficiency in breast tumors also predicts their response to taxanes: tumors expressing low levels of ATIP3 are associated with high CIN and are aneuploid, but paradoxically more responsive to taxane-based chemotherapy[17]. This phenomenon can be attributed to the detrimental levels of excessive aneuploidy resulting from combined ATIP3 depletion and taxane treatment, ultimately driving cell death[20,21]. Nonetheless, taxanes are highly toxic drugs with adverse side effects, highlighting the need for targeted therapies.

In the search for new targeted therapies for highly aneuploid breast cancers, we depleted ATIP3 to increase aneuploidy levels, and screened a panel of kinase inhibitors known to perturb the cell cycle. In this study, we focused on WEE1 kinase, a gatekeeper of the G2/M cell cycle checkpoint[22]. By inhibiting cyclin-dependent kinase 1 (CDK1) through phosphorylation of Tyr15, WEE1 helps to control the proper timing of cell division and prevents cells from entering mitosis until DNA replication and repair processes are completed, thus maintaining genome stability[23–25]. Here, we show that WEE1 inhibition is more cytotoxic in cells with high levels of aneuploidy. In these cells, WEE1 inhibition induces higher levels of replication stress and DNA damage in S-phase, which is responsible for severe chromosome pulverization in subsequent mitosis, causing massive cell death.

Results

The search for new therapeutic strategies against highly aneuploid breast cancers led us to perform a chemical synthetic lethality screen of 28 cell cycle kinase inhibitors in breast cancer cells in which ATIP3 protein was depleted to increase aneuploidy. The SUM52PE breast cancer cell line expressing or not ATIP3 was grown in 3-dimensions as multicellular spheroids (MCSs) to mimic the features of solid tumors and was treated with increasing doses of each inhibitor (Figure 1A, S1A). After 72 h of treatment, cell viability was assessed and the IC50 of each inhibitor was calculated. We considered an inhibitor as a differential hit if the IC50-fold change between control and ATIP3-depleted cells was equal to or higher than 2 (Figure 1B, Table S1). ATIP3 depletion improved the cytotoxic response to six different inhibitors targeting ATR, ATM, WEE1, Aurora, and PLK4 kinases (S1B-C). Among these differential inhibitors, we focused on AZD1775, which is a WEE1 kinase inhibitor. AZD1775 was more potent in ATIP3-depleted breast cancer MCSs, as indicated by their size (Figure 1C) and lower IC50 values (mean IC50 in shCtl is 1.31 µM *vs*. 0.43 µM in shATIP3) (Figure 1D). AZD1775 also exhibited lower IC50 values in two other breast cancer MCSs models in which ATIP3 expression was depleted (Figure S1D). Similar results were obtained with PD0166285, another WEE1 inhibitor (Figure S1E). In addition, AZD1775 abolished the phosphorylation of CDK1 at Tyr15, confirming target engagement (Figure S1F). Importantly, the doses of AZD1775 that caused maximal cell death in tumor cells had very little effects on diploid, non-transformed RPE-1 cells (Figure 1E). We investigated whether increased vulnerability of ATIP3-depleted aneuploid cells to WEE1 inhibition was

driven by aneuploidy *per se* or by ATIP3-specific effects. To address this question, we induced aneuploidy in RPE-1 cells using reversine, an inhibitor of MPS1 kinase that induces chromosome missegregation[26,27], and combined it with WEE1 inhibition (Figure S1G). MPS1 inhibition in RPE-1 cells resulted in aneuploidy, as shown by increased variability in chromosome numbers (Figure S1H). Aneuploidy induction by reversine in RPE-1 cells rendered them vulnerable to WEE1 inhibition, leading to cell death (Figure 1F), indicating that sensitivity to WEE1 inhibition is associated with aneuploidy. We then tested the efficacy of AZD1775 *in vivo* using xenografts of the MDA-MB-468 breast cancer cell line in which ATIP3 was depleted. AZD1775 was administered daily by oral gavage at a dose of 90 mg/kg for 3 weeks. ATIP3 depletion increased tumor growth, in line with the high aggressiveness of tumors expressing low levels of ATIP3 (Figure 1G). Treatment with AZD1775 prevented tumor growth and had a more prominent effect on ATIP3-depleted tumors (Fold change in tumor volume of 1.6 in shCtl *vs*. shCtl AZD1775 and 2.3 in shATIP3 *vs*. shATIP3 AZD1775) (Figure 1H) in agreement with *in vitro* observations.

WEE1 inhibition has been shown to induce premature mitotic entry of S-phase-arrested cells after induction of DNA damage[28]. To evaluate mitotic entry, we used live cell microscopy on control or ATIP3-depleted cells (Figure S2A) that were synchronized at the G1/S boundary and released in the presence or absence of AZD1775. Interestingly, in response to WEE1 inhibition, ATIP3-depleted cells entered mitosis an hour earlier than control cells (3.1 h post release for siATIP3 to enter mitosis vs. 4.2 h for siCtl), whereas a majority of untreated cells did not enter mitosis at 6 h post-release (Figure 2A-B). In addition, WEE1 inhibition increased the phosphorylation of both histone H3 (Figure S2B) and CDK1 substrates (Figure S2C), indicators of mitotic entry, in ATIP3 depleted cells. In line with these observations, the proportion of mitotic cells increased in ATIP3-depleted cells in both 2D (Figure 2C) and MCSs (Figure S2D-E). To gain further insights into the effects induced by WEE1 inhibition in mitosis, we filmed HeLa cells stably expressing mCherry-histone H2B in which we depleted ATIP3 to closely track the fate of individual cells. As described previously[17], untreated ATIP3-depleted cells spent more time in mitosis compared to control cells (Figure 2D-E, Movies S1 and S2). WEE1 inhibition further prolonged the time spent in mitosis. Notably, ATIP3-depleted cells treated with AZD1775 experienced significantly longer mitosis than control cells (Figure 2D-E, Movies S3 and S4). Strikingly, 75% of ATIP3-depleted cells treated with AZD1775 exhibited a back-and-

forth movement of their DNA around the mitotic spindle, compared to only 1% of control cells that behaved in this manner (Figure S2F, Movie S4), which is consistent with exceedingly long mitosis. AZD1775 induced two types of cell death. Cells either died during mitosis (mitotic catastrophe) (Figure 2D panel 3, Movie S3) or after mitotic exit (Figure 2D panel 4, Movie S4). Of note, cell death occurred in 95% of ATIP3-depleted cells treated with AZD1775 (63% after mitotic exit) and in 78% of control cells (12% after mitotic exit) (Figure 2F-G). Together, these results show that ATIP3 depletion accelerates mitotic entry, prolongs the time spent in mitosis, and exacerbates cell death upon exposure to WEE1 inhibitor.

WEE1 inhibition caused a very particular phenotype in mitosis, where a bulk of chromatin mass was on the outside of the mitotic spindle rather than in structured chromosomes aligned on the metaphase plate in both 2D (Figure 3A *enlarged panels*) and MCSs (Figure S2G). ATIP3 depletion exacerbated these mitotic abnormalities (Figure 3B). Similar results were obtained when WEE1 was depleted using siRNA, confirming that WEE1 kinase is the main target of AZD1775 (Figure S2H). We then investigated the impact of CDK1, a major kinase controlled by WEE1. The abnormal mitosis phenotype was completely abolished upon combining WEE1 inhibition with RO-3306, a CDK1 inhibitor (Figure S2I-J), confirming that the abnormal phenotype was due to the activation of CDK1 after WEE1 inhibition. The observation of such a phenotype, characterized by DNA exclusion from the spindle during mitosis, raises the question of the localization of centromere proteins (CENPs) in AZD1775-treated cells. Using anti-centromere antibodies (ACA) staining, we found that WEE1 inhibition caused the detachment of CENPs from the DNA, as evidenced by a chromatin mass located on the outside of the spindle and CENPs clustered on spindle fibers (Figure 3C). Similar results were obtained using CENP-A and CENP-B as centromeric markers (Figure S3A-B). We further distinguished two phenotypes, that we referred to as (i) **'central chromatin mass'** where the DNA is still mildly attached to the spindle (Figure 3D, central panel) and (ii) **'side chromatin mass'** where DNA is completely devoid of CENPs that are clustered on the spindle (Figure 3D, right panel). AZD1775-treated control and ATIP3-depleted cells exhibited equal proportions of the 'central chromatin mass' phenotype, whereas the 'side chromatin mass phenotype' was the major phenotype in ATIP3-depleted cells (Figure 3E). The detachment of DNA from the spindle prompted us to evaluate chromosome integrity by performing chromosome spreads. Following WEE1 inhibition, we observed two distinct types of chromosome spreads. The first

type, termed as "Cen^{ON}" showed CENPs attached to the chromosomes, although a few acentric chromosomes were present. In the second type, denoted as "Cen^{OFF}", CENPs were clustered and chromosomes were disintegrated, a state that we referred to as chromosome pulverization (Figure 3F, S3C). The latter spreads were largely reminiscent of the 'side chromatin mass' phenotype. Importantly, WEE1 inhibition increased the percentage of "Cen^{OFF}" spreads in ATIP3-depleted cells (65% compared to 23% in control cells) (Figure 3G). We examined whether WEE1 inhibition may trigger such chromosome pulverization in aneuploid cells, independently of ATIP3 deficiency. WEE1 inhibition induced chromosome pulverization in RPE-1 cells rendered aneuploid using reversine, but not in their near-diploid counterparts (Figure 3H-I). Similar results were obtained in the chromosomally stable HCT116 cancer cell line, where WEE1 inhibition alone exhibited negligible effects but triggered chromosome pulverization upon increasing aneuploidy using reversine (Figure S4A-C). Accordingly, elevating aneuploidy using reversine in HeLa cells, that are already aneuploid (Figure S4D), further increased the occurrence of chromosome pulverization (Figure S4E-F). These results underscore the crucial relationship between aneuploidy and cell sensitivity to WEE1 inhibition. To further examine centromeric aberrations, we investigated the binding of CENP-B to its specific DNA box, CENP-B box. Immunofluorescence coupled to Fluorescence *in situ* hybridization (FISH) was performed to reveal both CENP-B and CENP-B box. Following WEE1 inhibition, the CENP-B box was no longer detected in "Cen^{OFF}" spreads in which the protein CENP-B was clustered (Figure S4G-H), indicating loss or disruption of centromeric DNA. This suggests that inhibition of WEE1 results in DNA fragmentation in the centromeric region.

We then investigated the mechanisms leading to aberrant phenotypes in mitosis and chromosome pulverization after exposure to WEE1 inhibition. We hypothesized that chromosome pulverization during mitosis may stem from events that occur earlier in S-phase. WEE1 inhibition was previously shown to cause replication stress by exhausting replication origins, leading to replication fork stalling[25]. Stalled forks can then be recognized by a nuclease for processing[29]. Importantly, uncontrolled action of nucleases can lead to excessive fork degradation and massive DNA double-strand breaks (DSBs). To investigate the early effects of WEE1 inhibition in S-phase before mitotic entry, cells were treated for 2 h with AZD1775. WEE1 inhibition did not change the proportion of cells in S-phase, as indicated by the proportion of EdU-positive cells (Figure S5A-B). In line with higher DNA replication levels, WEE1 inhibition

induced higher levels of EdU incorporation although no differences were observed between control and ATIP3-depleted cells (Figure S5C). One of the early events of WEE1 inhibition was the induction of replication stress, as shown by elevated levels of phosphorylated replication protein A (RPA32 pS4/S8) (Figure 4A-B). Interestingly, ATIP3-depleted cells showed significantly higher levels of replication stress in response to WEE1 inhibition than control cells (Figure 4A-B). As excessive replication stress can induce the formation of DSBs[30], we assessed DNA damage by analyzing pan-nuclear H2AX phosphorylation (γH2AX). DNA damage levels were elevated upon WEE1 inhibition and even further in ATIP3-depleted cells (Figure 4C-D). In line with these results, our *in vivo* studies revealed that ATIP3-deficient tumors exhibit higher levels of DNA damage following treatment with AZD1775 (Figure S5D-E). Inversely, the percentage of EdU-positive cells with 53BP1 foci was reduced upon WEE1 inhibition, suggesting either an impaired DNA damaged response or reduced DNA repair activity (Figure S5F-G).

Importantly, after 6 h of treatment, when cells progressed to mitosis, the impact of WEE1 inhibition on DNA replication and damage remained pronounced in ATIP3-depleted cells. This is shown by the higher proportion of hyperphosphorylated RPA32 (Figure S6A-B) and γH2AX positive (Figure S6C-D) mitoses. Of note, EdU-positive mitotic cells also occurred following WEE1 inhibition, and to a greater extent in ATIP3-depleted cells (Figure S6C,E), indicating either replication stress-associated mitotic DNA synthesis (MIDAS)[31] or abrupt mitotic entry of replicating cells. The observed higher levels of damage in ATIP3-depleted mitotic cells led us to investigate whether they could be attributed to the presence of pre-existing replication stress prior to WEE1 inhibition. Cells were pretreated with a low dose of the DNA polymerase inhibitor aphidicolin for 2 h and then exposed for 6 h to AZD1775. When control cells were exposed to aphidicolin and AZD1775, they exhibited the same proportions of hyperphosphorylated RPA32 (Figure S7A-B) and γH2AX (Figure S7C-D) mitoses as those observed in ATIP3-depleted cells treated with AZD1775 alone. These results point towards the existence of low levels of endogenous replication stress or a compromised replication stress response in ATIP3-depleted cells. Indeed, ATIP3-depleted cells showed higher levels of endogenous 53BP1 nuclear bodies (Figure S7E-G) a marker of unresolved replication stress transmitted throughout the cell cycle[32].

We then investigated whether the effects of WEE1 inhibition in S-phase may be responsible for the detachment of CENPs from DNA and the chromosome pulverization observed during mitosis. To this end, G1/S synchronized cells were treated at different time points with AZD1775 following the scheme shown in Figure 4E. Control cells that completed at least half of their S-phase (mid-S and late-S) in the absence of AZD1775 presented much less abnormal phenotypes (side or central chromatin mass phenotypes) in mitosis (Figure 4F) and less chromosome pulverization (Figure 4G) compared to cells that were released into S-phase in the presence of AZD1775. Remarkably, a similar trend was observed in ATIP3-depleted cells. When allowed to progress into S phase before exposure to AZD1775, ATIP3-depleted cells displayed diminished occurrence of abnormal mitosis and chromosome pulverization in subsequent mitosis (Figure 4F-G). These results imply that the effects of the WEE1 inhibitor on DNA replication are crucial for the development of abnormalities during subsequent mitosis. Notably, allowing cells to partially replicate their DNA helps to alleviate mitotic abnormalities.

We investigated whether the restoration of DNA replication by adding nucleosides, which would counteract the nucleotide depletion caused by WEE1 inhibition[25], could prevent abnormal mitosis and chromosome pulverization. Simultaneous nucleoside supplementation in AZD1775-treated cells led to a comprehensive rescue of replication stress in S-phase (Figure S7H), as well as the subsequent abnormal mitoses (Figure S7I) and chromosome pulverization (Figure 4H-I) in both control and ATIP3-depleted cells, highlighting the dysregulation of DNA replication as a driving force behind mitotic aberrations induced by WEE1 inhibition.

Knowing that WEE1 inhibition during S phase results in chromosome pulverization in subsequent mitosis, we explored the potential involvement of key molecular players. Notably, the MUS81 endonuclease emerged as a candidate of interest due to its role in inducing DNA breakage at stalled replication forks after WEE1 inhibition[24]. We co-depleted MUS81 and ATIP3 (Figure S8A) and studied the extent of replication stress and DNA damage after WEE1 inhibition. MUS81 silencing in ATIP3-depleted cells led to a significant reduction in the levels of DNA damage (Figure 5A-B) and replication stress (Figure S8B-C) induced by WEE1 inhibition. Surprisingly, MUS81 depletion had no impact on the occurrence of the mitotic phenotypes (Figure S8D-E) or chromosome pulverization (Figure 5C-D), regardless of whether in control or ATIP3-depleted cells. This suggests that while MUS81 plays a role during S phase, it does not significantly contribute to abnormal mitosis nor chromosome pulverization, implying the

involvement of additional factors. This led us to test the implication of three other nucleases (EXO1, MRE11 and DNA2) which are involved in DNA resection during DNA repair (EXO1), DNA double-strand break sensing and processing (MRE11) and replication fork restart (DNA2)[33–35]. Given the intricate interplay between replication stress, DNA damage and mitotic processes, we reasoned that these nucleases might play roles in the mitotic phenotype and chromosome pulverization induced by WEE1 inhibition. Depletion of either EXO1 or MRE11 did not significantly influence abnormal mitoses (Figure S9A-C) or chromosome pulverization (Figure S9D-E), leading us to rule out their direct involvement as primary mediators of these effects. In contrast, DNA2 depletion rescued the abnormal mitotic phenotypes in ATIP3-depleted cells (Figure S10A-C) and prevented chromosome pulverization (15% 'Cen^{OFF}' spreads when DNA2 is co-depleted with ATIP3 *vs*. 55% 'Cen^{OFF}' spreads in ATIP3 depleted cells) (Figure 5E-F). Furthermore, the depletion of DNA2 prevented the excessive levels of DNA damage induced in ATIP3-deficient cells in response to WEE1 inhibition (Figure 5G-H). These findings point to a pivotal role of DNA2 in orchestrating the observed mitotic phenotypes subsequent to S-phase defects induced by WEE1 inhibition in aneuploid cancer cells.

Discussion

The findings presented in this study provide compelling evidence for increased sensitivity of aneuploid cells to WEE1 inhibition through severe chromosome pulverization. Using ATIP3 depletion as a model to increase aneuploidy levels, we demonstrate heightened susceptibility of highly aneuploid cells to WEE1 inhibition, driven by a combination of processes including increased levels of replication stress and DNA damage in S-phase combined with an accelerated cell cycle progression, ultimately leading to chromosome pulverization in mitosis and cell death.

In aneuploid cells, the uneven segregation of chromosomes and compromised DNA replication machinery routinely challenge cellular integrity[36,37](Figure 6 *left panel*). In these cells, WEE1 inhibition intensifies replication stress and DNA damage to catastrophic levels, culminating in replication failure. In this context, untimely activation of CDK1 by WEE1 inhibition triggers a premature entry into mitosis, which, when combined with the defects in S-phase, causes aberrant mitotic phenotypes, chromosome pulverization and massive cell death (Figure 6 *right panel*).

Importantly, the aberrant mitotic phenotypes, characterized by the detachment of centromere proteins from DNA and chromosome pulverization, are due to the effects of WEE1 inhibition in S-phase. Indeed, when cells are exposed to WEE1 inhibition after the completion of S-phase, the occurrence of aberrant mitosis and chromosome pulverization is drastically reduced. Our results favor the hypothesis that replication stress induced by WEE1 inhibition in aneuploid cells reaches intolerable levels that result in excessive nuclease activity during S-phase, leading to massive induction of double-strand breaks. In line with other studies[24,25,38], we found that the MUS81 endonuclease contributes to DNA damage induced by WEE1 inhibition in aneuploid cells. However, MUS81 depletion was not sufficient to rescue either the mitotic phenotypes or chromosome pulverization, pointing to the existence of additional molecular mechanisms.

The aberrant mitotic phenotypes are linked to the premature entry of cells into mitosis while having highly damaged and under-replicated genomes, as a consequence of untimely CDK1 activation. Late-replicating regions such as centromeric DNA would remain incompletely replicated despite cell cycle progression. Notably, proteins implicated in DNA repair and replication stress pathways become enriched during centromeric replication[39], as these genomic loci are fragile and challenging to replicate. The DNA2 helicase/nuclease, a putative substrate of CDK1[40], has high affinity for centromeric DNA[41]. Therefore, this enzyme emerges as a pivotal player in the context of centromeric DNA replication to resolve challenging DNA structures. Upon WEE1 inhibition, CDK1 ectopic activation may be responsible for unregulated activity of DNA2. Accordingly, depletion of DNA2 rescues both DNA damage and abnormal mitotic phenotypes, and prevents the severe chromosome pulverization associated with WEE1 inhibition.

Other studies have described a similar aberrant phenotype in response to WEE1 inhibition where cells underwent premature mitosis with under-replicated DNA. This phenotype was referred to as ‘centromere fragmentation’ based on the observation of centromeres being spatially separated from the main mass of chromosomes[42–44]. Our data provide further molecular insights into this phenotype and support a model in which centromere detachment from DNA is orchestrated by the action of nucleases. In mitosis, the distinctive "side chromatin mass" phenotype driven by WEE1 inhibition is a result of unregulated DNA2 activity, which breaks centromeric DNA causing the separation of CENPs from the DNA.

This study unveils intricate molecular mechanisms that underlie the consequences of WEE1 inhibition in aneuploid cells, and highlights the DNA2 helicase/nuclease as a new molecular player of cell cycle regulation upon inhibition of WEE1 kinase. Our findings hold significant implications for breast cancer therapies, particularly in revealing the vulnerability of highly aneuploid breast cancers to WEE1-targeted therapies.

Legends

Figure 1: Chemical synthetic screen identifies WEE1 kinase as a target for ATIP3-deficient breast cancer cells

(A) Pipeline scheme for drug screening using 28 cell cycle kinase inhibitors. The SUM52PE cell was cultured as MSCs. Screening was conducted in quadruplicates. **(B)** Plot representing the IC50 fold change of each inhibitor between shCtl and shATIP3. **(C)** Representative images of SUM52PE MCSs treated or not with 500 nM AZD1775 for 72 h *(Magnification 20x)*. **(D)** IC50 values of AZD1775 in MCSs (mean ± SEM. of N=6; two-tailed t-test; **p<0.01). **(E)** Plot representing viability of RPE-1 cells upon 72 h of treatment with increasing doses of AZD1775 (mean ± SEM. of N=3). **(F)** Plot representing viability of RPE-1 cells pre-treated with reversine for 48 h and 10 µM AZD1775 for 72 h (mean ± S.D.; one-way ANOVA; ****p<0.0001). **(G-H)** MDA-MB-468 shCtl or shATIP3 subcutaneous xenografts were treated or not with 90 mg/kg of AZD1775 by oral gavage (mean ± SEM; N=1 with 9 mice per group) **(G)** Tumor growth curve (the beginning of treatment is indicated by an arrow). **(H)** Tumor volume (mm^3) after 15 days of treatment (one-way ANOVA; *p<0.05 ****p<0.0001).

Figure 2: WEE1 inhibition accelerates mitotic entry in aneuploid cells and induces their cell death after failed mitosis

(A-B) HeLa cells expressing or not ATIP3 were synchronized at the G1/S boundary, released in the presence or absence of 500 nM AZD1775, and filmed for 6 h. **(A)** Representative images *(Magnification 10x)*. **(B)** Scattered dot plot showing the time to enter mitosis in response to AZD1775 (elapsed time between release and cell rounding). The number of analyzed cells is in brackets (mean ± S.D.; Mann-Whitney test; ****p<0.0001). **(C)** HeLa cells expressing or not ATIP3 were treated or not with 500 nM AZD1775 for 6 h. Mitotic index was determined as the ratio of mitotic cells to the cellular population (mean ± SEM. of N=4; a minimum of 177 cells were analyzed per group; one-way ANOVA; *p<0.05, **p<0.01, ****p<0.0001). **(D-G)** HeLa mCherry-H2B expressing not ATIP3 were stained with siR-tubulin and treated or not with 500 nM AZD1775, then analyzed by timelapse fluorescent imaging for 48 h. **(D)** Representative images. Time is indicated on the top left as h:min. Microtubules (siR-tubulin) are shown in cyan and DNA (mCherry-H2B) in red. **(E)** Scattered dot plot showing the duration of mitosis. The number of analyzed cells is in brackets (mean ± S.D.; Kruskal-Wallis test followed by Dunn's

multiple comparisons; ***p< 0.001, ****p<0.0001). **(F)** Cell fate profiles. **(G)** Proportion of cell fates measured in (F). Scale bar = 20 µm.

Figure 3: WEE1 inhibition causes severe mitotic defects and chromosome pulverization in highly aneuploid cells

HeLa cells expressing or not ATIP3 were treated or not with 500 nM AZD1775 for 6 h. **(A)** Immunofluorescence representative images showing centrosomes (pericentrin) in green, microtubules (tubulin) in red and DNA (DAPI) in blue. **(B)** Quantification of abnormal mitosis shown in (A) (mean ± SEM. of N=4; a minimum of 128 cells was analyzed; one-way ANOVA; **p<0.01, ***p<0.001, ****p<0.0001). **(C)** Immunofluorescence representative images showing CENPs (ACA) in magenta, microtubules (tubulin) in green and DNA (DAPI) in blue. Scale bar = 20 µm. **(D)** Immunofluorescence representative images of the mitotic phenotypes showing CENPs in magenta, microtubules in green and DNA in blue. Scale bar = 5 µm. **(E)** Quantification of the proportions of the mitotic phenotypes shown in (D) (mean ± SEM. of N=4; a minimum of 112 cells were analyzed per group; two-way ANOVA; side chromatin mass in siCtl *vs*. siATIP3 ****p<0.0001). **(F)** Immunofluorescence representative images of chromosome spreads showing CENP-A in green and DNA in red. **(G)** Quantification of the proportions of chromosome spreads shown in (F) (mean ± SEM. of N=6; a minimum of 145 spreads were analyzed per group; two-way ANOVA; siCtl Cen^{OFF} *vs*. siATIP3 Cen^{OFF} ****p<0.0001). **(H-I)** RPE-1 cells were treated with 500 nM reversine for 48 h then with 1 µM AZD1775 for 6 h. **(H)** Immunofluorescence representative images of chromosome spreads showing CENP-A in green and DNA in blue. **(I)** Quantification of the proportion of chromosome spreads from (H) (mean ± S.E.M of N=2; a minimum of 54 spreads were analyzed per group; two-way ANOVA; AZD1775 Cen^{OFF} vs AZD1775 + Reversine Cen^{OFF} ****p<0.0001). Scale bar = 5 µm.

Figure 4: Chromosome pulverization in mitosis is due to heightened levels of replication stress and DNA damage in S-phase

(A-D) HeLa cells expressing or not ATIP3 were treated or not with 500 nM AZD1775 for 2 h. **(A)** Immunofluorescence representative images showing phosphorylated RPA32 (S4/S8) in red and DNA in blue. **(B)** Scattered dot plot of phosphorylated RPA32 mean intensity per nucleus (normalized to DAPI). **(C)** Immunofluorescence representative photographs showing γH2AX in green and DNA in blue. **(D)** Scattered dot plot of γH2AX mean intensity per nucleus

(normalized to DAPI). **(B-D)** The number of analyzed cells is in brackets (mean ± S.D.; Kruskal-Wallis test followed by Dunn's multiple comparisons; ****p<0.0001). Scale bar = 20 µm. **(E)** Treatment scheme of HeLa cells synchronized at the G1/S boundary. Cells were either treated with 500 nM AZD1775 for 6 h directly after release from thymidine block (top axis, early-S); after 3 h into S phase progression (middle axis, mid-S), or after 6 h into S phase progression (bottom axis, late-S). **(F)** Quantification of the proportions of the mitotic phenotypes as described in (E) (mean ± SEM. of N=3; a minimum of 133 cells were analyzed per group; two-way ANOVA; side chromatin mass in siCtl early-S *vs*. late-S p<0.0001; side chromatin mass in siATIP3 early-S *vs*. late-S p<0.0001) **(G)** Quantification of the proportions of chromosome spreads as described in (E) (mean ± SEM. of N=3; a minimum of 80 spreads were analyzed per group; two-way ANOVA; Cen^{OFF} in siCtl early-S *vs*. late-S p<0.0001; Cen^{OFF} in siATIP3 early-S *vs*. late-S p<0.0001). **(H)** Immunofluorescence representative images of chromosome spreads from HeLa cells expressing or not ATIP3 and treated with 500 nM AZD1775 for 6 h in the presence or absence of nucleosides (1/50). CENP-A is shown in green and DNA in blue. **(I)** Quantification of the proportion of chromosome spreads shown in (H) (mean ± SEM. of N=2; a minimum of 61 spreads were analyzed per group; two-way ANOVA; Cen^{OFF} in siCtl AZD1775 *vs*. AZD1775 + Nucleosides p<0.0001; Cen^{OFF} in siATIP3 AZD1775 *vs*. siATIP3 AZD1775 + Nucleosides Cen^{OFF} p<0.0001). Scale bar = 5 µm.

Figure 5: DNA2 nuclease is responsible for chromosome pulverization in mitosis

(A-D) HeLa cells transfected with control, ATIP3, MUS81 or a combination of ATIP3 and MUS81 siRNAs were treated or not with 500 nM AZD1775 for 2 h (A-B) or 6 h (C-D). **(A)** Immunofluorescence representative images showing γH2AX in green and DNA in blue. **(B)** Scattered dot plot of γH2AX mean intensity per nucleus (normalized to DAPI). The number of analyzed cells is in brackets (mean ± S.D.; Kruskal-Wallis test followed by Dunn's multiple comparisons; ****p<0.0001; *<0.05). Scale bar = 20 µm **(C)** Immunofluorescence representative images of chromosome spreads showing CENP-A in green and DNA in red. **(D)** Quantification of the proportion of chromosome spreads shown in (C) (mean ± S.E.M of N=2; a minimum of 67 spreads were analyzed per group; two-way ANOVA showing no significance (p>0.99) between Cen^{OFF} in siATIP3 *vs*. siATIP3 + siMUS81). Scale bar = 5 µm. **(E-H)** HeLa cells transfected with control, ATIP3, DNA2 or a combination or ATIP3 and DNA2 siRNAs and treated or not with 500 nM AZD1775 for 6 h (E-F) or 2 h (G-H). **(E)** Immunofluorescence representative

images of chromosome spreads showing CENP-A in green and DNA in blue. **(F)** Quantification of the proportion of chromosomes spreads shown in (E) (mean ± S.E.M of N=2; a minimum of 78 spreads were analyzed per group; two-way ANOVA; Cen^{OFF} in siDNA2 *vs*. siDNA2 + siATIP3 **p<0.01). Scale bar = 5 µm. **(G)** Immunofluorescence representative images of chromosomes spreads showing γH2AX in green and DNA in blue. **(H)** Scattered dot plot of γH2AX mean intensity per nucleus (normalized to DAPI). The number of analyzed cells is in brackets (mean ± S.D.; Kruskal-Wallis test followed by Dunn's multiple comparisons; ****p<0.0001; *<0.05). Scale bar = 20 µm.

Figure 6: Graphical summary of the proposed working model

Left panel: During S-phase, aneuploid cells undergo replication stress due to the uneven allocation of chromosomes and flawed DNA replication machinery. This leads to the formation of DNA lesions and stalled replication forks. Consequently, DNA damage response pathways are activated with suboptimal DNA repair mechanisms. As aneuploid cells transition through mitosis, they experience chromosome missegregation causing dissemination of aneuploidy to subsequent daughter cells. ***Right panel:*** WEE1 inhibition in aneuploid cells increases levels of replication stress and DNA DSBs in S-phase through the unrestricted activity of the MUS81 endonuclease and the DNA2 helicase/nuclease. The untimely activation of CDK1 after WEE1 inhibition forces cells to enter mitosis prematurely with under-replicated and damaged DNA. DNA2 helicase/nuclease causes massive chromosome pulverization which leads to massive cell death.

Methods

Cell culture, synchronization, and treatment

All cell lines were grown in a sterile cell culture environment and were routinely tested for mycoplasma contamination. MDA-MB-231 (breast cancer cell line), MDA-MB-468 (breast cancer cell line), HeLa (cervical carcinoma cell line) and RPE-1 (hTERT immortalized retinal pigmented cell line) cells were cultured in Dulbecco's modified Eagle's medium (DMEM Gibco™, 61965026). SUM52PE (breast cancer cell line) and HCT116 (colon carcinoma cell line) cells were cultured in RPMI-1640 medium. All cell culture media were supplemented with 10% fetal bovine serum (FBS). MDA-MD-231 shCtl and shATIP3, SUM52PE shCtl and shATIP3, and

HeLa H2B-mCherry cells were previously described[17]. Cell lines were grown under standard cell culture conditions in CO_2 incubators (37 °C; 5% CO_2). Cells were routinely tested for absence of mycoplasma contamination using Venor® GeM Advance Kit (MB Minerva biolabs®).

For synchronization at the G1/S boundary, HeLa cells were treated with 2 mM thymidine for 18 h. Thymidine was washed out and cells were released into fresh media for 8 h followed by a second exposition to 2 mM thymidine for 18 h.

All drugs were purchased from Selleckchem and resuspended in DMSO. AZD1775 was used at 500 nM for all experiments except for cell viability assessment where it was used at increasing concentrations. RO-3306 was used at 10 µM, aphidicolin at 100 nM and reversine at 500 nM. Media was supplemented with nucleosides (EmbryoMax® Nucleosides, Sigma) 1/50 for DNA replication rescue experiments.

siRNA transfection

Specific and control scrambled siRNA oligonucleotides were purchased from Dharmacon (Horizon Discovery).

The following sequences were used:

ATIP3 (5'-UGGCAGAGGUUUAAGGUUA-3');

DNA2: GCUAAACCGUGAAGCAAGA, CUACGUCACUUUAAAGAUG,
ACAGUUGCCUGCAUUCUAA, UGAUAUAGAUACCCCAUUA;

EXO1: GAAGUUUCGUUACAUGUGU, GUAAAUGGACCUACUAACA,
ACUCGGAUCUCCUAGCUUU, GUUAGCAGCAUUUGGCAUA;

MRE11 GAUGAGAACUCUUGGUUUA, GAAAGGCUCUAUCGAAUGU,
GCUAAUGACUCUGAUGAUA, GAGUAUAGAUUUAGCAGAA;

MUS81: GGGAGCACCUGAAUCCUAA, CAGGAGCCAUCAAGAAUAA,
GGGUAUACCUGGUGGAAGA, CAGCCCUGGUGGAUCGAUA;

WEE1: AAUAGAACAUCUCGACUUA, AAUAUGAAGUCCCGGUAUA,
GAUCAUAUGCUUAUACAGA, CGACAGACUCCUCAAGUGA

All siRNAs (20 nM) were transfected for 48-72 h using Lipofectamine RNAiMAX (Invitrogen). Silencing efficiency was evaluated by qPCR or Western blot.

Drug screening

SUM52-PE breast cancer cells (2,000) were seeded in round bottom 96-well ultra-low attachment plates (Thermo Fisher) to form MCSs as previously described[17]. MCSs were treated with increasing doses of each kinase inhibitor for 3 days. Viability was determined by measurement of ATP using ATPlite assay (Perkin Elmer). Dose-response curves were generated and fitted with IC50 values using GraphPad Prism (dose-response with variable slope model).

Xenografts and drug treatment

For tumor formation, 5 million MDA-MB-468 (shCtl or shATIP3) cells were mixed with Geltrex (Gibco) and PBS (1:1) and injected in 100 µl subcutaneously into the left flank of 6–8-week-old NOD SCID gamma (NSG) mice (Charles River). Tumor growth was measured every 4 days using a caliper and volume was assessed as (length × width^2)/2. When the tumor volumes reached approximately 60-70 mm^3, mice were randomly segregated into 4 groups (n = 9 per group). Mice were treated daily with vehicle (0.5% methylcellulose) or 90 mg/kg AZD1775 (provided by AstraZeneca) (in 0.5% methylcellulose) via oral gavage for 26 days. Body weight was measured every 4 days as an indicator of toxicity. Animal experiments were performed in accordance with guidelines and approved by the ethical committee of the animal facility of Gustave Roussy Institute, Villejuif, France.

Live cell imaging

For quantification of mitotic entry, HeLa cells were transfected with control or ATIP3 siRNAs for 24 h then synchronized using double thymidine block. Cells were released in the presence or absence of 500 nM AZD1775 and filmed using an incucyte at a magnification of 10x every 10 minutes for 6 h. For fluorescent live cell imaging, HeLa-mCherryH2B cells were transfected for 48 h with control or ATIP3 siRNAs, then incubated with siR-Tubulin dye (10 nM) prior to treatment with 500 nM AZD1775. Cells were imaged using a confocal laser scanning microscope TCS SP8 MP (Leica) using a dry 40X objective, every 6 min for 48 h. Image analysis was performed using ImageJ software.

Immunofluorescence

Transfected cells were seeded on coverslips one day before treatment. For the analysis of mitotic phenotypes, cells were fixed with ice-cold methanol for 5 min then washed with PBS. For γH2AX and 53BP1 analysis, cells were fixed with 4% paraformaldehyde for 15 min then washed with PBS and permeabilized with 0.5% Triton X-100 in PBS for 30 min. For the analysis of phosphorylated RPA32, cells were pre-extracted using ice-cold 0.2% Triton X-100 for 1 min then fixed with 4% paraformaldehyde and permeabilized. Coverslips were subsequently blocked with 3% BSA in PBS for 1 h at room temperature and incubated with primary antibodies overnight at 4°C. Coverslips were washed with 3% BSA in PBS and incubated with Alexa Fluor-coupled secondary antibodies for 45 min at room temperature. Coverslips were counterstained with DAPI (1/1000) and mounted using FluorSave reagent (Millipore).

For detection of cells in S-phase, EdU incorporation was analyzed using the Click-iT EdU immunofluorescence kit (Invitrogen) according to the manufacturer's instructions. Cells were pulse labeled with 10 μM EdU for 30 min, fixed and subjected to the Click-iT reaction. The cells were then processed for immunofluorescence staining as described.

For immunofluorescence in 3D, MCSs were harvested and fixed in 4% paraformaldehyde, 0.5% Triton X-100 in PBS for 45 minutes, blocked in 3% BSA, 0.5% Triton X-100 in PBS overnight at 4°C and incubated 24 h in primary antibodies and overnight in secondary antibodies. MCSs were deposited onto slides and sealed with mounting media and coverslips.

The following primary antibodies were used: rabbit anti-pericentrin (ab4448; Abcam, 1/1000), rat anti-alpha-tubulin (ab6160; Abcam, 1/1000), rabbit anti-CENP-B (ab25734, Abcam, 1/1000), mouse anti-CENP-A (ADI-KAM-CC006-E, ENZO, 1/1000), human ACA (AB_2939058, Antibodies Inc., 1/2000), mouse γH2AX (05-630, Millipore, 1/1000), rabbit anti-53BP1 (ab172580, abcam 1/1000), RPA32 phospho S4/S8 (A300-245A, Bethyl, 1/1000), rabbit anti-phospho-histone H3 (06-570, Millipore, 1/1000). All secondary antibodies (Alexa Fluor dyes) were purchased from Jackson Immunoresearch.

Chromosome spreads and FISH

Transfected cells were seeded on coverslips at low density (30% confluency) one day before treatment. Colcemid (KaryoMAX, Gibco) was added to culture media 6 h before spreading at a final concentration of 0.1 μg/ml. Media was replaced with KCl buffer (75 mM) for 10 min at room temperature. Coverslips were centrifuged at 1800 rpm for 3 minutes and fixed with 4%

paraformaldehyde, blocked with 3% BSA 0,1% Triton X-100 in PBS for 30 min at room temperature then immunofluorescence was performed as previously described. IF-FISH for CENP-B box detection was modified from Chardon *et al.*[45]. Briefly, immunofluorescence was performed and cells were post-fixed in 2% formaldehyde for 10 mins. Cells were fixed in Carnoy's fixative for 15 min, rinsed in 80% ethanol and air-dried. Coverslips were incubated with CENP-B box probe-Cy3 (PNAbio) 1:1 in hybridization buffer (20mM Tris, pH 7.4, 60% formamide, 0.5% of blocking reagent (Roche 11096176001)). Samples and probes were denatured by heating on 75°C for 2 mins and incubated at 37°C overnight. Coverslips were washed with 0.4X SSC, counterstained with DAPI (1/1000) and mounted using FluorSave reagent (Millipore).

Image acquisition and analysis

Images were acquired with a confocal laser scanning microscope Dmi8- SP8 using a 63X objective. 5 to 10 fields were imaged/treatment. The pinhole diameter was set at 1 airy unit for all channels, and the exposure gain for each channel was kept constant in between image acquisition of all samples. Z-stack projection and image analysis was done using LAS-X analysis software. For intensity analysis (phosphorylated RPA32, γH2AX, EdU and DAPI), background was subtracted and areas of interest (nuclei) were delineated by ROIs. Mean intensities of each channel were calculated as the arithmetic mean of the determined gray-scale values in each ROI then normalized to DAPI mean intensities in the same ROI.

Quantitative PCR

RNA extraction and reverse transcription were performed as previously described[17]. Briefly, RNA was isolated using TRIzol reagent (Thermo Fisher). RNA concentration was assessed using a NanoDrop and Complementary DNA (cDNA) was generated using Superscript II reverse transcriptase (Thermo Fisher) following manufacturer's protocol.

Quantitative real-time PCR was performed on a Viia7 real-time PCR machine (Thermo Fisher). Gene expression was normalized to RPL13. The following oligonucleotides were used for assessment of gene silencing efficiency:

ATIP3 (F: GGCGGAACAGTGACAATA; R: GCAAATTCACCCATGACGA);

DNA2 (F: GATTTCTGGCACCAGCATAGCC; R: ACACCTCATGGAGAACCGTACC);

EXO1 (F: TCGGATCTCCTAGCTTTTGGCTG; R: AGCTGTCTGCACATTCCTAGCC);

MRE11 (F: CAGCAACCAACAAAGGAAGAGGC; R: GAGTTCCTGCTACGGGTAGAAG);

MUS81 (F: GATCCTACAGCACTTCGGAGAC; R: AAGAGTCCTGGACTTCCGCAAG);

WEE1 (F: GATGTGCGACAGACTCCTCAAG; R: CTGGCTTCCATGTCTTCACCAC).

Western blotting

Cells were lysed using RIPA buffer containing a cocktail of protease and phosphatase inhibitors. Protein lysates were denatured in Laemmli buffer, separated by SDS–PAGE and transferred onto a PVDF membrane. After blocking with 5% BSA in TBS-0.1% Tween-20, membranes were incubated with the following primary antibodies: rabbit anti-ATIP3 (Aviva ARP44419-P050, 1/1000), anti-phospho-histone H3 (06-570; Millipore, 1/1000), anti-phospho-tyrosine 15 Cdk1 (Cell Signaling Technology; 9111; 1:1,000 dilution), anti-CDK1 phosphorylated substrates (Cell signaling, 1/1000), rat anti-alpha-tubulin (ab6160; Abcam, 1/20000), goat anti-GAPDH (Novus biologicals, 1/50000). Proteins were visualized using horseradish-peroxidase-conjugated secondary antibodies followed by chemiluminescence detection with ECL (Clarity Western ECL substrate, Bio-Rad).

Statistical analysis

All statistical analysis was performed using GraphPad Prism 9 software. Statistical significance between two groups was determined using two-tailed t-test. When more than two groups were compared, statistical significance was determined using one or two-way ANOVA or Kruskal-Wallis when data distribution did not pass normality tests. P-values < 0.05 were considered significant.

References

1. Panagopoulos, A. & Altmeyer, M. The Hammer and the Dance of Cell Cycle Control. *Trends Biochem. Sci.* **46**, 301–314 (2021).

2. Hanahan, D. & Weinberg, R. A. Hallmarks of Cancer: The Next Generation. *Cell* **144**, 646–674 (2011).

3. Gordon, D. J., Resio, B. & Pellman, D. Causes and consequences of aneuploidy in cancer. *Nat. Rev. Genet.* **13**, 189–203 (2012).

4. Taylor, A. M. *et al.* Genomic and Functional Approaches to Understanding Cancer Aneuploidy. *Cancer Cell* **33**, 676-689.e3 (2018).

5. Torres, E. M. *et al.* Effects of Aneuploidy on Cellular Physiology and Cell Division in Haploid Yeast. *Science* **317**, 916–924 (2007).

6. Janssen, A., van der Burg, M., Szuhai, K., Kops, G. J. P. L. & Medema, R. H. Chromosome Segregation Errors as a Cause of DNA Damage and Structural Chromosome Aberrations. *Science* **333**, 1895–1898 (2011).

7. Ohashi, A. *et al.* Aneuploidy generates proteotoxic stress and DNA damage concurrently with p53-mediated post-mitotic apoptosis in SAC-impaired cells. *Nat. Commun.* **6**, 7668 (2015).

8. Sheltzer, J. M. & Amon, A. The aneuploidy paradox: costs and benefits of an incorrect karyotype. *Trends Genet.* **27**, 446–453 (2011).

9. Ferlay, J. *et al.* Cancer statistics for the year 2020: An overview. *Int. J. Cancer* **149**, 778–789 (2021).

10. Koboldt, D. C. *et al.* Comprehensive molecular portraits of human breast tumours. *Nature* **490**, 61–70 (2012).

11. Stephens, P. J. *et al.* Complex landscapes of somatic rearrangement in human breast cancer genomes. *Nature* **462**, 1005–1010 (2009).

12. Ciriello, G. *et al.* Comprehensive Molecular Portraits of Invasive Lobular Breast Cancer. *Cell* **163**, 506–519 (2015).

13. Danielsen, H. E., Pradhan, M. & Novelli, M. Revisiting tumour aneuploidy — the place of ploidy assessment in the molecular era. *Nat. Rev. Clin. Oncol.* **13**, 291–304 (2016).

14. Pinto, A. E. *et al.* DNA Ploidy is an Independent Predictor of Survival in Breast Invasive Ductal Carcinoma: A Long-term Multivariate Analysis of 393 Patients. *Ann. Surg. Oncol.* **20**, 1530–1537 (2013).

15. Hieronymus, H. *et al.* Tumor copy number alteration burden is a pan-cancer prognostic factor associated with recurrence and death. *eLife* **7**, e37294 (2018).

16. Cohen-Sharir, Y. *et al.* Aneuploidy renders cancer cells vulnerable to mitotic checkpoint inhibition. *Nature* **590**, 486–491 (2021).

17. Rodrigues-Ferreira, S. *et al.* Improving breast cancer sensitivity to paclitaxel by increasing aneuploidy. *Proc. Natl. Acad. Sci.* **116**, 23691–23697 (2019).

18. Rodrigues-Ferreira, S. *et al.* 8p22 MTUS1 Gene Product ATIP3 Is a Novel Anti-Mitotic Protein Underexpressed in Invasive Breast Carcinoma of Poor Prognosis. *PLOS ONE* **4**, e7239 (2009).

19. Molina, A. *et al.* ATIP3, a Novel Prognostic Marker of Breast Cancer Patient Survival, Limits Cancer Cell Migration and Slows Metastatic Progression by Regulating Microtubule Dynamics. *Cancer Res.* **73**, 2905–2915 (2013).

20. Rodrigues-Ferreira, S. & Nahmias, C. From tumorigenesis to cell death: the aneuploidy paradox. *Mol. Cell. Oncol.* **7**, 1709390 (2020).

21. Scribano, C. M. *et al.* Chromosomal instability sensitizes patient breast tumors to multipolar divisions induced by paclitaxel. *Sci. Transl. Med.* **13**, eabd4811 (2021).

22. Matheson, C. J., Backos, D. S. & Reigan, P. Targeting WEE1 Kinase in Cancer. *Trends Pharmacol. Sci.* **37**, 872–881 (2016).

23. Parker, L. L. & Piwnica-Worms, H. Inactivation of the p34cdc2-Cyclin B Complex by the Human WEE1 Tyrosine Kinase. *Science* **257**, 1955–1957 (1992).

24. Domínguez-Kelly, R. *et al.* Wee1 controls genomic stability during replication by regulating the Mus81-Eme1 endonuclease. *J. Cell Biol.* **194**, 567–579 (2011).

25. Beck, H. *et al.* Cyclin-Dependent Kinase Suppression by WEE1 Kinase Protects the Genome through Control of Replication Initiation and Nucleotide Consumption. *Mol. Cell. Biol.* **32**, 4226–4236 (2012).

26. Santaguida, S., Tighe, A., D'Alise, A. M., Taylor, S. S. & Musacchio, A. Dissecting the role of MPS1 in chromosome biorientation and the spindle checkpoint through the small molecule inhibitor reversine. *J. Cell Biol.* **190**, 73–87 (2010).

27. Sansregret, L. *et al.* APC/C Dysfunction Limits Excessive Cancer Chromosomal Instability. *Cancer Discov.* **7**, 218–233 (2017).

28. Aarts, M. *et al.* Forced Mitotic Entry of S-Phase Cells as a Therapeutic Strategy Induced by Inhibition of WEE1. *Cancer Discov.* **2**, 524–539 (2012).

29. Tye, S., Ronson, G. E. & Morris, J. R. A fork in the road: Where homologous recombination and stalled replication fork protection part ways. *Genome Stab.* **113**, 14–26 (2021).

30. Zeman, M. K. & Cimprich, K. A. Causes and consequences of replication stress. *Nat. Cell Biol.* **16**, 2–9 (2014).

31. Bhowmick, R., Minocherhomji, S. & Hickson, I. D. RAD52 Facilitates Mitotic DNA Synthesis Following Replication Stress. *Mol. Cell* **64**, 1117–1126 (2016).

32. Lukas, C. *et al.* 53BP1 nuclear bodies form around DNA lesions generated by mitotic transmission of chromosomes under replication stress. *Nat. Cell Biol.* **13**, 243–253 (2011).

33. Cotta-Ramusino, C. *et al.* Exo1 Processes Stalled Replication Forks and Counteracts Fork Reversal in Checkpoint-Defective Cells. *Mol. Cell* **17**, 153–159 (2005).

34. Bryant, H. E. *et al.* PARP is activated at stalled forks to mediate Mre11-dependent replication restart and recombination. *EMBO J.* **28**, 2601–2615 (2009).

35. Thangavel, S. *et al.* DNA2 drives processing and restart of reversed replication forks in human cells. *J. Cell Biol.* **208**, 545–562 (2015).

36. Passerini, V. *et al.* The presence of extra chromosomes leads to genomic instability. *Nat. Commun.* **7**, 10754 (2016).

37. Santaguida, S. *et al.* Chromosome Mis-segregation Generates Cell-Cycle-Arrested Cells with Complex Karyotypes that Are Eliminated by the Immune System. *Dev. Cell* **41**, 638-651.e5 (2017).

38. Duda, H. *et al.* A Mechanism for Controlled Breakage of Under-replicated Chromosomes during Mitosis. *Dev. Cell* **39**, 740–755 (2016).

39. Nassar, R., Thompson, L. & Fouquerel, E. Molecular mechanisms protecting centromeres from self-sabotage and implications for cancer therapy. *NAR Cancer* **5**, zcad019 (2023).

40. Kosugi, S., Hasebe, M., Tomita, M. & Yanagawa, H. Systematic identification of cell cycle-dependent yeast nucleocytoplasmic shuttling proteins by prediction of composite motifs. *Proc. Natl. Acad. Sci.* **106**, 10171–10176 (2009).

41. Li, Z. *et al.* hDNA2 nuclease/helicase promotes centromeric DNA replication and genome stability. *EMBO J.* **37**, e96729 (2018).

42. Lewis, C. W. *et al.* Prolonged mitotic arrest induced by Wee1 inhibition sensitizes breast cancer cells to paclitaxel. *Oncotarget Vol 8 No 43* (2017).

43. Lewis, C. W. *et al.* Upregulation of Myt1 Promotes Acquired Resistance of Cancer Cells to Wee1 Inhibition. *Cancer Res.* **79**, 5971–5985 (2019).

44. Bukhari, A. B. *et al.* Inhibiting Wee1 and ATR kinases produces tumor-selective synthetic lethality and suppresses metastasis. *J. Clin. Invest.* **129**, 1329–1344 (2019).

45. Chardon, F. *et al.* CENP-B-mediated DNA loops regulate activity and stability of human centromeres. *Mol. Cell* **82**, 1751-1767.e8 (2022).

Acknowledgments

We thank the Inserm, the CNRS, the Gustave Roussy cancer center, the Ligue Nationale Contre le cancer (LNCC), the associations Odyssea and Prolific, the Fondation Janssen Horizon, the Fondation Rothschild, the Ruban Rose association and the Taxe d'apprentissage of Gustave Roussy for financial support. This work has benefited from the facilities and expertise of PETRA (Nicolas Signolle), PFIC (Tudor Manoliu) and PFEP (Mélanie Polrot) platforms of the UMS AMMICa (CNRS UMS 3655 / Inserm US 23) - Gustave Roussy Cancer Campus Villejuif, France. Authors acknowledge help from Dr Daniele Fachinetti (Institut Curie, Paris, France) and Dr Michele Debatisse (Gustave Roussy, Villejuif, France) for providing reagents and Marianne Oulhen (Gustave Roussy, Villejuif, France) for technical assistance. We thank Dr Sophie Polo (Institut d'Epigénétique, Paris, France), Dr Daniele Fachinetti, Dr Renata Basto (Institut Curie, Paris, France), Dr Olivier Gavet and Dr Valeria Naim (Gustave Roussy, Villejuif, France) for constructive discussion throughout the project.

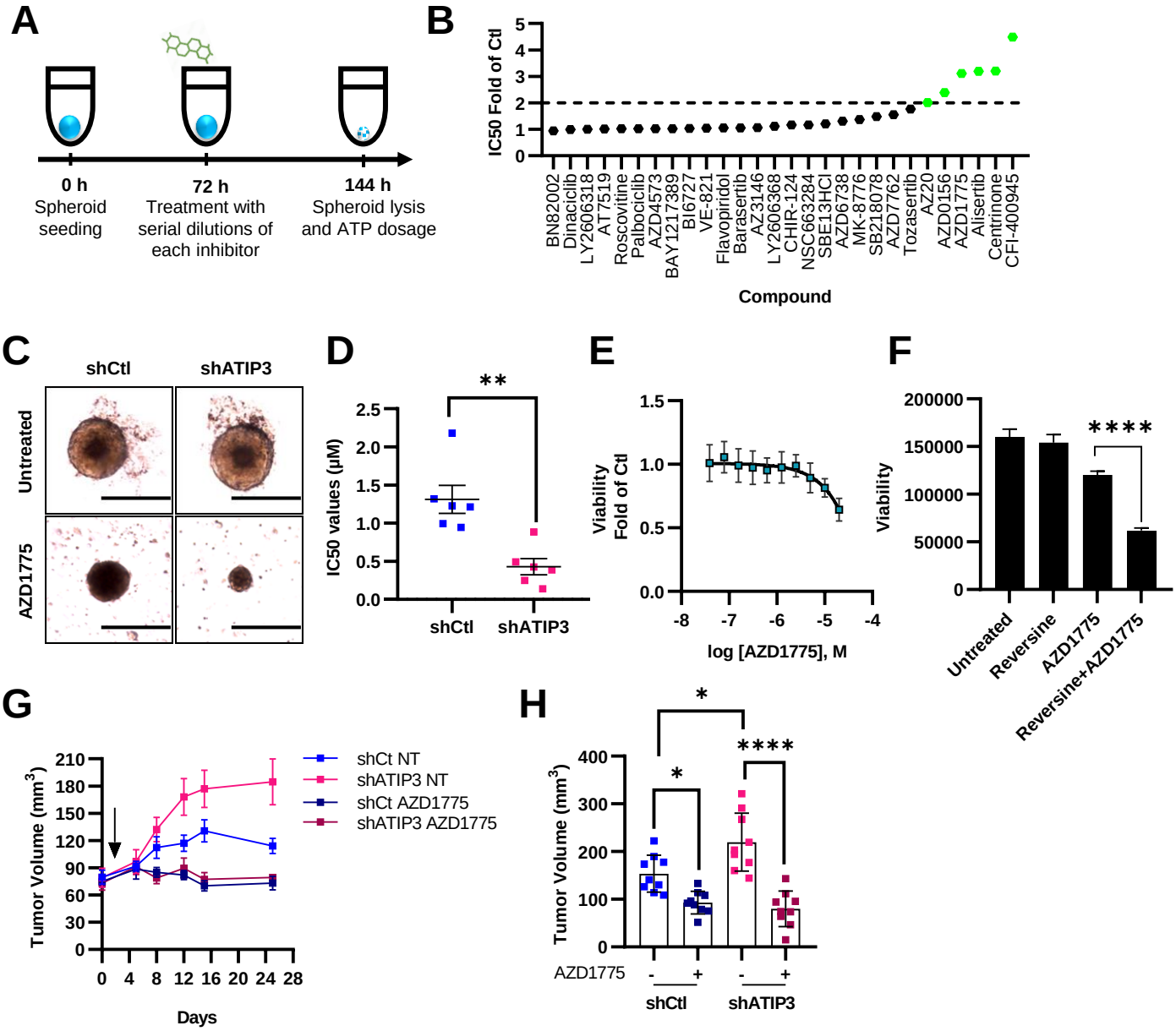
A
0 h
Spheroid seeding
72 h
Treatment with serial dilutions of each inhibitor
144 h
Spheroid lysis and ATP dosage
B
IC50 Fold of Ctl
BN82002
Dinaciclib
LY2606318
AT7519
Roscovitine
Palbociclib
AZD4573
BAY1217389
BI6727
VE-821
Flavopiridol
Barasertib
AZ3146
LY2606368
CHIR-124
NSC663284
SBE13HCl
AZD6738
MK-8776
SB218078
AZD7762
Tozasertib
AZ20
AZD0156
AZD1775
Alisertib
Centrinone
CFI-400945
Compound
C
shCtl
shATIP3
Untreated
AZD1775
D
IC50 values (µM)
shCtl
shATIP3
E
Viability Fold of Ctl
log [AZD1775], M
F
Viability
Untreated
Reversine
AZD1775
Reversine+AZD1775
G
Tumor Volume (mm3)
Days
shCt NT
shATIP3 NT
shCt AZD1775
shATIP3 AZD1775
H
Tumor Volume (mm3)
AZD1775
shCtl
shATIP3

Figure 1

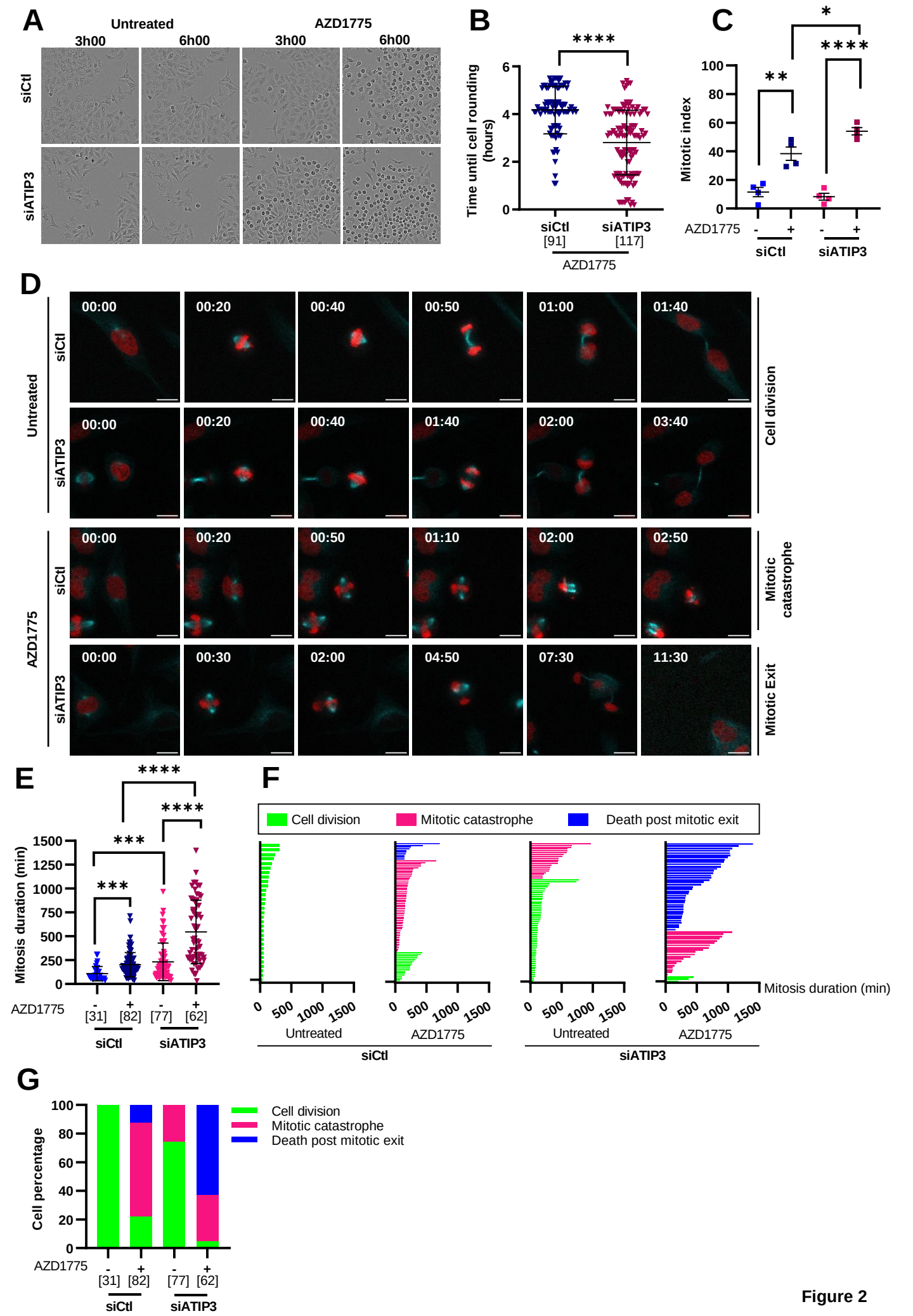
A
Untreated
AZD1775
3h00
6h00
3h00
6h00
siCtl
siATIP3
B
****
Time until cell rounding (hours)
siCtl
[91]
siATIP3
[117]
AZD1775
C
*
****
**
Mitotic index
AZD1775
siCtl
siATIP3
D
Untreated
AZD1775
siCtl
siATIP3
00:00
00:20
00:40
00:50
01:00
01:40
02:00
03:40
01:10
02:50
00:30
02:00
04:50
07:30
11:30
Cell division
Mitotic catastrophe
Mitotic Exit
E
****
***
Mitosis duration (min)
AZD1775
[31]
[82]
[77]
[62]
siCtl
siATIP3
F
Cell division
Mitotic catastrophe
Death post mitotic exit
Mitosis duration (min)
Untreated
AZD1775
siCtl
siATIP3
G
Cell percentage
Cell division
Mitotic catastrophe
Death post mitotic exit
AZD1775
[31]
[82]
[77]
[62]
siCtl
siATIP3

Figure 2

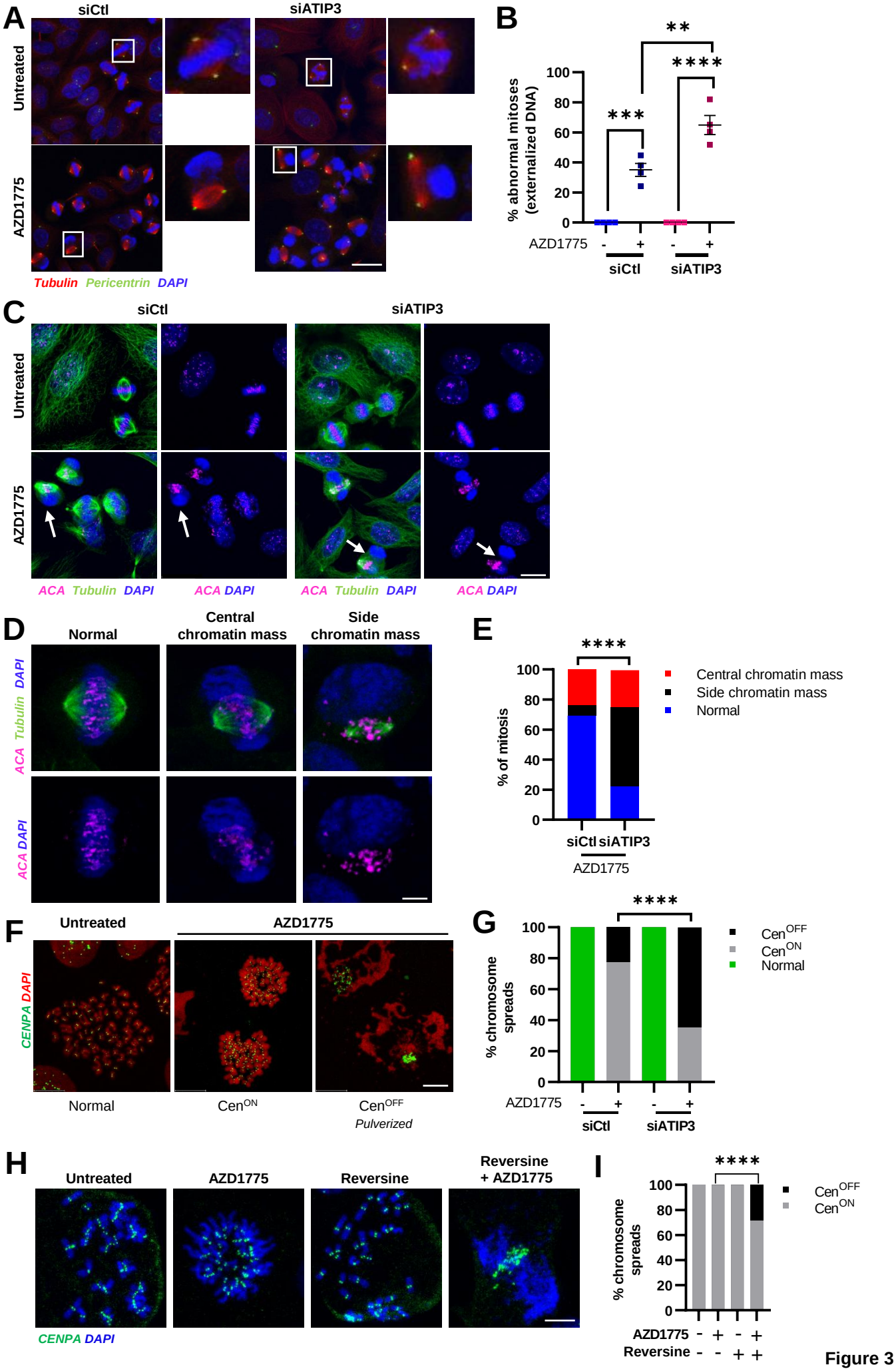
A
siCtl
siATIP3
Untreated
AZD1775
Tubulin Pericentrin DAPI
B
% abnormal mitoses (externalized DNA)
AZD1775
siCtl
siATIP3
C
siCtl
siATIP3
Untreated
AZD1775
ACA Tubulin DAPI
ACA DAPI
D
Normal
Central chromatin mass
Side chromatin mass
DAPI
Tubulin
ACA
E
% of mitosis
Central chromatin mass
Side chromatin mass
Normal
siCtl siATIP3
AZD1775
F
Untreated
AZD1775
CENPA DAPI
Normal
Cen^ON
Cen^OFF
Pulverized
G
% chromosome spreads
Cen^OFF
Cen^ON
Normal
AZD1775
siCtl
siATIP3
H
Untreated
AZD1775
Reversine
Reversine + AZD1775
CENPA DAPI
I
% chromosome spreads
Cen^OFF
Cen^ON
AZD1775
Reversine

Figure 3

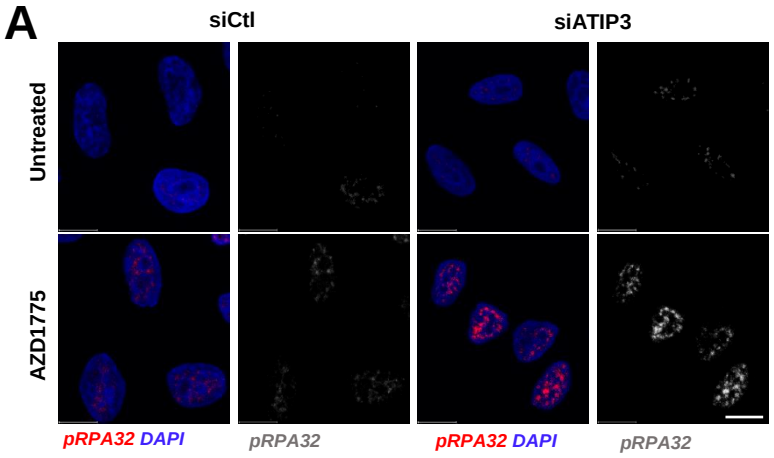
A
siCtl
siATIP3
Untreated
AZD1775
pRPA32 DAPI
pRPA32
pRPA32 DAPI
pRPA32

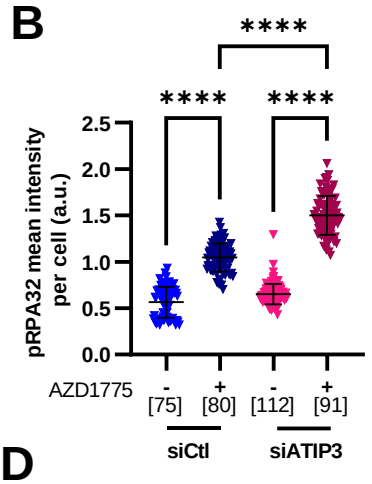
B
****
****
****
pRPA32 mean intensity per cell (a.u.)
2.5
2.0
1.5
1.0
0.5
0.0
AZD1775
-
+
-
+
[75]
[80]
[112]
[91]
siCtl
siATIP3

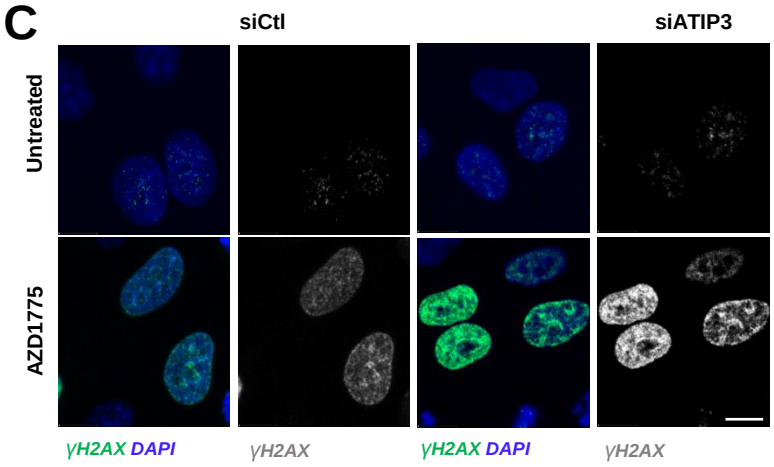
C
siCtl
siATIP3
Untreated
AZD1775
γH2AX DAPI
γH2AX
γH2AX DAPI
γH2AX

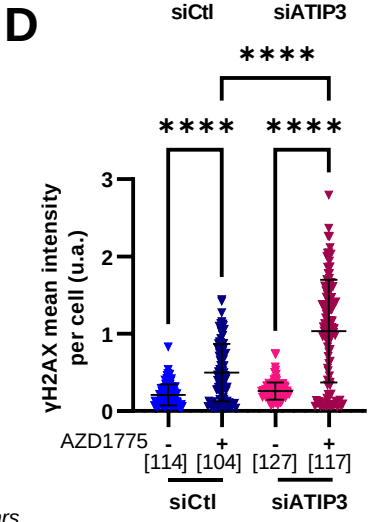
D
****
****
****
γH2AX mean intensity per cell (u.a.)
3
2
1
0
AZD1775
-
+
-
+
[114]
[104]
[127]
[117]
siCtl
siATIP3

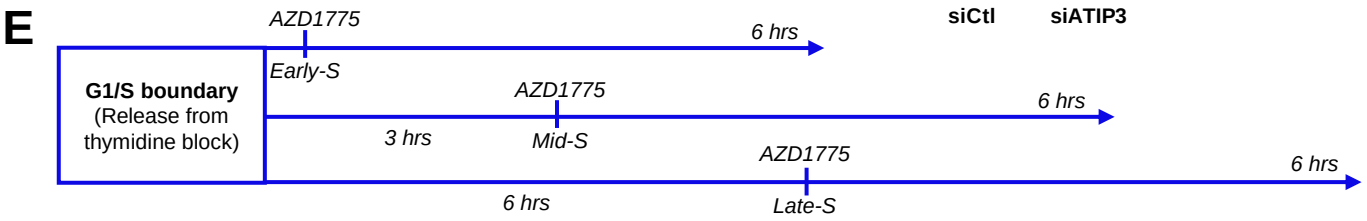
E
AZD1775
6 hrs
Early-S
G1/S boundary
(Release from
thymidine block)
AZD1775
6 hrs
3 hrs
Mid-S
AZD1775
6 hrs
6 hrs
Late-S

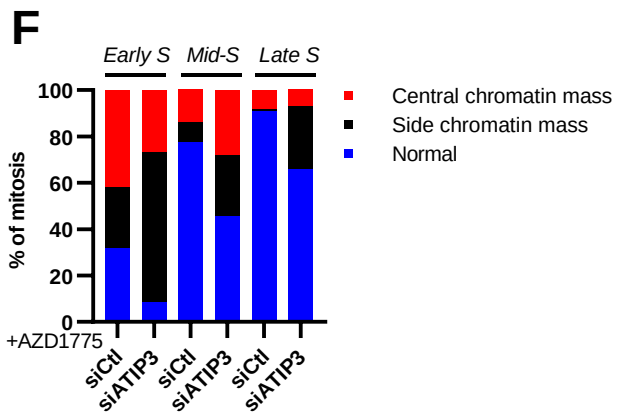
F
Early S
Mid-S
Late S
% of mitosis
100
80
60
40
20
0
Central chromatin mass
Side chromatin mass
Normal
+AZD1775
siCtl
siATIP3
siCtl
siATIP3
siCtl
siATIP3

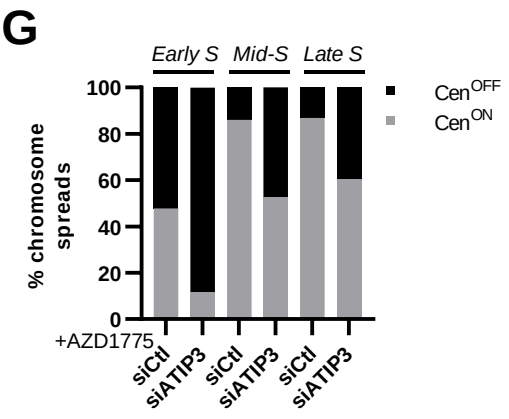
G
Early S
Mid-S
Late S
% chromosome spreads
100
80
60
40
20
0
CenOFF
CenON
+AZD1775
siCtl
siATIP3
siCtl
siATIP3
siCtl
siATIP3

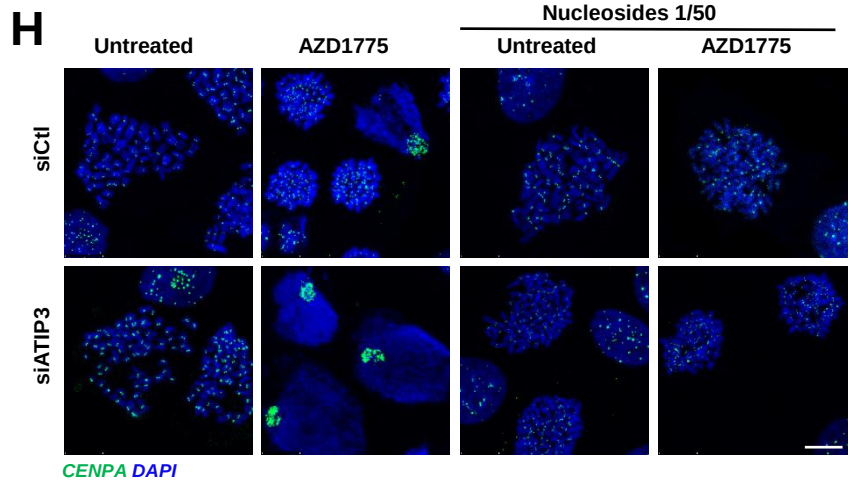
H
Nucleosides 1/50
Untreated
AZD1775
Untreated
AZD1775
siCtl
siATIP3
CENPA DAPI

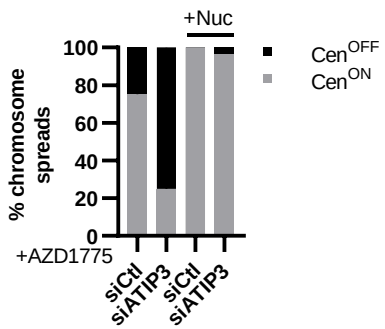
I
+Nuc
% chromosome spreads
100
80
60
40
20
0
CenOFF
CenON
+AZD1775
siCtl
siATIP3
siCtl
siATIP3

Figure 4

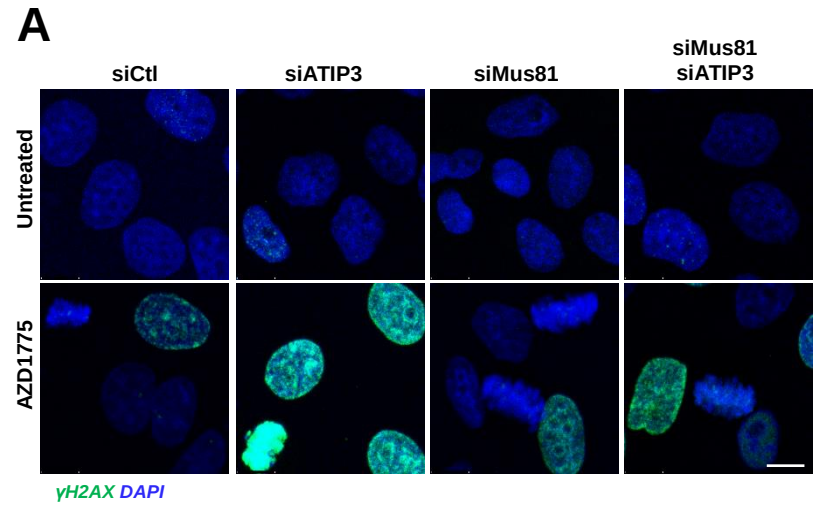
A
siCtl
siATIP3
siMus81
siMus81 siATIP3
Untreated
AZD1775
γH2AX DAPI

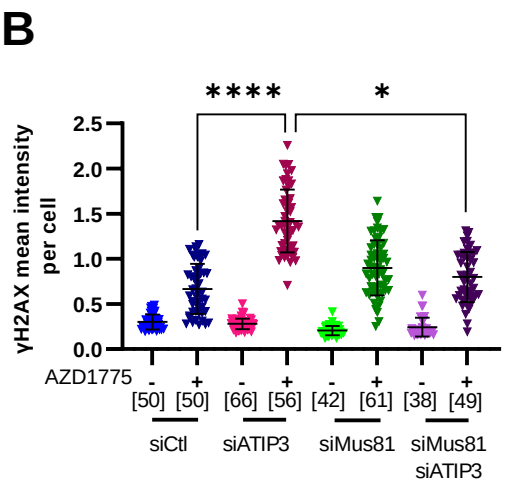
B
****
*
γH2AX mean intensity per cell
2.5
2.0
1.5
1.0
0.5
0.0
AZD1775
- + - + - + - +
[50] [50] [66] [56] [42] [61] [38] [49]
siCtl
siATIP3
siMus81
siMus81 siATIP3

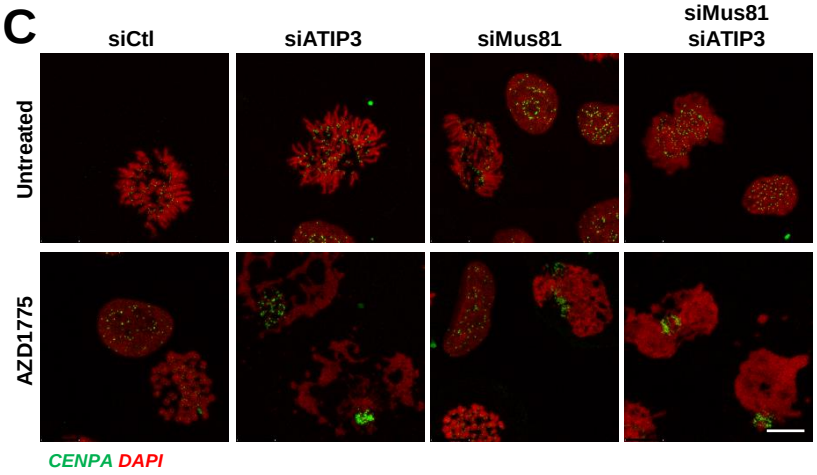
C
siCtl
siATIP3
siMus81
siMus81 siATIP3
Untreated
AZD1775
CENPA DAPI

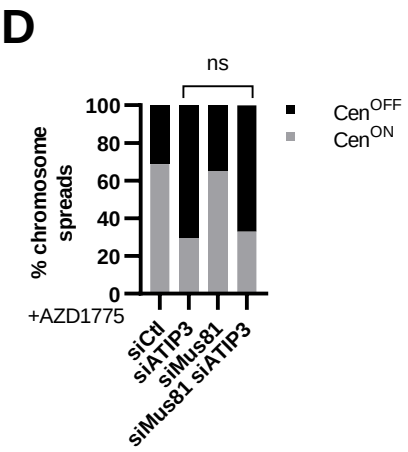
D
ns
% chromosome spreads
100
80
60
40
20
0
+AZD1775
Cen^OFF
Cen^ON
siCtl
siATIP3
siMus81
siMus81 siATIP3

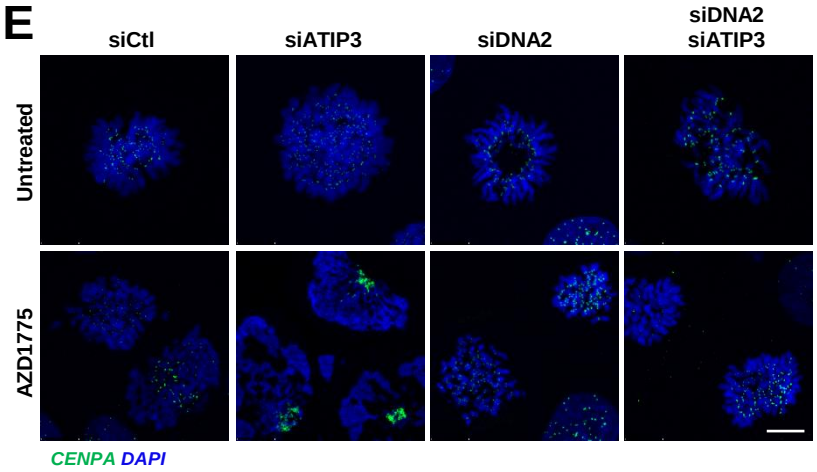
E
siCtl
siATIP3
siDNA2
siDNA2 siATIP3
Untreated
AZD1775
CENPA DAPI

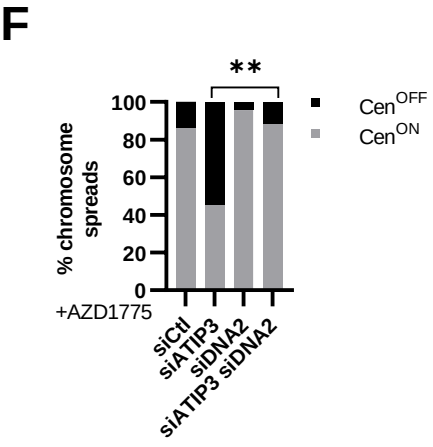
F
**
% chromosome spreads
100
80
60
40
20
0
+AZD1775
Cen^OFF
Cen^ON
siCtl
siATIP3
siDNA2
siATIP3 siDNA2

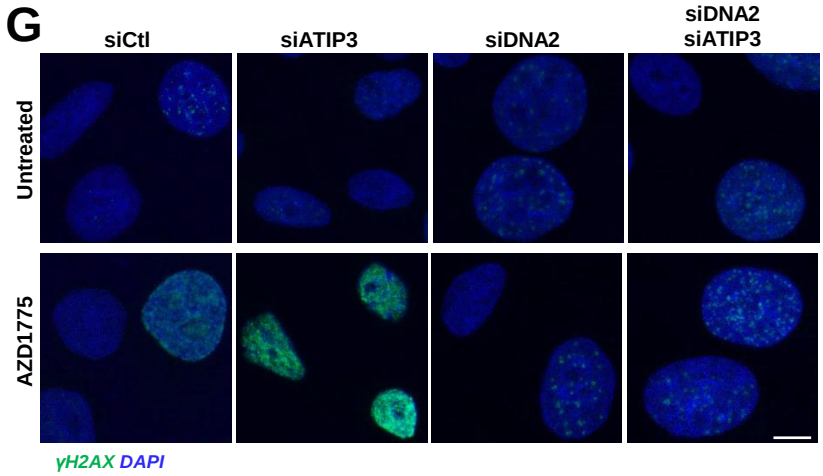
G
siCtl
siATIP3
siDNA2
siDNA2 siATIP3
Untreated
AZD1775
γH2AX DAPI

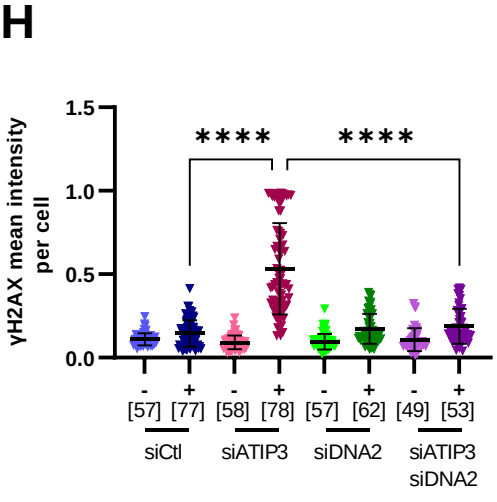
H
****
****
γH2AX mean intensity per cell
1.5
1.0
0.5
0.0
- + - + - + - +
[57] [77] [58] [78] [57] [62] [49] [53]
siCtl
siATIP3
siDNA2
siATIP3 siDNA2

Figure 5

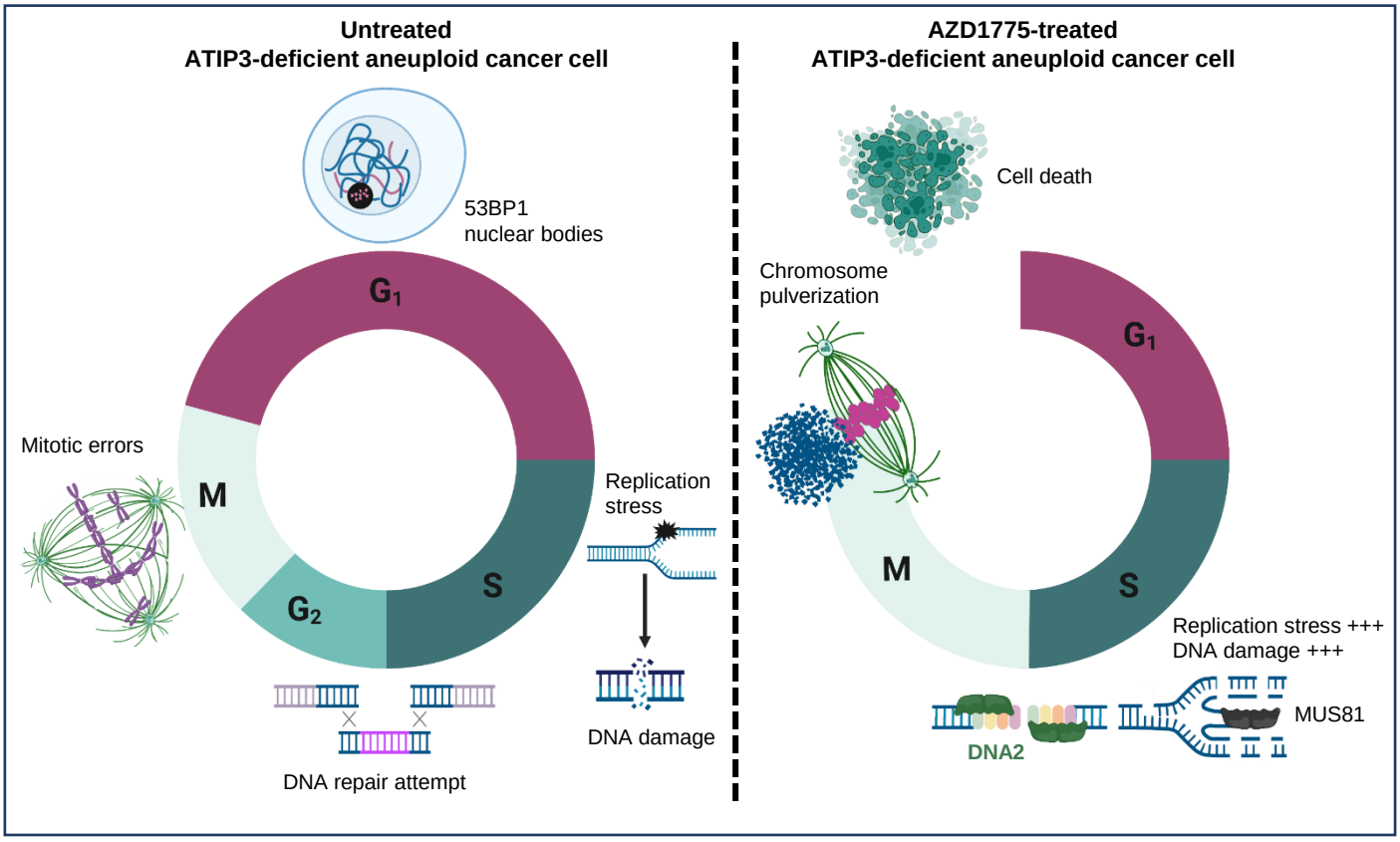
Untreated
ATIP3-deficient aneuploid cancer cell
53BP1
nuclear bodies
G1
S
G2
M
Mitotic errors
Replication
stress
DNA damage
DNA repair attempt
AZD1775-treated
ATIP3-deficient aneuploid cancer cell
Cell death
Chromosome
pulverization
G1
S
M
Replication stress +++
DNA damage +++
DNA2
MUS81

Figure 6

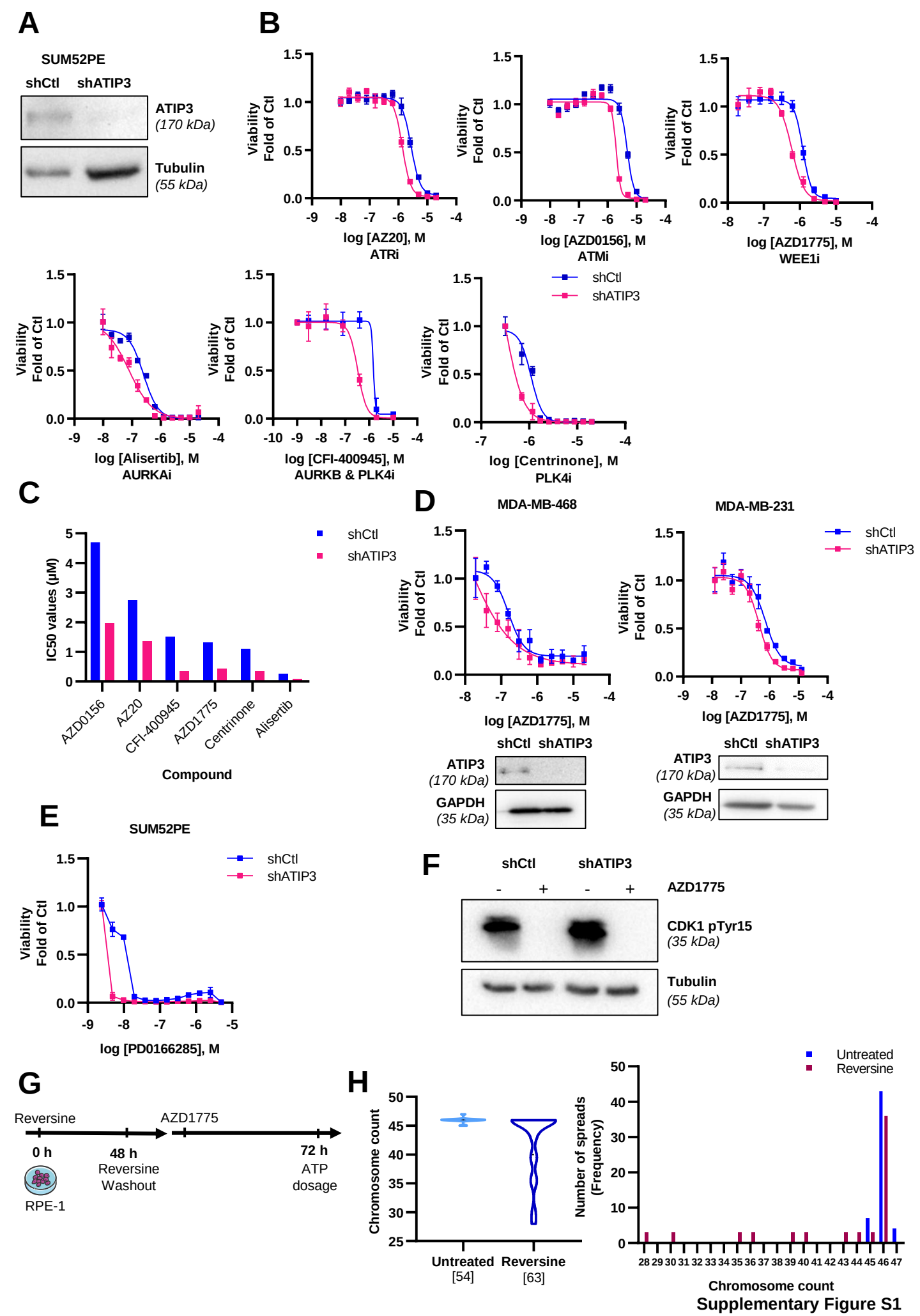

Supplementary Figure S1

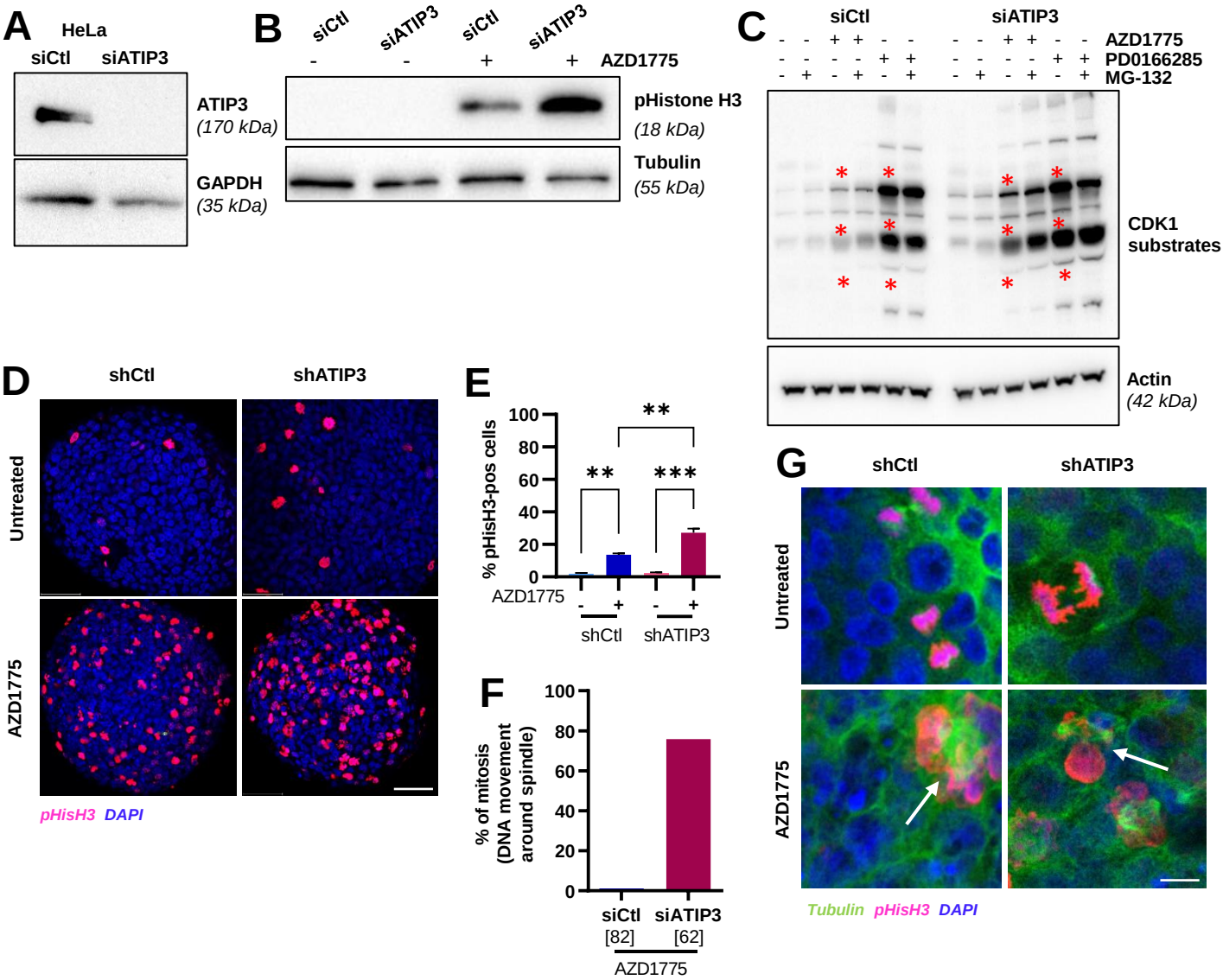

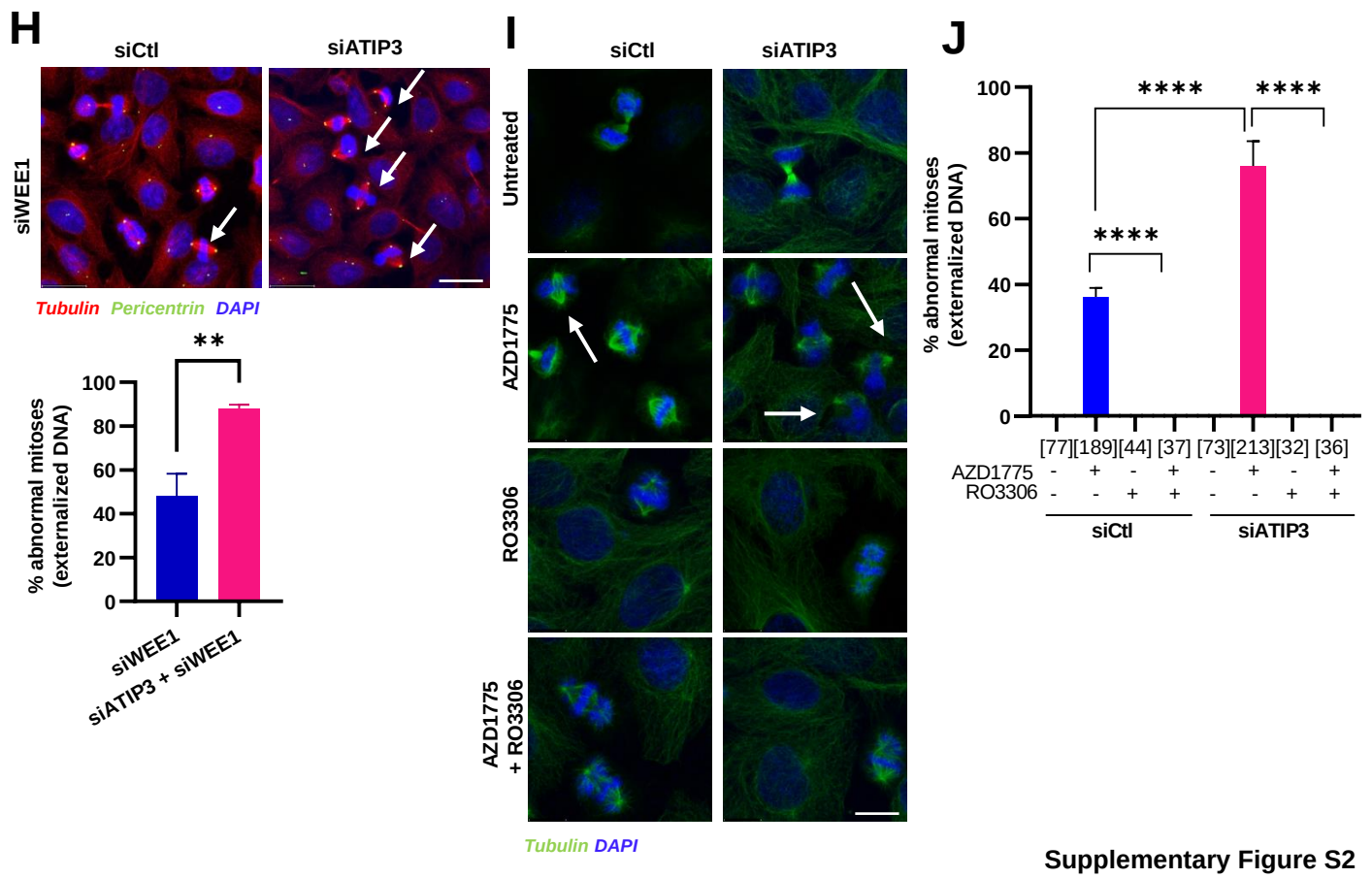

Supplementary Figure S2

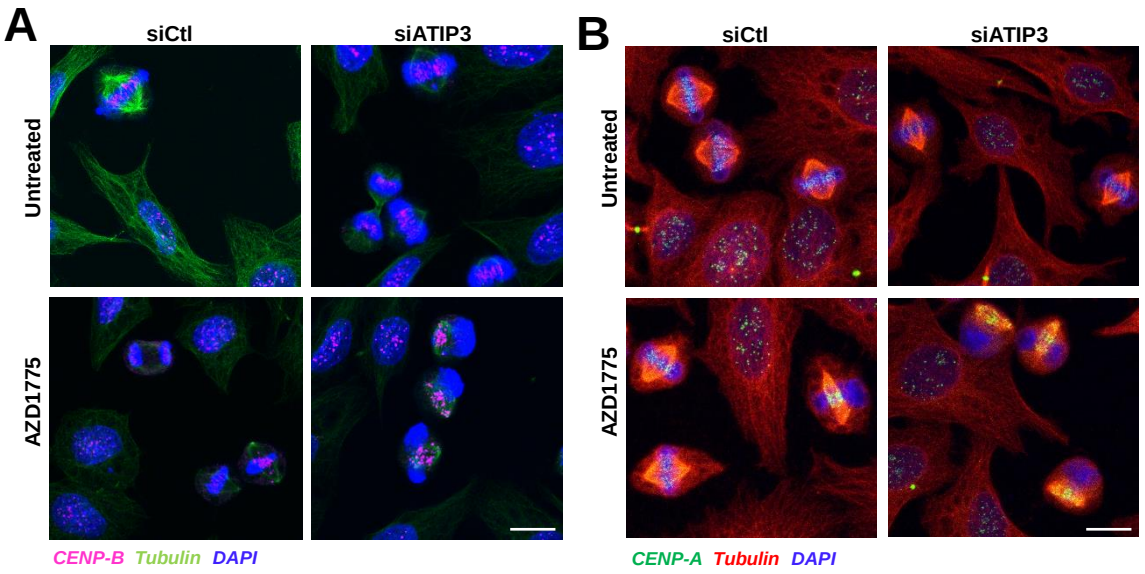

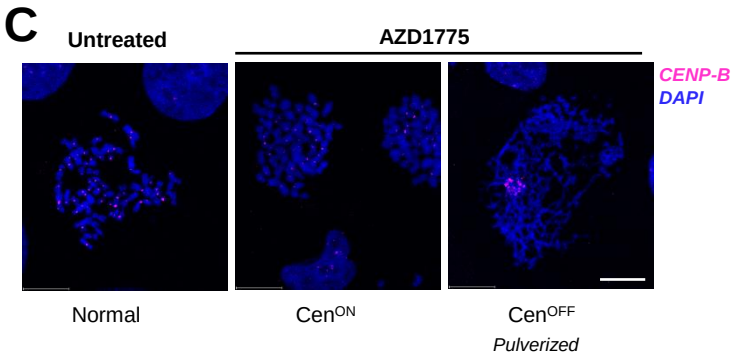

Supplementary Figure S3

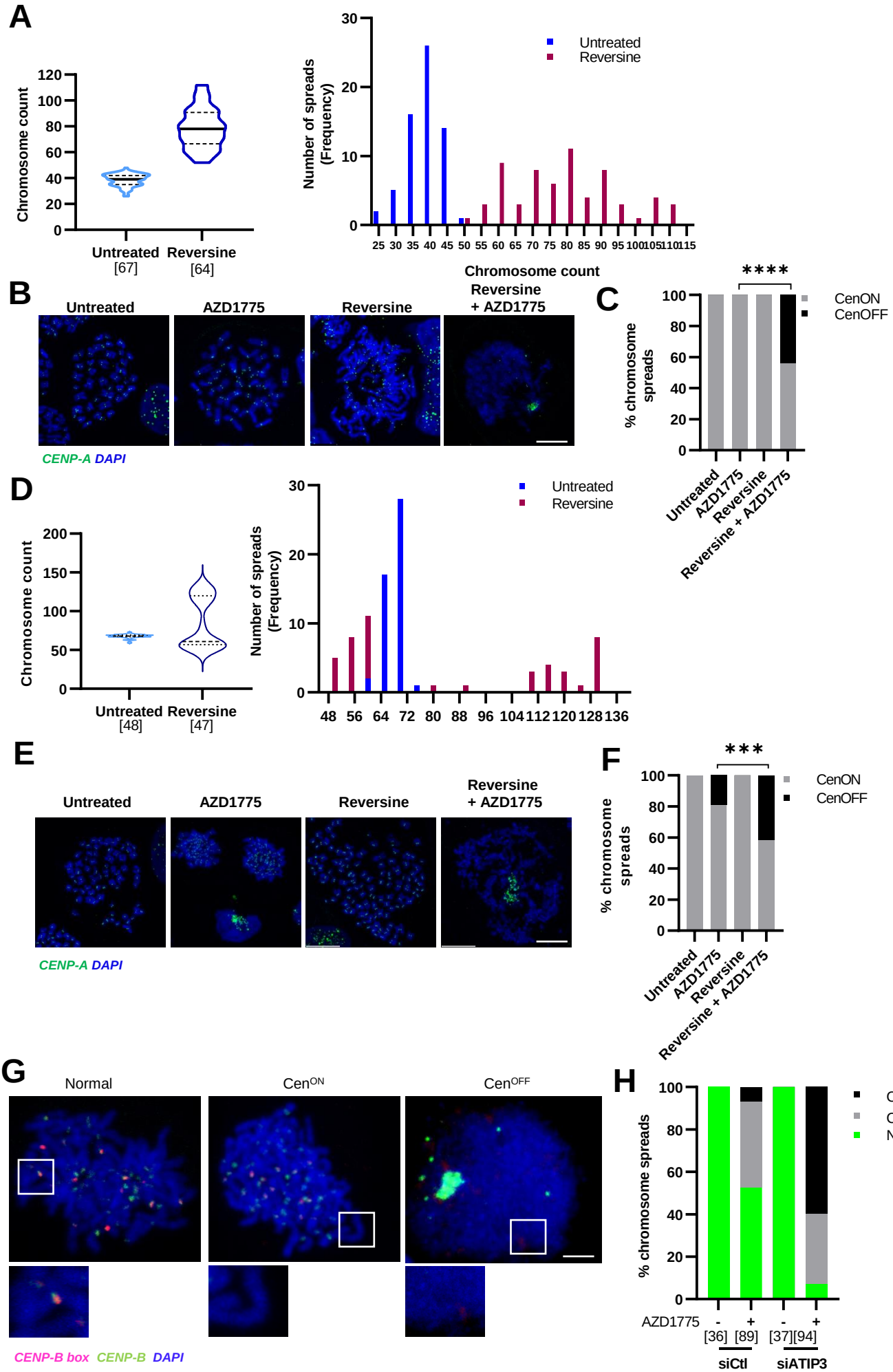

Supplementary Figure S4

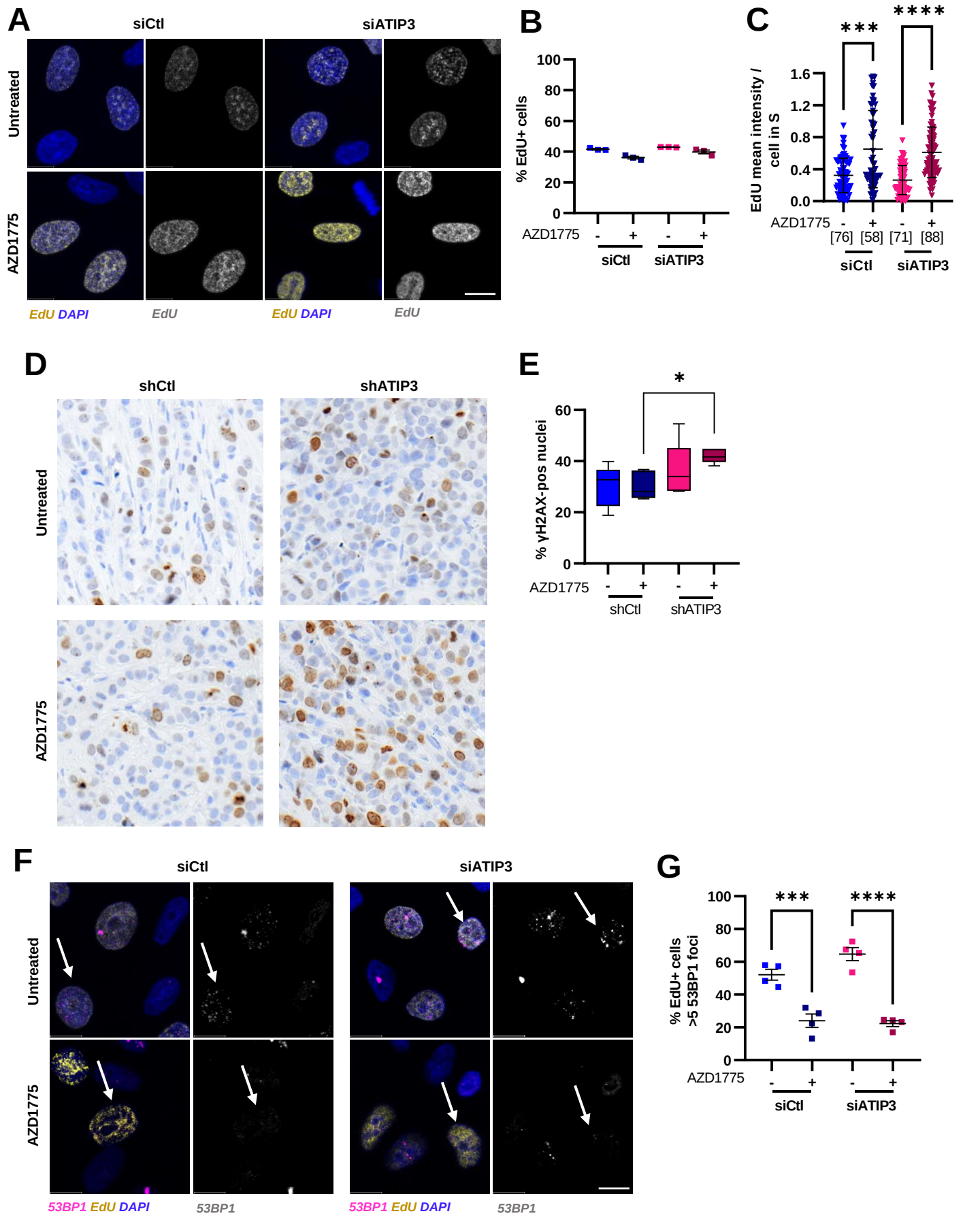

Supplementary Figure S5

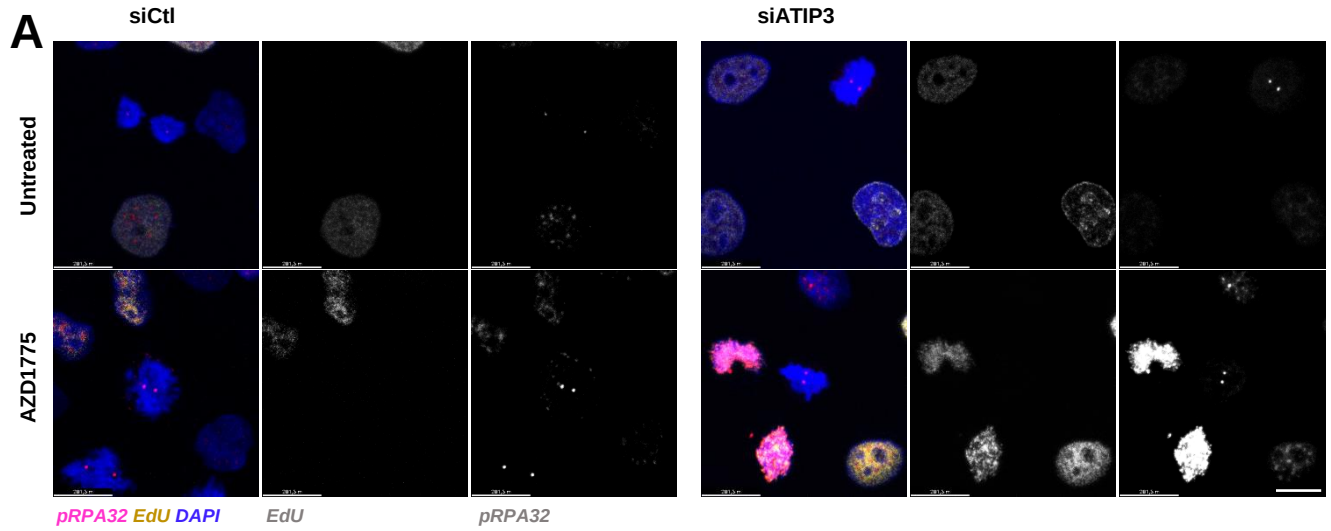

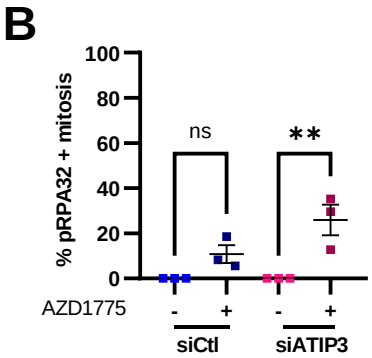

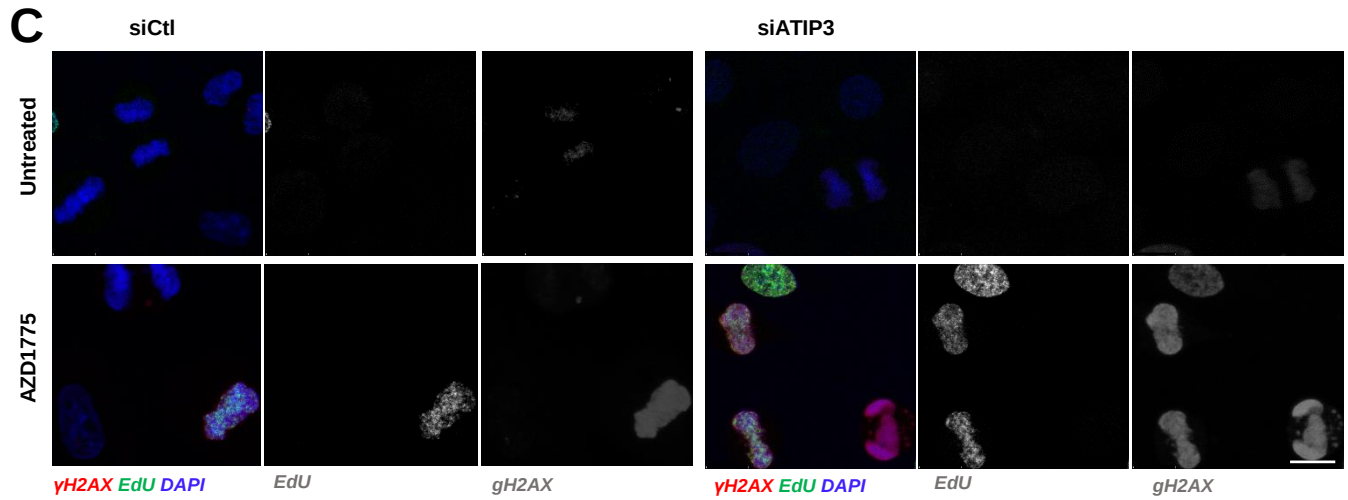

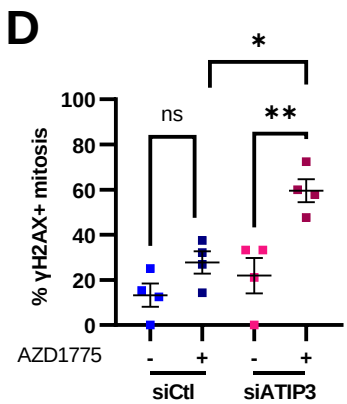

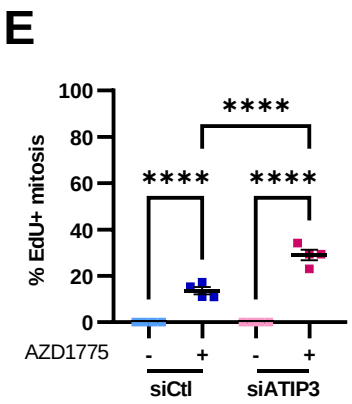

Supplementary Figure S6

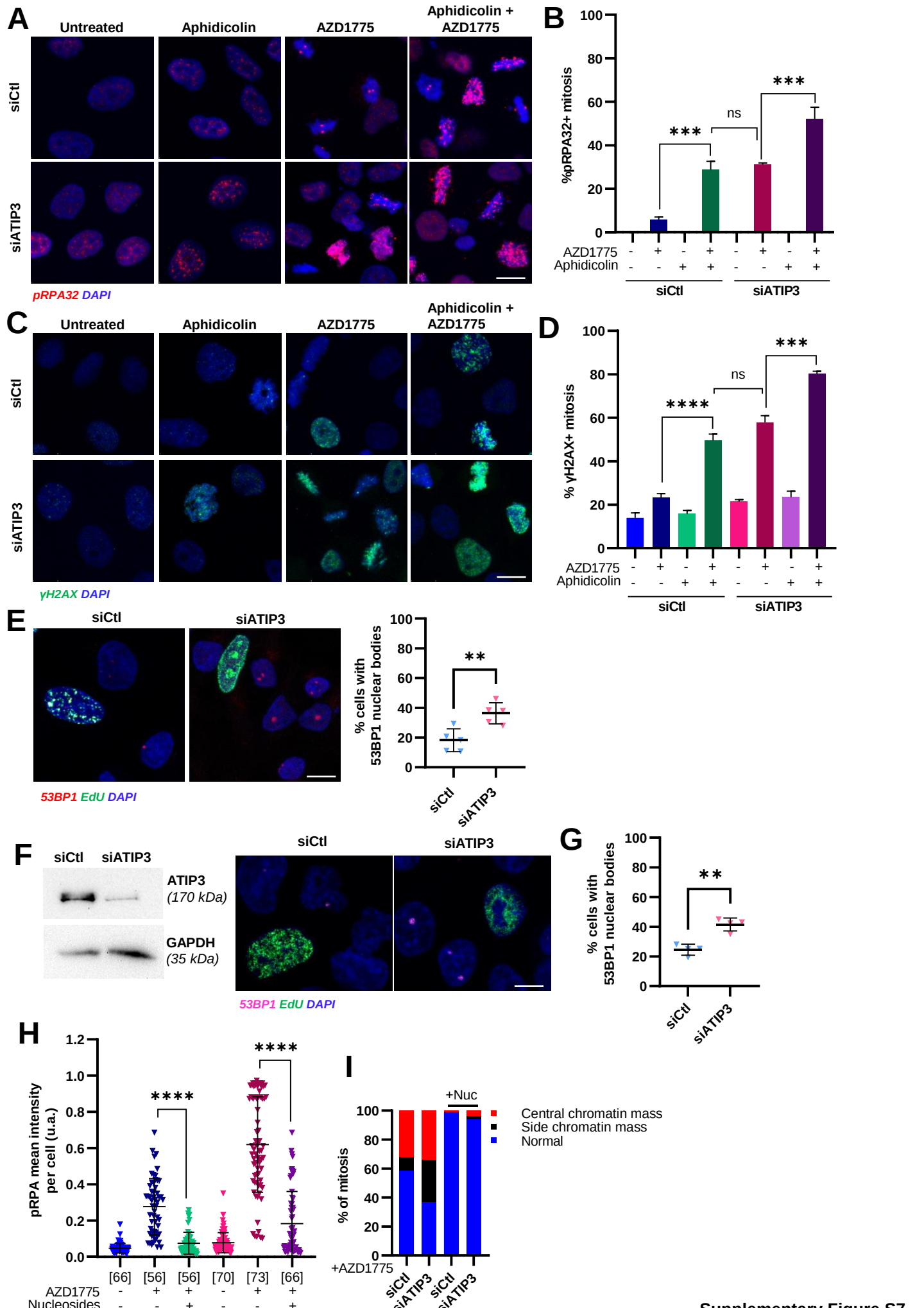

Supplementary Figure S7

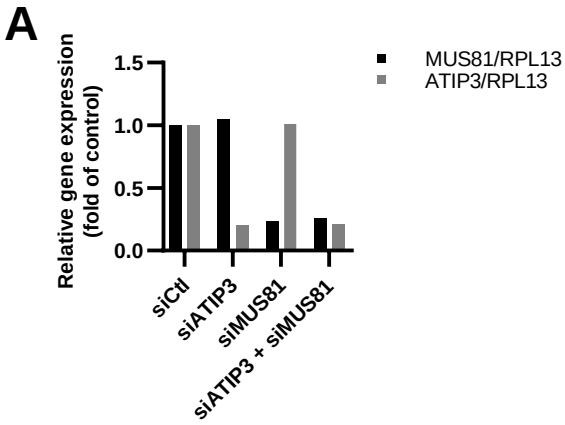

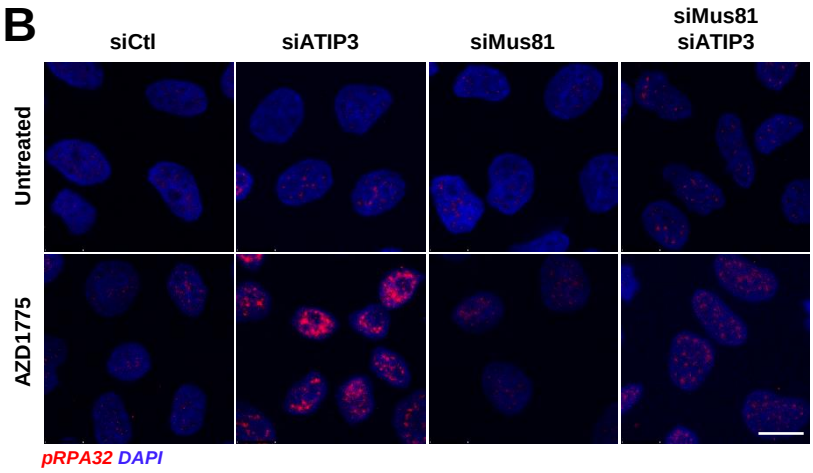

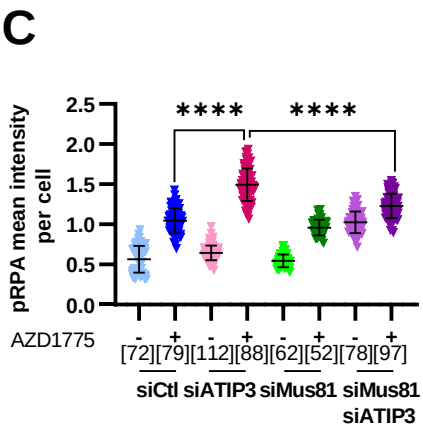

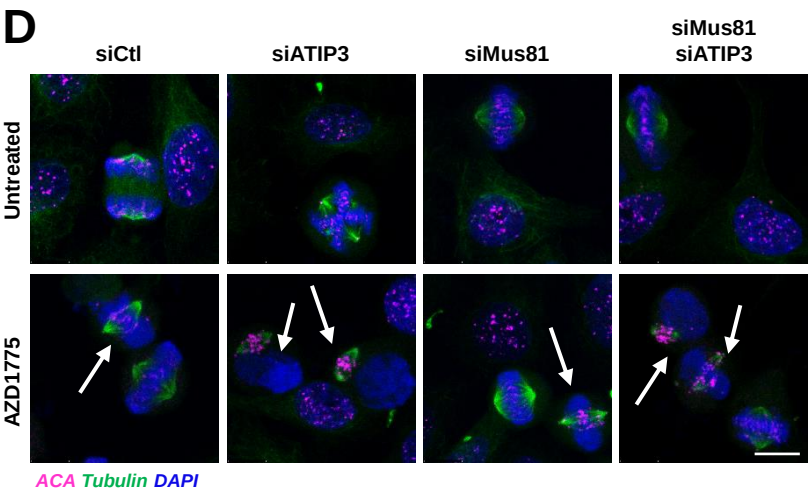

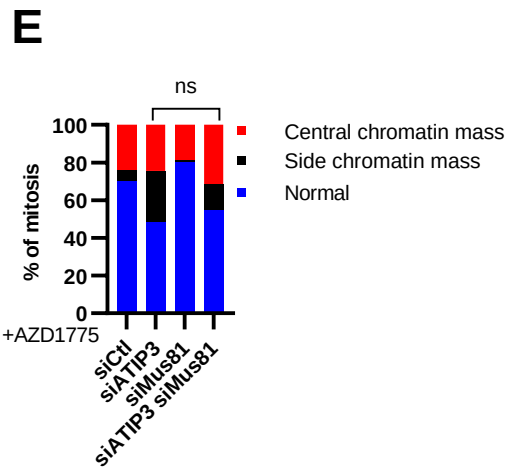

Supplementary Figure S8

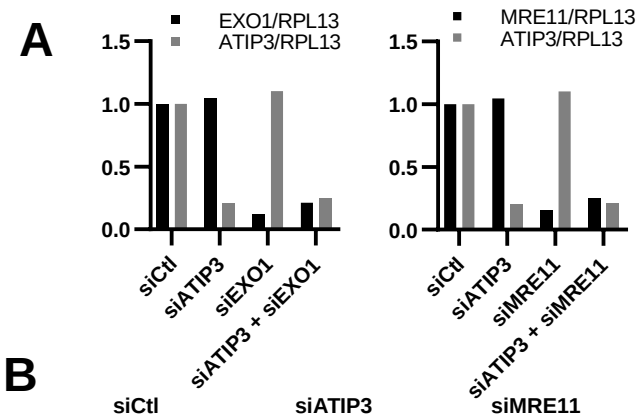

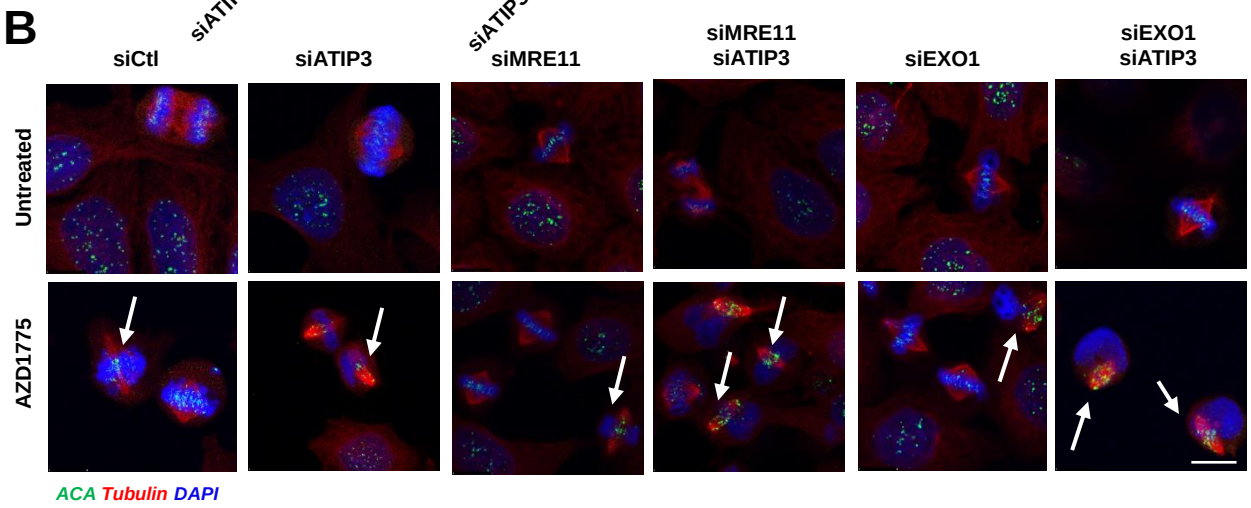

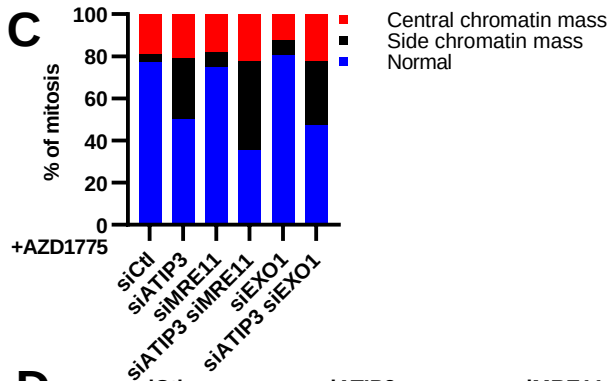

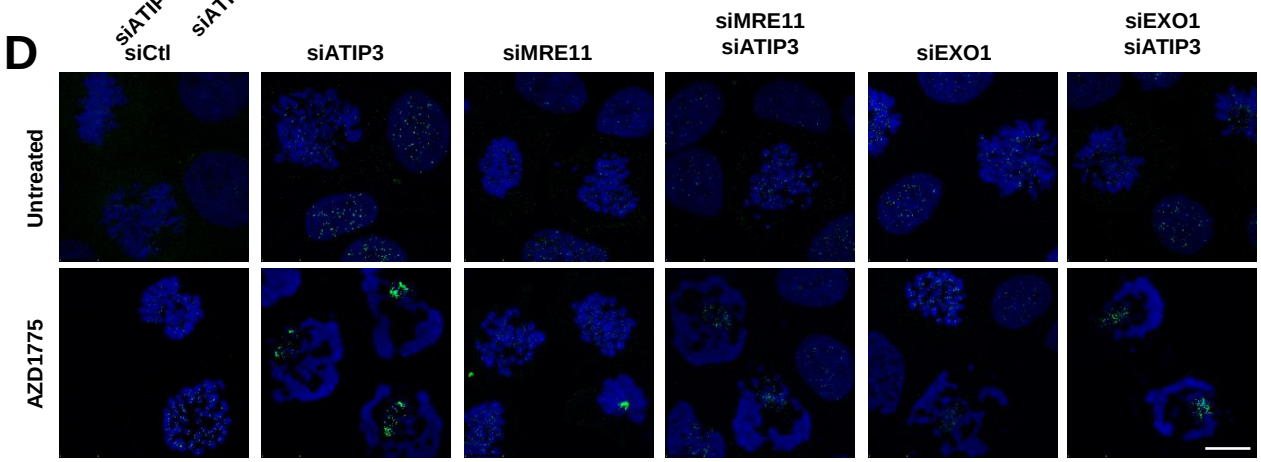

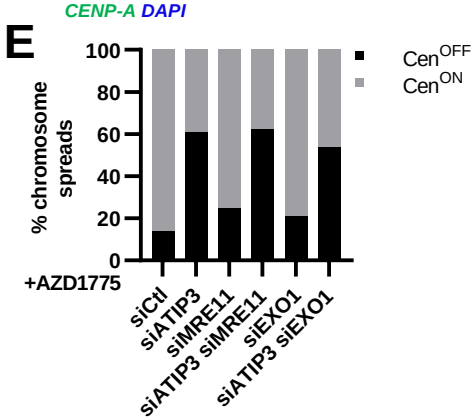

Supplementary Figure S9

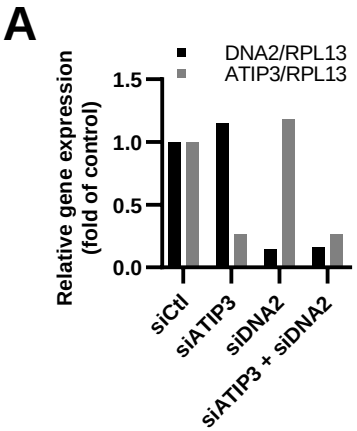

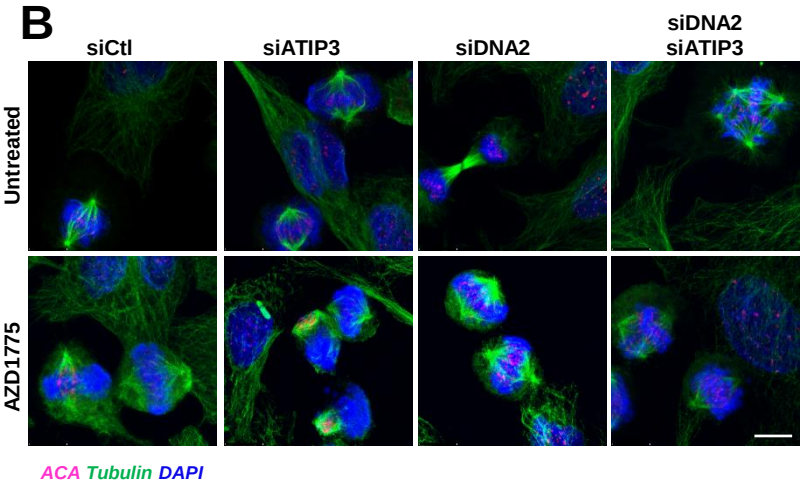

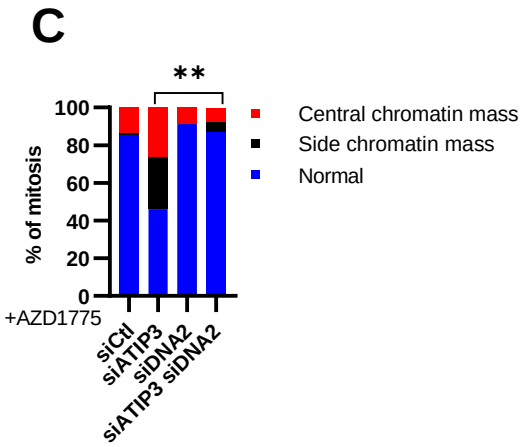

Supplementary Figure S10

Supplementary legends

Supplementary Figure S1: **(A)** Western blot of ATIP3 protein levels in SUM52PE shCtl or shATIP3 MCSs. Loading control: β-tubulin **(B)** Dose-response curves of the 6 differential inhibitors in SUM52PE shCtl or shATIP3 MCSs upon 72 h of treatment. **(C)** IC50 values in µM of each differential inhibitor in SUM52PE shCtl or shATIP3 MCSs upon 72 h of treatment. **(D)** *Top panels*: Dose-response curves of AZD1775 in MDA-MB-468 or MDA-MB-231 shCtl or shATIP3 MCSs upon 72 h of treatment. *Bottom panels*: Western blot of ATIP3 protein levels in shCtl or shATIP3 MCSs. Loading control: GAPDH. **(E)** Plot representing viability of in SUM52PE shCtl or shATIP3 MCSs upon 72 h of treatment with increasing doses of PD0166285. **(F)** Western blot analysis of CDK1 Tyr15 phosphorylation in SUM52PE shCtl or shATIP3 MCS treated or not with 500 nM AZD1775 for 6 h. Loading control: β-tubulin. **(G-H)** RPE-1 cells were treated for 48 h with 500 nM reversine. Reversine was washed out and cells were treated with 10 µM AZD1775 for 72 h before cell viability was assessed. **(G)** Treatment scheme of RPE-1 cells. **(H)** *Left panel*: Violin plot representing chromosome counts. The number of analyzed spreads is indicated between brackets. *Right panel:* Frequency distribution of chromosome counts.

Supplementary Figure S2: **(A-C)** HeLa cells transfected with control or ATIP3 siRNAs and treated with AZD1775 or PD0166285 for 6 h. **(A)** Western blot of ATIP3 protein levels. Loading control: GAPDH. **(B)** Western blot analysis for histone H3 Ser10 phosphorylation. Loading control: β-tubulin. **(C)** Western blot analysis of CDK1 phosphorylated substrates (pTPXK). Increased phosphorylated substrates are indicated in red. Loading control: Actin. **(D)** Immunofluorescence representative images of SUM52PE shCtl or shATIP3 MCSs treated with 500 nM AZD1775 for 14 h showing phosphorylated histone H3 in magenta and DNA in blue. Scale bar = 100 µm. **(E)** Quantification of the percentage of phospho-histone H3 positive cells in MCS shown in (D) (mean ± S.D.; Kruskal-Wallis test followed by Dunn's multiple comparisons; **p<0.01, ***p<0.001). **(F)** Percentage of cells exhibiting back and forth movement of their DNA around the spindle in mitosis. The number of analyzed cells in indicated between brackets. **(G)** Immunofluorescence representative images of SUM52PE shCtl or shATIP3 MCSs treated with 500 nM AZD1775 for 14 h showing phosphorylated histone H3 in magenta, microtubules in green and DNA in blue. White arrows indicate the exclusion of DNA from the mitotic spindle.

Scale bar = 10 µm. **(H)** HeLa cells transfected with control, WEE1, ATIP3 or both siRNAs. *Top panel*: Immunofluorescence representative images showing centrosomes in green, microtubules in red and DNA in blue. *Bottom panel:* quantification of abnormal mitosis (mean ± SEM. of N=3; a minimum of 97 cells were analyzed per group; two-tailed t-test; **p<0.01). **(I-J)** HeLa cells transfected with control or ATIP3 siRNAs were treated with 500 nM AZD1775, 10 µM RO-3306 or a combination of both drugs for 6 h. **(I)** Immunofluorescence representative images showing microtubules in green and DNA in blue. **(J)** Quantification of abnormal mitosis shown in (C) (mean ± SEM. of N=3; the number of analyzed cells is in brackets; one-way ANOVA; ****p<0.0001). Scale bar = 20 µm.

Supplementary Figure S3: HeLa cells transfected with control or ATIP3 siRNAs were treated with 500 nM AZD1775 for 6 h. **(A)** Immunofluorescence representative images showing CENP-B in magenta, microtubules in green and DNA in blue. **(B)** Immunofluorescence representative images showing CENP-A in green, microtubules in red and DNA in blue. **(C)** Immunofluorescence representative images of chromosome spreads showing CENP-B in magenta and DNA in blue. Scale bar = 20 µm.

Supplementary Figure S4: (A-C) HCT116 cells were treated for 48 h with 500 nM reversine. Reversine was washed out and cells were treated with 500 nM AZD1775 for 6 h before chromosome spreading. **(A)** *Left panel:* Violin plot representing chromosome counts. The number of analyzed spreads is indicated between brackets. *Right panel:* Frequency distribution of chromosome counts. **(B)** Representative images of chromosome spreads showing CENP-A in green and DNA in blue. **(C)** Quantification of the proportion of chromosome spreads shown in (C) (mean ± S.E.M of N=2; a minimum of 53 spreads were analyzed per group) two-way ANOVA; AZD1775 Cen^{OFF} vs AZD1775 + Reversine Cen^{OFF} ****p<0.0001). **(D-F)** HeLa cells were treated for 48 h with 500 nM reversine. Reversine was washed out and cells were treated with 500 nM AZD1775 for 6 h before chromosome spreading. **(D)** *Left panel:* Violin plot representing chromosome counts. The number of analyzed spreads is indicated between brackets. *Right panel:* Frequency distribution of chromosome counts. **(E)** Representative images of chromosome spreads showing CENP-A in green and DNA in blue. **(F)** Quantification of the proportion of chromosome spreads shown in (E) (mean ± S.E.M of N=2; a minimum of 57 spreads were analyzed per group) two-way ANOVA; AZD1775 Cen^{OFF} vs AZD1775 + Reversine Cen^{OFF} ***p<0.001). Scale bar = 5 µm. **(G-H)** HeLa cells transfected with control or ATIP3 siRNAs

were treated with 500 nM AZD1775 for 6 h. **(G)** Immunofluorescence representative images of IF-FISH showing CENP-B box in magenta, CENP-B in green and DNA in blue. **(H)** Quantification of the proportion of chromosome spreads shown in (G) (mean ± SEM. of N=2; the number of analyzed spreads is in brackets; two-way ANOVA; Cen^{OFF} in siCtl AZD1775 *vs*. siATIP3 AZD1775 ****p<0.0001). Scale bar = 5 µm.

Supplementary Figure S5: HeLa cells transfected with control or ATIP3 siRNAs were treated with 500 nM AZD1775 for 2 h (A-C). **(A)** Immunofluorescence representative images showing EdU in yellow and DNA in blue. The gray channel representing EdU is shown on the right to each condition. **(B)** Quantification of the percentage of EdU-positive cells shown in (A) (mean ± SEM. of N=3; a minimum of 73 cells were analyzed per group; one-way ANOVA; *ns*). **(C)** Quantification of EdU mean intensity per nucleus (normalized to DAPI) (mean ± S.D.; the number of analyzed cells is in brackets; Kruskal-Wallis test followed by Dunn's multiple comparisons; ***p<0.001, ****p<0.0001). **(D-E)** Mice xenografted with MDA-MB-468 shCtl or shATIP3 were treated or not with 90 mg/kg of AZD1775 by oral gavage daily for 4 days (1 mice per group) **(D)** Immunohistochemistry representative images showing γH2AX staining in xenografts. **(E)** Quantification of the percentage of γH2AX-positive nuclei shown in (D). **(F-G)** HeLa cells transfected with control or ATIP3 siRNAs were treated with 500 nM AZD1775 for 2 h. **(F)** Immunofluorescence representative images showing 53BP1 in magenta, EdU in yellow and DNA in blue. The gray channel representing 53BP1 is shown on the right to each condition. **(G)** Quantification of the percentage of EdU-positive cells with > 5 53BP1 foci shown in (F) (mean ± SEM. of N=4, a minimum of 173 cells were analyzed per group; one-way ANOVA; ***p<0.001, ****p<0.0001). Scale bar = 20 µm.

Supplementary Figure S6: HeLa cells transfected with control or ATIP3 siRNAs were treated with 500 nM AZD1775 for 6 h. **(A)** Immunofluorescence representative images showing phosphorylated RPA32 (S4/S8) in magenta, EdU in yellow and DNA in blue. The gray channels representing EdU or pRPA32 are shown on the right to each condition. **(B)** Quantification of the percentage of pRPA32-positive mitosis shown in (A) (mean ± SEM. of N=3; a minimum of 42 cells were analyzed per group; one-way ANOVA; *ns*, **p<0.01). **(C)** Immunofluorescence representative images showing γH2AX in red, EdU in green and DNA in blue. The gray channels representing EdU or γH2AX are shown on the right to each condition. **(D-E)** Quantification of the percentage of γH2AX-positive mitosis (D) and EdU-positive mitosis (E) shown in (C) (mean

± SEM. of N=4; a minimum of 50 cells were analyzed per group; one-way ANOVA; *ns*, *p<0.05, **p<0.01, ****p<0.0001). Scale bar = 20 µm.

Supplementary Figure S7: (A-D) HeLa cells transfected with control or ATIP3 siRNAs were pretreated with 100 nM Aphidicolin for 2 h then with 500 nM AZD1775 for 6 h. **(A)** Immunofluorescence representative images showing phosphorylated RPA32 (S4/S8) in magenta and DNA in blue. **(B)** Quantification of the percentage of pRPA32-positive mitosis shown in (A) (mean ± SEM. of N=2; a minimum of 51 cells were analyzed per group; one-way ANOVA; *ns*, ***p<0.001). **(C)** Immunofluorescence representative images showing γH2AX in green and DNA in blue. **(D)** Quantification of the percentage of γH2AX-positive mitosis shown in (C) (mean ± SEM. of N=2; a minimum of 58 cells were analyzed per group; one-way ANOVA; *ns*, ***p<0.001). **(E)** *Left panel:* Immunofluorescence representative images of HeLa cells transfected with control or ATIP3 siRNAs showing 53BP1 nuclear bodies in red, EdU in green and DNA in blue. *Right Panel:* Quantification of the percentage of G1 cells with 53BP1 nuclear bodies (mean ± SEM. of N=5; a minimum of 343 cells were analyzed per group; two-tailed t-test; *ns*, **p<0.01). **(F-G)** HCT116 cells were transfected with control or ATIP3 siRNAs. **(F)** *Right panel:* Western blot of ATIP3 protein levels. Loading control: GAPDH. *Left panel:* Immunofluorescence representative images showing 53BP1 nuclear bodies in magenta, EdU in green and DNA in blue. **(G)** Quantification of the percentage of G1 cells with 53BP1 nuclear bodies (mean ± SEM. of N=4; a minimum of 120 cells were analyzed per group; two-tailed t-test; *ns*, **p<0.01). Scale bar = 20 µm. **(H-I)** HeLa cells transfected with control or ATIP3 siRNAs were simultaneously with nucleosides (1/50) and 500 nM AZD1775 for 2 h (H) or 6 h (I). **(H)** Scattered dot-plot of phosphorylated RPA32 (S4/S8) per nucleus (normalized to DAPI). The number of analyzed cells is in brackets (mean ± S.D.; Kruskal-Wallis test followed by Dunn's multiple comparisons; ***p<0.001, ****p<0.0001). **(I)** Graph showing the % of mitotic phenotypes (mean ± SEM. of N=1; a minimum of 43 cells were analyzed per group; Side chromatin mass in siATIP3 AZD1775 *vs*. siATIP3 AZD1775 + Nuc p<0.0001).

Supplementary Figure S8: HeLa cells transfected with control, MUS81, ATIP3 or both siRNAs were treated with 500 nM AZD1775. **(A)** qPCR analysis of gene silencing efficiency. **(B)** Immunofluorescence representative images after 2 h of treatment showing phosphorylated RPA32 (S4/S8) in magenta and DNA in blue. **(C)** Quantification of phosphorylated RPA32 mean intensity per nucleus (normalized to DAPI) (mean ± S.D.; the number of analyzed cells is in

brackets; Kruskal-Wallis test followed by Dunn's multiple comparisons; ***p<0.001, ****p<0.0001). Scale bar = 20 µm. **(D)** Immunofluorescence representative images after 6 h of treatment showing CENPs in magenta, microtubules in green and DNA in blue. **(E)** Quantification of the proportions of mitotic phenotypes shown in (D) (mean ± SEM. of N=2; a minimum of 68 cells were analyzed per group; two-way ANOVA; Side chromatin mass in siATIP3 AZD1775 *vs*. siATIP3 + siMUS81 AZD1775 *ns*). Scale bar = 5 µm.

Supplementary Figure S9: HeLa cells transfected with control, EXO1, MRE11, ATIP3 or a combination of siRNAs were treated with 500 nM AZD1775 for 6 h. **(A)** qPCR analysis of gene silencing efficiency. **(B)** Immunofluorescence representative images showing CENPs in green, microtubules in red and DNA in blue. **(C)** Quantification of the proportion of mitotic phenotypes shown in (B) (mean ± SEM. of N=1; a minimum of 67 cells were analyzed per group; two-way ANOVA; Side chromatin mass in siATIP3 AZD1775 *vs*. siATIP3 siMRE11 AZD1775 *ns;* Side chromatin mass in siATIP3 AZD1775 *vs*. siATIP3 siEXO1 AZD1775 *ns*). **(D)** Immunofluorescence representative images of chromosome spreads showing CENP-A in green and DNA in blue. **(E)** Quantification of the proportions of chromosome spreads shown in (D) (mean ± SEM. of N=1; a minimum of 73 spreads were analyzed per group; two-way ANOVA; Cen^{OFF} in siATIP3 AZD1775 *vs*. siATIP3 siMRE11 AZD1775 *ns;* Cen^{OFF} in siATIP3 AZD1775 *vs*. siATIP3 siEXO1 AZD1775 *ns*). Scale bar = 20 µm.

Supplementary Figure S10: HeLa cells transfected with control, ATIP3, DNA2 or a combination or ATIP3 and DNA2 siRNAs and treated with 500 nM AZD1775 for 6 h. **(A)** qPCR analysis of gene silencing efficiency. **(B)** Immunofluorescence representative images of abnormal mitoses showing CENPs in magenta, microtubules in green and DNA in blue. **(C)** Quantification of the proportions of the mitotic phenotypes shown in (A) (mean ± S.E.M of N=2; a minimum of 88 cells were analyzed per group; two-way ANOVA; normal mitoses in siATIP3 *vs*. siATIP3 + siDNA2 **p<0.01). Scale bar = 20 µm.

Inhibitor	Target	IC50 in shCtl	IC50 in shATIP3	IC50 Fold change
CFI-400945	AURKB/PLK4	1,506	0,336	4,487
Centrinone	PLK4	1,092	0,341	3,199
Alisertib	AURKA	0,249	0,078	3,190
AZD1775	WEE1	1,310	0,430	3,110
AZD0156	ATM	4,699	1,965	2,391
AZ20	ATR	2,734	1,361	2,009
Tozasertib	panAurora	1,058	0,599	1,768
AZD7762	CHK1/2	0,396	0,256	1,548
SB218078	CHK1	0,225	0,152	1,486
MK-8776	CHK1	1,986	1,453	1,367
AZD6738	ATR	1,952	1,487	1,313
SBE13HCl	PLK1	0,225	0,187	1,206
NSC663284	CDC25	8,721	7,466	1,168
CHIR-124	CHK1	4,342	3,725	1,166
LY2606368	CHK1	2,809	2,509	1,120
AZ3146	MPS1	1,466	1,373	1,068
Barasertib	AURKB	2,335	2,210	1,057
Flavopiridol	panCDK	0,141	0,134	1,049
VE-821	ATR	6,475	6,228	1,040
BI6727	PLK1	0,868	0,838	1,035
BAY1217389	MPS1	1,074	1,047	1,025
AZD4573	CDK9	0,005	0,005	1,024
Palbociclib	CDK4/6	0,049	0,048	1,022
Roscovitine	CDK1/2	7,286	7,136	1,021
AT7519	panCDK	0,005	0,017	1,013
LY2606318	CHK1	5,138	5,148	0,998
Dinaciclib	CDK1/2/5/9	0,009	0,009	0,992
BN82002	CDC25	0,052	0,055	0,945

Table S1
IC50 values (µM) of the 28 inhibitors in SUM52PE multicellular spheroids expressing (shCtl) or not ATIP3 (shATIP3)
Compounds in green are differential with a fold change higher than 2

IV. DISCUSSION AND FUTURE DIRECTIONS

The comprehensive findings presented in our study not only unravel the intricate molecular mechanisms underlying the sensitivity of ATIP3-deficient cells to WEE1 inhibition but also pave the way for considering ATIP3 as a potential biomarker for guiding WEE1-targeted therapies.

To avoid redundancy with the discussion presented in the article, I will hereby discuss wider hypotheses, some unpublished results and the future directions of the current work.

1 ATIP3 AS A POTENTIAL BIOMARKER FOR RESPONSE TO WEE1 INHIBITORS

Our results point to the novel finding that increasing aneuploidy in cancer cells sensitizes to WEE1 inhibition. One study shows a slight correlation between the levels of WEE1 gene expression and the CIN25 gene signature ($R=0.53$, $p=0.027$)[296]. However, until now, no direct connections were made between the extent of aneuploidy and WEE1 inhibitor sensitivity.

To further explore this relationship, it will be of great interest to show that aneuploidy sensitizes to WEE1 inhibition in a range of different cancer cell lines, independently of ATIP3 depletion, by using reversine to induce aneuploidy or by overexpressing PLK4 to induce high rates of CIN[425]. Then, we would correlate the levels of CIN and extent of aneuploidy with the response to WEE1 inhibitor. Same correlative studies may be performed on breast cancer patient-derived xenografts (PDX). This should represent a basis for retrospective clinical data analysis of WEE1 inhibitor-treated breast cancer cohorts in which we would study the extent of aneuploidy and/or CIN levels and correlate them to pCR levels; should the data be publicly available one day.

As ATIP3 deficiency is associated with high levels of CIN and aneuploidy, we propose the use of ATIP3 as a potential biomarker for WEE1 inhibition. To consolidate the sensitizing effects of ATIP3 deficiency to WEE1 inhibition, it would be interesting to test the efficacy of WEE1 inhibition in breast cancer PDXs expressing known levels of ATIP3. AZD1775 has already been evaluated in PDX models but the RNAseq/whole exome sequencing data are not publicly available for us to correlate with ATIP3 expression levels. Nonetheless, previous work from our lab characterized ATIP3 levels in breast cancer PDXs[94], of which 3 PDXs were treated with AZD1775 in an independent study[426]. The response to AZD1775 and the levels of ATIP3 are represented in Figure 36. Although we cannot make any clear-cut conclusions because there are only 3 PDXs, the tendency is for a better response to AZD1775 when ATIP3 levels are low.

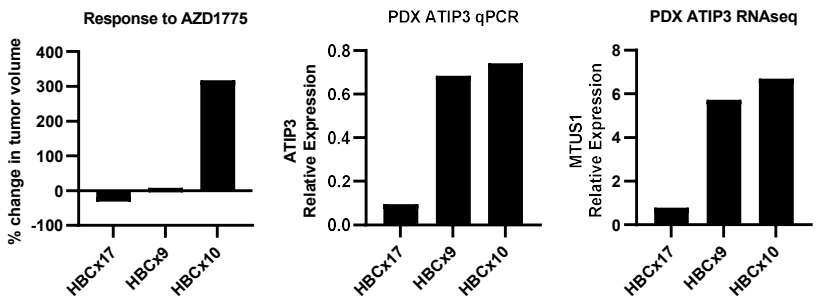

Figure 36: AZD1775-treated breast cancer PDXs

Currently, the lack of reliable predictive biomarkers for the response to WEE1 inhibitors hampers the success of clinical trials. It would be of great clinical benefit to identify the population of patients most likely to respond to treatment, and ATIP3 could here be of value.

2 EFFECTS OF WEE1 INHIBITION IN S-PHASE: IS CDK1 TO BLAME?

In dissecting the repercussions of WEE1 inhibition during S phase, our investigation has uncovered that WEE1 inhibition triggers a more pronounced replicative stress in aneuploid cells, in contrast to their less aneuploid counterparts. Furthermore,

the inhibition of WEE1 induces a surge in DNA damage which could be partly attributed to the activation of MUS81.

We are aware that SLX4, a regulator of MUS81-EME1, undergoes phosphorylation by CDK1[427]. This phosphorylation event is known for promoting the interaction with MUS81-EME1 during early mitosis[428]. Hence, the aberrant CDK1 activation due to WEE1 inhibition might prematurely activate SLX4, and consequently MUS81-EME1, during S phase instead of mitosis. This potentially untimely activation may transform stalled replication forks into DSBs. However, our observations suggest that MUS81 alone does not account for all damages, as these are not completely restored in the absence of MUS81. This aligns with a separate study indicating that premature CDK1 activation activates MUS81 in S phase but is insufficient to prevent all DNA damages when CDK1 is unleashed[429].

Therefore, determining what other factors, apart from MUS81, contribute to excessive DNA damage in S phase following aberrant CDK activation becomes of importance. We posit a hypothesis proposing an unscheduled nuclease activity under CDK control as a potential culprit responsible for the excessive DNA damage observed in S phase. An avenue of interest lies in the phosphorylation of Bloom's syndrome helicase (BLM) by CDK1[430], raising the possibility that an unscheduled activity of BLM could be a contributing factor. Furthermore, DNA2, a putative CDK1 substrate[431], could be a potential player in S-phase. To examine this, we would investigate the role of DNA2 in S-phase after WEE1 inhibition in the induction of DNA damage. The potential role of DNA2 in S-phase is supported by a study implicating DNA2 in the excessive degradation of stalled replication forks (using hydroxyurea), where WEE1 plays a protective role against DNA2[278]. However, this role of WEE1 was attributed to limiting CDK2 activity and not CDK1, adding an additional layer of complexity. This makes it challenging to pinpoint a single factor controlled by the WEE1-CDK1/2 pathway for ensuring fork stability, given the multitude of CDK phosphorylation targets. A prospective phosphoproteomic study

holds promise for shedding more light on this intricate regulatory network.

3 EFFECTS OF WEE1 INHIBITION ON MITOTIC ENTRY

The premature entry into mitosis observed following WEE1 inhibition in ATIP3-depleted cells raises a compelling question: Is this phenomenon a consequence of inherent properties of ATIP3 or a manifestation of the aneuploid state of these cells? And is the duration of S and G2 phases altered in ATIP3-depleted or aneuploid cells?

To unravel this, we would closely examine the length of the S and G2 phases using live microscopy of cells expressing fluorescently labelled Proliferating cell nuclear antigen (PCNA)[432]. We would examine the length of these phases in ATIP3-depeleted cells to discern whether their cell cycle is inherently compromised, potentially rendering WEE1 inhibition more efficient. Concurrently to the depletion of ATIP3, the same cell line would be rendered aneuploid using reversine or PLK4 overexpression, which would provide a comparative metric to evaluate whether any modifications in the lengths of S and G2 phases stem from aneuploidy *per se* or the absence of ATIP3.

The decision to enter mitosis is largely due to CDK1 activation, and we have observed higher phosphorylation of CDK1 substrates in response to WEE1 inhibition in ATIP3-depleted cells. To further explore the kinase activity of CDK1, it would be of interest to measure CDK1 activity after WEE1 inhibition using a CDK1 FRET sensor[433], as this approach would allow real-time monitoring and spatial resolution of CDK1 activity.

4 EFFECTS OF WEE1 INHIBITION IN MITOSIS: BEYOND DNA2 ACTIVITY

Our examination of the impact of WEE1 inhibition during mitosis raises the question of whether the observed effects are solely attributable to the enzymatic

activity of DNA2 or if other mechanisms are at play.

WEE1 inhibition leads to the formation of aberrant mitoses characterized by a detachment between centromeric proteins and unstructured DNA apparently pulverized in metaphase spreads. Two distinct aberrant mitotic phenotypes emerge: one with total detachment termed "side chromatin mass" and another where DNA is moderately attached referred to as "central chromatin mass." The evolutionary relationship between these two phenotypes prompts questions – does DNA undergo progressive pulverization during mitosis, or are these separate phenomena?

Our investigations attribute these mitotic phenotypes to the nuclease/helicase DNA2. In its absence, WEE1 inhibition no longer induces these characteristic phenotypes. Given DNA2's affinity for centromeric DNA, which is under-replicated in these conditions, we postulate that DNA2, when recruited or activated in mitosis, cleaves stalled replication forks in centromeric DNA, causing degradation and the separation of DNA from centromeric proteins. Examining the recruitment, localization, and activity of DNA2 in response to WEE1 inhibition, along with assessing replicative stress through combined DNA combing and FISH at the centromeric DNA under conditions of DNA2 depletion or presence, would offer valuable insights.

Chromosomes are moved inside the spindle by microtubules, first to the spindle center during prometaphase and then to spindle poles in anaphase. Microtubules attach to and pull on chromosomes at kinetochores[434]. Another fraction of microtubules contacts chromosome arms and generates polar ejection forces that push chromosomes away from the spindle poles[435] for congression. These forces generate a complex system with high tension. In a recent study, Schneider *et al.* observed, upon condensin-depletion in mitotic cells, an unstructured mass of compact chromatin forming a plate between the spindle poles. This phenotype also included kinetochores detached from the bulk mass of chromatin[436], which

echoes with our observations upon WEE1 inhibition. Their results also show that condensin is required for chromosomes to resist tension generated at kinetochores. So, there could be a potential condensation defect when WEE1 is inhibited. It would be informative to investigate this hypothesis with SMC2/4 labeling in mitosis or spreads. It may be plausible that the severely damaged DNA upon WEE1 inhibition, presents condensation defects making it unable to resist tension at kinetochores, in addition or partly due to enzymatic degradation by DNA2 at centromeric DNA.

We expected that highly degraded DNA during mitosis would be dispersed into small fragments within the cytoplasm. However, what we observe is a compact mass located adjacent to the spindle in the 'side chromatin mass' phenotype. This phenomenon could be attributed to either a more pronounced compaction of the broken DNA or the tethering of DSBs by DNA repair proteins known for chromatin remodeling, with the purpose of safeguarding genomic integrity during mitosis[437].

Of note, we observe the bulk chromatin mass moving around the spindle in ATIP3-depleted cells. This may be caused by deregulated polar ejection forces. It would then be of interest to examine the roles of chromokinesins like Kid or Kif4A or of depolymerizing kinesins such as Kif2C, a known ATIP3 partner of interaction, in the occurrence of the mitotic phenotypes after WEE1 inhibition.

Another striking feature lies in the spindle width, significantly reduced in cells with 'side chromatin mass' phenotype and increased in those with 'central chromatin mass' phenotype (Figure 37). The reduction in spindle width could be attributed to a decrease in chromatin quantity within the spindle because the chromosomes occupy the metaphase plate, therefore a reduction in the number of chromosomes should directly decrease the spindle width. This was observed to some extent in *C. elegans* where the manipulation of ploidy led to the observation that spindle width varies slightly with the number of chromosomes[438].

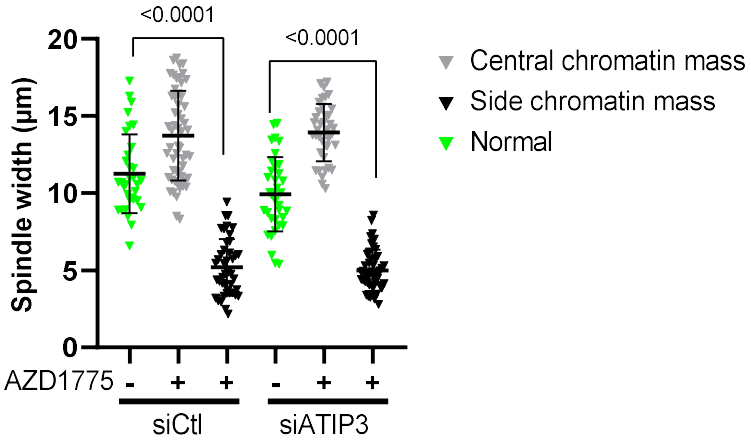

Figure 37: Variations in spindle width in response to WEE1 inhibition

The observed variations in spindle width require further investigation as very little is known about the regulation of spindle width. It would be interesting to determine whether the presence of chromosomes is necessary for the maintenance of a correct spindle size or if there are microtubule-regulatory mechanisms (MAPs, kinesins, …) that are impacted specifically in response to WEE1 inhibition.

5 A CROSSTALK BETWEEN ATIP3 AND WEE1?

Another interesting observation was the increase of WEE1 protein levels (Figure 38A) and activity (Figure 38B) upon ATIP3 depletion. These observations raised many questions.

As stated in the introduction, WEE1 turnover is ensured via $SCF^{\beta\text{-}TrCP}$ or $SCF^{TOME\text{-}1}$. ATIP3 is known to interact to S-phase kinase 1 (SKP1, unpublished results from the lab). One possibility may be that ATIP3 could represent a novel F-box for SCF recognition and degradation of WEE1. Hence, when ATIP3 is depleted, WEE1 levels rise as it would be less destined for degradation. It would be interesting to examine whether ATIP3 (1) controls WEE1 turnover using classic experiments of cycloheximide chase to determine WEE1 half-life; (2) antagonizes WEE1 degradation by the proteasome; (3) interferes with WEE1 ubiquitination patterns.

The fact that ATIP3-depleted cells are more sensitive to WEE1 inhibition could

result from the increased levels of WEE1. We can raise the hypothesis that the more abundant a protein is, the more targets there are for its inhibitor and as such, WEE1 inhibition would be more efficient in cells where WEE1 is more abundant.

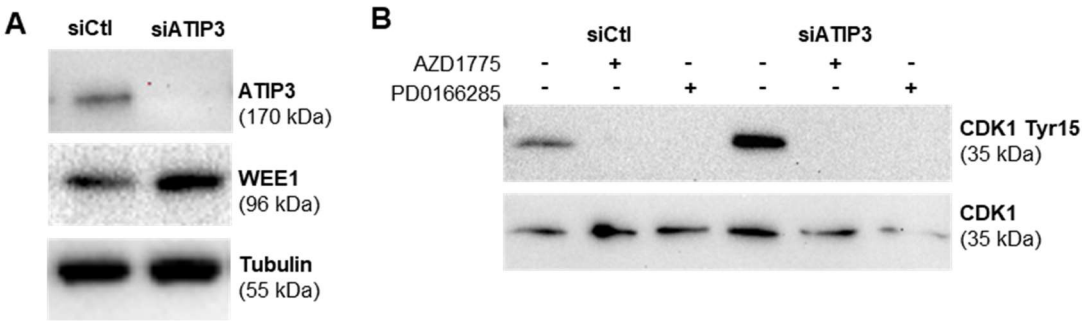

Figure 38: WEE1 protein levels and activity
(PD0166285 is the double WEE1/MYT1 inhibitor)

6 How could a MAP be implicated in nuclear-based events?

How could ATIP3, a microtubule-associated protein, be associated with heightened levels of replication stress and DNA damage in S-phase following WEE1 inhibition? One part is surely due to the fact that ATIP3-depleted cells are aneuploid and by definition would be more susceptible to damage and less prompt to repair their DNA. Nonetheless, could there be ATIP3-specific functions in S-phase or S-phase related processes that would render cells sensitive to WEE1 inhibition?

A previous study from the lab[91] showed that ATIP3 potentially interacts with nuclear proteins implicated in either DNA replication or repair and centromere maintenance. The hypothesis is that ATIP3 may be a direct regulator of one or more of these proteins, to aid in their recruitment to the nucleus or their timely export, or indirectly by the action of ATIP3 on proteasome-degradation pathways.

These factors include but are not restricted to CDC45, RIF1, TOPIIα (already mentioned in the introduction). It would be of need at first to validate that ATIP3 interacts with these proteins using co-immunoprecipitation or Proximity-ligation assays (PLA). Then an evaluation of the implication of these proteins in the observed effects in S-phase

after WEE1 inhibition in control or ATIP3-depleted cells.

As stated earlier, WEE1 inhibition causes unscheduled and excessive replication initiation, so the implication of the replication initiation factor CDC45 should be tested with the idea that WEE1 inhibition would increase the chromatin loading of CDC45[439], and possibly even to higher extent when ATIP3 is depleted. As for RIF1, a report has shown that WEE1 inhibition induces phosphorylation of MCM4 and RIF1[440], indicating dormant origin firing. As the major decatenating enzyme, TOPIIα removes supercoils and DNA loops during DNA replication and catenanes that hold sister chromatids together in mitosis. TOPIIα creates DSBs to allow changes in DNA topology[441], therefore an excessive action could be detrimental. Testing the effects of the depletion of TOPIIα would be too dramatical, but a timely inhibition specifically in cells in S-phase or mitosis could be informative as to its potential role in the excessive DNA damage and chromosome pulverization observed in ATIP3-depleted cells after exposure to WEE1 inhibitor.

A whole other scenario for ATIP3's role in S-phase events could be its involvement in DSBs mobility within the nucleus. It's not clear whether WEE1 inhibition induces more damage in ATIP3-depleted cells or if the damages induced are less well repaired. With the pioneering work of Aten *et al.*, demonstrating changes in DSB location and morphology within minutes following break induction, it's now clear that DSB are moved to 'repair centers' inside the nucleus by the concerted action of 53BP1 and microtubules[442,443]. Given the MT-stabilizing properties of ATIP3 and the increase in microtubule dynamics when ATIP3 is depleted, it would be very interesting to investigate if DSB motility is modified within the nucleus making damage less prompt to be repaired.

V. CLOSING STATEMENT

In conclusion, the interplay between WEE1 inhibition, ATIP3 depletion, and aneuploidy reveals a multifaceted landscape governing cellular responses during DNA replication and mitosis. The distinct phases of the cell cycle, particularly S-phase and mitosis, serve as critical arenas where ATIP3, as a microtubule-associated protein, emerges as a key orchestrator. From the augmented replication stress and DNA damage observed in S-phase to the peculiar mitotic aberrations, including centromere fragmentation and spindle abnormalities, the impact of ATIP3 depletion becomes increasingly apparent. As we navigate the intricate landscape of WEE1 inhibition and ATIP3 deficiency, the implications extend beyond a mere cascade of events. Instead, they underscore the choreography required for the faithful execution of DNA dynamics. Unraveling the complexities of ATIP3's role in these processes holds the promise of not only expanding our fundamental understanding of cell cycle regulation but also providing potential insights for targeted therapeutic interventions. Thus, this exploration stands as a testament to the continual pursuit of unraveling what governs the cellular symphony of life.

VI. REFERENCES

1. Hanahan, D. & Weinberg, R. A. The Hallmarks of Cancer. *Cell* **100**, 57–70 (2000).

2. Hanahan, D. & Weinberg, R. A. Hallmarks of Cancer: The Next Generation. *Cell* **144**, 646–674 (2011).

3. Hanahan, D. Hallmarks of Cancer: New Dimensions. *Cancer Discov.* **12**, 31–46 (2022).

4. Ferlay, J. *et al.* Cancer statistics for the year 2020: An overview. *Int. J. Cancer* **149**, 778–789 (2021).

5. DeSantis, C. E. *et al.* Breast cancer statistics, 2019. *CA. Cancer J. Clin.* **69**, 438–451 (2019).

6. Allemani, C. *et al.* Global surveillance of trends in cancer survival 2000–14 (CONCORD-3): analysis of individual records for 37 513 025 patients diagnosed with one of 18 cancers from 322 population-based registries in 71 countries. *The Lancet* **391**, 1023–1075 (2018).

7. Shiovitz, S. & Korde, L. A. Genetics of breast cancer: a topic in evolution. *Ann. Oncol.* **26**, 1291–1299 (2015).

8. Huen, M. S. Y., Sy, S. M. H. & Chen, J. BRCA1 and its toolbox for the maintenance of genome integrity. *Nat. Rev. Mol. Cell Biol.* **11**, 138–148 (2010).

9. Kuchenbaecker, K. B. *et al.* Risks of Breast, Ovarian, and Contralateral Breast Cancer for BRCA1 and BRCA2 Mutation Carriers. *JAMA* **317**, 2402–2416 (2017).

10. Amy Taylor *et al.* Consensus for genes to be included on cancer panel tests offered by UK genetics services: guidelines of the UK Cancer Genetics Group. *J. Med. Genet.* **55**, 372 (2018).

11. Chen, W. Y., Rosner, B., Hankinson, S. E., Colditz, G. A. & Willett, W. C. Moderate Alcohol Consumption During Adult Life, Drinking Patterns, and Breast Cancer Risk. *JAMA* **306**, 1884–1890 (2011).

12. Picon-Ruiz, M., Morata-Tarifa, C., Valle-Goffin, J. J., Friedman, E. R. & Slingerland, J. M. Obesity and adverse breast cancer risk and outcome: Mechanistic insights and strategies for intervention. *CA. Cancer J. Clin.* **67**, 378–397 (2017).

13. Mørch, L. S. *et al.* Contemporary Hormonal Contraception and the Risk of Breast Cancer. *N. Engl. J. Med.* **377**, 2228–2239 (2017).

14. Type and timing of menopausal hormone therapy and breast cancer risk: individual participant meta-analysis of the worldwide epidemiological evidence. *The*

Lancet **394**, 1159–1168 (2019).

15. Welch, D. R. Tumor Heterogeneity—A 'Contemporary Concept' Founded on Historical Insights and Predictions. *Cancer Res.* **76**, 4–6 (2016).

16. Tan, P. H. *et al.* The 2019 World Health Organization classification of tumours of the breast. *Histopathology* **77**, 181–185 (2020).

17. Wellings, S. R. & Jensen, H. M. On the Origin and Progression of Ductal Carcinoma in the Human Breast2. *JNCI J. Natl. Cancer Inst.* **50**, 1111–1118 (1973).

18. Bloom, H. J. G. & Richardson, W. W. Histological Grading and Prognosis in Breast Cancer. *Br. J. Cancer* **11**, 359–377 (1957).

19. ELSTON, C. W. & ELLIS, I. O. pathological prognostic factors in breast cancer. I. The value of histological grade in breast cancer: experience from a large study with long-term follow-up. *Histopathology* **19**, 403–410 (1991).

20. Fisher, B., Redmond, C. K. & Fisher, E. R. Evolution of Knowledge Related to Breast Cancer Heterogeneity: A 25-Year Retrospective. *J. Clin. Oncol.* **26**, 2068–2071 (2008).

21. Loibl, S. & Gianni, L. HER2-positive breast cancer. *The Lancet* **389**, 2415–2429 (2017).

22. Perou, C. M. *et al.* Molecular portraits of human breast tumours. *Nature* **406**, 747–752 (2000).

23. Sørlie, T. *et al.* Gene expression patterns of breast carcinomas distinguish tumor subclasses with clinical implications. *Proc. Natl. Acad. Sci.* **98**, 10869–10874 (2001).

24. Lehmann, B. D. *et al.* Identification of human triple-negative breast cancer subtypes and preclinical models for selection of targeted therapies. *J. Clin. Invest.* **121**, 2750–2767 (2011).

25. Lehmann, B. D. *et al.* Refinement of Triple-Negative Breast Cancer Molecular Subtypes: Implications for Neoadjuvant Chemotherapy Selection. *PLOS ONE* **11**, e0157368 (2016).

26. Masuda, H. *et al.* Differential Response to Neoadjuvant Chemotherapy Among 7 Triple-Negative Breast Cancer Molecular Subtypes. *Clin. Cancer Res.* **19**, 5533–5540 (2013).

27. Cortazar, P. *et al.* Pathological complete response and long-term clinical benefit in breast cancer: the CTNeoBC pooled analysis. *The Lancet* **384**, 164–172 (2014).

28. Carey, L. A. *et al.* The Triple Negative Paradox: Primary Tumor Chemosensitivity

of Breast Cancer Subtypes. *Clin. Cancer Res.* **13**, 2329–2334 (2007).

29. Liedtke, C. *et al.* Response to Neoadjuvant Therapy and Long-Term Survival in Patients With Triple-Negative Breast Cancer. *J. Clin. Oncol.* **26**, 1275–1281 (2008).

30. Bonotto, M. *et al.* Measures of Outcome in Metastatic Breast Cancer: Insights From a Real-World Scenario. *The Oncologist* **19**, 608–615 (2014).

31. Bianchini, G., De Angelis, C., Licata, L. & Gianni, L. Treatment landscape of triple-negative breast cancer — expanded options, evolving needs. *Nat. Rev. Clin. Oncol.* **19**, 91–113 (2022).

32. Polak, P. *et al.* A mutational signature reveals alterations underlying deficient homologous recombination repair in breast cancer. *Nat. Genet.* **49**, 1476–1486 (2017).

33. den Brok, W. D. *et al.* Homologous Recombination Deficiency in Breast Cancer: A Clinical Review. *JCO Precis. Oncol.* 1–13 (2017) doi:10.1200/PO.16.00031.

34. Ray Chaudhuri, A. & Nussenzweig, A. The multifaceted roles of PARP1 in DNA repair and chromatin remodelling. *Nat. Rev. Mol. Cell Biol.* **18**, 610–621 (2017).

35. Farmer, H. *et al.* Targeting the DNA repair defect in BRCA mutant cells as a therapeutic strategy. *Nature* **434**, 917–921 (2005).

36. Bryant, H. E. *et al.* Specific killing of BRCA2-deficient tumours with inhibitors of poly(ADP-ribose) polymerase. *Nature* **434**, 913–917 (2005).

37. Robson, M. *et al.* Olaparib for Metastatic Breast Cancer in Patients with a Germline BRCA Mutation. *N. Engl. J. Med.* **377**, 523–533 (2017).

38. Litton, J. K. *et al.* Talazoparib in Patients with Advanced Breast Cancer and a Germline BRCA Mutation. *N. Engl. J. Med.* **379**, 753–763 (2018).

39. Robson, M. E. *et al.* OlympiAD final overall survival and tolerability results: Olaparib versus chemotherapy treatment of physician's choice in patients with a germline BRCA mutation and HER2-negative metastatic breast cancer. *Ann. Oncol.* **30**, 558–566 (2019).

40. Litton, J. K. *et al.* Talazoparib versus chemotherapy in patients with germline BRCA1/2-mutated HER2-negative advanced breast cancer: final overall survival results from the EMBRACA trial. *Ann. Oncol.* **31**, 1526–1535 (2020).

41. Tutt, A. N. J. *et al.* Adjuvant Olaparib for Patients with BRCA1- or BRCA2-Mutated Breast Cancer. *N. Engl. J. Med.* **384**, 2394–2405 (2021).

42. Tung, N. M., Zakalik, D. & Somerfield, M. R. Adjuvant PARP Inhibitors in Patients With High-Risk Early-Stage HER2-Negative Breast Cancer and Germline BRCA

Mutations: ASCO Hereditary Breast Cancer Guideline Rapid Recommendation Update. *J. Clin. Oncol.* **39**, 2959–2961 (2021).

43. Drago, J. Z., Modi, S. & Chandarlapaty, S. Unlocking the potential of antibody–drug conjugates for cancer therapy. *Nat. Rev. Clin. Oncol.* **18**, 327–344 (2021).

44. Modi, S. *et al.* Trastuzumab Deruxtecan in Previously Treated HER2-Positive Breast Cancer. *N. Engl. J. Med.* **382**, 610–621 (2020).

45. Modi, S. *et al.* Antitumor Activity and Safety of Trastuzumab Deruxtecan in Patients With HER2-Low–Expressing Advanced Breast Cancer: Results From a Phase Ib Study. *J. Clin. Oncol.* **38**, 1887–1896 (2020).

46. Aslan, M. *et al.* Oncogene-mediated metabolic gene signature predicts breast cancer outcome. *Npj Breast Cancer* **7**, 141 (2021).

47. Bardia, A. *et al.* Sacituzumab Govitecan in Metastatic Triple-Negative Breast Cancer. *N. Engl. J. Med.* **384**, 1529–1541 (2021).

48. Hoxhaj, G. & Manning, B. D. The PI3K–AKT network at the interface of oncogenic signalling and cancer metabolism. *Nat. Rev. Cancer* **20**, 74–88 (2020).

49. Koboldt, D. C. *et al.* Comprehensive molecular portraits of human breast tumours. *Nature* **490**, 61–70 (2012).

50. Sharma, P. *et al.* Clinical and Biomarker Results from Phase I/II Study of PI3K Inhibitor Alpelisib plus Nab-paclitaxel in HER2-Negative Metastatic Breast Cancer. *Clin. Cancer Res.* **27**, 3896–3904 (2021).

51. Hortobagyi, G. N. *et al.* Ribociclib as First-Line Therapy for HR-Positive, Advanced Breast Cancer. *N. Engl. J. Med.* **375**, 1738–1748 (2016).

52. Luen, S., Virassamy, B., Savas, P., Salgado, R. & Loi, S. The genomic landscape of breast cancer and its interaction with host immunity. *The Breast* **29**, 241–250 (2016).

53. Sobral-Leite, M. *et al.* Assessment of PD-L1 expression across breast cancer molecular subtypes, in relation to mutation rate, BRCA1-like status, tumor-infiltrating immune cells and survival. *OncoImmunology* **7**, e1509820 (2018).

54. Stanton, S. E., Adams, S. & Disis, M. L. Variation in the Incidence and Magnitude of Tumor-Infiltrating Lymphocytes in Breast Cancer Subtypes: A Systematic Review. *JAMA Oncol.* **2**, 1354–1360 (2016).

55. Esteva, F. J., Hubbard-Lucey, V. M., Tang, J. & Pusztai, L. Immunotherapy and targeted therapy combinations in metastatic breast cancer. *Lancet Oncol.* **20**, e175–e186 (2019).

56. Schmid, P. *et al.* Atezolizumab and Nab-Paclitaxel in Advanced Triple-Negative Breast Cancer. *N. Engl. J. Med.* **379**, 2108–2121 (2018).

57. Schmid, P. *et al.* Pembrolizumab for Early Triple-Negative Breast Cancer. *N. Engl. J. Med.* **382**, 810–821 (2020).

58. Schmid, P. *et al.* Event-free Survival with Pembrolizumab in Early Triple-Negative Breast Cancer. *N. Engl. J. Med.* **386**, 556–567 (2022).

59. Domchek, S. M. *et al.* Olaparib and durvalumab in patients with germline BRCA-mutated metastatic breast cancer (MEDIOLA): an open-label, multicentre, phase 1/2, basket study. *Lancet Oncol.* **21**, 1155–1164 (2020).

60. Schmid, P. *et al.* BEGONIA: Phase 1b/2 study of durvalumab (D) combinations in locally advanced/metastatic triple-negative breast cancer (TNBC)—Initial results from arm 1, d+paclitaxel (P), and arm 6, d+trastuzumab deruxtecan (T-DXd). *J. Clin. Oncol.* **39**, 1023–1023 (2021).

61. Winer, E. P. *et al.* Association of tumor mutational burden (TMB) and clinical outcomes with pembrolizumab (pembro) versus chemotherapy (chemo) in patients with metastatic triple-negative breast cancer (mTNBC) from KEYNOTE-119. *J. Clin. Oncol.* **38**, 1013–1013 (2020).

62. Litchfield, K. *et al.* Meta-analysis of tumor- and T cell-intrinsic mechanisms of sensitization to checkpoint inhibition. *Cell* **184**, 596-614.e14 (2021).

63. Blank, C. U., Haanen, J. B., Ribas, A. & Schumacher, T. N. The "cancer immunogram". *Science* **352**, 658–660 (2016).

64. Cristescu, R. *et al.* Pan-tumor genomic biomarkers for PD-1 checkpoint blockade–based immunotherapy. *Science* **362**, eaar3593 (2018).

65. Zou, Y. *et al.* Efficacy and predictive factors of immune checkpoint inhibitors in metastatic breast cancer: a systematic review and meta-analysis. *Ther. Adv. Med. Oncol.* **12**, 1758835920940928 (2020).

66. Hiam-Galvez, K. J., Allen, B. M. & Spitzer, M. H. Systemic immunity in cancer. *Nat. Rev. Cancer* **21**, 345–359 (2021).

67. Elinav, E., Garrett, W. S., Trinchieri, G. & Wargo, J. The cancer microbiome. *Nat. Rev. Cancer* **19**, 371–376 (2019).

68. Sayaman, R. W. *et al.* Germline genetic contribution to the immune landscape of cancer. *Immunity* **54**, 367-386.e8 (2021).

69. Seibold, S. *et al.* Identification of a new tumor suppressor gene located at chromosome 8p21.3–22. *FASEB J.* **17**, 1180–1182 (2003).

70. Kinjo, T., Isomura, M., Iwamasa, T. & Nakamura, Y. Molecular cloning and characterization of two novel genes on chromosome 8p21.3. *J. Hum. Genet.* **45**, 12–17 (2000).

71. Wang, J. C. *et al.* Sequence-Ready Contig for the 1.4-cM Ductal Carcinoma in Situ Loss of Heterozygosity Region on Chromosome 8p22–p23. *Genomics* **60**, 1–11 (1999).

72. Nouet, S. *et al.* Trans-inactivation of Receptor Tyrosine Kinases by Novel Angiotensin II AT2 Receptor-interacting Protein, ATIP*. *J. Biol. Chem.* **279**, 28989–28997 (2004).

73. Nouet, S. & Nahmias, C. Signal Transduction from the Angiotensin II AT2 Receptor. *Trends Endocrinol. Metab.* **11**, 1–6 (2000).

74. Di Benedetto, M. *et al.* Structural organization and expression of human MTUS1, a candidate 8p22 tumor suppressor gene encoding a family of angiotensin II AT2 receptor-interacting proteins, ATIP. *Gene* **380**, 127–136 (2006).

75. KREZEL, M. A. *et al.* Gene Sequencing and Tissue Expression of Unknown Isoforms of an Angiotensin II Type 2 Receptor Interacting Protein, ATIP, in the Rat. *Biosci. Biotechnol. Biochem.* **75**, 414–418 (2011).

76. Rodrigues-Ferreira, S. & Nahmias, C. An ATIPical family of angiotensin II AT2 receptor-interacting proteins. *Trends Endocrinol. Metab.* **21**, 684–690 (2010).

77. Zuern, C. *et al.* Microtubule associated tumor suppressor 1 deficient mice develop spontaneous heart hypertrophy and SLE-like lymphoproliferative disease. *Int. J. Oncol.* **40**, 1079–1088 (2012).

78. Haykal, M. M., Rodrigues-Ferreira, S. & Nahmias, C. Microtubule-Associated Protein ATIP3, an Emerging Target for Personalized Medicine in Breast Cancer. *Cells* **10**, (2021).

79. Rodrigues-Ferreira, S. *et al.* 8p22 MTUS1 Gene Product ATIP3 Is a Novel Anti-Mitotic Protein Underexpressed in Invasive Breast Carcinoma of Poor Prognosis. *PLOS ONE* **4**, e7239 (2009).

80. Molina, A. *et al.* ATIP3, a Novel Prognostic Marker of Breast Cancer Patient Survival, Limits Cancer Cell Migration and Slows Metastatic Progression by Regulating Microtubule Dynamics. *Cancer Res.* **73**, 2905–2915 (2013).

81. Parbin, S. *et al.* DNA methylation regulates Microtubule-associated tumor suppressor 1 in human non-small cell lung carcinoma. *Exp. Cell Res.* **374**, 323–332 (2019).

82. Lv, Q., Dong, F., Zhou, Y., Cai, Z. & Wang, G. RNA-binding protein SORBS2

suppresses clear cell renal cell carcinoma metastasis by enhancing MTUS1 mRNA stability. *Cell Death Dis.* **11**, 1056 (2020).

83. Kara, M. *et al.* MTUS1 tumor suppressor and its miRNA regulators in fibroadenoma and breast cancer. *Gene* **587**, 173–177 (2016).

84. Ozcan, O. *et al.* MTUS1 and its targeting miRNAs in colorectal carcinoma: significant associations. *Tumor Biol.* **37**, 6637–6645 (2016).

85. Rodrigues-Ferreira, S. *et al.* Combinatorial expression of microtubule-associated EB1 and ATIP3 biomarkers improves breast cancer prognosis. *Breast Cancer Res. Treat.* **173**, 573–583 (2019).

86. Rodrigues-Ferreira, S., Molina, A. & Nahmias, C. Microtubule-associated tumor suppressors as prognostic biomarkers in breast cancer. *Breast Cancer Res. Treat.* **179**, 267–273 (2020).

87. Győrffy, B. Survival analysis across the entire transcriptome identifies biomarkers with the highest prognostic power in breast cancer. *Comput. Struct. Biotechnol. J.* **19**, 4101–4109 (2021).

88. Desai, A. & Mitchison, T. J. MICROTUBULE POLYMERIZATION DYNAMICS. *Annu. Rev. Cell Dev. Biol.* **13**, 83–117 (1997).

89. Akhmanova, A. & Steinmetz, M. O. Control of microtubule organization and dynamics: two ends in the limelight. *Nat. Rev. Mol. Cell Biol.* **16**, 711–726 (2015).

90. Velot, L. *et al.* Negative regulation of EB1 turnover at microtubule plus ends by interaction with microtubule-associated protein ATIP3. *Oncotarget Vol 6 No 41* (2015).

91. Nehlig, A. *et al.* Reciprocal regulation of Aurora kinase A and ATIP3 in the control of metaphase spindle length. *Cell. Mol. Life Sci.* **78**, 1765–1779 (2021).

92. Manning, A. L. *et al.* The Kinesin-13 Proteins Kif2a, Kif2b, and Kif2c/MCAK Have Distinct Roles during Mitosis in Human Cells. *Mol. Biol. Cell* **18**, 2970–2979 (2007).

93. Weaver, B. A. How Taxol/paclitaxel kills cancer cells. *Mol. Biol. Cell* **25**, 2677–2681 (2014).

94. Rodrigues-Ferreira, S. *et al.* Improving breast cancer sensitivity to paclitaxel by increasing aneuploidy. *Proc. Natl. Acad. Sci.* **116**, 23691–23697 (2019).

95. Rodrigues-Ferreira, S., Nehlig, A., Kacem, M. & Nahmias, C. ATIP3 deficiency facilitates intracellular accumulation of paclitaxel to reduce cancer cell migration and lymph node metastasis in breast cancer patients. *Sci. Rep.* **10**, 13217 (2020).

96. Rodrigues-Ferreira, S. & Nahmias, C. From tumorigenesis to cell death: the

aneuploidy paradox. *Mol. Cell. Oncol.* **7**, 1709390 (2020).

97. Dubrovsky, J. G. & Ivanov, V. B. Celebrating 50 years of the cell cycle. *Nature* **426**, 759–759 (2003).

98. Matthews, H. K., Bertoli, C. & de Bruin, R. A. M. Cell cycle control in cancer. *Nat. Rev. Mol. Cell Biol.* **23**, 74–88 (2022).

99. Pardee, A. B. A Restriction Point for Control of Normal Animal Cell Proliferation. *Proc. Natl. Acad. Sci.* **71**, 1286–1290 (1974).

100. Rubin, S. M., Sage, J. & Skotheim, J. M. Integrating Old and New Paradigms of G1/S Control. *Mol. Cell* **80**, 183–192 (2020).

101. Beroukhim, R. *et al.* The landscape of somatic copy-number alteration across human cancers. *Nature* **463**, 899–905 (2010).

102. Masai, H., Matsumoto, S., You, Z., Yoshizawa-Sugata, N. & Oda, M. Eukaryotic Chromosome DNA Replication: Where, When, and How? *Annu. Rev. Biochem.* **79**, 89–130 (2010).

103. Kotsantis, P., Jones, R. M., Higgs, M. R. & Petermann, E. Chapter Three - Cancer Therapy and Replication Stress: Forks on the Road to Perdition. in *Advances in Clinical Chemistry* (ed. Makowski, G. S.) vol. 69 91–138 (Elsevier, 2015).

104. Lindahl, T. Instability and decay of the primary structure of DNA. *Nature* **362**, 709–715 (1993).

105. Tubbs, A. & Nussenzweig, A. Endogenous DNA Damage as a Source of Genomic Instability in Cancer. *Cell* **168**, 644–656 (2017).

106. Lord, C. J. & Ashworth, A. The DNA damage response and cancer therapy. *Nature* **481**, 287–294 (2012).

107. Ciccia, A. & Elledge, S. J. The DNA Damage Response: Making It Safe to Play with Knives. *Mol. Cell* **40**, 179–204 (2010).

108. Matsuoka, S. *et al.* ATM and ATR Substrate Analysis Reveals Extensive Protein Networks Responsive to DNA Damage. *Science* **316**, 1160–1166 (2007).

109. Lee, J.-H. & Paull, T. T. ATM Activation by DNA Double-Strand Breaks Through the Mre11-Rad50-Nbs1 Complex. *Science* **308**, 551–554 (2005).

110. Burma, S., Chen, B. P., Murphy, M., Kurimasa, A. & Chen, D. J. ATM Phosphorylates Histone H2AX in Response to DNA Double-strand Breaks*. *J. Biol. Chem.* **276**, 42462–42467 (2001).

111. Paull, T. T. *et al.* A critical role for histone H2AX in recruitment of repair factors

to nuclear foci after DNA damage. *Curr. Biol.* **10**, 886–895 (2000).

112. Lou, Z. *et al.* MDC1 Maintains Genomic Stability by Participating in the Amplification of ATM-Dependent DNA Damage Signals. *Mol. Cell* **21**, 187–200 (2006).

113. Matsuoka, S., Huang, M. & Elledge, S. J. Linkage of ATM to Cell Cycle Regulation by the Chk2 Protein Kinase. *Science* **282**, 1893–1897 (1998).

114. Wade Harper, J., Adami, G. R., Wei, N., Keyomarsi, K. & Elledge, S. J. The p21 Cdk-interacting protein Cip1 is a potent inhibitor of G1 cyclin-dependent kinases. *Cell* **75**, 805–816 (1993).

115. Harper, J. W. *et al.* Inhibition of cyclin-dependent kinases by p21. *Mol. Biol. Cell* **6**, 387–400 (1995).

116. Agami, R. & Bernards, R. Distinct Initiation and Maintenance Mechanisms Cooperate to Induce G1 Cell Cycle Arrest in Response to DNA Damage. *Cell* **102**, 55–66 (2000).

117. Deckbar, D. *et al.* The Limitations of the G1-S Checkpoint. *Cancer Res.* **70**, 4412–4421 (2010).

118. Mailand, N. *et al.* Rapid Destruction of Human Cdc25A in Response to DNA Damage. *Science* **288**, 1425–1429 (2000).

119. Santra, M. K., Wajapeyee, N. & Green, M. R. F-box protein FBXO31 mediates cyclin D1 degradation to induce G1 arrest after DNA damage. *Nature* **459**, 722–725 (2009).

120. Smith, H. L., Southgate, H., Tweddle, D. A. & Curtin, N. J. DNA damage checkpoint kinases in cancer. *Expert Rev. Mol. Med.* **22**, e2 (2020).

121. DePamphilis, M. L. Chapter Two - Genome Duplication at the Beginning of Mammalian Development. in *Current Topics in Developmental Biology* (ed. DePamphilis, M. L.) vol. 120 55–102 (Academic Press, 2016).

122. Davidson, I. F., Li, A. & Blow, J. J. Deregulated Replication Licensing Causes DNA Fragmentation Consistent with Head-to-Tail Fork Collision. *Mol. Cell* **24**, 433–443 (2006).

123. Neelsen, K. J. *et al.* Deregulated origin licensing leads to chromosomal breaks by rereplication of a gapped DNA template. *Genes Dev.* **27**, 2537–2542 (2013).

124. Fragkos, M., Ganier, O., Coulombe, P. & Méchali, M. DNA replication origin activation in space and time. *Nat. Rev. Mol. Cell Biol.* **16**, 360–374 (2015).

125. McIntosh, D. & Blow, J. J. Dormant Origins, the Licensing Checkpoint, and the

Response to Replicative Stresses. *Cold Spring Harb. Perspect. Biol.* **4**, (2012).

126. Blow, J. J., Ge, X. Q. & Jackson, D. A. How dormant origins promote complete genome replication. *Trends Biochem. Sci.* **36**, 405–414 (2011).

127. Heller, R. C. *et al.* Eukaryotic Origin-Dependent DNA Replication In Vitro Reveals Sequential Action of DDK and S-CDK Kinases. *Cell* **146**, 80–91 (2011).

128. Labib, K. How do Cdc7 and cyclin-dependent kinases trigger the initiation of chromosome replication in eukaryotic cells? *Genes Dev.* **24**, 1208–1219 (2010).

129. Douglas, M. E., Ali, F. A., Costa, A. & Diffley, J. F. X. The mechanism of eukaryotic CMG helicase activation. *Nature* **555**, 265–268 (2018).

130. Zeman, M. K. & Cimprich, K. A. Causes and consequences of replication stress. *Nat. Cell Biol.* **16**, 2–9 (2014).

131. Vrtis, K. B. *et al.* Single-strand DNA breaks cause replisome disassembly. *Mol. Cell* **81**, 1309-1318.e6 (2021).

132. Branzei, D. & Foiani, M. Maintaining genome stability at the replication fork. *Nat. Rev. Mol. Cell Biol.* **11**, 208–219 (2010).

133. Sharma, S. *et al.* REV1 and polymerase ζ facilitate homologous recombination repair. *Nucleic Acids Res.* **40**, 682–691 (2012).

134. van Wietmarschen, N. *et al.* Repeat expansions confer WRN dependence in microsatellite-unstable cancers. *Nature* **586**, 292–298 (2020).

135. Aguilera, A. & García-Muse, T. R Loops: From Transcription Byproducts to Threats to Genome Stability. *Mol. Cell* **46**, 115–124 (2012).

136. Miller, K. M., Rog, O. & Cooper, J. P. Semi-conservative DNA replication through telomeres requires Taz1. *Nature* **440**, 824–828 (2006).

137. Zaratiegui, M. *et al.* CENP-B preserves genome integrity at replication forks paused by retrotransposon LTR. *Nature* **469**, 112–115 (2011).

138. Weinberg, G., Ullman, B. & Martin, D. W. Mutator phenotypes in mammalian cell mutants with distinct biochemical defects and abnormal deoxyribonucleoside triphosphate pools. *Proc. Natl. Acad. Sci.* **78**, 2447–2451 (1981).

139. Buisson, R., Boisvert, J. L., Benes, C. H. & Zou, L. Distinct but Concerted Roles of ATR, DNA-PK, and Chk1 in Countering Replication Stress during S Phase. *Mol. Cell* **59**, 1011–1024 (2015).

140. Saxena, S., Somyajit, K. & Nagaraju, G. XRCC2 Regulates Replication Fork Progression during dNTP Alterations. *Cell Rep.* **25**, 3273-3282.e6 (2018).

141. da Costa, A. A. B. A., Chowdhury, D., Shapiro, G. I., D'Andrea, A. D. & Konstantinopoulos, P. A. Targeting replication stress in cancer therapy. *Nat. Rev. Drug Discov.* **22**, 38–58 (2023).

142. Byun, T. S., Pacek, M., Yee, M., Walter, J. C. & Cimprich, K. A. Functional uncoupling of MCM helicase and DNA polymerase activities activates the ATR-dependent checkpoint. *Genes Dev.* **19**, 1040–1052 (2005).

143. Forrer Charlier, C. & Martins, R. A. P. Protective Mechanisms Against DNA Replication Stress in the Nervous System. *Genes* **11**, (2020).

144. Zou, L., Liu, D. & Elledge, S. J. Replication protein A-mediated recruitment and activation of Rad17 complexes. *Proc. Natl. Acad. Sci.* **100**, 13827–13832 (2003).

145. Kumagai, A., Lee, J., Yoo, H. Y. & Dunphy, W. G. TopBP1 Activates the ATR-ATRIP Complex. *Cell* **124**, 943–955 (2006).

146. Bass, T. E. *et al.* ETAA1 acts at stalled replication forks to maintain genome integrity. *Nat. Cell Biol.* **18**, 1185–1195 (2016).

147. Lee, Y.-C., Zhou, Q., Chen, J. & Yuan, J. RPA-Binding Protein ETAA1 Is an ATR Activator Involved in DNA Replication Stress Response. *Curr. Biol.* **26**, 3257–3268 (2016).

148. Branzei, D. & Foiani, M. Template Switching: From Replication Fork Repair to Genome Rearrangements. *Cell* **131**, 1228–1230 (2007).

149. Lopes, M., Foiani, M. & Sogo, J. M. Multiple Mechanisms Control Chromosome Integrity after Replication Fork Uncoupling and Restart at Irreparable UV Lesions. *Mol. Cell* **21**, 15–27 (2006).

150. Ashour, M. E. & Mosammaparast, N. Mechanisms of damage tolerance and repair during DNA replication. *Nucleic Acids Res.* **49**, 3033–3047 (2021).

151. De Piccoli, G. *et al.* Replisome Stability at Defective DNA Replication Forks Is Independent of S Phase Checkpoint Kinases. *Mol. Cell* **45**, 696–704 (2012).

152. Dungrawala, H. *et al.* The Replication Checkpoint Prevents Two Types of Fork Collapse without Regulating Replisome Stability. *Mol. Cell* **59**, 998–1010 (2015).

153. Neelsen, K. J. & Lopes, M. Replication fork reversal in eukaryotes: from dead end to dynamic response. *Nat. Rev. Mol. Cell Biol.* **16**, 207–220 (2015).

154. Zellweger, R. *et al.* Rad51-mediated replication fork reversal is a global response to genotoxic treatments in human cells. *J. Cell Biol.* **208**, 563–579 (2015).

155. Kolinjivadi, A. M. *et al.* Smarcal1-Mediated Fork Reversal Triggers Mre11-

Dependent Degradation of Nascent DNA in the Absence of Brca2 and Stable Rad51 Nucleofilaments. *Mol. Cell* **67**, 867-881.e7 (2017).

156. Vujanovic, M. *et al.* Replication Fork Slowing and Reversal upon DNA Damage Require PCNA Polyubiquitination and ZRANB3 DNA Translocase Activity. *Mol. Cell* **67**, 882-890.e5 (2017).

157. Bai, G. *et al.* HLTF Promotes Fork Reversal, Limiting Replication Stress Resistance and Preventing Multiple Mechanisms of Unrestrained DNA Synthesis. *Mol. Cell* **78**, 1237-1251.e7 (2020).

158. Schlacher, K. *et al.* Double-Strand Break Repair-Independent Role for BRCA2 in Blocking Stalled Replication Fork Degradation by MRE11. *Cell* **145**, 529–542 (2011).

159. Schlacher, K., Wu, H. & Jasin, M. A Distinct Replication Fork Protection Pathway Connects Fanconi Anemia Tumor Suppressors to RAD51-BRCA1/2. *Cancer Cell* **22**, 106–116 (2012).

160. Thangavel, S. *et al.* DNA2 drives processing and restart of reversed replication forks in human cells. *J. Cell Biol.* **208**, 545–562 (2015).

161. Cotta-Ramusino, C. *et al.* Exo1 Processes Stalled Replication Forks and Counteracts Fork Reversal in Checkpoint-Defective Cells. *Mol. Cell* **17**, 153–159 (2005).

162. Hanada, K. *et al.* The structure-specific endonuclease Mus81 contributes to replication restart by generating double-strand DNA breaks. *Nat. Struct. Mol. Biol.* **14**, 1096–1104 (2007).

163. Regairaz, M. *et al.* Mus81-mediated DNA cleavage resolves replication forks stalled by topoisomerase I–DNA complexes. *J. Cell Biol.* **195**, 739–749 (2011).

164. Pepe, A. & West, S. C. MUS81-EME2 Promotes Replication Fork Restart. *Cell Rep.* **7**, 1048–1055 (2014).

165. Yeo, J. E., Lee, E. H., Hendrickson, E. A. & Sobeck, A. CtIP mediates replication fork recovery in a FANCD2-regulated manner. *Hum. Mol. Genet.* **23**, 3695–3705 (2014).

166. Mijic, S. *et al.* Replication fork reversal triggers fork degradation in BRCA2-defective cells. *Nat. Commun.* **8**, 859 (2017).

167. El-Shemerly, M., Hess, D., Pyakurel, A. K., Moselhy, S. & Ferrari, S. ATR-dependent pathways control hEXO1 stability in response to stalled forks. *Nucleic Acids Res.* **36**, 511–519 (2008).

168. Kim, Y. *et al.* Regulation of multiple DNA repair pathways by the Fanconi anemia protein SLX4. *Blood* **121**, 54–63 (2013).

169. Ge, X. Q. & Blow, J. J. Chk1 inhibits replication factory activation but allows dormant origin firing in existing factories. *J. Cell Biol.* **191**, 1285–1297 (2010).

170. Zhao, H., Watkins, J. L. & Piwnica-Worms, H. Disruption of the checkpoint kinase 1/cell division cycle 25A pathway abrogates ionizing radiation-induced S and G2 checkpoints. *Proc. Natl. Acad. Sci.* **99**, 14795–14800 (2002).

171. Liu, H. *et al.* Phosphorylation of MLL by ATR is required for execution of mammalian S-phase checkpoint. *Nature* **467**, 343–346 (2010).

172. Guo, C. *et al.* Interaction of Chk1 with Treslin Negatively Regulates the Initiation of Chromosomal DNA Replication. *Mol. Cell* **57**, 492–505 (2015).

173. Toledo, L. I. *et al.* ATR Prohibits Replication Catastrophe by Preventing Global Exhaustion of RPA. *Cell* **155**, 1088–1103 (2013).

174. Karlsson-Rosenthal, C. & Millar, J. B. A. Cdc25: mechanisms of checkpoint inhibition and recovery. *Trends Cell Biol.* **16**, 285–292 (2006).

175. Boutros, R., Dozier, C. & Ducommun, B. The when and wheres of CDC25 phosphatases. *Cell Regul.* **18**, 185–191 (2006).

176. Sanchez, Y. *et al.* Conservation of the Chk1 Checkpoint Pathway in Mammals: Linkage of DNA Damage to Cdk Regulation Through Cdc25. *Science* **277**, 1497–1501 (1997).

177. Mankouri, H. W., Huttner, D. & Hickson, I. D. How unfinished business from S-phase affects mitosis and beyond. *EMBO J.* **32**, 2661–2671 (2013).

178. Stern, B. & Nurse, P. A quantitative model for the cdc2 control of S phase and mitosis in fission yeast. *Trends Genet.* **12**, 345–350 (1996).

179. Murray, A. W. Recycling the Cell Cycle: Cyclins Revisited. *Cell* **116**, 221–234 (2004).

180. Rahi, S. J., Pecani, K., Ondracka, A., Oikonomou, C. & Cross, F. R. The CDK-APC/C Oscillator Predominantly Entrains Periodic Cell-Cycle Transcription. *Cell* **165**, 475–487 (2016).

181. Akopyan, K. *et al.* Assessing Kinetics from Fixed Cells Reveals Activation of the Mitotic Entry Network at the S/G2 Transition. *Mol. Cell* **53**, 843–853 (2014).

182. Ly, T. *et al.* Proteomic analysis of cell cycle progression in asynchronous cultures, including mitotic subphases, using PRIMMUS. *eLife* **6**, e27574 (2017).

183. Lemmens, B. *et al.* DNA Replication Determines Timing of Mitosis by Restricting CDK1 and PLK1 Activation. *Mol. Cell* **71**, 117-128.e3 (2018).

184. Saldivar, J. C. *et al.* An intrinsic S/G2 checkpoint enforced by ATR. *Science* **361**, 806–810 (2018).

185. Lemmens, B. & Lindqvist, A. DNA replication and mitotic entry: A brake model for cell cycle progression. *J. Cell Biol.* **218**, 3892–3902 (2019).

186. Enders, G. H. Gauchos and ochos: a Wee1-Cdk tango regulating mitotic entry. *Cell Div.* **5**, 12 (2010).

187. Batty, P. & Gerlich, D. W. Mitotic Chromosome Mechanics: How Cells Segregate Their Genome. *Trends Cell Biol.* **29**, 717–726 (2019).

188. Gerlich, D., Hirota, T., Koch, B., Peters, J.-M. & Ellenberg, J. Condensin I Stabilizes Chromosomes Mechanically through a Dynamic Interaction in Live Cells. *Curr. Biol.* **16**, 333–344 (2006).

189. Ribeiro, S. A. *et al.* Condensin Regulates the Stiffness of Vertebrate Centromeres. *Mol. Biol. Cell* **20**, 2371–2380 (2009).

190. Houlard, M. *et al.* Condensin confers the longitudinal rigidity of chromosomes. *Nat. Cell Biol.* **17**, 771–781 (2015).

191. Sun, M., Biggs, R., Hornick, J. & Marko, J. F. Condensin controls mitotic chromosome stiffness and stability without forming a structurally contiguous scaffold. *Chromosome Res.* **26**, 277–295 (2018).

192. Peters, J.-M., Tedeschi, A. & Schmitz, J. The cohesin complex and its roles in chromosome biology. *Genes Dev.* **22**, 3089–3114 (2008).

193. Morales, C. & Losada, A. Establishing and dissolving cohesion during the vertebrate cell cycle. *Cell Nucl.* **52**, 51–57 (2018).

194. Wechsler, T., Newman, S. & West, S. C. Aberrant chromosome morphology in human cells defective for Holliday junction resolution. *Nature* **471**, 642–646 (2011).

195. Ono, T., Yamashita, D. & Hirano, T. Condensin II initiates sister chromatid resolution during S phase. *J. Cell Biol.* **200**, 429–441 (2013).

196. Gibcus, J. H. *et al.* A pathway for mitotic chromosome formation. *Science* **359**, eaao6135 (2018).

197. McKinley, K. L. & Cheeseman, I. M. The molecular basis for centromere identity and function. *Nat. Rev. Mol. Cell Biol.* **17**, 16–29 (2016).

198. Fachinetti, D. *et al.* DNA Sequence-Specific Binding of CENP-B Enhances the Fidelity of Human Centromere Function. *Dev. Cell* **33**, 314–327 (2015).

199. Fujita, R. *et al.* Stable complex formation of CENP-B with the CENP-A

nucleosome. *Nucleic Acids Res.* **43**, 4909–4922 (2015).

200. Otake, K. *et al.* CENP-B creates alternative epigenetic chromatin states permissive for CENP-A or heterochromatin assembly. *J. Cell Sci.* **133**, jcs243303 (2020).

201. Nassar, R., Thompson, L. & Fouquerel, E. Molecular mechanisms protecting centromeres from self-sabotage and implications for cancer therapy. *NAR Cancer* **5**, zcad019 (2023).

202. Cheeseman, I. M. The Kinetochore. *Cold Spring Harb. Perspect. Biol.* **6**, (2014).

203. Cheeseman, I. M. & Desai, A. Molecular architecture of the kinetochore–microtubule interface. *Nat. Rev. Mol. Cell Biol.* **9**, 33–46 (2008).

204. Screpanti, E. *et al.* Direct Binding of Cenp-C to the Mis12 Complex Joins the Inner and Outer Kinetochore. *Curr. Biol.* **21**, 391–398 (2011).

205. Przewloka, M. R. *et al.* CENP-C Is a Structural Platform for Kinetochore Assembly. *Curr. Biol.* **21**, 399–405 (2011).

206. Gascoigne, K. E. & Cheeseman, I. M. CDK-dependent phosphorylation and nuclear exclusion coordinately control kinetochore assembly state. *J. Cell Biol.* **201**, 23–32 (2013).

207. Suzuki, A., Badger, B. L., Wan, X., DeLuca, J. G. & Salmon, E. D. The Architecture of CCAN Proteins Creates a Structural Integrity to Resist Spindle Forces and Achieve Proper Intrakinetochore Stretch. *Dev. Cell* **30**, 717–730 (2014).

208. Amaro, A. C. *et al.* Molecular control of kinetochore-microtubule dynamics and chromosome oscillations. *Nat. Cell Biol.* **12**, 319–329 (2010).

209. Eibes, S. *et al.* CENP-E activation by Aurora A and B controls kinetochore fibrous corona disassembly. *Nat. Commun.* **14**, 5317 (2023).

210. Iemura, K. & Tanaka, K. Chromokinesin Kid and kinetochore kinesin CENP-E differentially support chromosome congression without end-on attachment to microtubules. *Nat. Commun.* **6**, 6447 (2015).

211. McIntosh, J. R. Structural and Mechanical Control of Mitotic Progression. *Cold Spring Harb. Symp. Quant. Biol.* **56**, 613–619 (1991).

212. Rieder, C. L., Cole, R. W., Khodjakov, A. & Sluder, G. The checkpoint delaying anaphase in response to chromosome monoorientation is mediated by an inhibitory signal produced by unattached kinetochores. *J. Cell Biol.* **130**, 941–948 (1995).

213. Foley, E. A. & Kapoor, T. M. Microtubule attachment and spindle assembly checkpoint signalling at the kinetochore. *Nat. Rev. Mol. Cell Biol.* **14**, 25–37 (2013).

214. Abrieu, A. *et al.* Mps1 Is a Kinetochore-Associated Kinase Essential for the Vertebrate Mitotic Checkpoint. *Cell* **106**, 83–93 (2001).

215. Tighe, A., Staples, O. & Taylor, S. Mps1 kinase activity restrains anaphase during an unperturbed mitosis and targets Mad2 to kinetochores. *J. Cell Biol.* **181**, 893–901 (2008).

216. London, N. & Biggins, S. Mad1 kinetochore recruitment by Mps1-mediated phosphorylation of Bub1 signals the spindle checkpoint. *Genes Dev.* **28**, 140–152 (2014).

217. Pines, J. Cubism and the cell cycle: the many faces of the APC/C. *Nat. Rev. Mol. Cell Biol.* **12**, 427–438 (2011).

218. McFarlane, R. J. & Humphrey, T. C. A role for recombination in centromere function. *Trends Genet.* **26**, 209–213 (2010).

219. Simi, S., Simili, M., Bonatti, S., Campagna, M. & Abbondandolo, A. Fragile sites at the centromere of Chinese hamster chromosomes: a possible mechanism of chromosome loss. *Mutat. Res. Mol. Mech. Mutagen.* **397**, 239–246 (1998).

220. Barra, V. & Fachinetti, D. The dark side of centromeres: types, causes and consequences of structural abnormalities implicating centromeric DNA. *Nat. Commun.* **9**, 4340 (2018).

221. Ly, P. & Cleveland, D. W. Rebuilding Chromosomes After Catastrophe: Emerging Mechanisms of Chromothripsis. *Trends Cell Biol.* **27**, 917–930 (2017).

222. Black, E. M. & Giunta, S. Repetitive Fragile Sites: Centromere Satellite DNA as a Source of Genome Instability in Human Diseases. *Genes* **9**, (2018).

223. Ly, P. *et al.* Chromosome segregation errors generate a diverse spectrum of simple and complex genomic rearrangements. *Nat. Genet.* **51**, 705–715 (2019).

224. Balzano, E. & Giunta, S. Centromeres under Pressure: Evolutionary Innovation in Conflict with Conserved Function. *Genes* **11**, (2020).

225. Chardon, F. *et al.* CENP-B-mediated DNA loops regulate activity and stability of human centromeres. *Mol. Cell* **82**, 1751-1767.e8 (2022).

226. Aze, A., Sannino, V., Soffientini, P., Bachi, A. & Costanzo, V. Centromeric DNA replication reconstitution reveals DNA loops and ATR checkpoint suppression. *Nat. Cell Biol.* **18**, 684–691 (2016).

227. Li, Z. *et al.* hDNA2 nuclease/helicase promotes centromeric DNA replication and genome stability. *EMBO J.* **37**, e96729 (2018).

228. Sundin, O. & Varshavsky, A. Terminal stages of SV40 DNA replication proceed via multiply intertwined catenated dimers. *Cell* **21**, 103–114 (1980).

229. Porter, A. C. G. & Farr, C. J. Topoisomerase II: untangling its contribution at the centromere. *Chromosome Res.* **12**, 569–583 (2004).

230. Wang, L. H.-C., Mayer, B., Stemmann, O. & Nigg, E. A. Centromere DNA decatenation depends on cohesin removal and is required for mammalian cell division. *J. Cell Sci.* **123**, 806–813 (2010).

231. Lukas, C. *et al.* 53BP1 nuclear bodies form around DNA lesions generated by mitotic transmission of chromosomes under replication stress. *Nat. Cell Biol.* **13**, 243–253 (2011).

232. Minocherhomji, S. *et al.* Replication stress activates DNA repair synthesis in mitosis. *Nature* **528**, 286–290 (2015).

233. Glover, T. W., Wilson, T. E. & Arlt, M. F. Fragile sites in cancer: more than meets the eye. *Nat. Rev. Cancer* **17**, 489–501 (2017).

234. Lezaja, A. & Altmeyer, M. Dealing with DNA lesions: When one cell cycle is not enough. *Cell Nucl.* **70**, 27–36 (2021).

235. Wyatt, H. D. M., Sarbajna, S., Matos, J. & West, S. C. Coordinated Actions of SLX1-SLX4 and MUS81-EME1 for Holliday Junction Resolution in Human Cells. *Mol. Cell* **52**, 234–247 (2013).

236. Palma, A. *et al.* Phosphorylation by CK2 regulates MUS81/EME1 in mitosis and after replication stress. *Nucleic Acids Res.* **46**, 5109–5124 (2018).

237. Bhowmick, R., Minocherhomji, S. & Hickson, I. D. RAD52 Facilitates Mitotic DNA Synthesis Following Replication Stress. *Mol. Cell* **64**, 1117–1126 (2016).

238. Chan, Y. W., Fugger, K. & West, S. C. Unresolved recombination intermediates lead to ultra-fine anaphase bridges, chromosome breaks and aberrations. *Nat. Cell Biol.* **20**, 92–103 (2018).

239. Tiwari, A., Addis Jones, O. & Chan, K.-L. 53BP1 can limit sister-chromatid rupture and rearrangements driven by a distinct ultrafine DNA bridging-breakage process. *Nat. Commun.* **9**, 677 (2018).

240. Harrigan, J. A. *et al.* Replication stress induces 53BP1-containing OPT domains in G1 cells. *J. Cell Biol.* **193**, 97–108 (2011).

241. Ochs, F. *et al.* Stabilization of chromatin topology safeguards genome integrity. *Nature* **574**, 571–574 (2019).

242. Lukas, J., Lukas, C. & Bartek, J. More than just a focus: The chromatin response to DNA damage and its role in genome integrity maintenance. *Nat. Cell Biol.* **13**, 1161–1169 (2011).

243. Nurse, P. Genetic control of cell size at cell division in yeast. *Nature* **256**, 547–551 (1975).

244. Thuriaux, P., Nurse, P. & Carter, B. Mutants altered in the control co-ordinating cell division with cell growth in the fission yeast Schizosaccharomyces pombe. *Mol. Gen. Genet. MGG* **161**, 215–220 (1978).

245. Russell, P. & Nurse, P. Negative regulation of mitosis by wee1+, a gene encoding a protein kinase homolog. *Cell* **49**, 559–567 (1987).

246. McGowan, C. H. & Russell, P. Cell cycle regulation of human WEE1. *EMBO J.* **14**, 2166–2175 (1995).

247. McGowan, C. H. & Russell, P. Human Wee1 kinase inhibits cell division by phosphorylating p34cdc2 exclusively on Tyr15. *EMBO J.* **12**, 75–85 (1993).

248. Parker, L. L. & Piwnica-Worms, H. Inactivation of the p34cdc2-Cyclin B Complex by the Human WEE1 Tyrosine Kinase. *Science* **257**, 1955–1957 (1992).

249. Villeneuve, J., Scarpa, M., Ortega-Bellido, M. & Malhotra, V. MEK1 inactivates Myt1 to regulate Golgi membrane fragmentation and mitotic entry in mammalian cells. *EMBO J.* **32**, 72–85 (2013).

250. Mueller, P. R., Coleman, T. R., Kumagai, A. & Dunphy, W. G. Myt1: A Membrane-Associated Inhibitory Kinase That Phosphorylates Cdc2 on Both Threonine-14 and Tyrosine-15. *Science* **270**, 86–90 (1995).

251. Liu, F., Stanton, J. J., Wu, Z. & Piwnica-Worms, H. The Human Myt1 Kinase Preferentially Phosphorylates Cdc2 on Threonine 14 and Localizes to the Endoplasmic Reticulum and Golgi Complex. *Mol. Cell. Biol.* **17**, 571–583 (1997).

252. Oh, J. S., Susor, A. & Conti, M. Protein Tyrosine Kinase Wee1B Is Essential for Metaphase II Exit in Mouse Oocytes. *Science* **332**, 462–465 (2011).

253. Featherstone, C. & Russell, P. Fission yeast p107wee1 mitotic inhibitor is a tyrosine/serine kinase. *Nature* **349**, 808–811 (1991).

254. Squire, C. J., Dickson, J. M., Ivanovic, I. & Baker, E. N. Structure and Inhibition of the Human Cell Cycle Checkpoint Kinase, Wee1A Kinase: An AtypicalTyrosine Kinase with a Key Role in CDK1 Regulation. *Structure* **13**, 541–550 (2005).

255. Bukhari, A. B., Chan, G. K. & Gamper, A. M. Targeting the DNA Damage Response for Cancer Therapy by Inhibiting the Kinase Wee1. *Front. Oncol.* **12**, (2022).

256. Mollapour, M. *et al.* Swe1Wee1-Dependent Tyrosine Phosphorylation of Hsp90 Regulates Distinct Facets of Chaperone Function. *Mol. Cell* **37**, 333–343 (2010).

257. Mollapour, M., Tsutsumi, S. & Neckers, L. Hsp90 phosphorylation, Wee1 and the cell cycle. *Cell Cycle* **9**, 2310–2316 (2010).

258. Kumagai, A. & Dunphy, W. G. Control of the Cdc2/cyclin B complex in Xenopus egg extracts arrested at a G2/M checkpoint with DNA synthesis inhibitors. *Mol. Biol. Cell* **6**, 199–213 (1995).

259. Lee, J., Kumagai, A. & Dunphy, W. G. Positive Regulation of Wee1 by Chk1 and 14-3-3 Proteins. *Mol. Biol. Cell* **12**, 551–563 (2001).

260. Watanabe, N., Broome, M. & Hunter, T. Regulation of the human WEE1Hu CDK tyrosine 15-kinase during the cell cycle. *EMBO J.* **14**, 1878–1891 (1995).

261. Watanabe, N. *et al.* M-phase kinases induce phospho-dependent ubiquitination of somatic Wee1 by SCFβ-TrCP. *Proc. Natl. Acad. Sci.* **101**, 4419–4424 (2004).

262. Watanabe, N. *et al.* Cyclin-dependent kinase (CDK) phosphorylation destabilizes somatic Wee1 via multiple pathways. *Proc. Natl. Acad. Sci.* **102**, 11663–11668 (2005).

263. Harvey, S. L., Charlet, A., Haas, W., Gygi, S. P. & Kellogg, D. R. Cdk1-Dependent Regulation of the Mitotic Inhibitor Wee1. *Cell* **122**, 407–420 (2005).

264. Yde, C. W., Olsen, B. B., Meek, D., Watanabe, N. & Guerra, B. The regulatory β-subunit of protein kinase CK2 regulates cell-cycle progression at the onset of mitosis. *Oncogene* **27**, 4986–4997 (2008).

265. Michael, W. M. & Newport, J. Coupling of Mitosis to the Completion of S Phase Through Cdc34-Mediated Degradation of Wee1. *Science* **282**, 1886–1889 (1998).

266. Ayad, N. G. *et al.* Tome-1, a Trigger of Mitotic Entry, Is Degraded during G1 via the APC. *Cell* **113**, 101–113 (2003).

267. Katayama, K., Fujita, N. & Tsuruo, T. Akt/Protein Kinase B-Dependent Phosphorylation and Inactivation of WEE1Hu Promote Cell Cycle Progression at G2/M Transition. *Mol. Cell. Biol.* **25**, 5725–5737 (2005).

268. Koh, S.-B. The expanding role of WEE1. *Cell. Signal.* **94**, 110310 (2022).

269. Chang, W. *et al.* Phosphorylation of MAP4 affects microtubule properties and cell cycle progression. *J. Cell Sci.* **114**, 2879–2887 (2001).

270. Mchedlishvili, N., Matthews, H. K., Corrigan, A. & Baum, B. Two-step interphase microtubule disassembly aids spindle morphogenesis. *BMC Biol.* **16**, 14 (2018).

271. Serpico, A. F., Febbraro, F., Pisauro, C. & Grieco, D. Compartmentalized control

of Cdk1 drives mitotic spindle assembly. *Cell Rep.* **38**, 110305 (2022).

272. David, A. F. *et al.* Augmin accumulation on long-lived microtubules drives amplification and kinetochore-directed growth. *J. Cell Biol.* **218**, 2150–2168 (2019).

273. Skoufias, D. A., Indorato, R.-L., Lacroix, F., Panopoulos, A. & Margolis, R. L. Mitosis persists in the absence of Cdk1 activity when proteolysis or protein phosphatase activity is suppressed. *J. Cell Biol.* **179**, 671–685 (2007).

274. Lianga, N. *et al.* A Wee1 checkpoint inhibits anaphase onset. *J. Cell Biol.* **201**, 843–862 (2013).

275. Wu, J. Q. *et al.* PP1-mediated dephosphorylation of phosphoproteins at mitotic exit is controlled by inhibitor-1 and PP1 phosphorylation. *Nat. Cell Biol.* **11**, 644–651 (2009).

276. Lucena, R., Alcaide-Gavilán, M., Anastasia, S. D. & Kellogg, D. R. Wee1 and Cdc25 are controlled by conserved PP2A-dependent mechanisms in fission yeast. *Cell Cycle* **16**, 428–435 (2017).

277. Visconti, R. *et al.* The Fcp1-Wee1-Cdk1 axis affects spindle assembly checkpoint robustness and sensitivity to antimicrotubule cancer drugs. *Cell Death Differ.* **22**, 1551–1560 (2015).

278. Elbæk, C. R., Petrosius, V. & Sørensen, C. S. WEE1 kinase limits CDK activities to safeguard DNA replication and mitotic entry. *Mutat. Res. Mol. Mech. Mutagen.* **819–820**, 111694 (2020).

279. Beck, H. *et al.* Cyclin-Dependent Kinase Suppression by WEE1 Kinase Protects the Genome through Control of Replication Initiation and Nucleotide Consumption. *Mol. Cell. Biol.* **32**, 4226–4236 (2012).

280. Pfister, S. X. *et al.* Inhibiting WEE1 Selectively Kills Histone H3K36me3-Deficient Cancers by dNTP Starvation. *Cancer Cell* **28**, 557–568 (2015).

281. Duda, H. *et al.* A Mechanism for Controlled Breakage of Under-replicated Chromosomes during Mitosis. *Dev. Cell* **39**, 740–755 (2016).

282. Domínguez-Kelly, R. *et al.* Wee1 controls genomic stability during replication by regulating the Mus81-Eme1 endonuclease. *J. Cell Biol.* **194**, 567–579 (2011).

283. Elbæk, C. R. *et al.* WEE1 kinase protects the stability of stalled DNA replication forks by limiting CDK2 activity. *Cell Rep.* **38**, 110261 (2022).

284. Petrosius, V., Benada, J., Nielsen, O., Schoof, E. M. & Sørensen, C. S. Temporal phosphoproteomics reveals WEE1-dependent control of 53BP1 pathway. *iScience* **26**, 105806 (2023).

285. Orthwein, A. *et al.* Mitosis Inhibits DNA Double-Strand Break Repair to Guard Against Telomere Fusions. *Science* **344**, 189–193 (2014).

286. Mukherjee, C. *et al.* RIF1 promotes replication fork protection and efficient restart to maintain genome stability. *Nat. Commun.* **10**, 3287 (2019).

287. Liu, W., Krishnamoorthy, A., Zhao, R. & Cortez, D. Two replication fork remodeling pathways generate nuclease substrates for distinct fork protection factors. *Sci. Adv.* **6**, eabc3598.

288. Meeks-Wagner, D. & Hartwell, L. H. Normal stoichiometry of histone dimer sets is necessary for high fidelity of mitotic chromosome transmission. *Cell* **44**, 43–52 (1986).

289. Mahajan, K., Fang, B., Koomen, J. M. & Mahajan, N. P. H2B Tyr37 phosphorylation suppresses expression of replication-dependent core histone genes. *Nat. Struct. Mol. Biol.* **19**, 930–937 (2012).

290. Mahajan, K. & Mahajan, N. P. WEE1 tyrosine kinase, a novel epigenetic modifier. *Trends Genet.* **29**, 394–402 (2013).

291. Fasulo, B. *et al.* Chk1 and Wee1 kinases coordinate DNA replication, chromosome condensation, and anaphase entry. *Mol. Biol. Cell* **23**, 1047–1057 (2012).

292. Alexandrow, M. G. & Hamlin, J. L. Chromatin decondensation in S-phase involves recruitment of Cdk2 by Cdc45 and histone H1 phosphorylation. *J. Cell Biol.* **168**, 875–886 (2005).

293. Roque, A., Ponte, I., Arrondo, J. L. R. & Suau, P. Phosphorylation of the carboxy-terminal domain of histone H1: effects on secondary structure and DNA condensation. *Nucleic Acids Res.* **36**, 4719–4726 (2008).

294. Hergeth, S. P. & Schneider, R. The H1 linker histones: multifunctional proteins beyond the nucleosomal core particle. *EMBO Rep.* **16**, 1439–1453 (2015).

295. Chang, K. *et al.* The Cancer Genome Atlas Pan-Cancer analysis project. *Nat. Genet.* **45**, 1113–1120 (2013).

296. Mir, S. E. *et al.* In Silico Analysis of Kinase Expression Identifies WEE1 as a Gatekeeper against Mitotic Catastrophe in Glioblastoma. *Cancer Cell* **18**, 244–257 (2010).

297. Magnussen, G. I. *et al.* High Expression of Wee1 Is Associated with Poor Disease-Free Survival in Malignant Melanoma: Potential for Targeted Therapy. *PLOS ONE* **7**, e38254 (2012).

298. Slipicevic, A. *et al.* Wee1 is a novel independent prognostic marker of poor survival in post-chemotherapy ovarian carcinoma effusions. *Gynecol. Oncol.* **135**, 118–

124 (2014).

299. Koh, S.-B. *et al.* Mechanistic Distinctions between CHK1 and WEE1 Inhibition Guide the Scheduling of Triple Therapy with Gemcitabine. *Cancer Res.* **78**, 3054–3066 (2018).

300. Ghelli Luserna Di Rorà, A. *et al.* Targeting WEE1 to enhance conventional therapies for acute lymphoblastic leukemia. *J. Hematol. Oncol.J Hematol Oncol* **11**, 99 (2018).

301. Aarts, M. *et al.* Forced Mitotic Entry of S-Phase Cells as a Therapeutic Strategy Induced by Inhibition of WEE1. *Cancer Discov.* **2**, 524–539 (2012).

302. Bridges, K. A. *et al.* MK-1775, a Novel Wee1 Kinase Inhibitor, Radiosensitizes p53-Defective Human Tumor Cells. *Clin. Cancer Res.* **17**, 5638–5648 (2011).

303. Rajeshkumar, N. V. *et al.* MK-1775, a Potent Wee1 Inhibitor, Synergizes with Gemcitabine to Achieve Tumor Regressions, Selectively in p53-Deficient Pancreatic Cancer Xenografts. *Clin. Cancer Res.* **17**, 2799–2806 (2011).

304. Webster, P. J. *et al.* AZD1775 induces toxicity through double-stranded DNA breaks independently of chemotherapeutic agents in p53-mutated colorectal cancer cells. *Cell Cycle* **16**, 2176–2182 (2017).

305. PosthumaDeBoer, J. *et al.* WEE1 inhibition sensitizes osteosarcoma to radiotherapy. *BMC Cancer* **11**, 156 (2011).

306. Fang, Y. *et al.* Sequential Therapy with PARP and WEE1 Inhibitors Minimizes Toxicity while Maintaining Efficacy. *Cancer Cell* **35**, 851-867.e7 (2019).

307. Wang, Y. *et al.* Radiosensitization of p53 Mutant Cells by PD0166285, a Novel G2 Checkpoint Abrogator. *Cancer Res.* **61**, 8211–8217 (2001).

308. Robert L. Panek *et al.* In Vitro Pharmacological Characterization of PD 166285, a New Nanomolar Potent and Broadly Active Protein Tyrosine Kinase Inhibitor. *J. Pharmacol. Exp. Ther.* **283**, 1433 (1997).

309. Hirai, H. *et al.* Small-molecule inhibition of Wee1 kinase by MK-1775 selectively sensitizes p53-deficient tumor cells to DNA-damaging agents. *Mol. Cancer Ther.* **8**, 2992–3000 (2009).

310. Wright, G. *et al.* Dual Targeting of WEE1 and PLK1 by AZD1775 Elicits Single Agent Cellular Anticancer Activity. *ACS Chem. Biol.* **12**, 1883–1892 (2017).

311. Serpico, A. F. *et al.* Wee1 Rather Than Plk1 Is Inhibited by AZD1775 at Therapeutically Relevant Concentrations. *Cancers* **11**, (2019).

312. Li, Z. *et al.* Development and Characterization of a Wee1 Kinase Degrader. *Cell Chem. Biol.* **27**, 57-65.e9 (2020).

313. Matheson, C. J., Backos, D. S. & Reigan, P. Targeting WEE1 Kinase in Cancer. *Trends Pharmacol. Sci.* **37**, 872–881 (2016).

314. Do, K. *et al.* Phase I Study of Single-Agent AZD1775 (MK-1775), a Wee1 Kinase Inhibitor, in Patients With Refractory Solid Tumors. *J. Clin. Oncol.* **33**, 3409–3415 (2015).

315. Leijen, S. *et al.* Phase I Study Evaluating WEE1 Inhibitor AZD1775 As Monotherapy and in Combination With Gemcitabine, Cisplatin, or Carboplatin in Patients With Advanced Solid Tumors. *J. Clin. Oncol.* **34**, 4371–4380 (2016).

316. Méndez, E. *et al.* A Phase I Clinical Trial of AZD1775 in Combination with Neoadjuvant Weekly Docetaxel and Cisplatin before Definitive Therapy in Head and Neck Squamous Cell Carcinoma. *Clin. Cancer Res.* **24**, 2740–2748 (2018).

317. Leijen, S. *et al.* Phase II Study of WEE1 Inhibitor AZD1775 Plus Carboplatin in Patients With TP53-Mutated Ovarian Cancer Refractory or Resistant to First-Line Therapy Within 3 Months. *J. Clin. Oncol.* **34**, 4354–4361 (2016).

318. Moore, K. N. *et al.* Adavosertib with chemotherapy (CT) in patients (pts) with platinum-resistant ovarian cancer (PPROC): An open label, four-arm, phase II study. *J. Clin. Oncol.* **37**, 5513–5513 (2019).

319. Cuneo, K. C. *et al.* Dose Escalation Trial of the Wee1 Inhibitor Adavosertib (AZD1775) in Combination With Gemcitabine and Radiation for Patients With Locally Advanced Pancreatic Cancer. *J. Clin. Oncol.* **37**, 2643–2650 (2019).

320. Huang, P. Q. *et al.* Discovery of ZN-c3, a Highly Potent and Selective Wee1 Inhibitor Undergoing Evaluation in Clinical Trials for the Treatment of Cancer. *J. Med. Chem.* **64**, 13004–13024 (2021).

321. Seligmann, J. F. *et al.* Inhibition of WEE1 Is Effective in TP53- and RAS-Mutant Metastatic Colorectal Cancer: A Randomized Trial (FOCUS4-C) Comparing Adavosertib (AZD1775) With Active Monitoring. *J. Clin. Oncol.* **39**, 3705–3715 (2021).

322. Van Linden, A. A. *et al.* Inhibition of Wee1 Sensitizes Cancer Cells to Antimetabolite Chemotherapeutics In Vitro and In Vivo, Independent of p53 Functionality. *Mol. Cancer Ther.* **12**, 2675–2684 (2013).

323. Zhou, L. *et al.* A regimen combining the Wee1 inhibitor AZD1775 with HDAC inhibitors targets human acute myeloid leukemia cells harboring various genetic mutations. *Leukemia* **29**, 807–818 (2015).

324. Kreahling, J. M. *et al.* MK1775, a Selective Wee1 Inhibitor, Shows Single-Agent Antitumor Activity against Sarcoma Cells. *Mol. Cancer Ther.* **11**, 174–182 (2012).

325. Chen, X. *et al.* Cyclin E Overexpression Sensitizes Triple-Negative Breast Cancer to Wee1 Kinase Inhibition. *Clin. Cancer Res.* **24**, 6594–6610 (2018).

326. Xu, H. *et al.* CCNE1 copy number is a biomarker for response to combination WEE1-ATR inhibition in ovarian and endometrial cancer models. *Cell Rep. Med.* **2**, 100394 (2021).

327. Fu, S. *et al.* Multicenter Phase II Trial of the WEE1 Inhibitor Adavosertib in Refractory Solid Tumors Harboring CCNE1 Amplification. *J. Clin. Oncol.* **41**, 1725–1734 (2023).

328. Lewis, C. W. *et al.* Upregulation of Myt1 Promotes Acquired Resistance of Cancer Cells to Wee1 Inhibition. *Cancer Res.* **79**, 5971–5985 (2019).

329. Duncan, A. W. *et al.* The ploidy conveyor of mature hepatocytes as a source of genetic variation. *Nature* **467**, 707–710 (2010).

330. Duncan, A. W. *et al.* Frequent Aneuploidy Among Normal Human Hepatocytes. *Gastroenterology* **142**, 25–28 (2012).

331. Duncan, A. W. *et al.* Aneuploidy as a mechanism for stress-induced liver adaptation. *J. Clin. Invest.* **122**, 3307–3315 (2012).

332. Rehen, S. K. *et al.* Chromosomal variation in neurons of the developing and adult mammalian nervous system. *Proc. Natl. Acad. Sci.* **98**, 13361–13366 (2001).

333. Kingsbury, M. A. *et al.* Aneuploid neurons are functionally active and integrated into brain circuitry. *Proc. Natl. Acad. Sci.* **102**, 6143–6147 (2005).

334. Baker, D. J. *et al.* BubR1 insufficiency causes early onset of aging-associated phenotypes and infertility in mice. *Nat. Genet.* **36**, 744–749 (2004).

335. Baker, D. J. *et al.* Increased expression of BubR1 protects against aneuploidy and cancer and extends healthy lifespan. *Nat. Cell Biol.* **15**, 96–102 (2013).

336. Knouse, K. A., Wu, J., Whittaker, C. A. & Amon, A. Single cell sequencing reveals low levels of aneuploidy across mammalian tissues. *Proc. Natl. Acad. Sci.* **111**, 13409–13414 (2014).

337. Pfau, S. J., Silberman, R. E., Knouse, K. A. & Amon, A. Aneuploidy impairs hematopoietic stem cell fitness and is selected against in regenerating tissues in vivo. *Genes Dev.* **30**, 1395–1408 (2016).

338. Gordon, D. J., Resio, B. & Pellman, D. Causes and consequences of aneuploidy in cancer. *Nat. Rev. Genet.* **13**, 189–203 (2012).

339. Siegel, J. J. & Amon, A. New Insights into the Troubles of Aneuploidy. *Annu. Rev.*

Cell Dev. Biol. **28**, 189–214 (2012).

340. McIntosh, J. R. Mitosis. *Cold Spring Harb. Perspect. Biol.* **8**, (2016).

341. Thompson, S. L. & Compton, D. A. Chromosome missegregation in human cells arises through specific types of kinetochore–microtubule attachment errors. *Proc. Natl. Acad. Sci.* **108**, 17974–17978 (2011).

342. Godek, K. M., Kabeche, L. & Compton, D. A. Regulation of kinetochore–microtubule attachments through homeostatic control during mitosis. *Nat. Rev. Mol. Cell Biol.* **16**, 57–64 (2015).

343. DeLuca, K. F., Lens, S. M. A. & DeLuca, J. G. Temporal changes in Hec1 phosphorylation control kinetochore–microtubule attachment stability during mitosis. *J. Cell Sci.* **124**, 622–634 (2011).

344. Gregan, J., Polakova, S., Zhang, L., Tolić-Nørrelykke, I. M. & Cimini, D. Merotelic kinetochore attachment: causes and effects. *Trends Cell Biol.* **21**, 374–381 (2011).

345. Bakhoum, S. F., Genovese, G. & Compton, D. A. Deviant Kinetochore Microtubule Dynamics Underlie Chromosomal Instability. *Curr. Biol.* **19**, 1937–1942 (2009).

346. Cimini, D., Wan, X., Hirel, C. B. & Salmon, E. D. Aurora Kinase Promotes Turnover of Kinetochore Microtubules to Reduce Chromosome Segregation Errors. *Curr. Biol.* **16**, 1711–1718 (2006).

347. Abad, M. A. *et al.* Structural basis for microtubule recognition by the human kinetochore Ska complex. *Nat. Commun.* **5**, 2964 (2014).

348. Molina, O. *et al.* Epigenetic engineering reveals a balance between histone modifications and transcription in kinetochore maintenance. *Nat. Commun.* **7**, 13334 (2016).

349. Molina, O., Kouprina, N., Masumoto, H., Larionov, V. & Earnshaw, W. C. Using human artificial chromosomes to study centromere assembly and function. *Chromosoma* **126**, 559–575 (2017).

350. Giam, M. & Rancati, G. Aneuploidy and chromosomal instability in cancer: a jackpot to chaos. *Cell Div.* **10**, 3 (2015).

351. Simon, J. E., Bakker, B. & Foijer, F. CINcere Modelling: What Have Mouse Models for Chromosome Instability Taught Us? in *Chromosomal Instability in Cancer Cells* (eds. Ghadimi, B. M. & Ried, T.) 39–60 (Springer International Publishing, 2015). doi:10.1007/978-3-319-20291-4_2.

352. Hanks, S. *et al.* Constitutional aneuploidy and cancer predisposition caused by biallelic mutations in BUB1B. *Nat. Genet.* **36**, 1159–1161 (2004).

353. Hernando, E. *et al.* Rb inactivation promotes genomic instability by uncoupling cell cycle progression from mitotic control. *Nature* **430**, 797–802 (2004).

354. Sotillo, R. *et al.* Mad2 Overexpression Promotes Aneuploidy and Tumorigenesis in Mice. *Cancer Cell* **11**, 9–23 (2007).

355. Kato, T. *et al.* Overexpression of MAD2 predicts clinical outcome in primary lung cancer patients. *Lung Cancer* **74**, 124–131 (2011).

356. Kabeche, L. & Compton, D. A. Checkpoint-Independent Stabilization of Kinetochore-Microtubule Attachments by Mad2 in Human Cells. *Curr. Biol.* **22**, 638–644 (2012).

357. Ryan, S. D. *et al.* Up-regulation of the mitotic checkpoint component Mad1 causes chromosomal instability and resistance to microtubule poisons. *Proc. Natl. Acad. Sci.* **109**, E2205–E2214 (2012).

358. Funk, L. C., Zasadil, L. M. & Weaver, B. A. Living in CIN: Mitotic Infidelity and Its Consequences for Tumor Promotion and Suppression. *Dev. Cell* **39**, 638–652 (2016).

359. Nigg, E. A. & Stearns, T. The centrosome cycle: Centriole biogenesis, duplication and inherent asymmetries. *Nat. Cell Biol.* **13**, 1154–1160 (2011).

360. Godinho, S. A. *et al.* Oncogene-like induction of cellular invasion from centrosome amplification. *Nature* **510**, 167–171 (2014).

361. Holland, A. J. & Cleveland, D. W. Boveri revisited: chromosomal instability, aneuploidy and tumorigenesis. *Nat. Rev. Mol. Cell Biol.* **10**, 478–487 (2009).

362. Nigg, E. A. Centrosome aberrations: cause or consequence of cancer progression? *Nat. Rev. Cancer* **2**, 815–825 (2002).

363. Ganem, N. J., Godinho, S. A. & Pellman, D. A mechanism linking extra centrosomes to chromosomal instability. *Nature* **460**, 278–282 (2009).

364. Kwon, M. *et al.* Mechanisms to suppress multipolar divisions in cancer cells with extra centrosomes. *Genes Dev.* **22**, 2189–2203 (2008).

365. Fujiwara, T. *et al.* Cytokinesis failure generating tetraploids promotes tumorigenesis in p53-null cells. *Nature* **437**, 1043–1047 (2005).

366. Zack, T. I. *et al.* Pan-cancer patterns of somatic copy number alteration. *Nat. Genet.* **45**, 1134–1140 (2013).

367. Dewhurst, S. M. *et al.* Tolerance of Whole-Genome Doubling Propagates Chromosomal Instability and Accelerates Cancer Genome Evolution. *Cancer Discov.* **4**, 175–185 (2014).

368. Ganem, N. J., Storchova, Z. & Pellman, D. Tetraploidy, aneuploidy and cancer. *Chromosom. Expr. Mech.* **17**, 157–162 (2007).

369. Gisselsson, D. *et al.* Generation of trisomies in cancer cells by multipolar mitosis and incomplete cytokinesis. *Proc. Natl. Acad. Sci.* **107**, 20489–20493 (2010).

370. Logarinho, E. *et al.* CLASPs prevent irreversible multipolarity by ensuring spindle-pole resistance to traction forces during chromosome alignment. *Nat. Cell Biol.* **14**, 295–303 (2012).

371. Barber, T. D. *et al.* Chromatid cohesion defects may underlie chromosome instability in human colorectal cancers. *Proc. Natl. Acad. Sci.* **105**, 3443–3448 (2008).

372. Mannini, L. & Musio, A. The dark side of cohesin: The carcinogenic point of view. *Mutat. Res. Mutat. Res.* **728**, 81–87 (2011).

373. Solomon, D. A. *et al.* Mutational Inactivation of STAG2 Causes Aneuploidy in Human Cancer. *Science* **333**, 1039–1043 (2011).

374. Zhang, N. *et al.* Overexpression of Separase induces aneuploidy and mammary tumorigenesis. *Proc. Natl. Acad. Sci.* **105**, 13033–13038 (2008).

375. Halazonetis, T. D., Gorgoulis, V. G. & Bartek, J. An Oncogene-Induced DNA Damage Model for Cancer Development. *Science* **319**, 1352–1355 (2008).

376. Gisselsson, D. Classification of chromosome segregation errors in cancer. *Chromosoma* **117**, 511–519 (2008).

377. Samoshkin, A. *et al.* Human Condensin Function Is Essential for Centromeric Chromatin Assembly and Proper Sister Kinetochore Orientation. *PLOS ONE* **4**, e6831 (2009).

378. Burrell, R. A. *et al.* Replication stress links structural and numerical cancer chromosomal instability. *Nature* **494**, 492–496 (2013).

379. Böhly, N. *et al.* Increased replication origin firing links replication stress to whole chromosomal instability in human cancer. *Cell Rep.* **41**, 111836 (2022).

380. Gorgoulis, V. G. *et al.* Activation of the DNA damage checkpoint and genomic instability in human precancerous lesions. *Nature* **434**, 907–913 (2005).

381. Hansford, S. & Huntsman, D. G. Boveri at 100: Theodor Boveri and genetic predisposition to cancer. *J. Pathol.* **234**, 142–145 (2014).

382. Bignold, L. P., Coghlan, B. L. D. & Jersmann, H. P. A. Hansemann, Boveri, chromosomes and the gametogenesis-related theories of tumours. *Cell Biol. Int.* **30**, 640–644 (2006).

383. Taylor, A. M. *et al.* Genomic and Functional Approaches to Understanding Cancer Aneuploidy. *Cancer Cell* **33**, 676-689.e3 (2018).

384. Weaver, B. A. A. & Cleveland, D. W. Aneuploidy: Instigator and Inhibitor of Tumorigenesis. *Cancer Res.* **67**, 10103–10105 (2007).

385. Torres, E. M. *et al.* Effects of Aneuploidy on Cellular Physiology and Cell Division in Haploid Yeast. *Science* **317**, 916–924 (2007).

386. Williams, B. R. *et al.* Aneuploidy Affects Proliferation and Spontaneous Immortalization in Mammalian Cells. *Science* **322**, 703–709 (2008).

387. Stingele, S. *et al.* Global analysis of genome, transcriptome and proteome reveals the response to aneuploidy in human cells. *Mol. Syst. Biol.* **8**, 608 (2012).

388. Sheltzer, J. M. & Amon, A. The aneuploidy paradox: costs and benefits of an incorrect karyotype. *Trends Genet.* **27**, 446–453 (2011).

389. Hoevenaar, W. H. M. *et al.* Degree and site of chromosomal instability define its oncogenic potential. *Nat. Commun.* **11**, 1501 (2020).

390. Santaguida, S. *et al.* Chromosome Mis-segregation Generates Cell-Cycle-Arrested Cells with Complex Karyotypes that Are Eliminated by the Immune System. *Dev. Cell* **41**, 638-651.e5 (2017).

391. Weaver, B. A. A., Silk, A. D., Montagna, C., Verdier-Pinard, P. & Cleveland, D. W. Aneuploidy Acts Both Oncogenically and as a Tumor Suppressor. *Cancer Cell* **11**, 25–36 (2007).

392. Ben-David, U. & Amon, A. Context is everything: aneuploidy in cancer. *Nat. Rev. Genet.* **21**, 44–62 (2020).

393. Duijf, P. H. G. & Benezra, R. The cancer biology of whole-chromosome instability. *Oncogene* **32**, 4727–4736 (2013).

394. Manning, A. L., Longworth, M. S. & Dyson, N. J. Loss of pRB causes centromere dysfunction and chromosomal instability. *Genes Dev.* **24**, 1364–1376 (2010).

395. Davoli, T. *et al.* Cumulative Haploinsufficiency and Triplosensitivity Drive Aneuploidy Patterns and Shape the Cancer Genome. *Cell* **155**, 948–962 (2013).

396. Silk, A. D. *et al.* Chromosome missegregation rate predicts whether aneuploidy will promote or suppress tumors. *Proc. Natl. Acad. Sci.* **110**, E4134–E4141 (2013).

397. Das, K. & Tan, P. Molecular cytogenetics: recent developments and applications in cancer. *Clin. Genet.* **84**, 315–325 (2013).

398. van den Bos, H., Bakker, B., Spierings, D. C. J., Lansdorp, P. M. & Foijer, F. Single-

cell sequencing to quantify genomic integrity in cancer. *Int. J. Biochem. Cell Biol.* **94**, 146–150 (2018).

399. Gazic, B. *et al.* S-phase fraction determined on fine needle aspirates is an independent prognostic factor in breast cancer – a multivariate study of 770 patients. *Cytopathology* **19**, 294–302 (2008).

400. Karra, H. *et al.* Securin predicts aneuploidy and survival in breast cancer. *Histopathology* **60**, 586–596 (2012).

401. Pinto, A. E. *et al.* DNA Ploidy is an Independent Predictor of Survival in Breast Invasive Ductal Carcinoma: A Long-term Multivariate Analysis of 393 Patients. *Ann. Surg. Oncol.* **20**, 1530–1537 (2013).

402. Danielsen, H. E., Pradhan, M. & Novelli, M. Revisiting tumour aneuploidy — the place of ploidy assessment in the molecular era. *Nat. Rev. Clin. Oncol.* **13**, 291–304 (2016).

403. Hieronymus, H. *et al.* Tumor copy number alteration burden is a pan-cancer prognostic factor associated with recurrence and death. *eLife* **7**, e37294 (2018).

404. Vasudevan, A. *et al.* Single-Chromosomal Gains Can Function as Metastasis Suppressors and Promoters in Colon Cancer. *Dev. Cell* **52**, 413-428.e6 (2020).

405. Andor, N. *et al.* Pan-cancer analysis of the extent and consequences of intratumor heterogeneity. *Nat. Med.* **22**, 105–113 (2016).

406. Rowald, K. *et al.* Negative Selection and Chromosome Instability Induced by Mad2 Overexpression Delay Breast Cancer but Facilitate Oncogene-Independent Outgrowth. *Cell Rep.* **15**, 2679–2691 (2016).

407. Ben-David, U. *et al.* Patient-derived xenografts undergo mouse-specific tumor evolution. *Nat. Genet.* **49**, 1567–1575 (2017).

408. Birkbak, N. J. *et al.* Paradoxical Relationship between Chromosomal Instability and Survival Outcome in Cancer. *Cancer Res.* **71**, 3447–3452 (2011).

409. Jamal-Hanjani, M. *et al.* Extreme chromosomal instability forecasts improved outcome in ER-negative breast cancer: a prospective validation cohort study from the TACT trial. *Ann. Oncol.* **26**, 1340–1346 (2015).

410. Laughney, A. M., Elizalde, S., Genovese, G. & Bakhoum, S. F. Dynamics of Tumor Heterogeneity Derived from Clonal Karyotypic Evolution. *Cell Rep.* **12**, 809–820 (2015).

411. Sheltzer, J. M. A Transcriptional and Metabolic Signature of Primary Aneuploidy Is Present in Chromosomally Unstable Cancer Cells and Informs Clinical Prognosis. *Cancer Res.* **73**, 6401–6412 (2013).

412. Sansregret, L. & Swanton, C. The Role of Aneuploidy in Cancer Evolution. *Cold Spring Harb. Perspect. Med.* **7**, (2017).

413. Janssen, A., Kops, G. J. P. L. & Medema, R. H. Elevating the frequency of chromosome mis-segregation as a strategy to kill tumor cells. *Proc. Natl. Acad. Sci.* **106**, 19108–19113 (2009).

414. Zasadil, L. M. *et al.* High rates of chromosome missegregation suppress tumor progression but do not inhibit tumor initiation. *Mol. Biol. Cell* **27**, 1981–1989 (2016).

415. Kawakami, M., Liu, X. & Dmitrovsky, E. New Cell Cycle Inhibitors Target Aneuploidy in Cancer Therapy. *Annu. Rev. Pharmacol. Toxicol.* **59**, 361–377 (2019).

416. Zasadil, L. M., Britigan, E. M. C. & Weaver, B. A. 2n or not 2n: Aneuploidy, polyploidy and chromosomal instability in primary and tumor cells. *WASPWAVE Proteins Expand. Memb. Funct. Role Ploidy Var. Cell. Adapt.* **24**, 370–379 (2013).

417. Maia, A. R. R. *et al.* Mps1 inhibitors synergise with low doses of taxanes in promoting tumour cell death by enhancement of errors in cell division. *Br. J. Cancer* **118**, 1586–1595 (2018).

418. de Cárcer, G. *et al.* Plk1 overexpression induces chromosomal instability and suppresses tumor development. *Nat. Commun.* **9**, 3012 (2018).

419. Godek, K. M. *et al.* Chromosomal Instability Affects the Tumorigenicity of Glioblastoma Tumor-Initiating Cells. *Cancer Discov.* **6**, 532–545 (2016).

420. Laucius, C. D., Orr, B. & Compton, D. A. Chromosomal instability suppresses the growth of K-Ras-induced lung adenomas. *Cell Cycle* **18**, 1702–1713 (2019).

421. Zasadil, L. M. *et al.* Cytotoxicity of Paclitaxel in Breast Cancer Is due to Chromosome Missegregation on Multipolar Spindles. *Sci. Transl. Med.* **6**, 229ra43-229ra43 (2014).

422. Scribano, C. M. *et al.* Chromosomal instability sensitizes patient breast tumors to multipolar divisions induced by paclitaxel. *Sci. Transl. Med.* **13**, eabd4811 (2021).

423. Maia, A. R. R. *et al.* Inhibition of the spindle assembly checkpoint kinase TTK enhances the efficacy of docetaxel in a triple-negative breast cancer model. *Ann. Oncol.* **26**, 2180–2192 (2015).

424. Cánovas, B. *et al.* Targeting p38α Increases DNA Damage, Chromosome Instability, and the Anti-tumoral Response to Taxanes in Breast Cancer Cells. *Cancer Cell* **33**, 1094-1110.e8 (2018).

425. Serçin, Ö. *et al.* Transient PLK4 overexpression accelerates tumorigenesis in p53-deficient epidermis. *Nat. Cell Biol.* **18**, 100–110 (2016).

426. Serra, V. *et al.* Identification of a Molecularly-Defined Subset of Breast and Ovarian Cancer Models that Respond to WEE1 or ATR Inhibition, Overcoming PARP Inhibitor Resistance. *Clin. Cancer Res.* **28**, 4536–4550 (2022).

427. Payliss, B. J. *et al.* Phosphorylation of the DNA repair scaffold SLX4 drives folding of the SAP domain and activation of the MUS81-EME1 endonuclease. *Cell Rep.* **41**, 111537 (2022).

428. Wyatt, H. D. M., Laister, R. C., Martin, S. R., Arrowsmith, C. H. & West, S. C. The SMX DNA Repair Tri-nuclease. *Mol. Cell* **65**, 848-860.e11 (2017).

429. Szmyd, R. *et al.* Premature activation of Cdk1 leads to mitotic events in S phase and embryonic lethality. *Oncogene* **38**, 998–1018 (2019).

430. Balbo Pogliano, C. *et al.* The CDK1-TOPBP1-PLK1 axis regulates the Bloom's syndrome helicase BLM to suppress crossover recombination in somatic cells. *Sci. Adv.* **8**, eabk0221.

431. Kosugi, S., Hasebe, M., Tomita, M. & Yanagawa, H. Systematic identification of cell cycle-dependent yeast nucleocytoplasmic shuttling proteins by prediction of composite motifs. *Proc. Natl. Acad. Sci.* **106**, 10171–10176 (2009).

432. Lockhead, S. *et al.* The Apparent Requirement for Protein Synthesis during G2 Phase Is due to Checkpoint Activation. *Cell Rep.* **32**, 107901 (2020).

433. Gavet, O. & Pines, J. Activation of cyclin B1–Cdk1 synchronizes events in the nucleus and the cytoplasm at mitosis. *J. Cell Biol.* **189**, 247–259 (2010).

434. Monda, J. K. & Cheeseman, I. M. The kinetochore–microtubule interface at a glance. *J. Cell Sci.* **131**, jcs214577 (2018).

435. Barisic, M., Aguiar, P., Geley, S. & Maiato, H. Kinetochore motors drive congression of peripheral polar chromosomes by overcoming random arm-ejection forces. *Nat. Cell Biol.* **16**, 1249–1256 (2014).

436. Schneider, M. W. G. *et al.* A mitotic chromatin phase transition prevents perforation by microtubules. *Nature* **609**, 183–190 (2022).

437. Audrey, A., de Haan, L., van Vugt, M. A. T. M. & de Boer, H. R. Processing DNA lesions during mitosis to prevent genomic instability. *Biochem. Soc. Trans.* **50**, 1105–1118 (2022).

438. Hara, Y. & Kimura, A. An allometric relationship between mitotic spindle width, spindle length, and ploidy in Caenorhabditis elegans embryos. *Mol. Biol. Cell* **24**, 1411–1419 (2013).

439. Hauge, S. *et al.* Combined inhibition of Wee1 and Chk1 gives synergistic DNA

damage in S-phase due to distinct regulation of CDK activity and CDC45 loading. *Oncotarget Vol 8 No 7* (2016).

440. Moiseeva, T. N., Qian, C., Sugitani, N., Osmanbeyoglu, H. U. & Bakkenist, C. J. WEE1 kinase inhibitor AZD1775 induces CDK1 kinase-dependent origin firing in unperturbed G1- and S-phase cells. *Proc. Natl. Acad. Sci.* **116**, 23891–23893 (2019).

441. Pommier, Y., Nussenzweig, A., Takeda, S. & Austin, C. Human topoisomerases and their roles in genome stability and organization. *Nat. Rev. Mol. Cell Biol.* **23**, 407–427 (2022).

442. Lottersberger, F., Karssemeijer, R. A., Dimitrova, N. & de Lange, T. 53BP1 and the LINC Complex Promote Microtubule-Dependent DSB Mobility and DNA Repair. *Cell* **163**, 880–893 (2015).

443. Shokrollahi, M. & Mekhail, K. Interphase microtubules in nuclear organization and genome maintenance. *Trends Cell Biol.* **31**, 721–731 (2021).

VII. APPENDICES

REVIEW 1 – PREDICTING AND OVERCOMING TAXANE CHEMORESISTANCE

In this article, we discussed the development of resistance to taxanes, which are commonly used as chemotherapy drugs for solid tumors, and what could be the ways to overcome this resistance to improve breast cancer patient outcomes.

We highlight the importance of identifying predictive biomarkers to select patients who will benefit from taxane-based chemotherapy and avoid ineffective treatment in patients with innate resistance. We also summarize insights into taxane resistance, including mitotic mechanisms and metabolic reprogramming.

Finally, we present the promising emerging strategies to overcome chemoresistance in the future, such as targeting mitotic fidelity and modulating cancer cell metabolism. The role of the tumor microenvironment in taxane resistance is briefly discussed, along with potential strategies to target non-cell autonomous mechanisms.

Overall, the article emphasizes the need for personalized medicine approaches to tailor treatment strategies for individual patients.

This review was published in February 2021.

CellPress

Trends in Molecular Medicine

Review

Predicting and Overcoming Taxane Chemoresistance

Sylvie Rodrigues-Ferreira,[1,2,3,*] Hadia Moindjie,[1,2] Maria M. Haykal,[1,2] and Clara Nahmias[1,2,*]

Taxanes are microtubule-targeting drugs used as cytotoxic chemotherapy to treat most solid tumors. The development of resistance to taxanes is a major cause of therapeutic failure and overcoming chemoresistance remains an important challenge to improve patient's outcome. Extensive efforts have been made recently to identify predictive biomarkers to select populations of patients who will benefit from taxane-based chemotherapy and avoid inefficient treatment of patients with innate resistance. This, together with the discovery of new mechanisms of resistance that include metabolic reprogramming and dialogue between tumor and its microenvironment, pave the way to a new era of personalized medicine. In this review, we recapitulate recent insights into taxane resistance and present promising emerging strategies to overcome chemoresistance in the future.

Highlights

Taxanes are widely used in the management of breast and ovarian cancer but drug resistance is frequently observed and represents a major limitation of the treatment. Major mechanisms of taxane resistance result from deregulation of mitotic functions and metabolic reprogramming as well as non-cell autonomous mechanisms involving tumor–microenvironment crosstalk.

Predictive biomarkers for taxane resistance that can be translated into the clinic are urgently needed to determine who will benefit from the therapy and avoid unnecessary treatment and side effects.

New predictive biomarkers, including microtubule-associated proteins, tumor-infiltrated lymphocytes, and predictive signatures, are currently under evaluation and machine learning approaches should further improve their accuracy.

Taxane analogs, new formulation dual inhibitors, and drug combinations are emerging strategies to circumvent chemoresistance.

Taxane-Based Chemotherapy: Clinical Applications and Limitations

Paclitaxel (brand name Taxol) is the founder member of the taxanes family that also includes docetaxel and cabazitaxel. Its potent antitumoral effects were rapidly established and the drug was approved by the FDA for treatment of solid tumors including gastric, prostate, head and neck, pancreatic, non-small cell lung, ovarian and breast cancers. Paclitaxel is generally used in sequential combination with DNA-targeting agents as cytotoxic chemotherapy for aggressive tumors. However, a substantial proportion of tumors are chemoresistant. As an example, almost 80% of breast tumors are resistant to chemotherapy [1]. For ovarian cancer, although 48–86% of high-grade serous tumors are chemosensitive [2], a large majority develops secondary resistance. Thus, toxicity and resistance to chemotherapy are major concerns that damper the use of these drugs. The challenge today is to be able to identify resistant patients and to provide them an efficient alternative therapy. In this review, we discuss emerging predictive biomarkers and promising targets to circumvent resistance to treatment, with a focus on breast and ovarian cancers. Understanding how paclitaxel affects microtubule dynamics to kill cancer cells and deciphering the mechanisms by which tumors resist to chemotherapy is paramount to design alternative strategies to overcome chemoresistance.

Paclitaxel: Binding Site and Mechanisms of Action

Pioneering studies of Susan B. Horwitz's group [3] revealed that paclitaxel is a tubulin-binding agent that promotes microtubule assembly and protects microtubules from depolymerization. Initially referred to as mitotic poison, paclitaxel used at relatively high concentrations (0.25–1 μM) was shown to behave as a strong antimitotic agent that arrests cells in M phase, leading to cell death by apoptosis. It was later realized that intratumoral concentrations of paclitaxel in locally advanced breast tumors are lower than previously estimated [4]. Clinically relevant doses of the drug at the tumor site are in the nanomolar range (5–50 nM) and do not affect microtubule polymer mass nor promote substantial mitotic arrest. They rather increase duration of mitosis and induce multipolar divisions leading to **aneuploidy** (see Glossary) [4–6]. Recent studies on the occupancy of taxane site in cells and animal models have confirmed that different drug

[1]Université Paris-Saclay, Institut Gustave Roussy, Inserm U981, Biomarqueurs prédictifs et nouvelles stratégies thérapeutiques en oncologie, 94800, Villejuif, France
[2]LabEx LERMIT, Université Paris Saclay, 92296 Châtenay-Malabry, France
[3]Inovarion, 75005 Paris, France

*Correspondence:
sylvie.rodrigues-ferreira@gustaveroussy.fr
sylvie.rodrigues-ferreira@inovarion.com
(S. Rodrigues-Ferreira), and
clara.nahmias@inserm.fr (C. Nahmias).

 https://doi.org/10.1016/j.molmed.2020.09.007

concentrations promote different biological effects and highlighted the formation of postmitotic micronuclei as an important consequence of paclitaxel action [7]. In addition, paclitaxel used at nonsaturating nanomolar concentrations – but not at high doses – was shown to control the dynamic behavior of growing microtubule ends (Box 1). *In vitro*, paclitaxel stabilizes microtubules by totally suppressing catastrophes [8,9]. In the presence of end-binding proteins (EBs), which contribute to the dynamicity of microtubule plus ends, paclitaxel increases catastrophes while strongly stimulating rescues [9]; a finding that illustrates the complex behavior of the drug.

Paclitaxel directly binds polymerized microtubules on the internal face of β-tubulin, in the so-called taxane-binding site [10,11]. Taxanes binding to β-tubulin induce conformational changes that strengthen longitudinal tubulin contacts by an allosteric mechanism, thereby promoting microtubule stabilization [12,13]. Other microtubule-stabilizing agents, such as epothilones and zampanolide A, bind to the same taxane pocket in β-tubulin but are believed to elicit different conformational changes at the microtubule ends [13–15]. Recent studies using fluorescent derivatives of paclitaxel at low doses revealed that taxanes tend to accumulate close to the plus ends of microtubules that are in a pre-catastrophe state [16]. Upon binding to these sites of perturbed microtubule growth, paclitaxel induces conformational transitions that convert these regions into rescue sites (Box 1). As a consequence, paclitaxel promotes microtubule stabilization at the plus ends that can propagate to the microtubule lattice. Thus, increased microtubule dynamic instability at plus ends paradoxically favors the accumulation of paclitaxel at these perturbed sites, and contributes rather than opposes to the stabilizing effects of the drug. These observations are of major importance for understanding the effects of taxanes in physiological and pathological situations. They also open important therapeutic perspectives regarding the interest of combining paclitaxel with microtubule-destabilizing drugs [17] for optimizing microtubule targeting agent-based treatments against cancer.

By stabilizing microtubules and promoting conformational transitions at microtubule ends, paclitaxel also likely modifies the complex network of proteins that regulate the microtubule cytoskeleton. By means of proteome quantitation of proteins crosslinks in HeLa cells, nanomolar concentrations of paclitaxel were recently shown to be sufficient to significantly modify the dynamics of global protein–protein interactions [18]. Paclitaxel treatment for 18 h induces a wide range of conformational changes in cytoskeletal proteins (microtubules, but also actin and intermediate filaments) and strikingly also elicits major changes in mitochondrial protein complexes [18]. Furthermore, low doses of paclitaxel promote changes in mRNA expression and stability [19], including coordinated upregulation of tubulin genes, that may contribute to microtubule homeostasis and self-repair [20]. Together these findings may orient the search for predictive biomarkers and mechanisms of acquired resistance to taxanes.

Predictive Biomarkers

Considering the rapidly developing area of personalized medicine, the stratification of patients who are likely to benefit from chemotherapy is of importance to improve treatment efficiency and patient outcome. Identifying patients who will not respond to chemotherapy is even more important to avoid unnecessary treatments that cause toxicities and adverse effects without any benefit. Today, the search for predictive biomarkers (Box 2) that may be translatable into clinical practice remains a challenge. In breast cancer, the estrogen receptor (ER) and human epidermal growth factor receptor-2 (HER2) oncogene are the only established biomarkers that are clinically used to predict response to hormonotherapy (tamoxifen) and HER2-targeted therapy (trastuzumab), respectively. Although ER-negative tumors are associated with increased

Glossary

Aneuploidy: presence of an abnormal number of chromosomes. This abnormality results from numerical and/or structural chromosomal aberrations and is considered as a hallmark of cancer.
Centrosome clustering: a process that contributes to bipolar division by promoting the gathering of extra centrosomes in two main poles.
Deep neural network: a machine learning method that uses multiple layers and networks to extract higher levels of features from the raw input.
Fatty acid synthesis: a process of synthesizing fatty acids from acetyl-CoA and NADPH through the action of fatty acid synthase enzymes.
Fatty acid oxidation: a lipid catabolic pathway that uses both exogenous and endogenous Fatty acids for energy production. Fatty acids are converted to fatty acyl-CoAs transported to the mitochondria, where they undergo multistep reactions to generate acetyl-CoA oxidized through the TCA.
Formulation: a process that combines an active drug and different chemical components to produce a final product with improved properties.
Glutaminolysis: a process of breaking the amino acid glutamine into glutamate, aspartate, CO2, pyruvate, lactate, alanine, and citrate.
Glycolysis: first step of the glucose metabolism pathway. Process of breaking down a molecule of glucose into two pyruvate molecules, while storing energy as ATP and NADH.
Machine learning: a method of artificial intelligence consisting of systems that automatically learn from raw inputs to extract informative features and generate algorithms for predictions or decisions.
Mitotic slippage: a process by which a cell exits a prolonged mitotic arrest when cyclin B1 levels drop below a threshold required to maintain the mitotic state.
Mitochondrial oxidative phosphorylation: a mitochondria-dependent energetic pathway that allows the phosphorylation of ADP to ATP thanks to the energy released by the oxidation of electron donors by the respiratory chain.
Pentose phosphate pathway: an alternative pathway of glycolysis that gives rise to several critical products for cancer metabolism, including a pentose (5-carbon sugar) or ribose-5-phosphate

Box 1. Microtubule Dynamics and Regulation

Microtubules are polarized and dynamic structures composed of α/β tubulin dimers that constantly alternate between periods of slow polymerization (growth) and rapid shrinkage (depolymerization). The transition between growth and shrinkage is defined as catastrophe and the reverse is defined as rescue (Figure I). This process, called dynamic instability, is essential for microtubules to explore the cytosol, target the cell cortex and organelles, and reorganize into a bipolar spindle during mitosis. Microtubule growth and shrinkage involve conformational changes at microtubule ends that are dependent on the nucleotide state of tubulin. Indeed, GTP hydrolysis in β-tubulin causes longitudinal compaction of protofilaments which in turn loosen their lateral interactions, thereby facilitating microtubule destabilization and shrinkage. In living cells, microtubules are submitted to local mechanical stress and damage, essentially due to microtubule crossing and bending [99], assaults of severing enzymes such as katanin or spastin [100], or mechanical obstacles [101,102]. These constraints promote the removal of tubulin dimers from the lattice and are responsible for a pre-catastrophe state. This local perturbation creates preferential sites of rescue on the microtubule shaft [16], illustrating microtubule lattice plasticity [20] and ability to self-repair [99,101,102] (Figure I). Thus, in a counterintuitive manner, increasing catastrophes favors microtubule repair and stabilization.

The microtubule cytoskeleton is also regulated by several hundred MAPs including structural, regulatory, and motor proteins that contribute to microtubule assembly, dynamics and/or functions. A family of MAPs, that preferentially associate with microtubule plus ends (+TIPs), are major regulators of microtubule dynamics. Among them, end-binding proteins (EBs) act as molecular platforms recruiting complex +TIP protein networks at the plus ends, such as CLIP-170 and CLASPs. Recent studies indicate that these +TIPs are also recruited to the microtubule lattice at particular sites of mechanical stress, severing or damage where they promote microtubule rescue [101,103] or facilitate self-repair [99,104].

Figure I shows the different phases of microtubule plus end dynamics (left) and self-repair of the lattice (right). Plus-end tracking proteins (end-binding proteins, CLASPs, and CLIP170) that contribute to both processes are indicated. Microtubule damage (black flash) promotes the loss of tubulin heterodimers (white square) that are replaced by GTP-loaded α/β tubulin (orange). The stabilizing effect of paclitaxel (PTX) is represented by a red arrow.

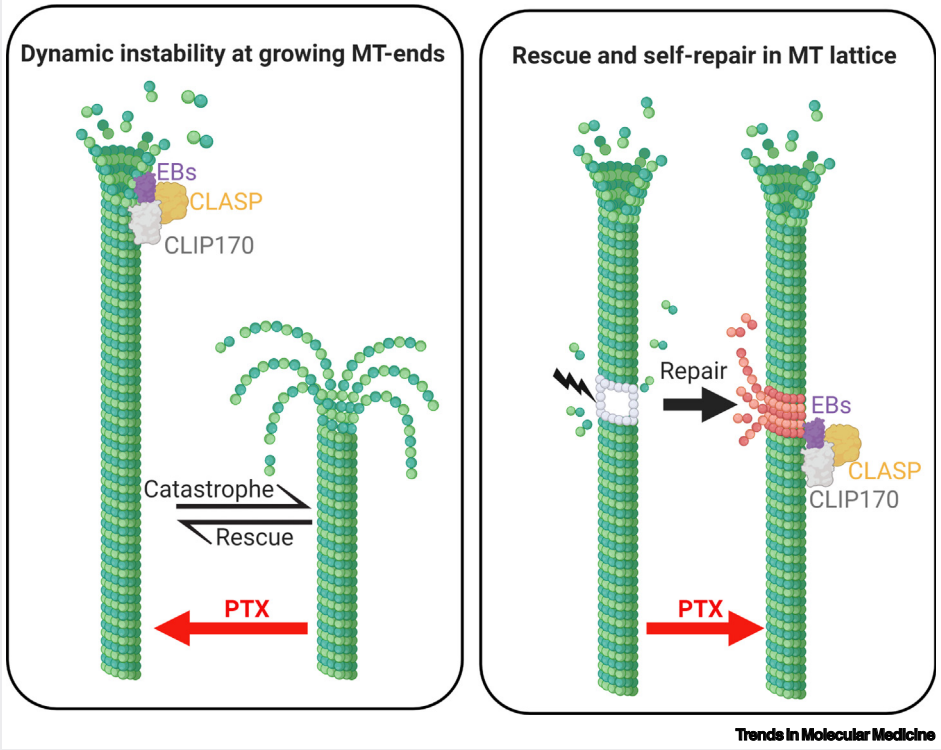

Figure I. Microtubule Dynamic Instability and Self-Repair.

which are precursors for the synthesis of nucleotides and nucleic acids.

PFKFB3: a kinase that catalyzes the production of fructose-2,6-biphosphate and ADP from fructose-6-phosphate and ATP.

Spindle assembly checkpoint: cellular surveillance mechanism that halts progression from metaphase to anaphase as long as chromosomes are not correctly attached to the mitotic spindle, hence preserving genomic integrity.

Tumor microenvironment: heterogeneous environment that surrounds cancer cells, formed by extracellular matrix components and several stromal cells including CAFs, infiltrating immune cells, cancer-associated adipocytes, and vascular/lymphatic endothelial cells.

Box 2. Predictive Biomarker: Definition and Methods

Predictive biomarkers are measurable indicators (genes, proteins, and signatures) used to identify patients more likely to respond favorably or unfavorably to treatment (Figure I). In breast cancer, when chemotherapy is administered in a neoadjuvant setting (i.e., before surgery), its efficiency is evaluated histologically at the time of surgery. The pCR is achieved when invasive tumor and invaded lymph nodes are absent according to Chevallier's criteria. In ovarian cancer, the efficiency of chemotherapy is evaluated by the clinical CR based on computed tomography scan or magnetic resonance imaging, according to RECIST (Response Evaluation Criteria In Solid Tumors) criteria, that include disappearance of all lesions, lymph node size <10 mm, and normalization of tumor marker levels. Tumors that do not achieve pCR or CR response are considered resistant to chemotherapy. Resistance can be innate, meaning present at diagnosis, or acquired following chemotherapy. The correlation between biomarker expression and sensitivity or resistance to chemotherapy is statistically analyzed to evaluate the predictive value of the biomarker. The performance of the biomarker, that is, its ability to accurately distinguish between responsive and resistant tumors, is established by its sensitivity (detection of true responder) and specificity (detection of true resistant) measured by a receiver operating characteristic curve. Additional multivariate analyses are performed to evaluate if the biomarker is independent or correlated with clinical or molecular parameters. Independent biomarkers are more reliable and ensure higher predictive performance.

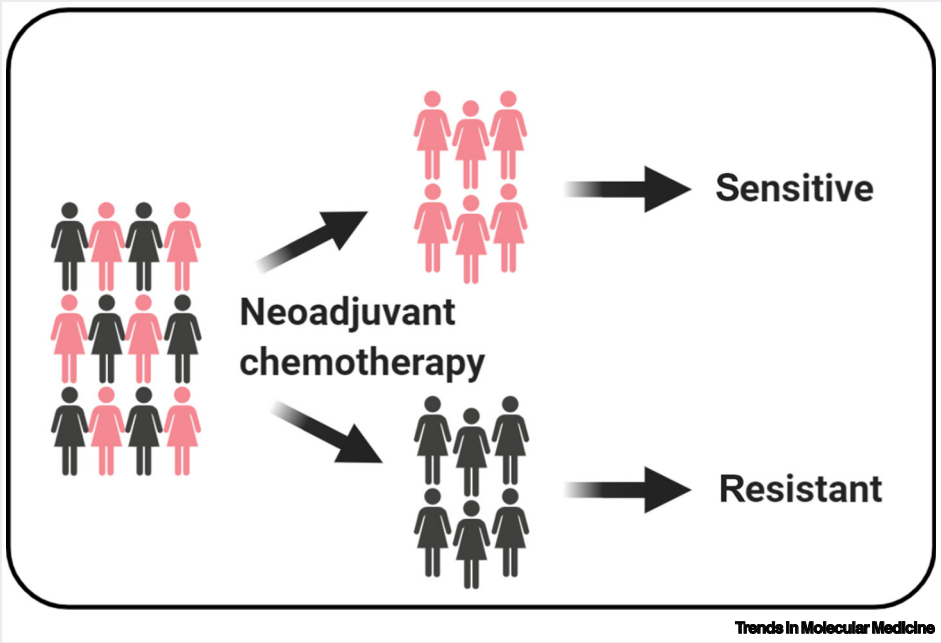

Figure I. Predictive Biomarker.

response rate to chemotherapy, robust predictive biomarkers of chemoresistance are still needed. In the past years, extensive studies have pointed to alterations of βIII-tubulin and drug transporters as major predictors of taxane chemoresistance [2,21]. Here, we discuss new promising predictive biomarkers of response to conventional chemotherapy containing taxanes and DNA targeting agents in breast and ovarian cancers (Table 1).

Microtubule-Associated Proteins (MAPs)

MAPs (Box 1), which bind and regulate microtubule assembly, dynamics, or functions, have long been considered as potential predictive biomarkers of taxane response [22]. High expression of either stabilizing (*MAPT/Tau*) or destabilizing (Stathmin/Ops18) MAPs is associated with chemoresistance in breast and ovarian cancer [23–27]. *MAPT/Tau* was described as the most highly upregulated gene in resistant breast tumors; however, it failed to remain an independent predictive biomarker when analyzed with clinical parameters in multivariate analyses, invalidating its use in clinics [26].

Table 1. Recent Predictive Biomarkers of Response to Taxane-Based Chemotherapy in Breast and Ovarian Cancers[a]

	Predictive biomarker	Cancer type	No. of patients	Biomarker evaluation method	Clinical evaluation	Predictive score[b] AUC (*P* value)	Independent predictive value	Refs
Microtubule-associated proteins	MAPT/Tau	Breast	3672	Immunohistochemistry / gene expression	pCR	nd	Contradictory	[25]
		Ovarian	74	IHC	PFS/OS	nd	No	[24]
	MTUS1/ATIP3	Breast	387	Gene expression	pCR	0.72 (0.007)	Yes	[27]
	STMN1/Stathmin	Breast	54	Gene expression	pCR	nd	Yes	[23]
		Ovarian	75	Gene expression	PFS/OS	nd	Nd	[22]
Signatures	Gene expression	Breast	250	Gene expression	pCR	nd	Nd	[39]
	lncRNA	Ovarian	46	Gene expression	CR	0.93 (nd)	Nd	[38]
	Methylation	Breast	53	methylation array	RCB	0.91 (nd)	Yes	[37]
Tumor microenvironment	Angiogenesis-related genes	Ovarian	39	Gene expression	CR	0.68 (0.097)	nd	[31]
	MMP2	Ovarian	35	Gene expression	CR	nd	nd	[29]
	SPARC	Breast	50	Gene expression	pCR	0.7 (nd)	nd	[28]
	Tumor-infiltrating lymphocytes	Breast	3771	Gene expression	pCR	nd	nd	[34]
		Breast	29	Hematoxylin eosin/gene expression	pCR	nd	yes	[36]

[a]Abbreviations: CR, complete response defined as absence of all radiographic evidence of disease after surgical resection and chemotherapy; nd, not determined; OS, overall survival; pCR, pathological complete response; PFS, progression-free survival; RCB, residual cancer burden.
[b]Predictive score evaluated by area under the curve and *P* value obtained from a receiver operating characteristic curve.

In a recent study, a total of 280 genes encoding microtubule-regulating proteins were analyzed in three independent cohorts of breast cancer patients treated in a neoadjuvant setting with taxane-based chemotherapy [28]. Seventeen genes were differentially expressed in chemoresistant tumors of all three cohorts. They belong to four major families of proteins comprising structural MAPs, microtubule end-binding proteins, spindle proteins, and kinesins. Among them, *MAPT* and *MTUS1* were among the most differentially regulated genes. As for *MAPT*, *MTUS1* encodes a stabilizing MAP (ATIP3) whose high expression is associated with breast cancer resistance to taxanes [28]. When analyzed together with clinicopathological parameters, *MTUS1* still significantly predicted the response to chemotherapy, indicating that *MTUS1* is an independent predictive biomarker. This study relaunches the interest of investigating microtubule-regulating proteins, either alone or in combination, to predict the response to chemotherapy.

Tumor Microenvironment

Besides cancer cells, the **tumor microenvironment** can influence cancer behavior including response to treatment. Components of the extracellular matrix such as the collagen-binding protein SPARC, or the metalloprotease MMP2 that degrade the matrix, have been shown to predict the response to chemotherapy in breast and ovarian tumors [29,30]. Low SPARC level and high MMP2 expression are associated with higher sensitivity to chemotherapy, suggesting that microenvironment remodeling may influence drug accessibility and subsequent tumor response to treatment. In agreement, by measuring intratumoral drug concentration, it was shown that abnormal vasculature reduces drug delivery to the tumor and contributes to chemoresistance [31]. Of note, hypoxia has also been shown to induce chemoresistance [32]. Thus investigating angiogenesis-related genes may be useful to predict tumor sensitivity to chemotherapy [33].

Accumulating evidence indicates that the immune system also contributes to the antitumor effect of chemotherapy [34,35]. Recently, using patient data from six randomized clinical trials, tumors with high amounts of tumor-infiltrated lymphocytes (TILs) were shown to be more prone to achieve a pathological complete response (pCR) after neoadjuvant chemotherapy [36]. In a Phase III study, inhibiting the interaction between TILs and cancer cells with immune checkpoint inhibitors has been shown to improve breast tumor response to chemotherapy [37,38]. TILs are thus associated with improved outcome in breast and ovarian tumors [36,39]. TIL level is measured directly on tumor samples by histopathological staining; however, it remains challenging to determine standardized methods and thresholds to predict sensitivity. To circumvent this problem, gene expression profile was used as an unbiased and reproducible method to evaluate TIL positivity in tumors [40]. A TIL genomic signature of 22 genes that correlates with TIL histological score was established. High TIL-genomic score independently predicts pCR to chemotherapy in breast cancer patients [40], indicating that genomic signatures may be useful to accurately predict response to chemotherapy and subsequently identify chemoresistant patients.

Predictive Signatures

Predictive signatures based on gene expression analysis were first attempts to distinguish sets of genes highly differentially expressed between resistant and sensitive tumors. More recently, signatures of epigenetic regulators [41] and long noncoding RNAs [32,42] have been identified as predictive biomarkers in breast and ovarian cancers.

The main challenge today is to improve computational analyses to propose robust and reproducible biomarkers with greater precision. In line with this idea, a qualitative transcriptional signature based on the ratio of expression values of selected gene pairs was developed [43]. Using a 61 gene-pairs signature, the authors identified more than 95% of the breast cancer patients achieving a pCR. This signature also selects the highly resistant patients and may thus represent an attractive tool to orient treatment decision [43]. To further improve performance, **machine learning** approaches are currently under investigation using either gene expression [44], DNA methylation, miRNA data [45], or histopathology images [46] as features for development of algorithms and training. The recent development of **deep neural network** models for prediction of drug response was found to outperform machine learning frameworks [47], providing a promising method to identify accurate predictive biomarkers.

Mechanisms of Taxane Resistance

Understanding how cancer cells escape chemotherapy-induced cell death is essential for the development of novel anticancer strategies. Many resistance mechanisms have been described over the past few years, including increased drug efflux, alteration of survival pathways, apoptosis evasion, and altered tubulin expression [21,48]. Here, we describe emerging taxane resistance mechanisms with a focus on mitotic and metabolic effects, either in a cell-intrinsic or non-cell autonomous manner (Figure 1).

Mitotic Mechanisms of Chemoresistance

Taxanes are known to affect microtubule dynamics, interfering with the assembly of the mitotic spindle and preventing the attachment of kinetochores to chromosomes. This leads to the activation of the **spindle assembly checkpoint** (SAC), the cell's feedback-control mechanism that ensures correct chromosome segregation. Failure to satisfy the SAC delays the degradation of cyclin B, thus impairing mitosis. Under prolonged mitosis induced by taxanes, cells are presented with two options: either experience death in mitosis through the activation of the apoptotic machinery; or undergo a process known as **mitotic slippage**, mainly due to a drop

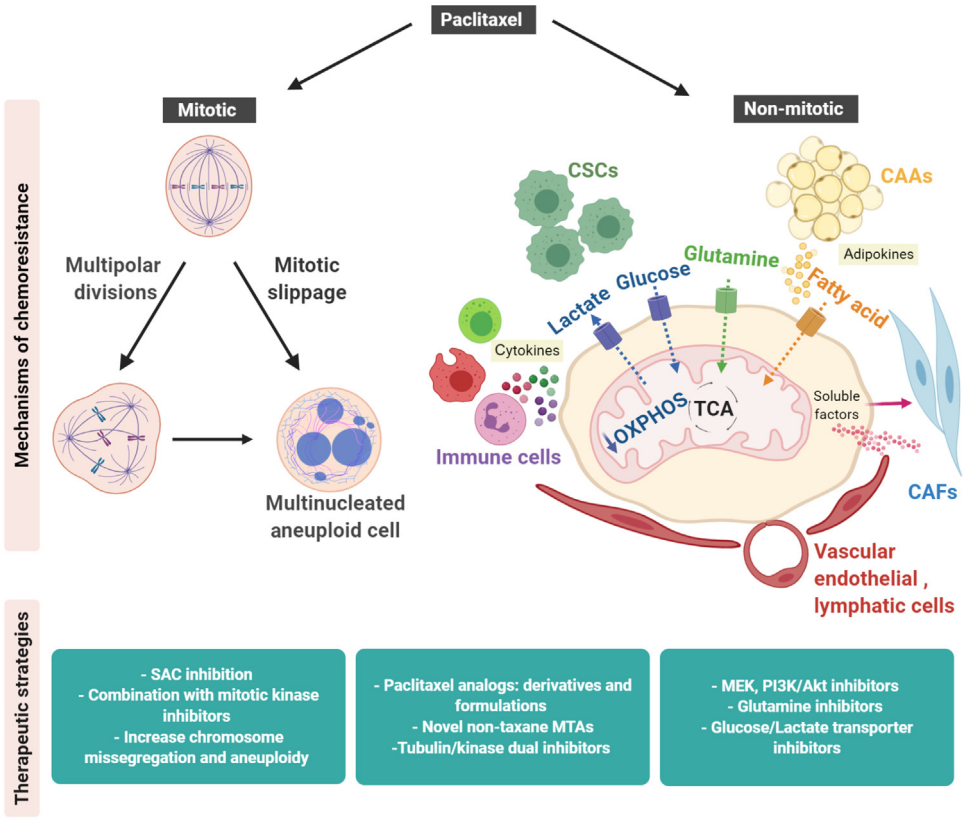

Figure 1. Mechanisms of Taxane-Mediated Chemoresistance. Tumor cells bypass taxane-mediated cell death through mitotic (left panel) or nonmitotic mechanisms, namely metabolic reprogramming and cues from the tumor microenvironment (right panel). Emerging strategies to circumvent resistance are depicted in the blue boxes below. Abbreviations: CAAs, cancer-associated adipocytes; CAFs, cancer-associated fibroblasts; CSCs, cancer stem cells; MEK, mitogen-activated protein kinase kinase; MTAs, microtubule-targeting agents; PI3K/Akt, phosphoinositide 3-kinase/Akt; SAC, spindle assembly checkpoint; TCA, tricarboxylic acid cycle.

in cyclin B levels. After mitotic slippage, cells progress into G1 phase without cytokinesis, generating polyploid cells and thus escaping cell death (Figure 1) [49].

The ability of cancer cells to survive taxane-induced prolonged mitosis by undergoing mitotic slippage represents a major resistance mechanism. Dysregulation of virtually any SAC protein or regulator in cancer cells has been shown to restore mitotic progression *in vitro* [50,51] and to correlate with chemoresistance in ovarian cancer patients [52]. Cancer cells can also rely on the modulation of cell death pathways in order to survive taxane-induced blockade of mitotic progression [53]. Overexpression of antiapoptotic proteins of the BCL2 family prevents death of mitotic cells long enough for cyclin B levels to drop below the threshold for slippage [54,55].

Paclitaxel promotes multipolar divisions, high rates of chromosome mis-segregation and aneuploid progenies, ultimately limiting cancer cell fitness and elevating cell death [4,28,56,57]. Nevertheless, cancer cells can shield themselves from high rates of chromosome mis-segregation by regulating mitotic fidelity proteins, independently of the SAC, to escape taxane-mediated cell death. Indeed, during mitosis, the assembly of the mitotic spindle and subsequent chromosome segregation are facilitated by MAPs, including kinesins, whose overexpression has been

shown to counteract paclitaxel-induced mitotic errors, conferring resistance [58,59]. Accordingly, in breast cancer patients, overexpression of the kinesin KIF20A is associated with poor prognosis [59]. **Centrosome clustering** that gathers centrosomes and shapes the multipolar spindle into pseudobipolar structures is another process allowing cells to divide and bypass taxane-induced prolonged mitosis. Likewise, recent studies associate breast cancer cell sensitivity to taxanes with pathways that control centrosome separation [60] or amplification [28].

Nonmitotic Mechanisms of Taxane Chemoresistance

Although taxanes are considered as potent antimitotic drugs, they are also effective against tumors with slow doubling times [5], raising the possibility that these drugs may also kill cancer cells through nonmitotic effects [61]. Indeed, taxanes have been shown to alter nucleocytoplasmic trafficking as well as autophagy, cell migration, inflammation, and metabolism [5,6,62].

Metabolic reprogramming is a recognized hallmark of cancer (Box 3), and it becomes increasingly clear that chemoresistant cancer cells undergo metabolic adaptations to escape the cellular stress induced by taxanes [63]. One of the best-known metabolic adaptations of resistant cancer cells is the set of stratagems used to promote energy production in a hostile microenvironment. Cancer cells that have acquired resistance to taxanes show increased metabolism due to overexpression or overactivation of several metabolic enzymes, ultimately leading to glucose or glutamine consumption, lactate release, and intracellular production of ATP, which is necessary for sustained cancer cell growth [64].

A dysregulated glycolytic state also promotes chemoresistance by an ATP-independent way involving the production of precursors for biological macromolecules such as carbon, amino acids, nucleotides, or lipids, which fuel tumorigenesis. As an example, the **pentose phosphate pathway** (PPP) links glucose metabolism and nucleotide synthesis in breast patient-derived xenograft models. Increased ribose synthesis through PPP is associated with chemoresistance and reduced survival in breast tumors and may contribute to chemoresistance by promoting the repair of DNA that had been damaged by chemotherapy [65].

Changes in lipid composition and abundance, that alter membrane fluidity and protein dynamics, have been shown to limit the intracellular transport and accumulation of chemotherapeutic drugs, with subsequent increase in chemoresistance [66]. Enhanced *de novo* **fatty acid synthesis** or ceramide metabolism upon paclitaxel exposure leads to chemoresistance by promoting several oncogenic signaling pathways such as Wnt/β-catenin, NF-κB or AKT in cancer cells and xenografts models [67,68]. Of note, the PI3K/AKT/mTOR pathway is a central signaling axis regulating various metabolic pathways including **glycolysis**, **glutaminolysis**, fatty acid synthesis, and **fatty acid oxidation**. This signaling pathway constitutes an interesting target to surmount chemoresistance in breast and ovarian cancers [69].

Mitochondria are other major players of chemoresistance. While Warburg's work suggested that defective mitochondria are partly responsible for the metabolic switch in tumors, it is now well known that cancer cells' mitochondria are functional and able to use **mitochondrial oxidative phosphorylation** (mtOXPHOS) as a source of energy [70]. In ovarian tumors, elevated mtOXPHOS and subsequent reactive oxygen species production were shown either to promote chemoresistance by acting on cancer stem cells (CSCs) [71] or to increase tumor sensitivity to conventional chemotherapy [72], suggesting that mtOXPHOS activity may have a 'double-edged sword' effect depending on the cellular context and microenvironment. Other emerging concepts, such as retrograde traffic from mitochondria to the nucleus following cellular stress, and horizontal transfer of mitochondria or its genetic material between healthy CSCs and

Box 3. Metabolic Reprogramming

Human cells synthesize energy in the form of ATP to fulfil important functions such as cell proliferation, migration, and invasion. ATP production comes from three major pathways that depend on glucose metabolism, namely glycolysis, tricarboxylic acid cycle (TCA), and mtOXPHOS (indicated in blue in Figure I). Healthy cells produce energy mainly through mtOXPHOS, whereas cancer cells exhibit an unconventional metabolism in which the energy requirements are satiated by aerobic glycolysis. This metabolic reprogramming, called the Warburg effect, is a hallmark of tumorigenesis and is necessary to sustain cancer cells survival and growth in a hostile microenvironment which is often characterized by hypoxia, low glucose levels, and/or nutrient deprivation [63]. The Warburg effect is mediated by upregulation and overactivation of several enzymes of the glycolytic cascade such as hexokinase 2 [105] or 6-phosphofructo-2-kinase/fructose-2,6-biphosphatase 3 (PFKFB3) kinases [106], the monocarboxylate transporter 1, or lactate dehydrogenase [107]. These promote glucose uptake, ATP production, and lactate release, with major consequences on acidification of the microenvironment and the promotion of tumor progression and metastasis. Although glutamine is considered to be a nonessential amino acid, some tumors become 'glutamine addicts' and upregulate the metabolism of glutamine to produce ATP. Glutamine is thus transformed into glutamate by glutaminase and then converted to α-ketoglutarate in order to enter into the TCA cycle [91]. Highly proliferating cancer cells show a strong lipid and cholesterol avidity which is satisfied by an increase of exogenous lipids import, cholesterol import, or activation of *de novo* fatty acid (FA) synthesis [63]. Overexpression or overactivation of lipogenic enzymes such as fatty acid synthase (FASN) activates several signal transduction cascades and oncogenic pathways to promote cell growth, migration, and metastasis [67,68]. Key enzymes implicated in metabolic reprogramming of cancer cells and upregulated or overexpressed in taxane-resistant cancer cells are shown in purple and italic in Figure I. Deregulation of different metabolic pathways (glucose, glutamine, lipids, ceramide, and mitochondrial metabolism) is correlated with tumor aggressiveness and chemoresistance [63]. This metabolic plasticity is dynamic and influenced by intrinsic factors as well as by extrinsic factors produced by the tumor microenvironment.

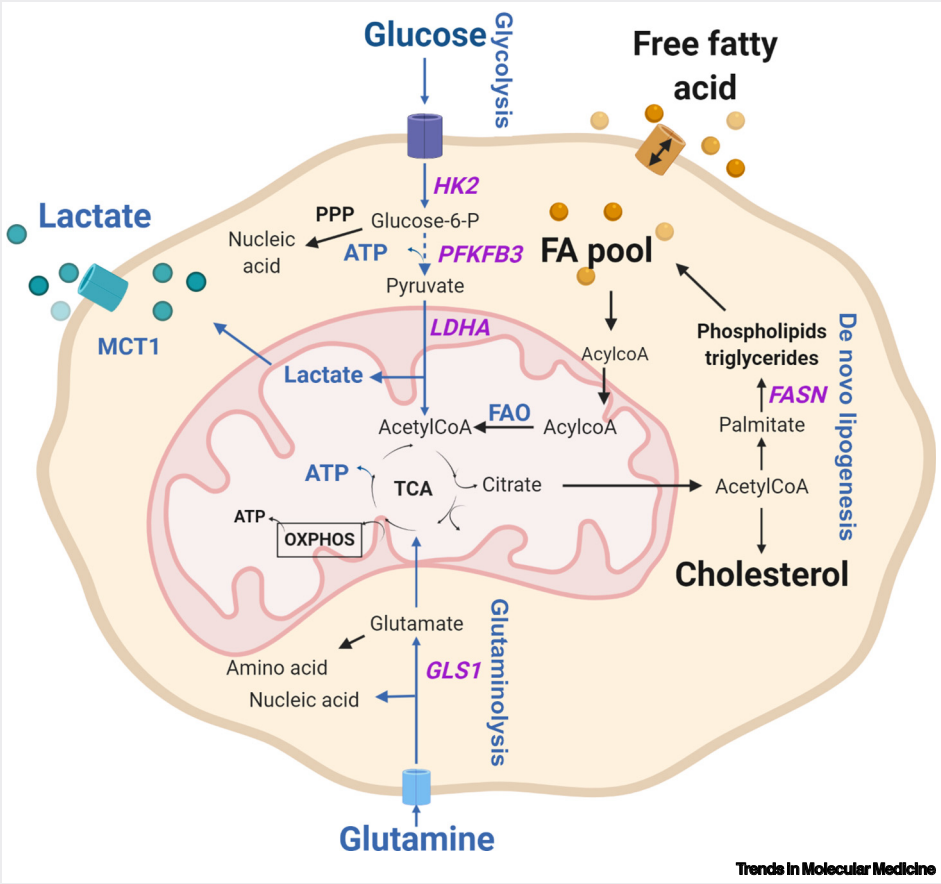

Figure I. Metabolic Reprogramming in Cancer Cells.

mitochondria-defective cancer cells [70], warrant further attention in the context of taxane resistance.

The metabolic and mitotic mechanisms of taxane resistance, although apparently independent, are tightly linked. Mitochondria are active during the energy-consuming process driving spindle formation and chromosome segregation. Upon taxane-induced prolonged mitosis, the mitochondrial mass declines [73] promoting AMPK-dependent phosphorylation of **PFKFB3**, which in turn results in increased glycolytic activity in mitotic cells. Mitotic cells thus present metabolic vulnerabilities, suggesting that mitotic cell death may be enhanced by exploiting the cell's energetic balance such as inhibition of glycolysis, to impede taxane chemoresistance [74].

Non-Cell Autonomous Mechanisms of Taxane-Based Chemoresistance

In addition to cell-intrinsic changes, many studies reported a role of the tumor microenvironment in taxane resistance. One of the difficulties in understanding how the metabolism of cancer cells affects chemotherapy comes from the intratumoral metabolic heterogeneity that is caused in part by the surrounding nontumor cells exposed to different microenvironmental conditions (hypoxia or nutrient deprivation). Indeed, stromal cells from the microenvironment communicate dynamically and reciprocally with cancer cells via direct interactions as well as paracrine signaling, including exosome secretion, to mediate the acquisition of chemoresistance (Figure 1).

Cancer cells secrete growth factors such as transforming growth factor β or platelet-derived growth factor that can change normal fibroblasts into activated cancer-associated fibroblasts (CAFs). In return, CAFs release exosomes transferring miR-21, which consequently inhibits ovarian cancer apoptosis in response to paclitaxel [75]. CAFs also secrete interleukin (IL)-6 and IL-8 to sustain cancer stemness, which consequently contributes to breast cancer chemoresistance [76]. Other components of the microenvironment, such as cancer-associated adipocytes, communicate with cancer cells and stromal cells by releasing various lipids, cytokines, inflammatory interleukins, adipokines, or miRNAs, that enhance cell viability in the presence of taxanes [77]. Finally, taxane chemoresistance is also driven by immune cells of the microenvironment. In particular, tumor-associated macrophages that infiltrate the tumor have been shown to promote mitotic slippage and cancer cell survival by reducing the duration of mitosis upon paclitaxel treatment [78].

Overcoming Taxane Resistance

Multidrug resistance (MDR) is frequently described as a major cause of taxane resistance and therapeutic failure in breast and ovarian cancer [79]. In chemoresistant cancer cell lines [79] and tumors [80], MDR has been associated with increased expression level of drug efflux pumps such as permeability glycoprotein (P-gp). To prevent MDR, studies have focused on optimizing taxane structures at specific positions to both improve drug solubility and bioavailability, and reduce affinity to drug efflux pumps. Thus, taxane derivatives obtained by modification of the C3, C10, or C3′ positions are poor substrates of P-gp and are useful to circumvent paclitaxel acquired resistance in breast and ovarian cancer cell lines [81–83]. Taxanes **formulations** have also been developed to bypass efflux-dependent drug resistance. Albumin-bound paclitaxel (nab-paclitaxel) was the first nanoformulation to receive FDA approval in 2005 for refractory, metastatic, or relapsed breast cancer [84]. Other conjugates that couple taxanes with nanoparticles or micelles have been shown to inhibit P-gp activity, increase paclitaxel delivery, and reverse paclitaxel resistance in ovarian cancer cells [85]. Several paclitaxel analogs and formulations are currently in clinical trials [84].

Besides paclitaxel analogs, new microtubule targeting agents that bind microtubules at non-taxane sites are under investigation [14,86]. Like taxanes, those inhibitors (such as epothilones and halichondrins) suppress microtubule dynamics and promote aberrant cell division and

Clinician's Corner

Taxane-based chemotherapy is the standard of care in breast and ovarian cancers. Resistance arises in a large number of patients and is an important issue in public health.

Several predictive biomarkers have been investigated but failed to translate into clinics due to lack of specificity and sensitivity.

Drugs able to overcome chemoresistance are currently being investigated in clinical trials.

The major issue today is the lack of efficient therapy for resistant tumors. New therapeutic strategies to surmount chemoresistance in conjunction with an appropriate companion biomarker are needed in the context of personalized medicine to improve patient care and outcome.

death, but they are poor substrates of P-gp and are consequently active in multidrug resistant cell lines [86]. Thus, investigating structural properties of microtubule binding sites may provide alternative therapeutic options to treat taxane-resistant tumors. In this context, a structure-based repurposing approach revealed pocket similarity between the ER and the β-tubulin taxane site. Selective ER modulators (SERMs) can bind to the taxane site and stabilize microtubules, suggesting that SERMs could represent an interesting strategy to overcome taxane resistance [87].

The identification of multiple mechanisms of taxane resistance, as described above, has oriented new strategies targeting mitotic fidelity, cell metabolism or tumor microenvironment to reverse the resistance (Figure 1). Prevention of mitotic exit by pharmacological inhibition of mitotic kinases [88], or by inhibiting regulators of chromosome segregation or the SAC effector APC/C [60,89,90], ultimately results in apoptosis and restores taxane sensitivity in breast and ovarian cancer models. Several studies have converged to a new paradigm where increasing mitotic abnormalities – and subsequent aneuploidy – confers higher sensitivity to taxane-based chemotherapy [28,57], presenting an attractive endpoint to novel therapeutic strategies.

Targeting the metabolic reprogramming induced by taxanes is another way to avoid chemoresistance. Indeed, metabolic modulators that target either glycolytic or glutaminolytic enzymes, glucose transporters, or lipid and mitochondria metabolism, have been shown to sensitize resistant cancer cells to paclitaxel [63,91]. Of note, targeting low proliferating CSCs either directly by the src kinase inhibitor dasatinib, or indirectly by targeting the CAFs, circumvents resistance to taxanes through induction of CSCs differentiation [92,93]. Deregulated metabolism in cancer cells may be driven by oncogenes, which points to inhibition of key signaling pathways as another option to overcome resistance. In particular, inhibiting the MEK or the PI3K/mTOR signaling pathways has been shown to reverse chemoresistance in ovarian and breast cancers [94,95].

Tubulin is a frequent nonkinase target of kinase inhibitors [96]. Thus, many inhibitors targeting either mitotic kinases, receptor tyrosine kinases, or intracellular kinases that regulate signaling and metabolic pathways such as src, PI3K, or PDK1, also interact with microtubules and modulate their dynamics [13,97,98]. By concomitantly targeting multiple pathways, tubulin/kinase dual inhibitors show improved efficiency in chemoresistant cancer cells while having reduced toxicity in normal cells, thereby overcoming the major limitations of taxanes. Dual inhibitors provide a new rationale for anticancer drug development that takes advantage of multiple target inhibition to kill cancer cells and reduce the risk of drug resistance.

Concluding Remarks

Overcoming taxane resistance is a major challenge and constitutes an active area of cancer research. New mechanisms of taxane resistance have been described, in particular the regulation of mitotic fidelity and metabolic reprogramming, opening the way to promising strategies with the hope to circumvent the resistance in the near future (see Outstanding Questions). Alternative therapies are currently in clinical trials but efforts are still needed for the development of accurate predictive biomarkers translatable into clinics. Machine learning and deep learning are emerging approaches that warrant further development. In the context of personalized medicine, the management of breast and ovarian cancers will greatly benefit from associating a companion biomarker – to identify resistant patients – with an adapted therapy to circumvent chemoresistance and improve patients' outcome (see Clinician's Corner).

Outstanding Questions

Could the development of machine learning algorithms improve the identification of accurate predictive biomarkers in breast and ovarian cancer?

What is the impact of the tumor microenvironment versus cell-autonomous mechanisms in the control of taxane resistance?

Could inhibitors of mitotic fidelity and/or metabolic reprogramming represent future therapies against chemoresistant cancers?

How can we translate the knowledge in taxane resistance mechanisms into clinical settings?

Will taxane analogues or drug combination be successful treatments to bypass chemoresistance?

Acknowledgments

This work was funded by Gustave Roussy Cancer Center, the Agence Nationale de la Recherche grant MMO ANR-10-IBHU-0001, the Comité Ile-de-France of the Ligue Nationale contre le Cancer, the Ligue contre le Cancer 94/Val-de-Marne, the

Fondation ARC, the Centre National de la Recherche Scientifique, the Institut National de la Santé et de la Recherche Médicale, the Fondation Janssen Horizon, the Fonds de Dotation Agnès b., AG2R LA MONDIALE, the Fondation Rothschild, the association Odyssea and Prolific.

References

1. Houssami, N. *et al.* (2012) Meta-analysis of the association of breast cancer subtype and pathologic complete response to neoadjuvant chemotherapy. *Eur. J. Cancer* 48, 3342–3354
2. Pokhriyal, R. *et al.* (2019) Chemotherapy resistance in advanced ovarian cancer patients. *Biomark. Cancer* 11, 1–19
3. Schiff, P.B. *et al.* (1979) Promotion of microtubule assembly *in vitro* by taxol. *Nature* 277, 665–667
4. Zasadil, L.M. *et al.* (2014) Cytotoxicity of paclitaxel in breast cancer is due to chromosome missegregation on multipolar spindles. *Sci. Transl. Med.* 6, 229ra43
5. Weaver, B.A. (2014) How taxol/paclitaxel kills cancer cells. *Mol. Biol. Cell* 25, 2677–2681
6. Mitchison, T.J. *et al.* (2017) Is inflammatory micronucleation the key to a successful anti-mitotic cancer drug? *Open Biol.* 7, 170182
7. Pineda, J.J. *et al.* (2018) Site occupancy calibration of taxane pharmacology in live cells and tissues. *Proc. Natl. Acad. Sci. U. S. A.* 115, E11406–E11414
8. Dumontet, C. and Jordan, M.A. (2010) Microtubule-binding agents: a dynamic field of cancer therapeutics. *Nat. Rev. Drug Discov.* 9, 790–803
9. Mohan, R. *et al.* (2013) End-binding proteins sensitize microtubules to the action of microtubule-targeting agents. *Proc. Natl. Acad. Sci. U. S. A.* 110, 8900–8905
10. Nogales, E. *et al.* (1995) Structure of tubulin at 6.5 A and location of the taxol-binding site. *Nature* 375, 424–427
11. Yang, C.-P.H. and Horwitz, S.B. (2017) Taxol®: the first microtubule stabilizing agent. *Int. J. Mol. Sci.* 18, 1733
12. Elie-Caille, C. *et al.* (2007) Straight GDP-tubulin protofilaments form in the presence of taxol. *Curr. Biol.* 17, 1765–1770
13. Steinmetz, M.O. and Prota, A.E. (2018) Microtubule-targeting agents: strategies to hijack the cytoskeleton. *Trends Cell Biol.* 28, 776–792
14. Prota, A.E. *et al.* (2013) Molecular mechanism of action of microtubule-stabilizing anticancer agents. *Science* 339, 587–590
15. Kellogg, E.H. *et al.* (2017) Insights into the distinct mechanisms of action of taxane and non-taxane microtubule stabilizers from cryo-EM structures. *J. Mol. Biol.* 429, 633–646
16. Rai, A. *et al.* (2020) Taxanes convert regions of perturbed microtubule growth into rescue sites. *Nat. Mater.* 19, 355–365
17. Peronne, L. *et al.* (2020) Two antagonistic microtubule targeting drugs act synergistically to kill cancer cells. *Cancers* 12, 2196
18. Chavez, J.D. *et al.* (2019) Cellular interactome dynamics during paclitaxel treatment. *Cell Rep.* 29, 2371–2383
19. Gasic, I. *et al.* (2019) Tubulin mRNA stability is sensitive to change in microtubule dynamics caused by multiple physiological and toxic cues. *PLoS Biol.* 17, e3000225
20. Gasic, I. and Mitchison, T.J. (2019) Autoregulation and repair in microtubule homeostasis. *Curr. Opin. Cell Biol.* 56, 80–87
21. Fuksa, L. *et al.* (2012) Predictive biomarkers in breast cancer: their value in neoadjuvant chemotherapy. *Cancer Investig.* 30, 663–678
22. McGrogan, B.T. *et al.* (2008) Taxanes, microtubules and chemoresistant breast cancer. *Biochim. Biophys. Acta* 1785, 96–132
23. Su, D. *et al.* (2009) Stathmin and tubulin expression and survival of ovarian cancer patients receiving platinum treatment with and without paclitaxel. *Cancer* 115, 2453–2463
24. Meng, X.-L. *et al.* (2012) Low expression of stathmin in tumor predicts high response to neoadjuvant chemotherapy with docetaxel-containing regimens in locally advanced breast cancer. *Genet. Test. Mol. Biomark.* 16, 689–694
25. Smoter, M. *et al.* (2013) Tau protein as a potential predictive marker in epithelial ovarian cancer patients treated with paclitaxel/platinum first-line chemotherapy. *J. Exp. Clin. Cancer Res.* 32, 25
26. Bonneau, C. *et al.* (2015) Predictive and prognostic value of the tau protein in breast cancer. *Anticancer Res.* 35, 5179–5184
27. Xie, S. *et al.* (2016) Microtubule-binding proteins as promising biomarkers of paclitaxel sensitivity in cancer chemotherapy. *Med. Res. Rev.* 36, 300–312
28. Rodrigues-Ferreira, S. *et al.* (2019) Improving breast cancer sensitivity to paclitaxel by increasing aneuploidy. *Proc. Natl Acad. Sci. USA* 116, 23691–23697
29. Nakazawa, Y. *et al.* (2020) The pathological complete response and secreted protein acidic and rich in cysteine expression in patients with breast cancer receiving neoadjuvant nab-paclitaxel chemotherapy. *Oncol. Lett.* 19, 2705–2712
30. Jeleniewicz, W. *et al.* (2019) *MMP-2* mRNA expression in ovarian cancer tissues predicts patients' response to platinum-taxane chemotherapy. *Anticancer Res.* 39, 1821–1827
31. Jain, R.K. (2013) Normalizing tumor microenvironment to treat cancer: bench to bedside to biomarkers. *J. Clin. Oncol.* 31, 2205–2218
32. Pucci, P. *et al.* (2018) Hypoxia and noncoding RNAs in taxane resistance. *Trends Pharmacol. Sci.* 39, 695–709
33. Mendiola, M. *et al.* (2018) Predicting response to standard first-line treatment in high-grade serous ovarian carcinoma by angiogenesis-related genes. *Anticancer Res.* 38, 5393–5400
34. Denkert, C. *et al.* (2010) Tumor-associated lymphocytes as an independent predictor of response to neoadjuvant chemotherapy in breast cancer. *J. Clin. Oncol.* 28, 105–113
35. Yu, X. *et al.* (2016) Prognostic and predictive value of tumor-infiltrating lymphocytes in breast cancer: a systematic review and meta-analysis. *Clin. Transl. Oncol.* 18, 497–506
36. Denkert, C. *et al.* (2018) Tumour-infiltrating lymphocytes and prognosis in different subtypes of breast cancer: a pooled analysis of 3771 patients treated with neoadjuvant therapy. *Lancet Oncol.* 19, 40–50
37. Schmid, P. *et al.* (2020) Pembrolizumab for early triple-negative breast cancer. *N. Engl. J. Med.* 382, 810–821
38. Schmid, P. *et al.* (2020) Atezolizumab plus nab-paclitaxel as first-line treatment for unresectable, locally advanced or metastatic triple-negative breast cancer (IMpassion130): updated efficacy results from a randomised, double-blind, placebo-controlled, phase 3 trial. *Lancet Oncol.* 21, 44–59
39. Li, J. *et al.* (2017) The prognostic value of tumor-infiltrating T lymphocytes in ovarian cancer. *Oncotarget* 8, 15621
40. Kochi, M. *et al.* (2018) Tumour-infiltrating lymphocytes (TILs)-related genomic signature predicts chemotherapy response in breast cancer. *Breast Cancer Res. Treat.* 167, 39–47
41. Pineda, B. *et al.* (2019) A two-gene epigenetic signature for the prediction of response to neoadjuvant chemotherapy in triple-negative breast cancer patients. *Clin. Epigenet.* 11, 33
42. Wang, L. *et al.* (2017) Identification of long non-coding RNA signature for paclitaxel-resistant patients with advanced ovarian cancer. *Oncotarget* 8, 64191–64202
43. Chen, Y. *et al.* (2020) A qualitative transcriptional signature for predicting extreme resistance of ER-negative breast cancer to paclitaxel, doxorubicin, and cyclophosphamide neoadjuvant chemotherapy. *Front. Mol. Biosci.* 7, 34
44. Feng, X. *et al.* (2019) Gene expression-based predictive markers for paclitaxel treatment in ER+ and ER− breast cancer. *Front. Genet.* 10, 156
45. Bomane, A. *et al.* (2019) Paclitaxel response can be predicted with interpretable multi-variate classifiers exploiting DNA-methylation and miRNA data. *Front. Genet.* 10, 1041
46. Lu, Z. *et al.* (2020) Deep-learning-based characterization of tumor-infiltrating lymphocytes in breast cancers from histopathology images and multiomics data. *JCO Clin. Cancer Informat.* 4, 480–490
47. Sakellaropoulos, T. *et al.* (2019) A deep learning framework for predicting response to therapy in cancer. *Cell Rep.* 29, 3367–3373

48. Murray, S. *et al.* (2012) Taxane resistance in breast cancer: mechanisms, predictive biomarkers and circumvention strategies. *Cancer Treat. Rev.* 38, 890–903
49. Gascoigne, K.E. and Taylor, S.S. (2008) Cancer cells display profound intra- and interline variation following prolonged exposure to antimitotic drugs. *Cancer Cell* 14, 111–122
50. Tambe, M. *et al.* (2016) Novel Mad2-targeting miR-493-3p controls mitotic fidelity and cancer cells' sensitivity to paclitaxel. *Oncotarget* 7, 12267–12285
51. Chong, T. *et al.* (2018) Deregulation of the spindle assembly checkpoint is associated with paclitaxel resistance in ovarian cancer. *J. Ovarian Res.* 11, 27
52. Etemadmoghadam, D. *et al.* (2009) Integrated genome-wide DNA copy number and expression analysis identifies distinct mechanisms of primary chemoresistance in ovarian carcinomas. *Clin. Cancer Res.* 15, 1417–1427
53. Haschka, M. *et al.* (2018) Perturbing mitosis for anti-cancer therapy: is cell death the only answer? *EMBO Rep.* 19, e45440
54. Wertz, I.E. *et al.* (2011) Sensitivity to antitubulin chemotherapeutics is regulated by MCL1 and FBW7. *Nature* 471, 110–114
55. Sloss, O. *et al.* (2016) Mcl-1 dynamics influence mitotic slippage and death in mitosis. *Oncotarget* 7, 5176–5192
56. Silk, A.D. *et al.* (2013) Chromosome missegregation rate predicts whether aneuploidy will promote or suppress tumors. *Proc. Natl. Acad. Sci. U. S. A.* 110, E4134–E4141
57. Rodrigues-Ferreira, S. and Nahmias, C. (2020) From tumorigenesis to cell death: the aneuploidy paradox. *Mol. Cell. Oncol.* 7, 1709390
58. Ganguly, A. *et al.* (2011) Overexpression of mitotic centromere-associated kinesin stimulates microtubule detachment and confers resistance to paclitaxel. *Mol. Cancer Ther.* 10, 929–937
59. Khongkow, P. *et al.* (2016) Paclitaxel targets FOXM1 to regulate KIF20A in mitotic catastrophe and breast cancer paclitaxel resistance. *Oncogene* 35, 990–1002
60. Roberts, M.S. *et al.* (2020) LIN9 and NEK2 are core regulators of mitotic fidelity that can be therapeutically targeted to overcome taxane resistance. *Cancer Res.* 80, 1693–1706
61. Komlodi-Pasztor, E. *et al.* (2011) Mitosis is not a key target of microtubule agents in patient tumors. *Nat. Rev. Clin. Oncol.* 8, 244–250
62. Rodrigues-Ferreira, S. *et al.* (2020) ATIP3 deficiency facilitates intracellular accumulation of paclitaxel to reduce cancer cell migration and lymph node metastasis in breast cancer patients. *Sci. Rep.* 10, 13217
63. Desbats, M.A. *et al.* (2020) Metabolic plasticity in chemotherapy resistance. *Front. Oncol.* 10, 281
64. Zaal, E.A. and Berkers, C.R. (2018) The influence of metabolism on drug response in cancer. *Front. Oncol.* 8, 500
65. Li, Q. *et al.* (2020) Rac1 activates non-oxidative pentose phosphate pathway to induce chemoresistance of breast cancer. *Nat. Commun.* 11, 1456
66. Peetla, C. *et al.* (2013) Biophysics of cell membrane lipids in cancer drug resistance: Implications for drug transport and drug delivery with nanoparticles. *Adv. Drug Deliv. Rev.* 65, 1686–1698
67. Swanton, C. *et al.* (2007) Regulators of mitotic arrest and ceramide metabolism are determinants of sensitivity to paclitaxel and other chemotherapeutic drugs. *Cancer Cell* 11, 498–512
68. Heuer, T.S. *et al.* (2017) FASN inhibition and taxane treatment combine to enhance anti-tumor efficacy in diverse xenograft tumor models through disruption of tubulin palmitoylation and microtubule organization and FASN inhibition-mediated effects on oncogenic signaling and gene expression. *EBioMedicine* 16, 51–62
69. Wu, Y.-H. *et al.* (2020) Comparing PI3K/Akt inhibitors used in ovarian cancer treatment. *Front. Pharmacol.* 11, 206
70. Guerra, F. *et al.* (2017) Mitochondria and cancer chemoresistance. *Biochim. Biophys. Acta Bioenerg.* 1858, 686–699
71. Emmings, E. *et al.* (2019) Targeting mitochondria for treatment of chemoresistant ovarian cancer. *Int. J. Mol. Sci.* 20, 229
72. Gentric, G. *et al.* (2019) PML-regulated mitochondrial metabolism enhances chemosensitivity in human ovarian cancers. *Cell Metab.* 29, 156–173
73. Domènech, E. *et al.* (2015) AMPK and PFKFB3 mediate glycolysis and survival in response to mitophagy during mitotic arrest. *Nat. Cell Biol.* 17, 1304–1316
74. Taylor, C. *et al.* (2017) Loss of PFKFB4 induces cell death in mitotically arrested ovarian cancer cells. *Oncotarget* 8, 17960–17980
75. Au Yeung, C.L. *et al.* (2016) Exosomal transfer of stroma-derived miR21 confers paclitaxel resistance in ovarian cancer cells through targeting APAF1. *Nat. Commun.* 7, 11150
76. Su, S. *et al.* (2018) CD10+GPR77+ cancer-associated fibroblasts promote cancer formation and chemoresistance by sustaining cancer stemness. *Cell* 172, 841–856
77. Yang, J. *et al.* (2019) Adipocytes promote ovarian cancer chemoresistance. *Sci. Rep.* 9, 13316
78. Olson, O.C. *et al.* (2017) Tumor-associated macrophages suppress the cytotoxic activity of antimitotic agents. *Cell Rep.* 19, 101–113
79. Greenberger, L.M. and Sampath, D. (2006) Resistance to taxanes. In *Cancer Drug Resistance* (Teicher, B.A., ed.), pp. 329–358, Humana Press
80. Clarke, R. *et al.* (2005) Multidrug resistance/P-glycoprotein and breast cancer: review and meta-analysis. *Semin. Oncol.* 32, 9–15
81. Jing, Y.-R. *et al.* (2020) T-13 and T-26, the novel taxanes with improved oral bioavailability in rats. *Sci. Rep.* 10, 3211
82. Jelínek, M. *et al.* (2018) Substituents at the C3′ and C3′N positions are critical for taxanes to overcome acquired resistance of cancer cells to paclitaxel. *Tox. Appl. Pharmacol.* 347, 79–91
83. Matesanz, R. *et al.* (2014) Taxanes with high potency inducing tubulin assembly overcome tumoural cell resistances. *Bioorg. Med. Chem.* 22, 5078–5090
84. Ojima, I. *et al.* (2016) Taxane anticancer agents: a patent perspective. *Expert Opin. Ther. Pat.* 26, 1–20
85. Chen, F. *et al.* (2017) Reversal of paclitaxel resistance in human ovarian cancer cells with redox-responsive micelles consisting of α-tocopheryl succinate-based polyphosphoester copolymers. *Acta Pharmacol. Sin.* 38, 859–873
86. Ning, N. *et al.* (2018) A novel microtubule inhibitor overcomes multidrug resistance in tumors. *Cancer Res.* 78, 5949–5957
87. Lo, Y.-C. *et al.* (2019) Pocket similarity identifies selective estrogen receptor modulators as microtubule modulators at the taxane site. *Nat. Commun.* 10, 1033
88. Peng, Y. *et al.* (2019) USP7 is a novel deubiquitinase sustaining PLK1 protein stability and regulating chromosome alignment in mitosis. *J. Exp. Clin. Cancer Res.* 38, 468
89. Raab, M. *et al.* (2020) Boosting the apoptotic response of high-grade serous ovarian cancers with *CCNE1* amplification to paclitaxel *in vitro* by targeting APC/C and the pro-survival protein MCL-1. *Int. J. Cancer* 146, 1086–1098
90. Raab, M. *et al.* (2019) Blocking mitotic exit of ovarian cancer cells by pharmaceutical inhibition of the anaphase-promoting complex reduces chromosomal instability. *Neoplasia* 21, 363–375
91. Masamha, C.P. and LaFontaine, P. (2018) Molecular targeting of glutaminase sensitizes ovarian cancer cells to chemotherapy. *J. Cell. Biochem.* 119, 6136–6145
92. Tian, J. *et al.* (2018) Dasatinib sensitises triple negative breast cancer cells to chemotherapy by targeting breast cancer stem cells. *Br. J. Cancer* 119, 1495–1507
93. Cazet, A.S. *et al.* (2018) Targeting stromal remodeling and cancer stem cell plasticity overcomes chemoresistance in triple negative breast cancer. *Nat. Commun.* 9, 2897
94. Oudin, M.J. *et al.* (2017) MENA confers resistance to paclitaxel in triple-negative breast cancer. *Mol. Cancer Ther.* 16, 143–155
95. Choi, H.J. *et al.* (2019) A novel PI3K/mTOR dual inhibitor, CMG002, overcomes the chemoresistance in ovarian cancer. *Gynecol. Oncol.* 153, 135–148
96. Munoz, L. (2017) Non-kinase targets of protein kinase inhibitors. *Nat. Rev. Drug Discov.* 16, 424–440
97. Arnst, K.E. *et al.* (2019) Current advances of tubulin inhibitors as dual acting small molecules for cancer therapy. *Med. Res. Rev.* 39, 1398–1426

98. Tanabe, K. (2017) Microtubule depolymerization by kinase inhibitors: unexpected findings of dual inhibitors. *Int. J. Mol. Sci.* 18, 2508
99. Aumeier, C. *et al.* (2016) Self-repair promotes microtubule rescue. *Nat. Cell Biol.* 18, 1054–1064
100. Vemu, A. *et al.* (2018) Severing enzymes amplify microtubule arrays through lattice GTP-tubulin incorporation. *Science* 361, 768
101. de Forges, H. *et al.* (2016) Localized mechanical stress promotes microtubule rescue. *Curr. Biol.* 26, 3399–3406
102. Schaedel, L. *et al.* (2015) Microtubules self-repair in response to mechanical stress. *Nat. Mater.* 14, 1156–1163
103. Henrie, H. *et al.* (2020) Stress-induced phosphorylation of CLIP-170 by JNK promotes microtubule rescue. *J. Cell Biol.* 219, e201909093
104. Aher, A. *et al.* (2020) CLASP mediates microtubule repair by restricting lattice damage and regulating tubulin incorporation. *Curr. Biol.* 30, 2175–2183
105. Yang, T. *et al.* (2018) PIM2-mediated phosphorylation of hexokinase 2 is critical for tumor growth and paclitaxel resistance in breast cancer. *Oncogene* 37, 5997–6009
106. Mondal, S. *et al.* (2019) Therapeutic targeting of PFKFB3 with a novel glycolytic inhibitor PFK158 promotes lipophagy and chemosensitivity in gynecologic cancers. *Int. J. Cancer* 144, 178–189
107. Hou, L. *et al.* (2019) Interfering cellular lactate homeostasis overcomes Taxol resistance of breast cancer cells through the microRNA-124-mediated lactate transporter (MCT1) inhibition. *Cancer Cell Int.* 19, 193

Review 2 - ATIP3, an Emerging Target for Personalized Medicine in Breast Cancer

The purpose of this review was to describe in details all that we know about ATIP3, from our lab and others. As there is a need for robust biomarkers to guide personalized treatment for breast cancer patients. In this review, we focus on ATIP3's role as a prognostic biomarker of patient survival and a predictive biomarker of breast tumors' response to taxane-based chemotherapy. Additionally, we discuss the deregulated molecular mechanisms associated with ATIP3 deficiency such as centrosome amplification and aneuploidy. We propose the targeting of ATIP3-associated molecular complexes and/or exploiting aneuploidy as potential novel therapeutic approaches for ATIP3-deficient breast tumors.

This review was published on the 1st of May 2021.

cells

MDPI

Review

Microtubule-Associated Protein ATIP3, an Emerging Target for Personalized Medicine in Breast Cancer

Maria M. Haykal [1,2], Sylvie Rodrigues-Ferreira [1,2,3] and Clara Nahmias [1,2,*]

1 Institut Gustave Roussy, Université Paris-Saclay, Inserm U981, Biomarqueurs Prédictifs et Nouvelles Stratégies Thérapeutiques en Oncologie, 94800 Villejuif, France; maria.haykal@gustaveroussy.fr (M.M.H.); sylvie.rodrigues-ferreira@gustaveroussy.fr (S.R.-F.)
2 LERMIT Laboratory, 92296 Chatenay-Malabry, France
3 Inovarion, 75005 Paris, France
* Correspondence: clara.nahmias@inserm.fr

Abstract: Breast cancer is the leading cause of death by malignancy among women worldwide. Clinical data and molecular characteristics of breast tumors are essential to guide clinician's therapeutic decisions. In the new era of precision medicine, that aims at personalizing the treatment for each patient, there is urgent need to identify robust companion biomarkers for new targeted therapies. This review focuses on ATIP3, a potent anti-cancer protein encoded by candidate tumor suppressor gene *MTUS1*, whose expression levels are markedly down-regulated in breast cancer. ATIP3 is a microtubule-associated protein identified both as a prognostic biomarker of patient survival and a predictive biomarker of breast tumors response to taxane-based chemotherapy. We present here recent studies pointing out ATIP3 as an emerging anti-cancer protein and a potential companion biomarker to be combined with future personalized therapy against ATIP3-deficient breast cancer.

Keywords: *MTUS1*; tumor suppressor; breast cancer; prognostic biomarker; predictive biomarker; microtubule; taxanes; chemotherapy; targeted therapy

Citation: Haykal, M.M.; Rodrigues-Ferreira, S.; Nahmias, C. Microtubule-Associated Protein ATIP3, an Emerging Target for Personalized Medicine in Breast Cancer. *Cells* **2021**, *10*, 1080. https://doi.org/10.3390/cells10051080

Academic Editor: Frank Schnütgen

Received: 12 April 2021
Accepted: 29 April 2021
Published: 1 May 2021

1. ATIP3 and the *MTUS1* Gene, a Historical Point of View

The microtubule-associated tumor suppressor (*MTUS1*) gene was first identified in 2003 under the name *MTSG1* [1]. This gene is located at chromosomal position 8p22, a region frequently reported to be lost in a number of solid tumors, including breast cancer [2,3]. In their search for new tumor suppressor genes, Seibold and collaborators used a differential display RT-PCR strategy and identified the *MTSG1* transcript as being up-regulated in 3-dimensional cultures of quiescent versus differentiated human endothelial cells [1]. *MTSG1* was reported to encode a 436 amino-acids polypeptide (48 KDa) co-localizing with mitochondria, that was down-regulated in pancreatic cancer and inhibited cell proliferation when expressed into pancreatic cancer cells.

In an independent study published a few months later by our group, the same polypeptide was identified in a yeast two-hybrid system as an intracellular interacting partner of the human angiotensin II AT2 receptor and was designated ATIP1 [4]. AT2 is a rare example of a seven transmembrane receptor that controls cell proliferation through intracellular pathways that do not use typical G-protein signaling [5]. ATIP1 was, thus, identified as a scaffold protein mediating the anti-proliferative effects of AT2 in a constitutive fashion, even in the absence of receptor stimulation [4].

The functional relevance of ATIP1-AT2 receptor complexes was further demonstrated in a number of cell types of cardiovascular, adipose, and neuronal origins [6–12]. Transgenic animals overexpressing ATIP1 were useful for demonstrating the role of the AT2/ATIP1 axis in pathophysiological models of neointima formation [6,7], vascular senescence [8] and endothelial dysfunction [9], as well as neuronal differentiation [10] and adipose tissue inflammation [11]. The observation that ATIP1 and AT2 transcripts are co-regulated by

PARP-1 [12] further supported the tight link between these two proteins. ATIP1 was also described as a Golgi-associated protein involved in intracellular trafficking of the AT2 receptor to the cell membrane [13]. Thus, ATIP1 mainly appears as a regulator of AT2 receptor functions in cardiovascular and central nervous systems.

ATIP1 belongs to the family of evolutionary conserved AT2-interacting proteins (ATIP), that includes ATIP3 and ATIP4. All ATIPs share the same C-terminal amino-acid sequence of 396 residues comprising the AT2 receptor binding site and several coiled-coil motifs involved in homo- and hetero-dimerization [4]. ATIP1, ATIP3, and ATIP4 are the products of alternative splicing and different promoter usage of the same *MTUS1* gene, organized into 17 coding exons [14,15]. *MTUS1* encodes two splice variants of ATIP3, designated ATIP3a and ATIP3b, that differ by a single in-phase exon encoding a sequence of 60 amino-acids in the N-terminal portion of the proteins. To date, no functional difference has been reported between the two polypeptides. In rodents, the ortholog *MTUS1* gene comprises 15 coding exons that are also alternatively spliced [13,16] to generate 3 different ATIP isoforms (designated ATBP50, ATBP135, and ATBP60 in the mouse) with high sequence homology to human ATIP1, ATIP3 and ATIP4, respectively. The *Xenopus MTUS1* gene ortholog encodes the ICIS protein, which exhibits structural homology with the mammalian ATIP3 isoform [14].

The ATIP1 and ATIP3 transcripts display an ubiquitous profile with high expression in the brain, ATIP3 being the prominent isoform in peripheral tissues, whereas ATIP4 is exclusively expressed in the central nervous system [14]. The presence of a canonical transmembrane domain in its polypeptide sequence suggests close interaction of ATIP4 with the AT2 receptor at the plasma membrane. However, this isoform has never been characterized at the molecular nor functional level.

Consistent with the initial report that *MTUS1* may be a candidate tumor suppressor gene in pancreatic cancer [1], inactivation of the gene in knock-out animals was associated with B cell lymphoproliferative disease [17]. Furthermore, p53-regulation of ATIP1 transcripts suggested a link between *MTUS1* gene regulation and cancer [18]. Indeed, *MTUS1* down-regulation in cancer tissues was frequently reported, including in tumors from the breast [19–23], bladder [24,25], colon [26–29], gallbladder [30], gastric tissues [31,32], lung (NSCLC) [33], head-and-neck [34–39], clear cell renal cell carcinoma (cc-RCC) [40,41], and uveal melanoma [42], with the exception of prostate cancer, in which *MTUS1* expression was reported to increase with cancer progression [43,44] (Table 1). Only few studies were designed to discriminate between different ATIP isoforms, and they all pointed to ATIP3 as the major *MTUS1* isoform altered in human malignancies [19,21,36,43], ATIP1 being a minor form expressed in normal peripheral tissues [14].

The present review focuses on the characterization of ATIP3 in breast cancer. We summarize recent results investigating intracellular mechanisms regulated by this protein and we present evidence that ATIP3 is a prognostic and predictive biomarker in breast tumors. Finally, we discuss data suggesting that ATIP3 studies may open the way to important emerging targets for anti-cancer therapy.

Table 1. *MTUS1* gene status in human cancers.

Cancer Type	*MTUS1* Isoform	Detection Method	Expression Level	Prognosis *	Reference
Bladder	N.D.	IHC	Underexpressed	OS	[25]
	N.D.	RT-qPCR	Underexpressed	DFS	[24]
Breast	N.D.	Microarray	Underexpressed	N.D.	[23]
	ATIP3	Microarray		OS/MFS	[21]
	ATIP3	Microarray/IHC		N.D.	[19]
	ATIP3	Microarray/IHC		OS	[22]
Colorectal	N.D.	RNA-seq	Underexpressed	OS	[29]
	N.D.	IHC		N.D.	[27]
	N.D.	RT-qPCR/WB		N.D.	[26]
	N.D.	RT-qPCR		N.D.	[28]
Gallbladder	N.D.	Microarray/IHC	Underexpressed	DFS	[30]
Gastric	N.D.	RT-qPCR	Underexpressed	N.D.	[32]
Non small cell lung	N.D.	Microarray	Underexpressed	OS	[33]
Oral	N.D.	RT-qPCR	Underexpressed	N.D.	[38]
	ATIP3	IHC		OS	[36]
	N.D.	Microarray/IHC		OS	[34]
Prostate	ATIP1/ATIP3	RT-qPCR/IHC	Overexpressed	N.D.	[43]
Renal	N.D.	IHC	Underexpressed	N.D.	[41]
Uveal melanoma	N.D.	Microarray	Underexpressed	MFS	[42]

N.D. Not determined; OS: Overall survival, DFS: disease-free survival, MFS: metastasis free survival; IHC: immunohistochemistry, RT-qPCR: Reverse transcription quantitative polymerase chain reaction; RNAseq: RNA sequencing; WB: Western blot. * Underexpression of *MTUS1* is associated with reduced OS, MFS, and DFS.

2. ATIP3 Is a Microtubule-Associated Protein

ATIP3 is a 1270 amino-acids polypeptide organized into an unstructured N-terminal region of 874 amino-acids and a coiled-coil C-terminal region shared with other ATIP members [14,20]. Initial analyses of its intracellular localization clearly indicated that ATIP3 decorates the microtubule cytoskeleton and the centrosome in interphase, and localizes at the mitotic spindle during all stages of mitosis. In microtubule co-sedimentation assays, ATIP3 was found to associate with stable microtubules rather than soluble tubulin [19]. Studies of ATIP3 deletion mutants revealed that ATIP3 binds microtubules through a positively charged, central region (D2) of the protein [21]. These basic residues are believed to interact with the acidic charges of tubulin tails, as reported for other microtubule-associated proteins (MAPs).

The microtubule cytoskeleton plays an essential role in cell homeostasis by controlling not only cell shape, but also intracellular trafficking of proteins and organelles, as well as cell migration and mitosis. Microtubules are polarized and very dynamic structures formed by the assembly of a/b tubulin dimers at their growing (plus) ends, in a GTP-dependent manner. Microtubule ends are constantly alternating between phases of growth (polymerization) and shrinkage (depolymerization), in a process known as "dynamic instability" [45]. This process is essential to allow rapid adaptation of the cytoskeleton to cell changes, such as formation of the mitotic spindle and response to extracellular cues. Microtubule assembly and dynamics are tightly regulated by a large number of MAPs, including structural MAPs that localize along the microtubule fibers, and microtubule plus ends-tracking proteins (+TIPs) that decorate the rapidly growing plus ends [46]. Among +TIPs, End-Binding proteins EB1 and EB3 play a central role in regulating microtubule dynamics. EB1 directly binds the microtubule plus ends [47], where it acts as a platform to

recruit many other regulatory +TIPs [46]. Furthermore, EB1 binding by itself was shown to accelerate the maturation of microtubule plus ends, thereby contributing to dynamic instability [48].

ATIP3 is a structural MAP localized all along the microtubule lattice, and a potent microtubule stabilizer [19]. Strikingly, ATIP3 reduces microtubule dynamics at plus ends although it does not bind to this location [21]. ATIP3 was actually found to interact with EB1 in the cytosol and reduce free EB1 turnover on its preferential site at the plus ends [49]. In this regard, ATIP3 may be considered as an "endogenous antagonist" of EB1, like other structural MAPs, such as MAP1B, MAP2, or MAP-Tau, that all interact with EB1 to restrain its accumulation at growing ends [50]. By preventing EB1 accumulation at plus ends, cytosolic ATIP3/EB1 complexes control the rate of microtubule growth and shrinkage, thereby regulating microtubule targeting to the cell cortex, and subsequent cell polarity and migration [49] (Figure 1). In the absence of ATIP3, EB1 is free to accumulate on plus ends, which accelerates microtubule dynamics. This in turn increases cancer cell motility, in agreement with increased metastatic behavior of ATIP3-deficient breast tumors.

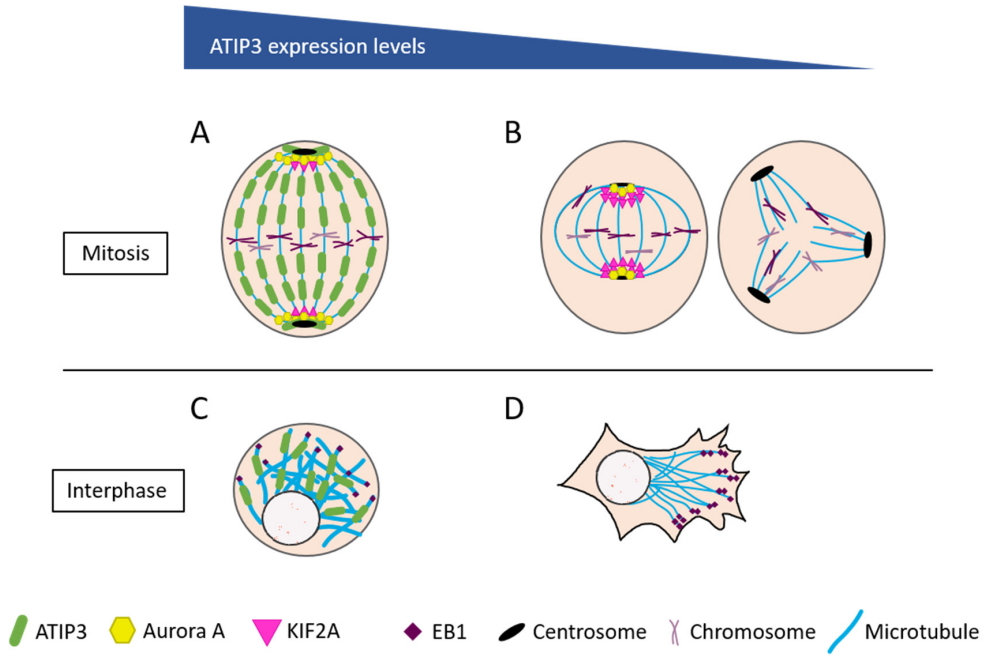

Figure 1. ATIP3-associated molecular mechanisms. (**A**) ATIP3 controls microtubule depolymerization by preventing KIF2A localization to the poles. (**B**) Left: ATIP3-deficient cells have a short metaphase spindle, due to increased KIF2A at the poles. Right: ATIP3-deficient cells show centrosome amplification and multipolar spindle formation, leading to aneuploidy. (**C**) ATIP3 stabilizes microtubules by negatively regulating EB1 turnover at microtubule plus-ends. (**D**) ATIP3-deficient cells are prone to increased directional migration and polarization, due to increased microtubule dynamics.

3. Cancer-Related Molecular Mechanisms Controlled by ATIP3

The microtubule stabilizing properties of ATIP3 are consistent with its potent anti-cancer effects. Indeed, ectopic expression of ATIP3 in breast cancer cells was shown to markedly reduce tumor growth [19] and distant metastasis [21] in pre-clinical models. In line with these in vivo studies, ATIP3 expression reduces cell proliferation, prolongs the time spent in mitosis and reduces cell polarity and migration. However, the intracellular mechanisms associated with the anti-cancer effects of ATIP3 have only recently emerged.

A major step towards the understanding of ATIP3-associated molecular mechanisms was recently provided by a proteomic approach that aimed at identifying intracellular interacting partners of ATIP3 in breast cancer cells. Co-immunoprecipitation experiments followed by mass spectrometry led to the identification of 145 ATIP3-interacting proteins,

among which, nine were related to the microtubule cytoskeleton and/or mitosis [51]. Interestingly, ATIP3 interacts with KIF2A—a microtubule depolymerizing kinesin of the KinI family—and its regulator, Dda3, via a minimal sequence of 112 amino-acids present in the central basic region of the protein. The ATIP3/KIF2A/Dda3 complex prevents the accumulation of KIF2A at the poles of the mitotic spindle, and therefore controls microtubule depolymerization and spindle dynamics at minus ends (Figure 1). As a consequence, ATIP3 regulates the microtubule poleward flux—a mechanism of concerted polymerization at plus ends and depolymerization at minus ends of the spindle—that takes place in metaphase to maintain a constant size of the mitotic spindle [52]. In ATIP3-depleted cells, the mitotic spindle is significantly shortened [51]. This mitotic abnormality, among others, is expected to provoke major defects in chromosome segregation and subsequent aneuploidy.

The stability of the ATIP3/KIF2A/Dda3 molecular complex requires phosphorylation by the mitotic kinase, Aurora A, a major kinase deregulated in cancer, including breast cancer [53,54]. Aurora kinase A is known to localize at the spindle poles where it phosphorylates KIF2A to reduce both the amount, and the depolymerizing activity, of the kinesin at this location. Of importance, ATIP3 was shown to maintain an active pool of Aurora kinase A at the poles, as a mechanism to control KIF2A activity and mitotic spindle integrity [51] (Figure 1). In an independent study conducted in renal cancer cells, ATIP3 was found to regulate the phosphorylation of KIF2C (also designated MCAK), another microtubule depolymerizing kinesin of the KinI family. A recombinant fragment of ATIP3 was shown to contribute to KIF2C phosphorylation on serine 192 by Aurora kinase B, and increase tubulin polymerization, consistent with its microtubule stabilizing effects [40].

Interestingly, the ATIP3 ortholog in *Xenopus*, named ICIS, is also a microtubule-associated protein that interacts with XKCM1 (the *Xenopus* ortholog of MCAK) and with Aurora B kinase to control the integrity of the mitotic spindle [55]. However, in contrast to human ATIP3, ICIS does not decorate the mitotic spindle but localizes both at centromeres and centrosomes in mitotic cells. Furthermore, ICIS stimulates, rather than inhibits, the depolymerizing activity of MCAK to control spindle dynamics at the kinetochores and chromosome segregation in anaphase. Other studies [56] have shown that in *Xenopus* mitotic extracts, ICIS interacts with both MCAK and KIF2A in addition to Aurora B, INCENP, and TD-60, all members of the chromosome passenger complex (CPC, a master regulator of faithful mitosis), supporting the notion that ICIS functions as a scaffold located at the inner centromere to regulate microtubule depolymerization and dynamics at the kinetochore. Together, these studies raise a common scenario for ATIP3 mechanisms of action on mitotic spindle integrity and chromosome segregation in different cellular models. Depending on the organism and cell type, ATIP3 interacts with different kinesins of the KinI family (either KIF2A and/or MCAK) to regulate their depolymerizing activity through Aurora (A or B) kinase-dependent phosphorylation, with a major effect on microtubule dynamics and mitosis (Table 2).

Besides its prominent effects on microtubule dynamics through interaction with EB1, KinI kinesins, and Aurora kinases, it is likely that ATIP3 may control other molecular mechanisms that may account for its potent anti-cancer and anti-metastatic effects in different malignancies. In salivary adenoid cystic carcinoma [36] and squamous carcinoma of the tongue [37], ATIP3 was found to inhibit the phosphorylation of extracellular regulated kinases ERK1/2, as well as the expression of epithelial to mesenchymal (EMT) markers slug and vimentin. In ovarian cancer cell lines, anti-migratory and anti-metastatic effects of ATIP3 were also related to inhibition of the ERK/EMT axis [57]. More recently, ATIP3 expression has been associated with reduced ERK1/2 phosphorylation, cell proliferation, and migration in gastric cancer [32]. In this model, ATIP3 was also found to inhibit the activity of CDC25B phosphatase, leading to phosphorylation and inhibition of the master cell cycle kinase CDK1 [32]. Interestingly, previous studies have revealed that expression of the ATIP1 isoform reduces ERK1/2 activity induced by receptor tyrosine kinases [4], which further links the ATIP family with inhibition of the ERK pathway (Table 2). While

the molecular mechanisms by which ATIP3 inhibits ERK1/2 phosphorylation remain to be clarified, these findings clearly warrant further investigation in breast cancer.

Table 2. ATIP3 localization and function in human and *Xenopus* cells.

	Human ATIP3	Reference	*Xenopus* ICIS	Reference
Localization	Microtubule Mitotic Spindle Centrosome	[19]	Centromere Centrosome	[55]
Interacts with	EB1 KIF2A DDA3	[49,51]	XKCM1 KIF2A AURKB INCENP TD-60	[55,56]
Signaling	ERK AURKA KIF2C CDC25B CDK1	[4,32,51,57]		
Function	Microtubule dynamics Spindle size Centrosome number Proliferation Migration Polarization EMT	[19,21,32,49,51, 57,58]	Microtubule dynamics Mitotic spindle integrity	[55,56]

4. ATIP3 Is a Prognostic Biomarker in Breast Cancer

Breast cancer is the leading cause of death by malignancy in women all over the world. Major difficulties faced by clinicians in treating their patients are related to the high heterogeneity of breast tumors and their ability to metastasize to distant organs. At the onset of the 21st century, the classification of breast tumors into distinct molecular subtypes (luminal, HER2, or triple-negative breast cancer (TNBC)), based on the expression of hormone receptors for estrogen (ER) and progesterone (PR), and amplification of the HER2 oncogene, has changed the paradigm and oriented clinical decisions [59,60]. Over the past few years, the rapid development of high-throughput molecular techniques investigating genomic, epigenetic, and transcriptional alterations in breast tumors has launched a new area of cancer research. Precision medicine, which aims at administrating the right treatment to the right patient based on unique molecular properties of each tumor, is considered today as a major endpoint in the fight against cancer. This approach mainly relies on the identification of biomarkers to select the appropriate population of patients for personalized treatment.

With the aim of identifying new molecular markers in breast cancer, the expression levels of the *MTUS1* gene were analyzed in a DNA array study of 151 breast tumors compared to normal breast tissue [19]. These studies revealed for the first time that *MTUS1* is markedly down-regulated in approximately 50% of all breast cancers and 70% of TNBC, which represent the most aggressive tumors. Real-time RT-PCR analyses using specific oligonucleotides indicated that ATIP3 is the major transcript expressed in normal mammary gland and down-regulated in breast tumors. In several independent cohorts of patients, low levels of ATIP3 mRNA were significantly associated with TNBC subtype [61,62], high grade, and metastatic breast tumors [19], thereby linking low ATIP3 expression and breast cancer aggressiveness.

The mechanisms by which ATIP3 mRNA levels are reduced in breast cancer have not yet been clarified. It is to note that the human ATIP3 promoter contains several CpG islands, suggesting possible regulation by promoter methylation at these sites. Although this possibility has not been directly addressed in breast cancer, recent studies have indeed

reported promoter methylation as a possible mechanism for *MTUS1* down-regulation in non-small cell lung (NSCLC) carcinoma [33]. Another mechanism for regulation of *MTUS1* mRNA stability by the RNA binding protein SORBS2 was recently reported in clear cell renal cell carcinoma [40]. Long non-coding RNAs were shown to control the stability of *MTUS1* transcripts via microRNAs in gastric [32] and cervical cancer [63]. In several other cancer types, including breast [64], colorectal [28], lung [65], gallbladder cancer [30], and osteosarcoma [66], microRNAs also down-regulate *MTUS1* expression. Most microRNAs were found to target the 3'UTR of the gene, which is common to all ATIP isoforms. At the genomic level, alterations of ATIP3-specific coding exons by somatic mutation have been identified in hepatocellular carcinoma [67] but mutational analysis of *MTUS1* in breast cancer remains to be performed. A single study has reported genomic deletion of a sequence corresponding to ATIP3-specific exon 4 in association with increased familial risk of breast cancer [68]. Together these studies suggest that ATIP3 alterations in cancer are a consequence of deregulated gene expression rather than genomic variations.

To investigate whether ATIP3 may represent a prognostic biomarker of breast cancer patient survival, Kaplan-Meyer curves were extracted from different cohorts of breast cancer patients. These studies indicated that low ATIP3 levels are significantly associated with poor clinical outcome and reduced 5-years survival [21]. ATIP3 was also identified as a prognostic biomarker of relapse-free survival and overall survival among patients with metastatic disease. Of interest, the *MTUS1* gene was also described as an interesting prognostic biomarker of patient clinical outcome in other cancer types (Table 1).

The increasing amount of publicly available large-scale molecular studies of breast tumors, associated with clinical data of the patients, have opened the possibility to explore the prognostic value of biomarker combinations, that are likely to be more accurate and informative than single biomarkers. In this context, the prognostic value of ATIP3 was studied in combination with its interacting partner EB1, that was shown to be up-regulated in aggressive breast tumors [69]. Functional studies mentioned above [49,50] showing that ATIP3 antagonizes the effects of EB1 on microtubule dynamics, raised the possibility that tumors with low ATIP3 and high EB1 levels may be associated with increased malignancy and worse prognosis compared with other breast tumors. Studies conducted on 5 independent cohorts of breast cancer patients indeed confirmed the increased prognostic value of combined ATIP3/EB1 expression compared with each biomarker alone [22,70].

In this regard, it will be interesting to further investigate the value of combined expression of ATIP3 with other partners involved in important molecular complexes, such as the depolymerizing kinesins (KIF2A/KIF2C) and mitotic (Aurora) kinases that have also been described as prognostic biomarkers of breast cancer patient survival [71–74]. Other MAPs have been identified as prognostic biomarkers in breast cancer [70]. They are part of protein networks that coordinately regulate microtubule dynamics and functions. Prognostic value of their combined expression warrants further examination.

5. ATIP3 Is a Predictive Biomarker of Taxane-Based Chemotherapy in Breast Cancer

The observation that ATIP3 is a stabilizing MAP raised the possibility that its expression may impact the effects of taxanes on cancer cells. Taxanes (paclitaxel and docetaxel) are chemotherapeutic agents widely used for the treatment of breast cancer. They are generally used in neoadjuvant settings (to reduce tumor size before surgery) and in adjuvant treatment for TNBC and metastatic breast tumors. Taxanes are also frequently used for treating other malignancies, such as ovarian, prostate, lung, and pancreatic cancers. These drugs, also called mitotic poisons, bind microtubules at the "taxane site" and block microtubule dynamics. By stabilizing spindle microtubules in mitosis, taxanes promote mitotic arrest at the spindle assembly checkpoint (SAC), which results in apoptotic cell death. At very low doses of a few nanomolar range, taxanes induce the formation of multipolar spindles and other mitotic defects leading to aneuploidy [75].

Because microtubules are essential components of all cell types, taxanes have very severe side effects characterized by neuropathies and immune system defects, which strongly

hamper patient's quality of life. Importantly, besides inducing undesirable adverse effects, conventional taxane-containing chemotherapy only benefits to a minor fraction (15–20%) of primary breast tumors. It is therefore of utmost importance to identify biomarkers able to select with high confidence the patients who are at high risk to resist to chemotherapy. These predictive biomarkers represent a necessary step towards therapeutic de-escalation and future design of new targeted strategies for chemoresistant breast tumors [76].

In a transcriptomic analysis of three independent cohorts of breast cancer patients treated in neo-adjuvant settings with taxanes, 17 genes encoding microtubule-regulating proteins were found differentially expressed in chemoresistant breast tumors [58], and one of the most strongly deregulated genes was *MTUS1*. Interestingly, ATIP3 expression was significantly down-regulated in taxane-sensitive tumors achieving pathological complete response to chemotherapy [58], including in the BL1 subtype of TNBC [77]. Lymph node metastases were also significantly less frequent among low-ATIP3 expressing tumors following treatment with paclitaxel, compared with high-ATIP3 tumors [78]. These results were rather unexpected as ATIP3 deficiency is associated with increased microtubule dynamics [21], which is opposite to the microtubule-stabilizing effect of taxanes.

At the molecular level, ATIP3 depletion leads to increased accumulation of paclitaxel along the microtubule lattice [78], which accounts for higher sensitivity to low doses of chemotherapy. These results are consistent with in vitro findings that microtubule instability at the plus ends may improve Taxol binding to microtubules [79]. During mitosis, ATIP3 deficiency induces centrosome amplification and formation of multipolar spindles, which are sources of aneuploidy. In the presence of low doses of taxanes, these mitotic abnormalities accumulate above a tolerable level and promote massive cell death [80]. Thus, ATIP3 deficiency induces aneuploidy, which paradoxically sensitizes cancer cells to paclitaxel treatment. In line with these molecular data, human breast tumors expressing low *MTUS1* levels were shown to exhibit elevated aneuploidy and chromosome instability (Figure 1).

Thus, by increasing microtubule dynamics at growing plus ends, ATIP3 deficiency both favors increased paclitaxel binding to microtubules in interphase and promotes the formation of multipolar spindles in mitosis. The potent effects of taxane-based chemotherapy in ATIP3-deficient breast tumors likely arise from a combination of both mechanisms.

6. New ATIP3-Associated Emerging Targets for Breast Cancer Therapy?

In conclusion, studies conducted over the past ten years with the aim to depict the expression and function of ATIP3 in breast cancer have successfully pointed out this protein as a robust prognostic biomarker of patient survival and a strong predictive biomarker for resistance to taxane-based chemotherapy. Down-regulation of *MTUS1* is associated with tumor progression and poor outcome for the patients, suggesting that therapies designed to restore physiological levels of *MTUS1* transcripts may be valuable. Epigenetic mechanisms underlying *MTUS1* down-regulation in various cancers include promoter methylation and regulation of ATIP mRNA turnover and stability by RNA binding proteins, long non-coding RNA and microRNAs. Although still challenging, epigenetic-targeted therapeutic strategies are rapidly developing [81,82] and may open new avenues for restoring endogenous ATIP3 levels in ATIP3-deficient breast tumors. Epidrugs (compounds targeting epigenetic enzymes) and antagomirs (that block the effects of inhibitory microRNAs) [83] are being considered as promising future therapeutic options in cancer and progresses are being made to improve their delivery [84]. However, strategies for targeting ATIP3-deficiency in breast tumors still require better knowledge of epigenetic mechanisms involved in *MTUS1* gene alterations in cancer.

Recent studies have also unveiled interesting molecular mechanisms associated with ATIP3 intracellular effects, both in interphase and mitosis. ATIP3 contributes to cellular homeostasis by regulating microtubule dynamics and maintaining mitotic spindle integrity. The demonstration ATIP3 interacts with EB1 in the cytosol and with KIF2A/Aurora A at the spindle pole, provides clues to the design of molecular therapies targeting ATIP3-deficient

tumors. Indeed, high throughput screening of small molecules (either synthetic compounds or small peptides), able to mimic or prevent ATIP3 participation into these molecular complexes, may represent an interesting strategy to restore ATIP3 intracellular functions in ATIP3-deficient tumors. Furthermore, ATIP3 deficiency in breast tumors has been associated with increased centrosome amplification and aneuploidy, which renders them more susceptible to taxane-based chemotherapy [58]. While aneuploidy is a recognized hallmark of aggressive cancer, it also appears as an Achille's heel of tumors as far as taxane treatment is concerned. This paradigm shift opens new therapeutic strategies to exploit cancer vulnerability. Increasing cancer cell aneuploidy above a threshold using low doses of microtubule-stabilizing drugs may represent a novel way to induce tumor shrinkage [80]. Future in-depth characterization of ATIP3-associated intracellular mechanisms in normal and cancer cells are warranted to facilitate the design of new molecular therapies targeting a subpopulation of ATIP3-deficient breast cancer patients. With approximately 170,000 new cases of ATIP3-deficient TNBC tumors diagnosed annually worldwide, such an ATIP3-associated targeted approach will likely represent a major step forward to face a major public health problem. Other ATIP3-deficient solid tumors may additionally benefit from these therapeutic advances.

Author Contributions: M.M.H., S.R.-F. and C.N. have written the manuscript and agreed to the published version. All authors have read and agreed to the published version of the manuscript.

Funding: This work has been funded by Gustave Roussy, the ANR grant MMO ANR-10-IBHU-0001, the Fondation Janssen Horizon, the Taxe d'Apprentissage TA2020 (University Paris Saclay, France), AG2R LA MONDIALE, the Comité Ile-de-France of the Ligue Nationale contre le Cancer, the Ligue contre le Cancer 94/Val-de-Marne, the Fonds de Dotation Agnès b., the CNRS, the INSERM, the association Odyssea and Prolific. Authors wish to thank Francis Destombes for financial support.

Institutional Review Board Statement: Not applicable.

Informed Consent Statement: Not applicable.

Data Availability Statement: Not applicable.

Conflicts of Interest: Authors declare that they have no conflict of interest.

References

1. Seibold, S.; Rudroff, C.; Weber, M.; Galle, J.; Wanner, C.; Marx, M. Identification of a New Tumor Suppressor Gene Located at Chromosome 8p21.3-22. *FASEB J.* **2003**, *17*, 1180–1182. [CrossRef]
2. Kinjo, T.; Isomura, M.; Iwamasa, T.; Nakamura, Y. Molecular Cloning and Characterization of Two Novel Genes on Chromosome 8p21.3. *J. Hum. Genet.* **2000**, *45*, 12–17. [CrossRef] [PubMed]
3. Wang, J.C.; Radford, D.M.; Holt, M.S.; Helms, C.; Goate, A.; Brandt, W.; Parik, M.; Phillips, N.J.; DeSchryver, K.; Schuh, M.E.; et al. Sequence-Ready Contig for the 1.4-CM Ductal Carcinoma in Situ Loss of Heterozygosity Region on Chromosome 8p22–P23. *Genomics* **1999**, *60*, 1–11. [CrossRef] [PubMed]
4. Nouet, S.; Amzallag, N.; Li, J.-M.; Louis, S.; Seitz, I.; Cui, T.-X.; Alleaume, A.-M.; Di Benedetto, M.; Boden, C.; Masson, M.; et al. Trans-Inactivation of Receptor Tyrosine Kinases by Novel Angiotensin II AT2 Receptor-Interacting Protein, ATIP. *J. Biol. Chem.* **2004**, *279*, 28989–28997. [CrossRef]
5. Nouet, S.; Nahmias, C. Signal Transduction from the Angiotensin II AT2 Receptor. *Trends Endocrinol. Metab.* **2000**, *11*, 1–6. [CrossRef]
6. Fujita, T.; Mogi, M.; Min, L.-J.; Iwanami, J.; Tsukuda, K.; Sakata, A.; Okayama, H.; Iwai, M.; Nahmias, C.; Higaki, J.; et al. Attenuation of Cuff-Induced Neointimal Formation by Overexpression of Angiotensin II Type 2 Receptor-Interacting Protein 1. *Hypertension* **2009**, *53*, 688–693. [CrossRef]
7. Kukida, M.; Mogi, M.; Ohshima, K.; Nakaoka, H.; Iwanami, J.; Kanno, H.; Tsukuda, K.; Chisaka, T.; Min, L.-J.; Wang, X.-L.; et al. Angiotensin II Type 2 Receptor Inhibits Vascular Intimal Proliferation With Activation of PPARγ. *AJHYPE* **2016**, *29*, 727–736. [CrossRef]
8. Min, L.-J.; Mogi, M.; Iwanami, J.; Jing, F.; Tsukuda, K.; Ohshima, K.; Horiuchi, M. Angiotensin II Type 2 Receptor-Interacting Protein Prevents Vascular Senescence. *J. Am. Soc. Hypertens* **2012**, *6*, 179–184. [CrossRef]
9. Soda, K.; Nakada, Y.; Iwanari, H.; Hamakubo, T. AT2 Receptor Interacting Protein 1 (ATIP1) Mediates COX-2 Induction by an AT2 Receptor Agonist in Endothelial Cells. *Biochem. Biophys. Rep.* **2020**, *24*, 100850. [CrossRef]
10. Li, J.-M.; Mogi, M.; Tsukuda, K.; Tomochika, H.; Iwanami, J.; Min, L.-J.; Nahmias, C.; Iwai, M.; Horiuchi, M. Angiotensin II-Induced Neural Differentiation via Angiotensin II Type 2 (AT2) Receptor-MMS2 Cascade Involving Interaction between AT2

Receptor-Interacting Protein and Src Homology 2 Domain-Containing Protein-Tyrosine Phosphatase 1. *Mol. Endocrinol.* **2007**, *21*, 499–511. [CrossRef]
11. Jing, F.; Mogi, M.; Min, L.-J.; Ohshima, K.; Nakaoka, H.; Tsukuda, K.; Wang, X.; Iwanami, J.; Horiuchi, M. Effect of Angiotensin II Type 2 Receptor-Interacting Protein on Adipose Tissue Function via Modulation of Macrophage Polarization. *PLoS ONE* **2013**, *8*, e60067. [CrossRef] [PubMed]
12. Reinemund, J.; Seidel, K.; Steckelings, U.M.; Zaade, D.; Klare, S.; Rompe, F.; Katerbaum, M.; Schacherl, J.; Li, Y.; Menk, M.; et al. Poly(ADP-Ribose) Polymerase-1 (PARP-1) Transcriptionally Regulates Angiotensin AT2 Receptor (AT2R) and AT2R Binding Protein (ATBP) Genes. *Biochem. Pharmacol.* **2009**, *77*, 1795–1805. [CrossRef] [PubMed]
13. Wruck, C.J.; Funke-Kaiser, H.; Pufe, T.; Kusserow, H.; Menk, M.; Schefe, J.H.; Kruse, M.L.; Stoll, M.; Unger, T. Regulation of Transport of the Angiotensin AT2 Receptor by a Novel Membrane-Associated Golgi Protein. *ATVB* **2005**, *25*, 57–64. [CrossRef] [PubMed]
14. Di Benedetto, M.; Bièche, I.; Deshayes, F.; Vacher, S.; Nouet, S.; Collura, V.; Seitz, I.; Louis, S.; Pineau, P.; Amsellem-Ouazana, D.; et al. Structural Organization and Expression of Human MTUS1, a Candidate 8p22 Tumor Suppressor Gene Encoding a Family of Angiotensin II AT2 Receptor-Interacting Proteins, ATIP. *Gene* **2006**, *380*, 127–136. [CrossRef]
15. Yu, J.; Liu, X.; Ye, H.; Zhou, X. Genomic Characterization of the Human Mitochondrial Tumor Suppressor Gene 1 (MTUS1): 5′ Cloning and Preliminary Analysis of the Multiple Gene Promoters. *BMC Res. Notes* **2009**, *2*, 109. [CrossRef]
16. Krezel, M.A.; Rezmann, L.A.; Varghayee, N.; Pete, J.; Frauman, A.G.; Louis, S.N.S. Gene Sequencing and Tissue Expression of Unknown Isoforms of an Angiotensin II Type 2 Receptor Interacting Protein, ATIP, in the Rat. *Biosci. Biotechnol. Biochem.* **2011**, *75*, 414–418. [CrossRef]
17. Zuern, C.; Krenacs, L.; Starke, S.; Heimrich, J.; Palmetshofer, A.; Holtmann, B.; Sendtner, M.; Fischer, T.; Galle, J.; Wanner, C.; et al. Microtubule Associated Tumor Suppressor 1 Deficient Mice Develop Spontaneous Heart Hypertrophy and SLE-like Lymphoproliferative Disease. *Int. J. Oncol.* **2012**, *40*, 1079–1088. [CrossRef]
18. Chen, Z.; Liu, X.; Wang, C.; Jin, Y.; Wang, Y.; Wang, A.; Zhou, X. P53 Regulates the Expression of Human Angiotensin II AT(2) Receptor Interacting Protein (ATIP1) Gene. *Oncol. Lett.* **2011**, *2*, 919–922. [CrossRef]
19. Rodrigues-Ferreira, S.; Di Tommaso, A.; Dimitrov, A.; Cazaubon, S.; Gruel, N.; Colasson, H.; Nicolas, A.; Chaverot, N.; Molinié, V.; Reyal, F.; et al. 8p22 MTUS1 Gene Product ATIP3 Is a Novel Anti-Mitotic Protein Underexpressed in Invasive Breast Carcinoma of Poor Prognosis. *PLoS ONE* **2009**, *4*, e7239. [CrossRef]
20. Rodrigues-Ferreira, S.; Nahmias, C. An ATIPical Family of Angiotensin II AT2 Receptor-Interacting Proteins. *Trends Endocrinol. Metab.* **2010**, *21*, 684–690. [CrossRef]
21. Molina, A.; Velot, L.; Ghouinem, L.; Abdelkarim, M.; Bouchet, B.P.; Luissint, A.-C.; Bouhlel, I.; Morel, M.; Sapharikas, E.; Di Tommaso, A.; et al. ATIP3, a Novel Prognostic Marker of Breast Cancer Patient Survival, Limits Cancer Cell Migration and Slows Metastatic Progression by Regulating Microtubule Dynamics. *Cancer Res.* **2013**, *73*, 2905–2915. [CrossRef]
22. Rodrigues-Ferreira, S.; Nehlig, A.; Monchecourt, C.; Nasr, S.; Fuhrmann, L.; Lacroix-Triki, M.; Garberis, I.; Scott, V.; Delaloge, S.; Pistilli, B.; et al. Combinatorial Expression of Microtubule-Associated EB1 and ATIP3 Biomarkers Improves Breast Cancer Prognosis. *Breast Cancer Res. Treat.* **2019**, *173*, 573–583. [CrossRef] [PubMed]
23. Yuan, P.; Liu, D.; Deng, M.; Liu, J.; Wang, J.; Zhang, L.; Liu, Q.; Zhang, T.; Chen, Y.; Jin, G. Identification of Differently Expressed Genes with Specific SNP Loci for Breast Cancer by the Integration of SNP and Gene Expression Profiling Analyses. *Pathol. Oncol. Res.* **2015**, *21*, 469–475. [CrossRef]
24. Xiao, J.; Chen, J.-X.; Zhu, Y.-P.; Zhou, L.-Y.; Shu, Q.-A.; Chen, L.-W. Reduced Expression of MTUS1 MRNA Is Correlated with Poor Prognosis in Bladder Cancer. *Oncol. Lett.* **2012**, *4*, 113–118. [CrossRef]
25. Rogler, A.; Hoja, S.; Giedl, J.; Ekici, A.B.; Wach, S.; Taubert, H.; Goebell, P.J.; Wullich, B.; Stöckle, M.; Lehmann, J.; et al. Loss of MTUS1/ATIP Expression Is Associated with Adverse Outcome in Advanced Bladder Carcinomas: Data from a Retrospective Study. *BMC Cancer* **2014**, *14*, 214. [CrossRef] [PubMed]
26. Zuern, C.; Heimrich, J.; Kaufmann, R.; Richter, K.K.; Settmacher, U.; Wanner, C.; Galle, J.; Seibold, S. Down-Regulation of MTUS1 in Human Colon Tumors. *Oncol. Rep.* **2010**, *23*, 183–189. [CrossRef]
27. Melcher, R.; Hartmann, E.; Zopf, W.; Herterich, S.; Wilke, P.; Müller, L.; Rosler, E.; Kudlich, T.; Al-Taie, O.; Rosenwald, A.; et al. LOH and Copy Neutral LOH (CnLOH) Act as Alternative Mechanism in Sporadic Colorectal Cancers with Chromosomal and Microsatellite Instability. *Carcinogenesis* **2011**, *32*, 636–642. [CrossRef]
28. Ozcan, O.; Kara, M.; Yumrutas, O.; Bozgeyik, E.; Bozgeyik, I.; Celik, O.I. MTUS1 and Its Targeting MiRNAs in Colorectal Carcinoma: Significant Associations. *Tumour Biol.* **2016**, *37*, 6637–6645. [CrossRef] [PubMed]
29. Zheng, W.; Yang, C.; Qiu, L.; Feng, X.; Sun, K.; Deng, H. Transcriptional Information Underlying the Generation of CSCs and the Construction of a Nine-MRNA Signature to Improve Prognosis Prediction in Colorectal Cancer. *Cancer Biol. Ther.* **2020**, *21*, 688–697. [CrossRef] [PubMed]
30. Sim, J.; Kim, Y.; Kim, H.; Bang, S.; Jee, S.; Park, S.; Shin, S.-J.; Jang, K. Loss of MTUS1 Expression Is Associated With Poor Prognosis in Patients With Gallbladder Carcinoma. *In Vivo* **2020**, *34*, 125–132. [CrossRef]
31. Li, X.; Liu, H.; Yu, T.; Dong, Z.; Tang, L.; Sun, X. Loss of MTUS1 in Gastric Cancer Promotes Tumor Growth and Metastasis. *Neoplasma* **2014**, *61*, 128–135. [CrossRef] [PubMed]
32. Zhao, J.; Li, X.; Fu, L.; Zhang, N.; Yang, J.; Cai, J. LncRNA LIFR-AS1 Inhibits Gastric Carcinoma Cell Proliferation, Migration and Invasion by Sponging MiR-4698. *Mol. Med. Rep.* **2021**, *23*, 1. [CrossRef] [PubMed]

33. Parbin, S.; Pradhan, N.; Das, L.; Saha, P.; Deb, M.; Sengupta, D.; Patra, S.K. DNA Methylation Regulates Microtubule-Associated Tumor Suppressor 1 in Human Non-Small Cell Lung Carcinoma. *Exp. Cell Res.* **2019**, *374*, 323–332. [CrossRef] [PubMed]
34. Ding, X.; Zhang, N.; Cai, Y.; Li, S.; Zheng, C.; Jin, Y.; Yu, T.; Wang, A.; Zhou, X. Down-Regulation of Tumor Suppressor MTUS1/ATIP Is Associated with Enhanced Proliferation, Poor Differentiation and Poor Prognosis in Oral Tongue Squamous Cell Carcinoma. *Mol. Oncol.* **2012**, *6*, 73–80. [CrossRef]
35. Ribeiro, I.P.; Marques, F.; Caramelo, F.; Ferrão, J.; Prazeres, H.; Julião, M.J.; Rifi, W.; Savola, S.; de Melo, J.B.; Baptista, I.P.; et al. Genetic Imbalances Detected by Multiplex Ligation-Dependent Probe Amplification in a Cohort of Patients with Oral Squamous Cell Carcinoma—The First Step towards Clinical Personalized Medicine. *Tumor Biol.* **2014**. [CrossRef]
36. Zhao, T.; Ding, X.; Chang, B.; Zhou, X.; Wang, A. MTUS1/ATIP3a down-Regulation Is Associated with Enhanced Migration, Invasion and Poor Prognosis in Salivary Adenoid Cystic Carcinoma. *BMC Cancer* **2015**, *15*, 203. [CrossRef]
37. Zhao, T.; He, Q.; Liu, Z.; Ding, X.; Zhou, X.; Wang, A. Angiotensin II Type 2 Receptor-Interacting Protein 3a Suppresses Proliferation, Migration and Invasion in Tongue Squamous Cell Carcinoma via the Extracellular Signal-Regulated Kinase-Snai2 Pathway. *Oncol. Lett.* **2016**, *11*, 340–344. [CrossRef]
38. Mahjabeen, I.; Kayani, M.A. Loss of Mitochondrial Tumor Suppressor Genes Expression Is Associated with Unfavorable Clinical Outcome in Head and Neck Squamous Cell Carcinoma: Data from Retrospective Study. *PLoS ONE* **2016**, *11*, e0146948. [CrossRef]
39. Bozgeyik, I.; Yumrutas, O.; Bozgeyik, E. MTUS1, a Gene Encoding Angiotensin-II Type 2 (AT2) Receptor-Interacting Proteins, in Health and Disease, with Special Emphasis on Its Role in Carcinogenesis. *Gene* **2017**, *626*, 54–63. [CrossRef]
40. Lv, Q.; Dong, F.; Zhou, Y.; Cai, Z.; Wang, G. RNA-Binding Protein SORBS2 Suppresses Clear Cell Renal Cell Carcinoma Metastasis by Enhancing MTUS1 MRNA Stability. *Cell Death Dis.* **2020**, *11*, 1056. [CrossRef]
41. Sim, J.; Wi, Y.C.; Park, H.Y.; Park, S.Y.; Yoon, Y.E.; Bang, S.; Kim, Y.; Jang, K.; Paik, S.S.; Shin, S.-J. Clinicopathological Significance of MTUS1 Expression in Patients With Renal Cell Carcinoma. *Anticancer Res.* **2020**, *40*, 2961–2967. [CrossRef]
42. Luo, H.; Ma, C. Identification of Prognostic Genes in Uveal Melanoma Microenvironment. *PLoS ONE* **2020**, *15*, e0242263. [CrossRef]
43. Louis, S.N.S.; Chow, L.T.C.; Varghayee, N.; Rezmann, L.A.; Frauman, A.G.; Louis, W.J. The Expression of MTUS1/ATIP and Its Major Isoforms, ATIP1 and ATIP3, in Human Prostate Cancer. *Cancers* **2011**, *3*, 3824–3837. [CrossRef]
44. Guimond, M.-O.; Battista, M.-C.; Nikjouitavabi, F.; Carmel, M.; Barres, V.; Doueik, A.A.; Fazli, L.; Gleave, M.; Sabbagh, R.; Gallo-Payet, N. Expression and Role of the Angiotensin II AT2 Receptor in Human Prostate Tissue: In Search of a New Therapeutic Option for Prostate Cancer. *Prostate* **2013**, *73*, 1057–1068. [CrossRef]
45. Mitchison, T.; Kirschner, M. Dynamic Instability of Microtubule Growth. *Nature* **1984**, *312*, 237–242. [CrossRef] [PubMed]
46. Akhmanova, A.; Steinmetz, M.O. Control of Microtubule Organization and Dynamics: Two Ends in the Limelight. *Nat. Rev. Mol. Cell Biol.* **2015**, *16*, 711–726. [CrossRef]
47. Guesdon, A.; Bazile, F.; Buey, R.M.; Mohan, R.; Monier, S.; García, R.R.; Angevin, M.; Heichette, C.; Wieneke, R.; Tampé, R.; et al. EB1 Interacts with Outwardly Curved and Straight Regions of the Microtubule Lattice. *Nat. Cell Biol.* **2016**, *18*, 1102–1108. [CrossRef]
48. Maurer, S.P.; Cade, N.I.; Bohner, G.; Gustafsson, N.; Boutant, E.; Surrey, T. EB1 Accelerates Two Conformational Transitions Important for Microtubule Maturation and Dynamics. *Curr. Biol.* **2014**, *24*, 372–384. [CrossRef] [PubMed]
49. Velot, L.; Molina, A.; Rodrigues-Ferreira, S.; Nehlig, A.; Bouchet, B.P.; Morel, M.; Leconte, L.; Serre, L.; Arnal, I.; Braguer, D.; et al. Negative Regulation of EB1 Turnover at Microtubule plus Ends by Interaction with Microtubule-Associated Protein ATIP3. *Oncotarget* **2015**, *6*, 43557–43570. [CrossRef]
50. Nehlig, A.; Molina, A.; Rodrigues-Ferreira, S.; Honoré, S.; Nahmias, C. Regulation of End-Binding Protein EB1 in the Control of Microtubule Dynamics. *Cell Mol. Life Sci.* **2017**, *74*, 2381–2393. [CrossRef] [PubMed]
51. Nehlig, A.; Seiler, C.; Steblyanko, Y.; Dingli, F.; Arras, G.; Loew, D.; Welburn, J.; Prigent, C.; Barisic, M.; Nahmias, C. Reciprocal Regulation of Aurora Kinase A and ATIP3 in the Control of Metaphase Spindle Length. *Cell Mol. Life Sci.* **2021**, *78*, 1765–1779. [CrossRef]
52. Ganem, N.J.; Compton, D.A. Functional Roles of Poleward Microtubule Flux during Mitosis. *Cell Cycle* **2006**, *5*, 481–485. [CrossRef]
53. Cirak, Y.; Furuncuoglu, Y.; Yapicier, O.; Aksu, A.; Cubukcu, E. Aurora A Overexpression in Breast Cancer Patients Induces Taxane Resistance and Results in Worse Prognosis. *J. BUON* **2015**, *20*, 1414–1419.
54. Yan, M.; Wang, C.; He, B.; Yang, M.; Tong, M.; Long, Z.; Liu, B.; Peng, F.; Xu, L.; Zhang, Y.; et al. Aurora-A Kinase: A Potent Oncogene and Target for Cancer Therapy. *Med. Res. Rev.* **2016**, *36*, 1036–1079. [CrossRef]
55. Ohi, R.; Coughlin, M.L.; Lane, W.S.; Mitchison, T.J. An Inner Centromere Protein That Stimulates the Microtubule Depolymerizing Activity of a KinI Kinesin. *Dev. Cell* **2003**, *5*, 309–321. [CrossRef]
56. Knowlton, A.L.; Vorozhko, V.V.; Lan, W.; Gorbsky, G.J.; Stukenberg, P.T. ICIS and Aurora B Coregulate the Microtubule Depolymerase Kif2a. *Curr. Biol.* **2009**, *19*, 758–763. [CrossRef]
57. Ping, H.; Guo, L.; Xi, J.; Wang, D. Angiotensin II Type 2 Receptor-Interacting Protein 3a Inhibits Ovarian Carcinoma Metastasis via the Extracellular HMGA2-Mediated ERK/EMT Pathway. *Tumour Biol.* **2017**, *39*, 1010428317713389. [CrossRef] [PubMed]
58. Rodrigues-Ferreira, S.; Nehlig, A.; Moindjie, H.; Monchecourt, C.; Seiler, C.; Marangoni, E.; Chateau-Joubert, S.; Dujaric, M.-E.; Servant, N.; Asselain, B.; et al. Improving Breast Cancer Sensitivity to Paclitaxel by Increasing Aneuploidy. *Proc. Natl. Acad. Sci. USA* **2019**, *116*, 23691–23697. [CrossRef]
59. Perou, C.M.; Sørlie, T.; Eisen, M.B.; van de Rijn, M.; Jeffrey, S.S.; Rees, C.A.; Pollack, J.R.; Ross, D.T.; Johnsen, H.; Akslen, L.A.; et al. Molecular Portraits of Human Breast Tumours. *Nature* **2000**, *406*, 747–752. [CrossRef] [PubMed]

60. Sørlie, T.; Perou, C.M.; Tibshirani, R.; Aas, T.; Geisler, S.; Johnsen, H.; Hastie, T.; Eisen, M.B.; van de Rijn, M.; Jeffrey, S.S.; et al. Gene Expression Patterns of Breast Carcinomas Distinguish Tumor Subclasses with Clinical Implications. *Proc. Natl. Acad. Sci. USA* **2001**, *98*, 10869–10874. [CrossRef] [PubMed]
61. Lehmann, B.D.; Bauer, J.A.; Chen, X.; Sanders, M.E.; Chakravarthy, A.B.; Shyr, Y.; Pietenpol, J.A. Identification of Human Triple-Negative Breast Cancer Subtypes and Preclinical Models for Selection of Targeted Therapies. *J. Clin. Investig.* **2011**, *121*, 2750–2767. [CrossRef] [PubMed]
62. Lehmann, B.D.; Jovanović, B.; Chen, X.; Estrada, M.V.; Johnson, K.N.; Shyr, Y.; Moses, H.L.; Sanders, M.E.; Pietenpol, J.A. Refinement of Triple-Negative Breast Cancer Molecular Subtypes: Implications for Neoadjuvant Chemotherapy Selection. *PLoS ONE* **2016**, *11*, e0157368. [CrossRef]
63. Ou, L.; Xiang, T.-Y.; Hao, X.-Y.; Wang, D.-Z.; Zeng, Q. Reduced Long Non-Coding RNA PTENP1 Contributed to Proliferation and Invasion via MiR-19b/MTUS1 Axis in Patients with Cervical Cancer. *Eur. Rev. Med. Pharmacol. Sci.* **2020**, *24*, 4132–4144. [CrossRef]
64. Kara, M.; Kaplan, M.; Bozgeyik, I.; Ozcan, O.; Celik, O.I.; Bozgeyik, E.; Yumrutas, O. MTUS1 Tumor Suppressor and Its MiRNA Regulators in Fibroadenoma and Breast Cancer. *Gene* **2016**, *587*, 173–177. [CrossRef] [PubMed]
65. Gu, Y.; Liu, S.; Zhang, X.; Chen, G.; Liang, H.; Yu, M.; Liao, Z.; Zhou, Y.; Zhang, C.-Y.; Wang, T.; et al. Oncogenic MiR-19a and MiR-19b Co-Regulate Tumor Suppressor MTUS1 to Promote Cell Proliferation and Migration in Lung Cancer. *Protein Cell* **2017**, *8*, 455–466. [CrossRef]
66. Lv, D.-B.; Zhang, J.-Y.; Gao, K.; Yu, Z.-H.; Sheng, W.-C.; Yang, G.; Gao, Y.-Z. MicroRNA-765 Targets MTUS1 to Promote the Progression of Osteosarcoma via Mediating ERK/EMT Pathway. *Eur. Rev. Med Pharmacol. Sci.* **2019**, *23*, 4618–4628. [CrossRef]
67. Di Benedetto, M.; Pineau, P.; Nouet, S.; Berhouet, S.; Seitz, I.; Louis, S.; Dejean, A.; Couraud, P.O.; Strosberg, A.D.; Stoppa-Lyonnet, D.; et al. Mutation Analysis of the 8p22 Candidate Tumor Suppressor Gene ATIP/MTUS1 in Hepatocellular Carcinoma. *Mol. Cell Endocrinol.* **2006**, *252*, 207–215. [CrossRef]
68. Frank, B.; Bermejo, J.L.; Hemminki, K.; Sutter, C.; Wappenschmidt, B.; Meindl, A.; Kiechle-Bahat, M.; Bugert, P.; Schmutzler, R.K.; Bartram, C.R.; et al. Copy Number Variant in the Candidate Tumor Suppressor Gene MTUS1 and Familial Breast Cancer Risk. *Carcinogenesis* **2007**, *28*, 1442–1445. [CrossRef] [PubMed]
69. Dong, X.; Liu, F.; Sun, L.; Liu, M.; Li, D.; Su, D.; Zhu, Z.; Dong, J.-T.; Fu, L.; Zhou, J. Oncogenic Function of Microtubule End-Binding Protein 1 in Breast Cancer: EB1 in Breast Cancer. *J. Pathol.* **2010**, *220*, 361–369. [CrossRef] [PubMed]
70. Rodrigues-Ferreira, S.; Molina, A.; Nahmias, C. Microtubule-Associated Tumor Suppressors as Prognostic Biomarkers in Breast Cancer. *Breast Cancer Res. Treat.* **2020**, *179*, 267–273. [CrossRef]
71. Wang, J.; Ma, S.; Ma, R.; Qu, X.; Liu, W.; Lv, C.; Zhao, S.; Gong, Y. KIF2A Silencing Inhibits the Proliferation and Migration of Breast Cancer Cells and Correlates with Unfavorable Prognosis in Breast Cancer. *BMC Cancer* **2014**, *14*, 461. [CrossRef]
72. Li, T.-F.; Zeng, H.-J.; Shan, Z.; Ye, R.-Y.; Cheang, T.-Y.; Zhang, Y.-J.; Lu, S.-H.; Zhang, Q.; Shao, N.; Lin, Y. Overexpression of Kinesin Superfamily Members as Prognostic Biomarkers of Breast Cancer. *Cancer Cell Int.* **2020**, *20*, 123. [CrossRef] [PubMed]
73. Nadler, Y.; Camp, R.L.; Schwartz, C.; Rimm, D.L.; Kluger, H.M.; Kluger, Y. Expression of Aurora A (but Not Aurora B) Is Predictive of Survival in Breast Cancer. *Clin. Cancer Res.* **2008**, *14*, 4455–4462. [CrossRef] [PubMed]
74. Ali, H.R.; Dawson, S.-J.; Blows, F.M.; Provenzano, E.; Pharoah, P.D.; Caldas, C. Aurora Kinase A Outperforms Ki67 as a Prognostic Marker in ER-Positive Breast Cancer. *Br. J. Cancer* **2012**, *106*, 1798–1806. [CrossRef]
75. Weaver, B.A. How Taxol/Paclitaxel Kills Cancer Cells. *MBoC* **2014**, *25*, 2677–2681. [CrossRef]
76. Rodrigues-Ferreira, S.; Moindjie, H.; Haykal, M.M.; Nahmias, C. Predicting and Overcoming Taxane Chemoresistance. *Trends Mol. Med.* **2021**, *27*, 138–151. [CrossRef]
77. Masuda, H.; Baggerly, K.A.; Wang, Y.; Zhang, Y.; Gonzalez-Angulo, A.M.; Meric-Bernstam, F.; Valero, V.; Lehmann, B.D.; Pietenpol, J.A.; Hortobagyi, G.N.; et al. Differential Response to Neoadjuvant Chemotherapy among 7 Triple-Negative Breast Cancer Molecular Subtypes. *Clin. Cancer Res.* **2013**, *19*, 5533–5540. [CrossRef] [PubMed]
78. Rodrigues-Ferreira, S.; Nehlig, A.; Kacem, M.; Nahmias, C. ATIP3 Deficiency Facilitates Intracellular Accumulation of Paclitaxel to Reduce Cancer Cell Migration and Lymph Node Metastasis in Breast Cancer Patients. *Sci. Rep.* **2020**, *10*, 13217. [CrossRef]
79. Rai, A.; Liu, T.; Glauser, S.; Katrukha, E.A.; Estévez-Gallego, J.; Rodríguez-García, R.; Fang, W.-S.; Díaz, J.F.; Steinmetz, M.O.; Altmann, K.-H.; et al. Taxanes Convert Regions of Perturbed Microtubule Growth into Rescue Sites. *Nat. Mater.* **2020**, *19*, 355–365. [CrossRef]
80. Rodrigues-Ferreira, S.; Nahmias, C. From Tumorigenesis to Cell Death: The Aneuploidy Paradox. *Mol. Cell. Oncol.* **2020**, *7*, 1709390. [CrossRef]
81. Nebbioso, A.; Tambaro, F.P.; Dell'Aversana, C.; Altucci, L. Cancer Epigenetics: Moving Forward. *PLoS Genet.* **2018**, *14*, e1007362. [CrossRef] [PubMed]
82. Miranda Furtado, C.L.; Dos Santos Luciano, M.C.; Silva Santos, R.D.; Furtado, G.P.; Moraes, M.O.; Pessoa, C. Epidrugs: Targeting Epigenetic Marks in Cancer Treatment. *Epigenetics* **2019**, *14*, 1164–1176. [CrossRef] [PubMed]
83. Krützfeldt, J.; Rajewsky, N.; Braich, R.; Rajeev, K.G.; Tuschl, T.; Manoharan, M.; Stoffel, M. Silencing of MicroRNAs in Vivo with "Antagomirs". *Nature* **2005**, *438*, 685–689. [CrossRef]
84. Forterre, A.; Komuro, H.; Aminova, S.; Harada, M. A Comprehensive Review of Cancer MicroRNA Therapeutic Delivery Strategies. *Cancers* **2020**, *12*, 1852. [CrossRef] [PubMed]

ARTICLE 2 – A NETWORK OF 17 MICROTUBULE-RELATED GENES HIGHLIGHTS FUNCTIONAL DEREGULATIONS IN BREAST CANCER

In this study, we investigated the role of 17 microtubule-related genes (MT-Rel) in breast cancer, with a focus on their expression, prognostic value, and functional impact. Among them, 14 genes, including KIF4A, ASPM, and AURKB, are notably overexpressed in breast tumors compared to normal tissues. These genes, associated with microtubule dynamics, are linked to poor prognosis in breast cancer patients. We also employed a Systems Biology approach to reveal functional gene networks and their implications in breast cancer. Three major sub-networks are identified, corresponding to crucial cellular processes: spindle organization, mitotic sister chromatid segregation, and cytokinesis. The analysis underscores the role of microtubule dynamics in these processes and emphasizes the potential impact on cancer initiation and progression. Furthermore, we identified specific MT-Rel genes, such as AURKB, TPX2, and KIF4A, as essential for cell viability, suggesting their potential as therapeutic targets.

This study advocates for the exploration of these genes, considering their association with mitotic pathways, aneuploidy, and chromosome instability in breast cancer. The findings propose avenues for developing personalized medicine and therapeutic strategies, possibly in combination with taxane-based chemotherapy, to address the challenges of breast cancer treatment.

This article was accepted for publishing on the 4th of October 2023.

cancers

MDPI

Article

A network of 17 microtubule-related genes highlights functional deregulations in breast cancer

Sylvie RODRIGUES-FERREIRA[1,2,3], Morgane MORIN[1,2*], Gwenn GUICHAOUA[4,5*], Hadia MOINDJIE[1,2#], Maria HAYKAL[1,2], Olivier COLLIER[6], Véronique STOVEN[4,5] and Clara NAHMIAS[1,2]

1. Gustave Roussy Cancer Center, F-94800 Villejuif, France.
2. INSERM U981, Université Paris-Saclay, F-94800 Villejuif, France.
3. Inovarion, F-75005 Paris, France
4. CBIO, Mines Paris-PSL, PSL Research University, F-75005 Paris, France.
5. INSERM U900, Institut Curie, F-75005 Paris, France.
6. MODAL'X, UPL, Université Paris Nanterre, CNRS, F-92000 Nanterre, France.

* Equal contribution

Present address : 1. Université Paris-Saclay, UVSQ, INRAE, BREED, F-78350, Jouy-en-Josas, France ; 2. Ecole Nationale Vétérinaire d'Alfort, BREED, F-94700, Maisons-Alfort, France.

Corresponding authors: C.N. clara.nahmias@inserm.fr and V.S. veronique.stoven@minesparis.psl.eu

Simple Summary: The microtubule cytoskeleton is a key component of the cell and an important target for breast cancer therapy. Microtubule organization and function are tightly regulated by a panel of microtubule-related proteins (MT-Rel) to ensure cellular homeostasis. Deregulation of MT-rel genes is likely to impact microtubule dynamics and subsequent cell functions. In this study, we evaluate the prognostic value of a panel of 17 MT-Rel in breast tumors and the functional consequence of their deregulation using a Systems Biology approach. This study highlights MT-Rel as potential prognostic biomarkers and interesting therapeutical targets to evaluate in breast cancer.

Abstract: A wide panel of microtubule-associated proteins and kinases is involved in coordinated regulation of the microtubule cytoskeleton and may thus represent valuable molecular markers contributing to major cellular pathways deregulated in cancer. We previously identified a panel of 17 microtubule-related (MT-Rel) genes that are differentially expressed in breast tumors showing resistance to taxane-based chemotherapy. In the present study, we evaluated the expression, prognostic value and functional impact of these genes in breast cancer. We show that 14 MT-Rel genes (KIF4A, ASPM, KIF20A, KIF14, TPX2, KIF18B, KIFC1, AURKB, KIF2C, GTSE1, KIF15, KIF11, RACGAP1, STMN1) are up-regulated in breast tumors compared with adjacent normal tissue. Six of them (KIF4A, ASPM, KIF20A, KIF14, TPX2, KIF18B) are overexpressed by more than 10-fold in tumor samples and four of them (KIF11, AURKB, TPX2 and KIFC1) are essential for cell survival. Overexpression of all 14 genes, and underexpression of 3 other MT-Rel genes (MAST4, MAPT and MTUS1) are associated with poor breast cancer patient survival. A Systems Biology approach highlighted three major functional networks connecting the 17 MT-Rel genes and partners, which are centered on spindle assembly, chromosome segregation and cytokinesis. Together our studies identified mitotic Aurora kinases and their substrates as major targets for therapeutic approaches against breast cancer.

Keywords: Aurora kinases; biomarker; kinesins; mitotic defects; prognostic value; Systems Biology; therapeutic targets

Citation: To be added by editorial staff during production.

Academic Editor: Firstname Lastname

Received: date
Revised: date
Accepted: date
Published: date

1. Introduction

Breast cancer is a leading cause of death by malignancy in women worldwide. The classification of breast tumors into distinct histological and molecular subtypes has been paramount to orient clinicians in their decision to deliver appropriate treatments to the patients. While hormonotherapy and HER2-targeted therapy are considered as treatments of choice for patients with luminal - Estrogen Receptor (ER)-positive - and HER2-amplified breast cancer subtypes [1], only few therapies are available for breast tumors that become resistant to treatment and for triple-negative breast cancer (TNBC), that do not express ER nor HER2 receptors. In addition to chemotherapy, immunotherapy and targeted therapies are being developed for TNBC [2] but additional therapeutic strategies are warranted for this aggressive type of cancer. In the rapidly developing area of precision medicine, with the objective to deliver the right treatment to the right patient, it is of utmost importance to identify new prognostic and predictive biomarkers in order to select patients who need close medical follow up and adapted treatments [3].

Attention has been drawn since more than 50 years on the microtubule cytoskeleton in the fight against cancer. Mitotic poisons - including taxanes, that bind and stabilize microtubules - have been used in combination with DNA targeting agents for breast cancer chemotherapy. Microtubules are essential components of the cytoskeleton involved in different steps of cell division, migration and intracellular transport of proteins and organelles - all these processes being deregulated in cancer. Microtubules are polarized structures formed by the assembly of tubulin dimers, that rapidly alternate between phases of polymerization and depolymerization at the microtubule ends, in a process called dynamic instability [4,5].

The dynamic property of microtubules is crucial to their function. It ensures proper assembly of the mitotic spindle during mitosis and correct attachment of chromosomes to the kinetochores in metaphase to promote equal chromosome segregation during cell division. Microtubule dynamicity is essential for intracellular transport and is also required to establish cell polarity, explore the cytosol and target the cell cortex during migration. Microtubule assembly, dynamics and functions are tightly regulated by a large panel of microtubule-associated and regulatory proteins including MAPs, kinesins and kinases [6–8]. Defects in the expression or function of these microtubule-related proteins (designated MT-Rel) may thus provoke major cellular alterations with subsequent consequences on cancer initiation or progression [9–11]. Resistance to chemotherapeutic agents targeting the microtubule cytoskeleton may also result from dysregulation of MT-Rel, among other molecular mechanisms [9,12].

In a recent study, we took advantage of large databases containing both molecular and clinical data for breast cancer patients to investigate whether MT-Rel may represent new predictive biomarkers of breast cancer chemoresistance [13]. To this end, we compared the expression levels of a panel of 280 MT-Rel encoding genes in transcriptomic studies from three independent cohorts of patients with breast tumors classified as sensitive or resistant to chemotherapy. Bioinformatics studies identified a total of 117 MT-Rel genes that were significantly deregulated in sensitive versus resistant breast tumors, among which 17 genes were deregulated in all three cohorts of patients [13].

In the present study, we examined the possibility that these 17 predictive MT-Rel genes may be connected and represent a functional network for breast cancer prognosis. To this end, we examined expression levels of these genes and their co-regulation in mammary tumors and adjacent normal tissues. We also evaluated their potential value as prognostic biomarkers of patient survival and the functional consequence of their depletion on cell viability. Finally, we used a Systems Biology method to highlight gene networks potentially associated with important biological functions altered in breast cancer.

2. Materials and Methods

Gene expression and Kaplan-Meier analyses

MT-Rel mRNA expression levels were analysed using the TNMplot database (http://www.tnmplot.com) [14] of 112 breast tumor samples and their corresponding adjacent normal tissues. Comparison of normal and tumor samples was performed by the Mann–Whitney U test.

Expression values of each MT-Rel gene were downloaded from TNMplot for correlation analysis. Unsupervised hierarchical clustering was performed using the JMP7 software. Pearson correlation coefficients were calculated using graphPad Prism9 software.

Association of MT-Rel expression with Overall Survival (OS) and Relapse-Free Survival (RFS) was determined using Kaplan–Meier plotter database (http://www.kmplot.com) [15]. For each gene, the best probeset was used (Jetset) and the best cut-off was selected to distinguish between tumors expressing low and high levels of the gene.

RNAi screen and Cancer dependency map

MDA-MB-231 and MDA-MB-468 breast cancer cell lines were cultured as described [16,17]. Cells were transiently transfected with siRNA library (Dharmacon ON-TARGETplus) targeting each of the 14 overexpressed MT-Rel genes (4 individual siRNAs per gene) and a non-targeting control pool siRNA. Before primary screening, pilot experiments were performed in which siRNA doses and incubation times were titrated to optimize assay responses to negative and positive controls. Transfection was conducted in 96-well plates (5000 cells/well) containing 0,2 pmol of siRNA/well using Lipofectamine RNAiMAX transfection reagent (Invitrogen). Cell viability was determined after 96 hours using CellTiterGlo luminescent cell viability assay (Promega).

The dependency data used in this manuscript were derived from the publicly available data set (DepMap Public 23Q2+Score, Chronos), consisting of dependency data for our 14 genes of interest across 47 breast cancer cell lines. These data are available online at https://depmap.org/portal/download/custom/.

Systems biology

The goal was to build a small and interpretable network connecting the 17 differentially expressed MT-Rel genes in order to highlight functional interplays and cellular processes that are deregulated in breast cancer. We used the Python module pypath 0.14.48 to process post-translational activity flow databases where we searched for direct interactors known for each of the 17 genes. This did not allow connecting the 17 genes into a single network, leaving MTUS1 and ASPM unconnected. To address this issue, we "manually" connected MTUS1 based on known interactions in available scientific publications. Indeed, MTUS1 gene product ATIP3 was shown to interact with KIF2A [18]. ASPM was connected thanks to its first neighbor CDK4, known to interact with CDK1. We observed that some of the network nodes that have been extensively studied, such as AURKB, MAPT, RACGAP1 and STMN1 had many first neighbors that were otherwise not connected to any other node of the network. In order to build the smallest possible network with only relevant information related to breast cancer, among these direct neighbors, we only retained the genes belonging to the 280 MT-related genes that are differentially expressed in tumor versus normal samples. This led to a network of 43 nodes and 87 edges involving the 17 genes. We completed this network by adding all interactions known between the 43 nodes of the network (41 genes, including 2 complexes). In some cases in which contrary information exists in the literature, we choose the interactions of the SIGNOR 3.0 database (https://signor.uniroma2.it [19]. Network analysis unveiled several sub-networks corresponding to specific cellular processes, labeled based on Gene Ontology (GO) biological process enrichment analysis conducted using Gprofiler

(https://biit.cs.ut.ee/gprofiler). Enrichment analysis was conducted on the 41 genes of the network with the Benjamini-Hochberg FDR correction.

3. Results

3.1. Regulation of expression of 17 MT-Rel genes in breast tumors

A total of 17 genes encoding microtubule-related proteins (MT-Rel) were selected in a previous search for potential biomarkers of breast cancer chemoresistance [13]. To get further insight into the potential regulation and biological relevance of these 17 genes in breast cancer, we compared the expression levels of each gene in 112 tumors relative to adjacent normal tissues, using RNA-seq analyses available in public databases (www.tnmplot.com). As shown in Fig.1A and Suppl Table S1, all genes were significantly differentially expressed in tumors compared to paired normal breast tissues.

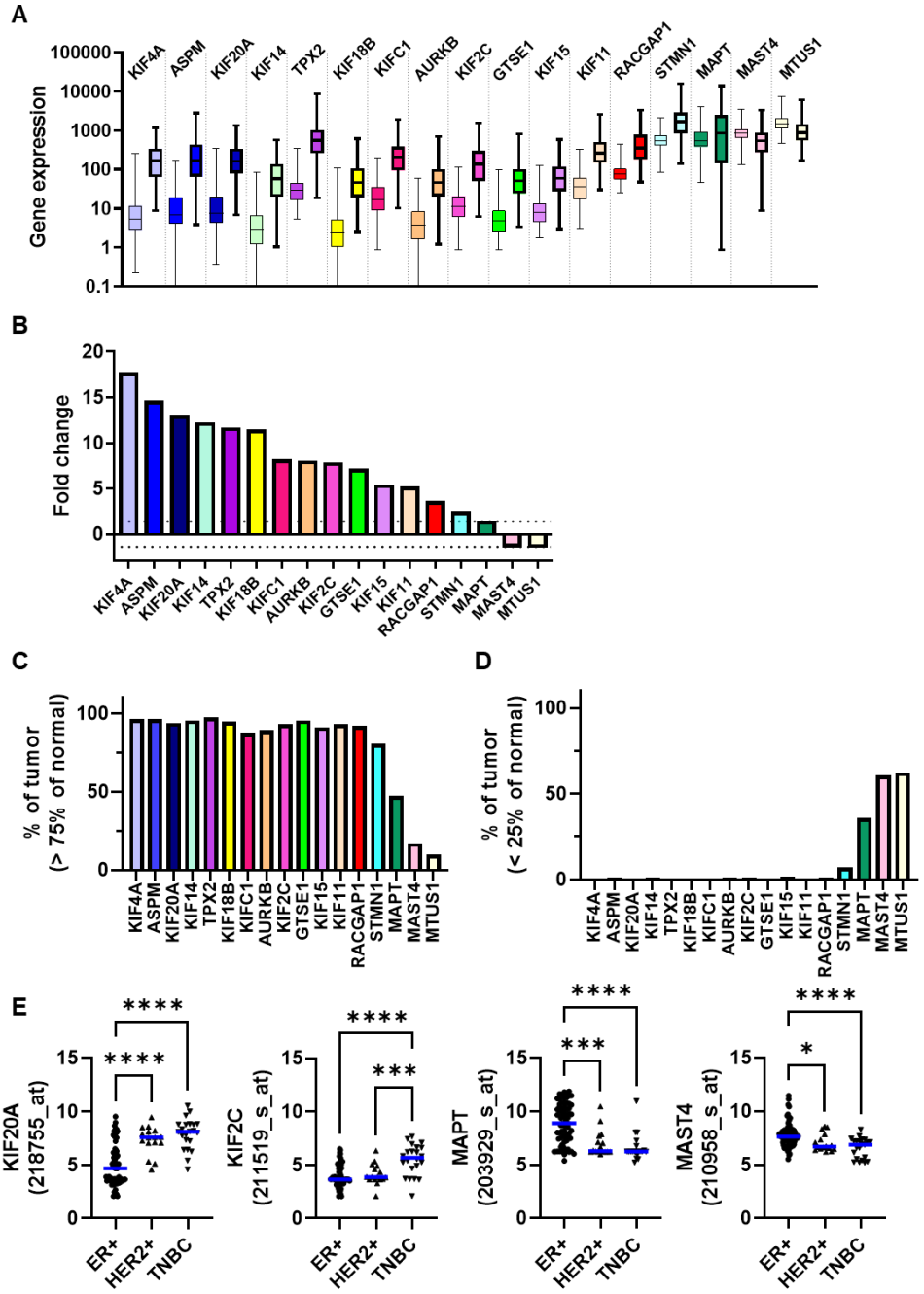

Figure 1. Expression of 17 MT-Rel genes in breast tumors and normal tissues.
(A) Boxplots of mRNA expression level of the 17 MT-Rel genes in 112 breast tumors (bold boxplot) and their adjacent normal tissues (thin boxplot) from the TNMplot database (tnmplot.com). (**B**) Histograms of fold change of gene expression between tumor and normal breast tissues. Dotted line indicates a fold change value of 1.4. (**C**) Proportion of tumor samples showing higher expression of a given gene compared to normal samples using the third quartile as cutoff value. (**D**) Proportion of tumor samples showing lower expression of a given gene compared to normal samples using the first quartile as cutoff value. (E) Probeset intensities for each indicated gene in breast tumors from the REMAGUS02 cohort [20] classified according to their molecular subtype. A blue line indicates the median value. *p<0.05; ***p<0.001; ****p<0.0001.

Fourteen genes (KIF4A, ASPM, KIF20A, KIF14, TPX2, KIF18B, KIFC1, AURKB, KIF2C, GTSE1, KIF15, KIF11, RACGAP1, STMN1) were up-regulated in tumors compared to normal tissues, with fold changes ranging from 2.5 up to 17.8 (Fig.1B, Suppl Table S1). Each of these 14 genes was overexpressed (expression level higher than 75% of normal levels) in more than 80% of breast tumors (Fig.1C, Suppl Fig.S1). Six of them (KIF4A, ASPM, KIF20A, KIF14, TPX2, KIF18B) warrant particular attention as they show increased expression by more than 10-fold in tumor samples compared to normal tissues (Fig.1B, Suppl Table S1).

The MAPT gene was moderately but significantly up-regulated (fold change 1.44) in malignant compared to adjacent normal tissues (Fig.1B, suppl Table 1). Notably, MAPT was overexpressed in 47.3% of tumors (Fig.1C, Suppl Fig.S1) and underexpressed (lower than 25% of normal levels) in 35.7% of tumors (Fig.1D, Suppl Fig.S1). Whether strong variation in MAPT expression in tumors depends on breast cancer molecular subtypes will require further investigation with larger cohorts of patients. The two other genes, namely MAST4 and MTUS1, were modestly (fold change 1.4 to 1.5) but significantly down-regulated in malignant tissues compared to normal breast (Fig.1B, Suppl Table S1). Both genes were found underexpressed in 60% of the tumors (Fig. 1D, Suppl Fig.S1).

Expression levels of each gene were compared among breast tumors classified according to molecular subtypes. As shown in Fig.1E and Suppl Fig.S2, tumors of the TNBC subtype expressed significantly higher levels of KIF4A, ASPM, KIF20A, KIF14, TPX2, KIF18B, KIFC1, AURKB, KIF2C, GTSE1, KIF15, KIF11, RACGAP1, STMN1 genes, and lower levels of MAPT, MAST4 and MTUS1 genes, compared with luminal ER-positive breast tumors.

We then explored the possibility that expression of the 17 MT-Rel genes may be co-regulated. Unsupervised hierarchical clustering of 112 breast tumors and adjacent non-tumoral breast (www.tnmplot.com), based on mRNA levels of the 17 MT-Rel genes, allowed to distinguish two populations of breast tumors that differ from normal tissues (Fig.2A). In one of them (cluster 1), representing one third of breast tumors, the majority of the 17 genes was overexpressed compared to adjacent non-tumoral tissues.

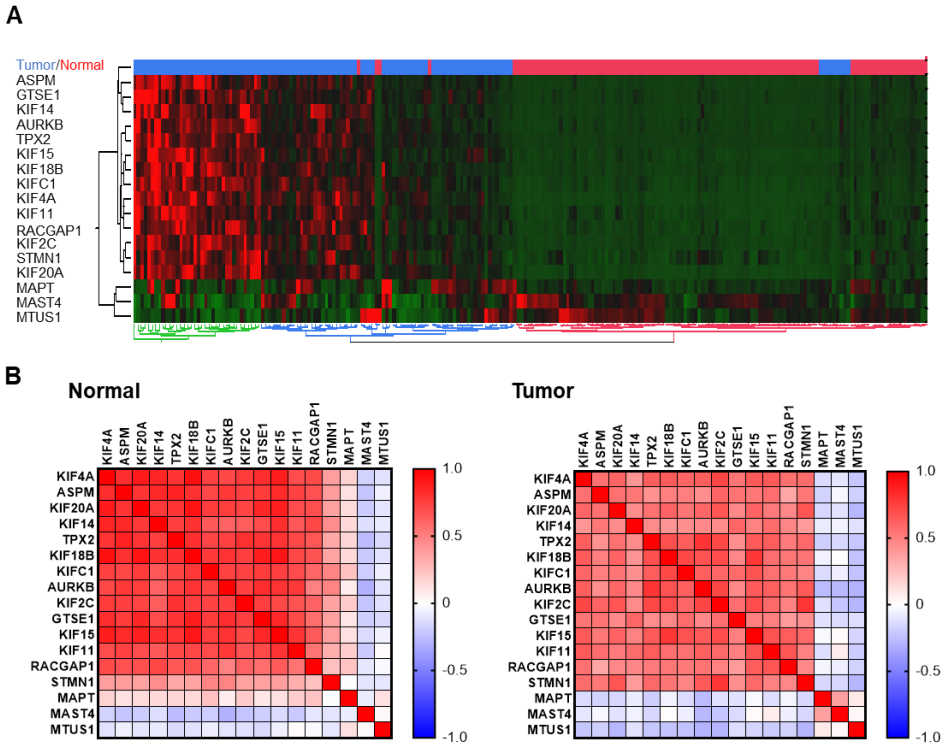

Figure 2. Co-regulation of 17 MT-Rel gene expression in breast tumor and normal tissues.

(**A**) Heat map hierarchical clustering of the 17 MT-Rel genes in normal (red) and tumor (blue) breast samples. Dendogram at the bottom shows the clustering of normal samples in red (cluster 3), and two clusters of tumors in blue (cluster 1) and green (cluster 2). (**B**) Heat map of Pearson correlation coefficient (r) in normal (left) and tumor (right) breast samples.

Co-regulation of expression of each of the 17 genes was analyzed in more details in normal and cancer samples (Fig.2B). In normal tissues, a marked correlation (r=0.55 to 0.94) was found between 13 up-regulated genes - STMN1 being the exception - (Fig.2B, Suppl Table S2), suggesting that coordinated expression of these genes may be conserved to maintain microtubule cytoskeleton homeostasis. In paired breast tumors however, correlation between the 13 up-regulated genes was weaker (r=0.35 to 0.79) (Fig.2B, Suppl Table S3), indicating some degree of variability in the profile of MT-Rel in breast cancer, in line with the heat map shown in Fig.2A.

MAPT, MAST4 and MTUS1 formed a distinct group of genes that were not significantly correlated with any other gene (suppl Tables S2 and S3). Notably, a weak but significant correlation between MAST4 and MAPT gene expression (r=0.37, p=0.0001) was depicted in tumor samples but not in normal tissues.

We asked whether MT-Rel gene expression in breast tumors may be prognostic of patient survival. Kaplan-Meyer curves of patient overall survival (OS) and relapse-free survival (RFS) from the kmplotter database (kmplot.com) revealed that each MT-Rel gene has a potential prognostic value in breast cancer. High levels of each of the 14 overexpressed genes, and low levels of MAPT, MAST4 and MTUS1, are significantly associated with poor patient survival (Fig. 3A, 3B, Suppl. Table S4, Suppl Fig.S3).

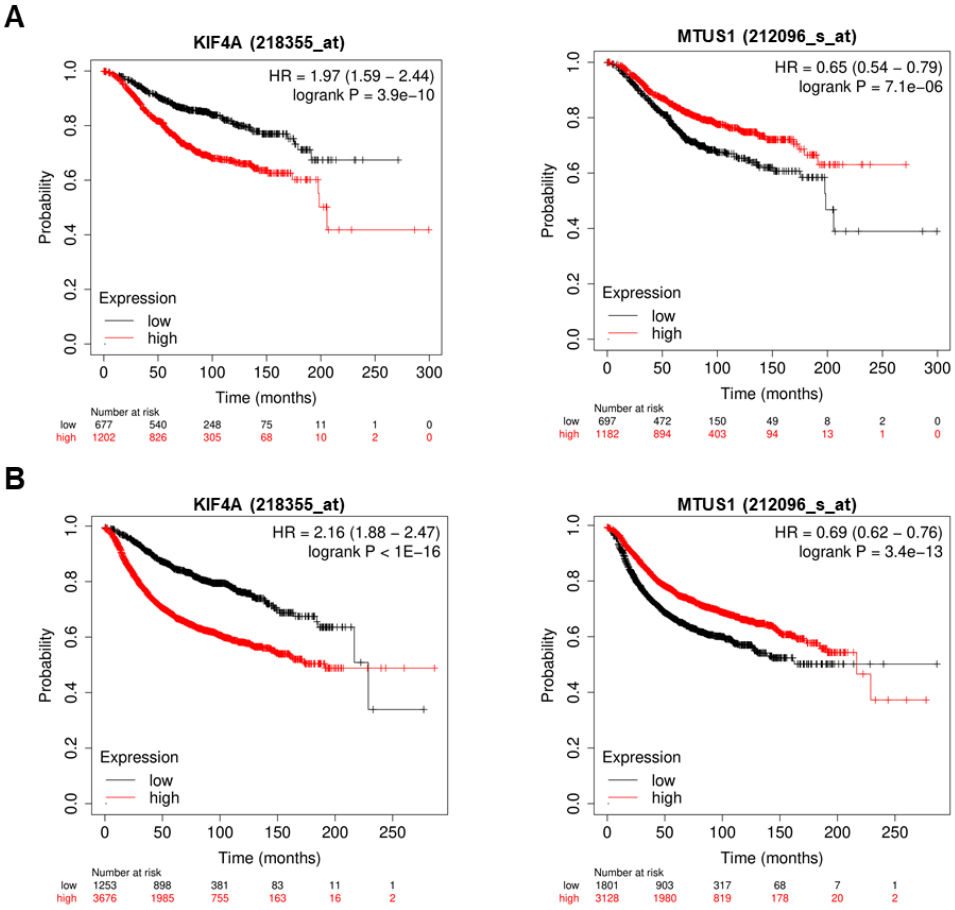

Figure 3. Survival curves of breast cancer patients according to MT-Rel gene expression level.

(A) Overall survival curves of breast cancer patients according to KIF4A (218355_at) or MTUS1 (212096_s_at) probeset intensities from kmplotter (kmplot.com). (**B**) Relapse-free survival curves as in (A).

We further addressed the functional relevance of MT-Rel deregulation in breast cancer cells. To this end, a library of siRNAs targeting each of the 14 overexpressed MT-Rel genes was transfected into two breast cancer cell lines (MDA-MB-231 and MDA-MB-468) and cell viability was measured after 96 hrs. Results revealed that KIF11, AURKB, TPX2 and KIFC1 are essential genes whose depletion in both breast cancer cell lines impacts cell viability (Fig. 4A, 4B, Suppl Table S5). Cancer dependency map (depmap.org) further highlighted KIF11, AURKB, RACGAP1 and TPX2 as genes with essential effects in 47 breast cancer cell lines (Fig. 4C, Suppl Table S6).

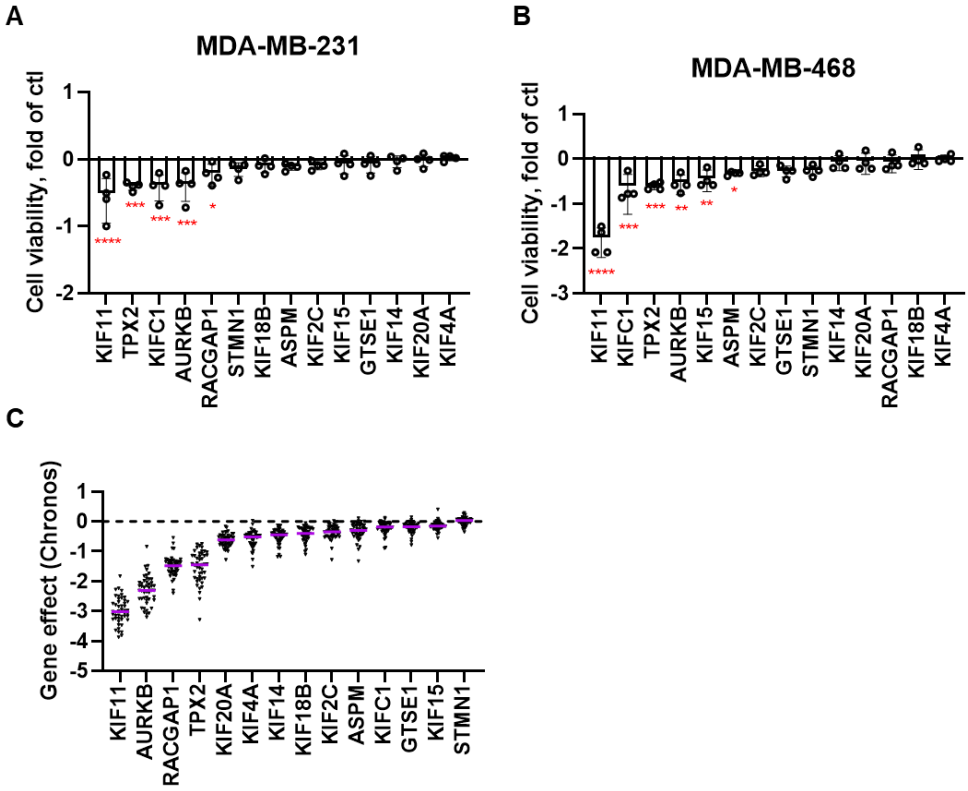

Figure 4. Effect of MT-Rel gene silencing on breast cancer cell viability.

Cell viability was measured following silencing of each MT-rel gene by siRNA transfection (96h) into MDA-MB-231 (A) and MDA-MB-468 (B) breast cancer cell lines. *p<0.05, **p<0.01, ***p<0.001, ****p<0.00001. (C) Scattered dot plot of gene dependency score (Chronos). A lower Chronos score indicates a higher likelihood that the gene of interest is essential in a given cell line. A score of 0 indicates that a gene is non-essential.

3.2. Systems Biology analysis of functional interplays and gene networks

In a second part of our study, we investigated whether the 17 MT-Rel genes may also be functionally connected into gene networks and linked to specific biological functions and molecular mechanisms altered in cancer. To tackle this question, we undertook a Systems Biology approach centered on these 17 genes. We built the smallest network starting from the 17 MT-Rel genes, further extended to their functional partners in order to connect them within a single network, as detailed in Materials and Methods. The extended network comprises 43 nodes (41 genes and 2 complexes) and 87 edges representing 42 functional activations, 32 inhibitions and 13 protein-protein interactions (PPI) (Fig.5A). The 17 genes and their partners are linked by edges displayed in green for activations and red for inhibitions. Formation of protein complexes is represented by gray lines. The Systems Biology approach also integrates information on differential regulation of each gene in breast cancer. Thus, among the 41 genes of the network, 26 are up-regulated (fold change > 1.5), and 8 are down regulated (fold change < 0.66) in breast tumors compared to normal breast.

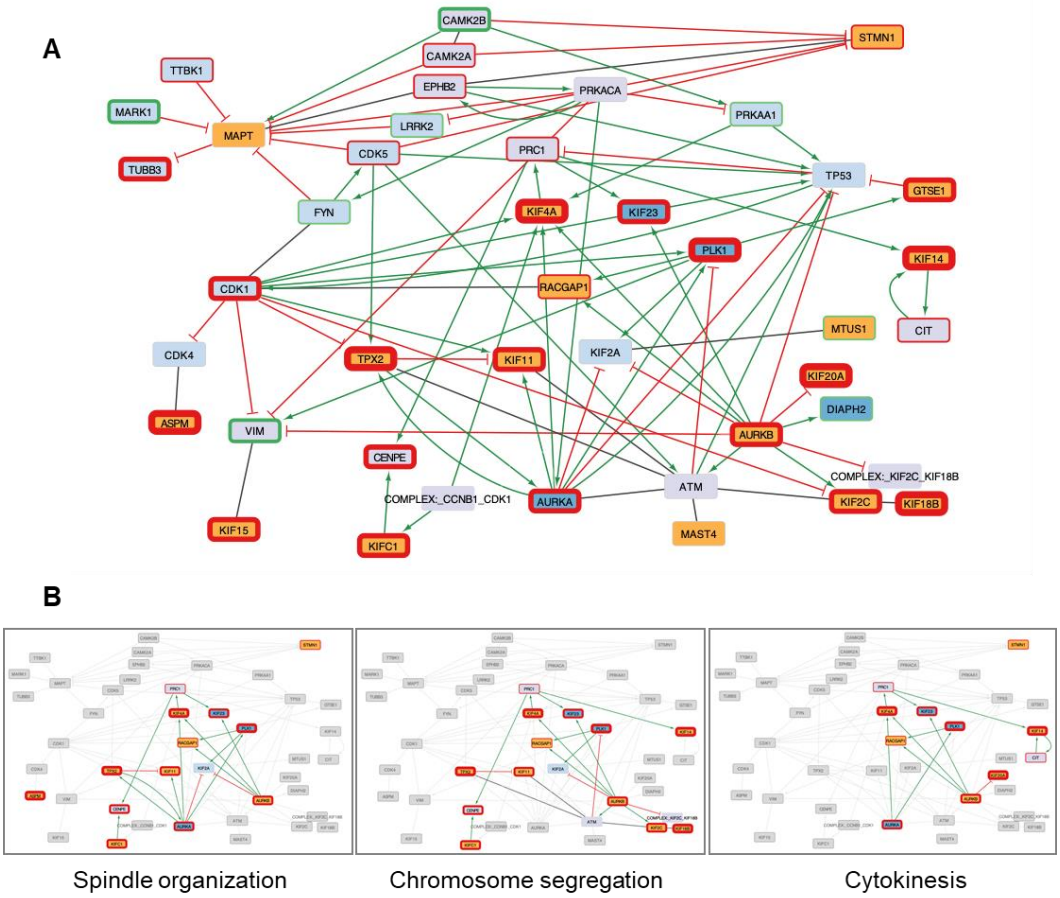

Figure 5. Systems Biology-derived networks connecting 17 MT-Rel genes.

(**A**). The 17 MT-Rel genes (in orange) and their partners are linked by edges displayed in red for inhibitions, green for activations, and black for protein-protein interactions. Node colors were assigned as follows: orange for the 17 MT-Rel genes differentially expressed in the 3 considered breast cancer transcriptomic datasets, blue for 17 MT-Rel genes differentially expressed in two of these datasets, light blue for genes with normal expression in breast cancer but present in the initial list of 280 MT-Rel genes, and light purple for genes not present in the list of 280 MT-Rel genes. Using the tnmplot.com site, we annotated on the node the fold change between normal and breast cancer tissues: red contour if the gene is up-regulated, and green contour if the gene is down-regulated. The thicker is the border, the higher is the fold change. (**B**) Sub-networks extracted from the network shown in (A) are associated with following enriched GO terms "spindle organization" (GO:0007051, p=6.10e-16) (left panel), "Mitotic sister chromatid segregation" (GO:0000070, p=2.10e-17) (middle panel) and "cytokinesis" GO:0000910, p=3.10e-11) (right panel).

Detailed analysis of the network highlighted 3 major clusters (or sub-networks) in which the 17 MT-Rel genes and their partners present dense connections (Fig.5B). These clusters are related to the cellular processes associated with the following enriched GO terms: (i) spindle organization, (ii) mitotic sister chromatid segregation and (iii) cytokinesis (Fig.6). Notably, three genes (AURKB, KIF4A and RACGAP1) contribute to all three gene sub-networks.

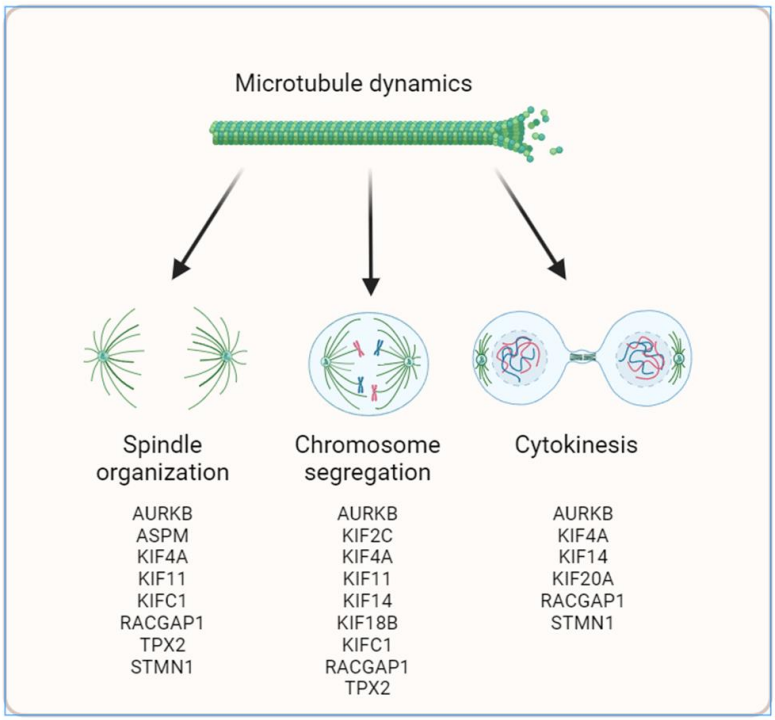

Figure 6. Schematic representation recapitulating the functional impact of MT-Rel genes in breast cancer.

Three major steps of mitosis were highlighted by the Systems Biology analysis, namely Spindle assembly, Chromosome segregation and Cytokinesis. These cellular processes are likely controlled by fine regulation of microtubule dynamic instability.

4. Discussion

In this study, we have evaluated the prognostic value and functional relevance of a panel of 17 genes encoding MT-Rel proteins that were previously identified as potential predictive biomarkers of chemoresistance. Fourteen MT-Rel genes (KIF4A, ASPM, KIF20A, KIF14, TPX2, KIF18B, KIFC1, AURKB, KIF2C, GTSE1, KIF15, KIF11, RACGAP1, STMN1) were found significantly up-regulated in breast tumors compared with paired adjacent normal tissue, and were overexpressed in the aggressive TNBC subtype compared with luminal breast tumors. Notably, six of them (KIF4A, ASPM, KIF20A, KIF14, TPX2, KIF18B) were overexpressed by more than ten-fold. High expression of each of these genes was associated with poor clinical outcome for the patient - with both reduced overall survival and relapse-free survival - pointing to their potential value as prognostic biomarkers in breast cancer.

In line with our studies, other groups reported that ASPM, KIF20A, TPX2, AURKA and KIF2C are among the top 11 up-regulated hub key genes identified as potential breast cancer prognostic biomarkers [21]. ASPM and AURKB also recently appeared as key genes up-regulated in TNBC [22]. Furthermore, a meta-analysis identified KIF20A and ASPM among the top 55 overexpressed genes when comparing tumor and normal samples across the ten most frequent human cancers [14]. It is to note that the majority (8 out of 14) of up-regulated MT-Rel genes encode kinesins which are molecular motors involved in the intracellular transport of proteins and organelles along microtubules. Kinesins have been recently highlighted as prognostic biomarkers in breast cancer [23,24] and a 6-KIFs-based risk score (among which 4 MT-Rel genes KIF4A, KIF15, KIF18B, KIF20A) was reported to accurately predict outcomes [24].

Among the 17 MT-Rel genes studied here, 3 (MAPT, MTUS1, MAST4) have a different pattern of expression. They are only moderately up-regulated (MAPT) or down-regulated (MTUS1, MAST4) in breast cancer and are not co-regulated with other MT-Rel genes. Low levels of all three genes are associated with TNBC subtype, malignancy and poor prognosis for breast cancer patients, in line with previous reports for MAPT [25,26] and MTUS1 [16,17], MAST4 being much less studied.

Thus, differential regulation of all 17 MT-Rel genes in breast tumors (14 being overexpressed and 3 down-regulated) is associated with poor prognosis.

Noticeably, 8 out of the 17 MT-Rel genes (MAPT, MTUS1, STMN1, KIF2C, KIF18B, GTSE1, ASPM, KIFC1) are involved in the regulation of microtubule dynamics and stability. Genes that are underexpressed (MAPT, MTUS1) encode microtubule stabilizers (Tau and ATIP3 proteins, respectively) [16–18,27] whereas genes that are overexpressed (STMN1, KIF2C, KIF18B) encode proteins that either destabilize [28] or depolymerize [29–32] microtubules, respectively. Other overexpressed genes (GTSE1, ASPM, KIFC1) indirectly control microtubule dynamics. The microtubule plus-end binding protein GTSE1 inhibits KIF2C and its overexpression increases spindle microtubule dynamics [33,34], as does the minus-end binding protein ASPM by interacting with citron kinase (CIT) [35] whereas in interphase ASPM interacts with katanin to promote severing and disassembly of dynamic microtubules [36]. Finally, the molecular motor KIFC1 (also called HSET) binds to, and disrupts, microtubule plus ends, thereby inducing catastrophe and increasing microtubule dynamic instability [37]. Globally, the emerging picture is an imbalance favoring microtubule destabilization, likely driven by the upregulation of genes encoding microtubule destabilizing or depolymerizing proteins and down-regulation of those encoding microtubule stabilizers, with a net tendency to increase microtubule dynamics in cancer cells. This in turn, alters the proper organization and shape of the cytoskeleton, leading to cellular abnormalities.

To further highlight cellular abnormalities driven by de-regulation of the 17 MT-Rel genes, we undertook a Systems Biology approach that extends beyond the 17 genes and takes into account differential gene expression. These studies allowed to draw a functional gene network that comprises 41 genes (including 2 protein complexes) and 87 edges contributing to major biological functions altered in breast tumors. Probing GO terms in public databases revealed that all 14 up-regulated MT-Rel genes are connected into 3 major functional sub-networks specifying different steps of mitosis, namely prometaphase/metaphase (control of mitotic spindle organization and integrity), anaphase (equal separation of chromosomes in each daughter cell) and cytokinesis (completion of division into two daughter cells). Defects in mitotic spindle assembly, chromosome segregation or cytokinesis likely result from altered microtubule dynamics. These defects are major drivers of aneuploidy due to improper chromosome attachment to the spindle in metaphase, chromosome lagging in anaphase and/or multinucleated cells due to cytokinesis failure. Aneuploidy and subsequent DNA damage are recognized hallmarks of cancer and are among the most important features associated with breast cancer aggressiveness.

To our surprise, despite the presence of 8 kinesins and 8 proteins regulating microtubule dynamics in the network, pathways involved in cell migration were not significantly highlighted in our study. Although the GO term "microtubule motor activity" (GO:0003777 with p-value of 9.175e-17) reached considerable significance, the genes associated with this GO term exhibited minimal connectivity within our network. Consequently, the intracellular transport pathway would not add significant insights in terms of Systems Biology perspective. These findings further underscore the profound impact of mitotic pathways within this gene network.

By combining gene expression, prognostic studies, functional data and Systems Biology methods, our study points to important genes to target in breast cancer. We identify here 3 champions, namely AURKB, TPX2 and KIF4A. These are highly up-regulated

and/or essential genes, contributing as hubs to several functional sub-networks in deregulated breast cancer. AURKB encodes the mitotic kinase Aurora B, that phosphorylates components at the kinetochore - where chromosomes attach microtubules - and regulates the microtubule depolymerizing activity of KIF2C [38,39]. TPX2 (Targeting Protein for Xlp2) is both a substrate and a regulator of Aurora kinase A (AURKA) that also phosphorylates a wide range of substrates in mitosis and controls the depolymerizing activity of KIF2A kinesin at the spindle pole [18,40]. AURK and TPX2 have previously been identified as prognostic biomarkers of breast cancer patient survival [21]. Furthermore, both Aurora kinases and their substrates KIF2A and KIF2C are actionable proteins for which specific inhibitors have been developed in the past years [41–43]. Targeting Aurora kinases has been extensively explored and several clinical trials have been performed or are still ongoing, including in breast cancer, to evaluate the efficiency and the safety of Aurora kinase inhibition in cancer patients [42,44].

5. Conclusions

In conclusion, breast tumors with deregulated expression of MT-Rel genes are prone to cytoskeletal alterations that likely promote aneuploidy and chromosome instability. This study opens new perspectives where targeting druggable MT-Rel proteins and their functional partners, alone or in combination with taxane-based chemotherapy, may represent an interesting therapeutical strategy in the fight against breast cancer. Together, these results may fill the gap towards the development of personalized medicine in breast cancer.

Supplementary Materials: The following supporting information can be downloaded at: www.mdpi.com/xxx/s1; **Figure S1**: Expression of 17 MT-Rel genes in breast tumors and normal tissues; **Figure S2:** Expression of 17 MT-Rel genes in breast tumors according to molecular subtypes; **Figure S3**: Survival curves of breast cancer patients according to MT-Rel gene expression level; **Table S1**: Differential expression of 17 MT-Rel genes in breast tumor samples relative to adjacent normal tissues; **Table S2**: Pearson's correlation (r) values and associated p-values in normal breast tissues; **Table S3**: Pearson's correlation (r) values and associated p-values in breast tumors; **Table S4**: Overall survival (OS) and Relapse-free survival (RFS) analysis in breast cancer patients; **Table S5**: Functional consequences of MT-Rel silencing on breast cancer cell viability; **Table S6**: DepMap analysis of MT-Rel gene depletion on viability of 47 breast cancer cell lines.

Author Contributions: Conceptualization, S.R-F, V.S and C.N.; software, G.G. O.C and V.S.; investigation, S.R-F, M.M, G.G, M.H, H.M and V.S.; supervision, V.S. and C.N.; writing—original draft preparation, S.R-F, G.G, V.S, C.N.; writing-review and editing, S.R-F., M.M, G.G., V.S. and C.N.; funding acquisition, M.M, H.M, M.H, O.C., V.S and C.N. All authors have read and agreed to the published version of the manuscript.

Funding: We wish to thank the Inserm, the CNRS, the Gustave Roussy cancer center, the Ligue Nationale Contre le cancer (LNCC), the associations Odyssea and Prolific, the Fondation Rothschild, the LERMIT/HEALTHI Emergence, the Ruban Rose association for financial support to CN, and the Fondation Janssen Horizon for support to CN and MH. This work has been supported by the Paris Île-de-France Région in the framework of DIM AI4IDF (GG) and by fellowships from the Ligue Nationale Contre le Cancer (LNCC) for MM and MH and from the Fondation ARC and FRM for HM. OC's research has been conducted within the FP2M federation (CNRS FR 2036), as part of the project Labex MME-DII (ANR11-LBX-0023-01).

Institutional Review Board Statement: Not applicable.

Informed Consent Statement: Not applicable.

Data Availability Statement: Publicly available datasets analyzed in this study can be found in following sites : TNMplot (http://www.tnmplot.com), KMplot (http://www.kmplot.com), DepMap Public 23Q2 (https://depmap.org/portal/download/custom/), SIGNOR 3.0 database (https://signor.uniroma2.it) and Gprofiler (https://biit.cs.ut.ee/gprofiler).

Conflicts of Interest: The authors declare no conflict of interest.

References

1. Brenton, J.D.; Carey, L.A.; Ahmed, A.A.; Caldas, C. Molecular Classification and Molecular Forecasting of Breast Cancer: Ready for Clinical Application? *J. Clin. Oncol.* **2005**, *23*, 7350–7360, doi:10.1200/JCO.2005.03.3845.
2. Lu, B.; Natarajan, E.; Balaji Raghavendran, H.R.; Markandan, U.D. Molecular Classification, Treatment, and Genetic Biomarkers in Triple-Negative Breast Cancer: A Review. *Technol. Cancer Res. Treat.* **2023**, *22*, 153303382211452, doi:10.1177/15330338221145246.
3. Rodrigues-Ferreira, S.; Nahmias, C. Predictive Biomarkers for Personalized Medicine in Breast Cancer. *Cancer Lett.* **2022**, *545*, 215828, doi:10.1016/j.canlet.2022.215828.
4. Mitchison, T.; Kirschner, M. Dynamic Instability of Microtubule Growth. *Nature* **1984**, *312*, 237–242, doi:10.1038/312237a0.
5. Brouhard, G.J. Dynamic Instability 30 Years Later: Complexities in Microtubule Growth and Catastrophe. *Mol. Biol. Cell* **2015**, *26*, 1207–1210, doi:10.1091/mbc.E13-10-0594.
6. Hirokawa, N. Microtubule Organization and Dynamics Dependent on Microtubule-Associated Proteins. *Curr. Opin. Cell Biol.* **1994**, *6*, 74–81, doi:10.1016/0955-0674(94)90119-8.
7. Akhmanova, A.; Steinmetz, M.O. Control of Microtubule Organization and Dynamics: Two Ends in the Limelight. *Nat. Rev. Mol. Cell Biol.* **2015**, *16*, 711–726, doi:10.1038/nrm4084.
8. Shigematsu, H.; Imasaki, T.; Doki, C.; Sumi, T.; Aoki, M.; Uchikubo-Kamo, T.; Sakamoto, A.; Tokuraku, K.; Shirouzu, M.; Nitta, R. Structural Insight into Microtubule Stabilization and Kinesin Inhibition by Tau Family MAPs. *J. Cell Biol.* **2018**, *217*, 4155–4163, doi:10.1083/jcb.201711182.
9. Bhat, K.M.R.; Setaluri, V. Microtubule-Associated Proteins as Targets in Cancer Chemotherapy. *Clin. Cancer Res.* **2007**, *13*, 2849–2854, doi:10.1158/1078-0432.CCR-06-3040.
10. Khwaja, S.; Kumar, K.; Das, R.; Negi, A.S. Microtubule Associated Proteins as Targets for Anticancer Drug Development. *Bioorganic Chem.* **2021**, *116*, 105320, doi:10.1016/j.bioorg.2021.105320.
11. Wattanathamsan, O.; Pongrakhananon, V. Emerging Role of Microtubule-Associated Proteins on Cancer Metastasis. *Front. Pharmacol.* **2022**, *13*, doi:10.3389/fphar.2022.935493.
12. Rodrigues-Ferreira, S.; Moindjie, H.; Haykal, M.M.; Nahmias, C. Predicting and Overcoming Taxane Chemoresistance. *Trends Mol. Med.* **2021**, *27*, 138–151, doi:10.1016/j.molmed.2020.09.007.
13. Rodrigues-Ferreira, S.; Nehlig, A.; Moindjie, H.; Monchecourt, C.; Seiler, C.; Marangoni, E.; Chateau-Joubert, S.; Dujaric, M.-E.; Servant, N.; Asselain, B.; et al. Improving Breast Cancer Sensitivity to Paclitaxel by Increasing Aneuploidy. *Proc. Natl. Acad. Sci.* **2019**, *116*, 23691–23697, doi:10.1073/pnas.1910824116.
14. Bartha, Á.; Győrffy, B. TNMplot.com: A Web Tool for the Comparison of Gene Expression in Normal, Tumor and Metastatic Tissues. *Int. J. Mol. Sci.* **2021**, *22*, doi:10.3390/ijms22052622.
15. Győrffy, B. Survival Analysis across the Entire Transcriptome Identifies Biomarkers with the Highest Prognostic Power in Breast Cancer. *Comput. Struct. Biotechnol. J.* **2021**, *19*, 4101–4109, doi:10.1016/j.csbj.2021.07.014.
16. Rodrigues-Ferreira, S.; Di Tommaso, A.; Dimitrov, A.; Cazaubon, S.; Gruel, N.; Colasson, H.; Nicolas, A.; Chaverot, N.; Molinié, V.; Reyal, F.; et al. 8p22 MTUS1 Gene Product ATIP3 Is a Novel Anti-Mitotic Protein Underexpressed in Invasive Breast Carcinoma of Poor Prognosis. *PloS One* **2009**, *4*, e7239, doi:10.1371/journal.pone.0007239.
17. Molina, A.; Velot, L.; Ghouinem, L.; Abdelkarim, M.; Bouchet, B.P.; Luissint, A.-C.; Bouhlel, I.; Morel, M.; Sapharikas, E.; Di Tommaso, A.; et al. ATIP3, a Novel Prognostic Marker of Breast Cancer Patient Survival, Limits Cancer Cell Migration and Slows Metastatic Progression by Regulating Microtubule Dynamics. *Cancer Res.* **2013**, *73*, 2905–2915, doi:10.1158/0008-5472.CAN-12-3565.
18. Nehlig, A.; Molina, A.; Rodrigues-Ferreira, S.; Honoré, S.; Nahmias, C. Regulation of End-Binding Protein EB1 in the Control of Microtubule Dynamics. *Cell. Mol. Life Sci.* **2017**, *74*, 2381–2393, doi:10.1007/s00018-017-2476-2.

19. Lo Surdo, P.; Iannuccelli, M.; Contino, S.; Castagnoli, L.; Licata, L.; Cesareni, G.; Perfetto, L. SIGNOR 3.0, the SIGnaling Network Open Resource 3.0: 2022 Update. *Nucleic Acids Res.* **2023**, *51*, D631–D637, doi:10.1093/nar/gkac883.
20. Valet, F.; de Cremoux, P.; Spyratos, F.; Servant, N.; Dujaric, M.E.; Gentien, D.; Lehmann-Che, J.; Scott, V.; Sigal-Zafrani, B.; Mathieu, M.C.; et al. Challenging Single- and Multi-Probesets Gene Expression Signatures of Pathological Complete Response to Neoadjuvant Chemotherapy in Breast Cancer: Experience of the REMAGUS 02 Phase II Trial. *The Breast* **2013**, *22*, 1052–1059, doi:10.1016/j.breast.2013.08.015.
21. Chen, G.; Yu, M.; Cao, J.; Zhao, H.; Dai, Y.; Cong, Y.; Qiao, G. Identification of Candidate Biomarkers Correlated with Poor Prognosis of Breast Cancer Based on Bioinformatics Analysis. *Bioengineered* **2021**, *12*, 5149–5161, doi:10.1080/21655979.2021.1960775.
22. Alam, M.S.; Sultana, A.; Wang, G.; Haque Mollah, M.N. Gene Expression Profile Analysis to Discover Molecular Signatures for Early Diagnosis and Therapies of Triple-Negative Breast Cancer. *Front. Mol. Biosci.* **2022**, *9*, 1049741, doi:10.3389/fmolb.2022.1049741.
23. Lucanus, A.J.; Yip, G.W. Kinesin Superfamily: Roles in Breast Cancer, Patient Prognosis and Therapeutics. *Oncogene* **2018**, *37*, 833–838, doi:10.1038/onc.2017.406.
24. Li, T.-F.; Zeng, H.-J.; Shan, Z.; Ye, R.-Y.; Cheang, T.-Y.; Zhang, Y.-J.; Lu, S.-H.; Zhang, Q.; Shao, N.; Lin, Y. Overexpression of Kinesin Superfamily Members as Prognostic Biomarkers of Breast Cancer. *Cancer Cell Int.* **2020**, *20*, 123, doi:10.1186/s12935-020-01191-1.
25. Bonneau, C.; Gurard-Levin, Z.A.; Andre, F.; Pusztai, L.; Rouzier, R. Predictive and Prognostic Value of the TauProtein in Breast Cancer. *Anticancer Res.* **2015**, *35*, 5179–5184.
26. Darlix, A.; Hirtz, C.; Thezenas, S.; Maceski, A.; Gabelle, A.; Lopez-Crapez, E.; De Forges, H.; Firmin, N.; Guiu, S.; Jacot, W.; et al. The Prognostic Value of the Tau Protein Serum Level in Metastatic Breast Cancer Patients and Its Correlation with Brain Metastases. *BMC Cancer* **2019**, *19*, doi:10.1186/s12885-019-5287-z.
27. Prezel, E.; Elie, A.; Delaroche, J.; Stoppin-Mellet, V.; Bosc, C.; Serre, L.; Fourest-Lieuvin, A.; Andrieux, A.; Vantard, M.; Arnal, I. Tau Can Switch Microtubule Network Organizations: From Random Networks to Dynamic and Stable Bundles. *Mol. Biol. Cell* **2018**, *29*, 154–165, doi:10.1091/mbc.E17-06-0429.
28. Holmfeldt, P.; Sellin, M.E.; Gullberg, M. Upregulated Op18/stathmin Activity Causes Chromosomal Instability through a Mechanism That Evades the Spindle Assembly Checkpoint. *Exp. Cell Res.* **2010**, *316*, 2017–2026, doi:10.1016/j.yexcr.2010.04.008.
29. Hunter, A.W.; Caplow, M.; Coy, D.L.; Hancock, W.O.; Diez, S.; Wordeman, L.; Howard, J. The Kinesin-Related Protein MCAK Is a Microtubule Depolymerase That Forms an ATP-Hydrolyzing Complex at Microtubule Ends. *Mol. Cell* **2003**, *11*, 445–457, doi:10.1016/S1097-2765(03)00049-2.
30. Stout, J.R.; Yount, A.L.; Powers, J.A.; LeBlanc, C.; Ems-McClung, S.C.; Walczak, C.E. Kif18B Interacts with EB1 and Controls Astral Microtubule Length during Mitosis. *Mol. Biol. Cell* **2011**, *22*, 3070–3080, doi:10.1091/mbc.e11-04-0363.
31. Tanenbaum, M.E.; Macurek, L.; van der Vaart, B.; Galli, M.; Akhmanova, A.; Medema, R.H. A Complex of Kif18b and MCAK Promotes Microtubule Depolymerization and Is Negatively Regulated by Aurora Kinases. *Curr. Biol.* **2011**, *21*, 1356–1365, doi:10.1016/j.cub.2011.07.017.
32. McHugh, T.; Welburn, J.P.I. Potent Microtubule-Depolymerizing Activity of a Mitotic Kif18b–MCAK–EB Network. *J. Cell Sci.* **2023**, *136*, doi:10.1242/jcs.260144.
33. Tipton, A.R.; Wren, J.D.; Daum, J.R.; Siefert, J.C.; Gorbsky, G.J. GTSE1 Regulates Spindle Microtubule Dynamics to Control Aurora B Kinase and Kif4A Chromokinesin on Chromosome Arms. *J. Cell Biol.* **2017**, *216*, 3117–3132, doi:10.1083/jcb.201610012.
34. Singh, D.; Schmidt, N.; Müller, F.; Bange, T.; Bird, A.W. Destabilization of Long Astral Microtubules via Cdk1-Dependent Removal of GTSE1 from Their Plus Ends Facilitates Prometaphase Spindle Orientation. *Curr. Biol.* **2021**, *31*, 766–781.e8, doi:10.1016/j.cub.2020.11.040.

35. Gai, M.; Bianchi, F.T.; Vagnoni, C.; Vernì, F.; Bonaccorsi, S.; Pasquero, S.; Berto, G.E.; Sgrò, F.; Chiotto, A.M.; Annaratone, L.; et al. ASPM and CITK Regulate Spindle Orientation by Affecting the Dynamics of Astral Microtubules. *EMBO Rep.* **2016**, *17*, 1396–1409, doi:10.15252/embr.201541823.
36. Jiang, K.; Rezabkova, L.; Hua, S.; Liu, Q.; Capitani, G.; Altelaar, A.F.M.; Heck, A.J.R.; Kammerer, R.A.; Steinmetz, M.O.; Akhmanova, A. Microtubule Minus-End Regulation at Spindle Poles by an ASPM–katanin Complex. *Nat. Cell Biol.* **2017**, *19*, 480–492, doi:10.1038/ncb3511.
37. Ogren, A.; Parmar, S.; Mukherjee, S.; Gonzalez, S.J.; Plooster, M.; McClellan, M.; Mannava, A.G.; Davidson, E.; Davis, T.N.; Gardner, M.K. Kinesin-14 Motors Participate in a Force Balance at Microtubule plus-Ends to Regulate Dynamic Instability. *Proc. Natl. Acad. Sci.* **2022**, *119*, doi:10.1073/pnas.2108046119.
38. Andrews, P.D.; Ovechkina, Y.; Morrice, N.; Wagenbach, M.; Duncan, K.; Wordeman, L.; Swedlow, J.R. Aurora B Regulates MCAK at the Mitotic Centromere. *Dev. Cell* **2004**, *6*, 253–268, doi:10.1016/S1534-5807(04)00025-5.
39. Lan, W.; Zhang, X.; Kline-Smith, S.L.; Rosasco, S.E.; Barrett-Wilt, G.A.; Shabanowitz, J.; Hunt, D.F.; Walczak, C.E.; Stukenberg, P.T. Aurora B Phosphorylates Centromeric MCAK and Regulates Its Localization and Microtubule Depolymerization Activity. *Curr. Biol.* **2004**, *14*, 273–286, doi:10.1016/j.cub.2004.01.055.
40. Jang, C.-Y.; Coppinger, J.A.; Seki, A.; Yates, J.R.; Fang, G. Plk1 and Aurora A Regulate the Depolymerase Activity and the Cellular Localization of Kif2a. *J. Cell Sci.* **2009**, *122*, 1334–1341, doi:10.1242/jcs.044321.
41. Damodaran, A.P.; Vaufrey, L.; Gavard, O.; Prigent, C. Aurora A Kinase Is a Priority Pharmaceutical Target for the Treatment of Cancers. *Trends Pharmacol. Sci.* **2017**, *38*, 687–700, doi:10.1016/j.tips.2017.05.003.
42. Kovacs, A.H.; Zhao, D.; Hou, J. Aurora B Inhibitors as Cancer Therapeutics. *Molecules* **2023**, *28*, 3385, doi:10.3390/molecules28083385.
43. Smith, J.C.; Husted, S.; Pilrose, J.; Ems-McClung, S.C.; Stout, J.R.; Carpenter, R.L.; Walczak, C.E. MCAK Inhibitors Induce Aneuploidy in Triple-Negative Breast Cancer Models. *Cancers* **2023**, *15*, 3309, doi:10.3390/cancers15133309.
44. Du, R.; Huang, C.; Liu, K.; Li, X.; Dong, Z. Targeting AURKA in Cancer: Molecular Mechanisms and Opportunities for Cancer Therapy. *Mol. Cancer* **2021**, *20*, doi:10.1186/s12943-020-01305-3.

Supplementary Materials

A network of 17 microtubule-related genes highlights functional deregulations in breast cancer

RODRIGUES-FERREIRA Sylvie, MORIN Morgane, GUICHAOUA Gwenn, MOINDJIE Hadia, HAYKAL Maria, COLLIER Olivier, STOVEN Veronique, NAHMIAS Clara.

Legends to Supplemental Figures

Supplemental Figure S1: **Expression of 17 MT-Rel genes in breast tumors and normal tissues.**

Proportions of tumor samples that show higher expression of the selected genes compared to adjacent normal samples at each of the quantile cutoff values (minimum Min, 1st quartile Q1, median Med, 3rd quartile Q3, maximum Max). Specificity (in red) is calculated by dividing the number of tumor samples (T) with the sum of tumor and normal samples (T+N) as described in [1].

Supplemental Figure S2: Expression of 17 MT-Rel genes in breast tumors according to molecular subtypes.

Probeset intensities of each appropriate gene in breast tumors from the REMAGUS02 cohort, classified according to molecular subtypes: ER+ (ER-positive), HER2+ (HER2-overexressing) and TNBC (Triple negative breast cancer subtype). A blue line indicates the median value. *p<0.05; **p<0.01; ***p<0.001; ****p<0.0001.

Supplemental Figure S3: Survival curves of breast cancer patients according to MT-Rel gene expression level.

(A) Overall survival curves of breast cancer patients according to the 17 MT-Rel genes probeset intensities from kmplotter (kmplot.com). **(B)** Relapse-free survival curves as in **(A).** For each gene, the best probeset was used (Jetset) and the best cut-off was selected to distinguish between tumors expressing low and high levels of the gene.

Legends to Supplemental Tables

Supplemental Table S1. Differential expression of 17 MT-Rel genes in breast tumor samples relative to adjacent normal tissues.

Median fold change and associated Mann-Whitney p-value were determined for each MT-Rel gene in 112 breast tumors and adjacent normal tissues from TNMplot.org.

Supplemental Table S2. Pearson's correlation (r) values and associated p-values in normal breast tissues.

p-values that do not reach significance are indicated in grey. Genes are ordered according to their fold change in breast tumor vs normal tissue as shown in Fig. 1B.

Supplemental Table S3. Pearson's correlation (r) values and associated p-values in breast tumors.

p values that do not reach significance are indicated in grey. Genes are ordered as in Suppl Table S2.

Supplemental Table S4. Overall survival (OS) and Relapse-free survival (RFS) analysis in breast cancer patients.

Best probeset and best cut-off for each gene were determined from kmplot.com. HR: Hazard Ratio; CI: Confidence Interval; n: number of patients analyzed. Genes are ordered as in Suppl Table S2.

Supplemental Table S5. Functional consequences of MT-Rel silencing on breast cancer cell viability.

Mean fold change and standard error mean (sem) in cell viability of breast cancer cell lines MDA-MB-231 and MDA-MB-468 following silencing of 14 overexpressed MT-Rel genes by siRNA screening. Significant p-values are indicated in blue. Shown are the results of four independent experiments performed in quadruplicate. Results are normalized to control siRNA.

Supplemental Table S6. DepMap analysis of MT-Rel gene depletion on viability of 47 breast cancer cell lines.

Chronos dependency score values across the 47 breast cancer cell lines. Genes are presented by alphabetical order.

Reference

1. Bartha, Á.; Győrffy, B. TNMplot.com: A Web Tool for the Comparison of Gene Expression in Normal, Tumor and Metastatic Tissues. *Int. J. Mol. Sci.* **2021**, *22*, doi:10.3390/ijms22052622.

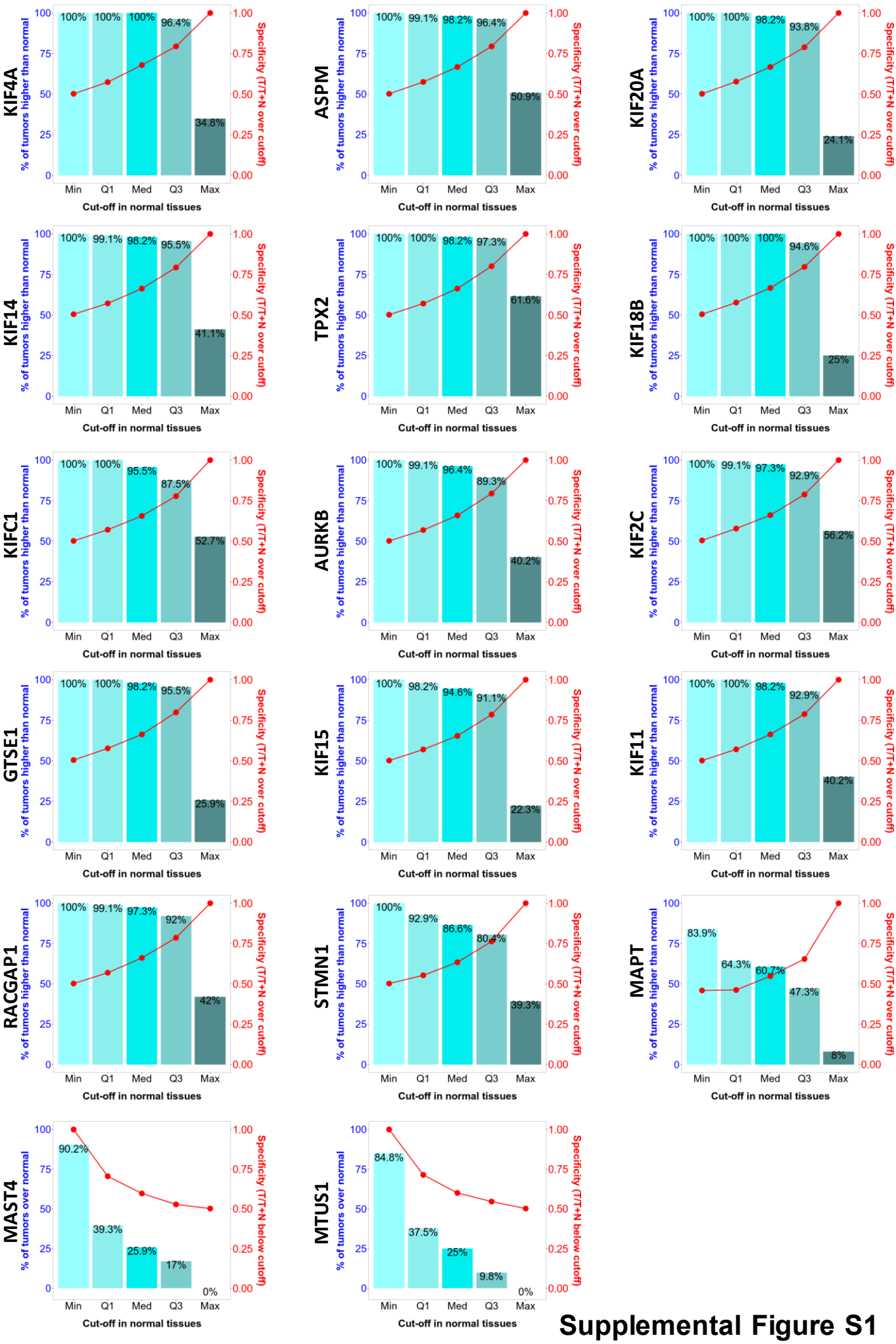

Supplemental Figure S1

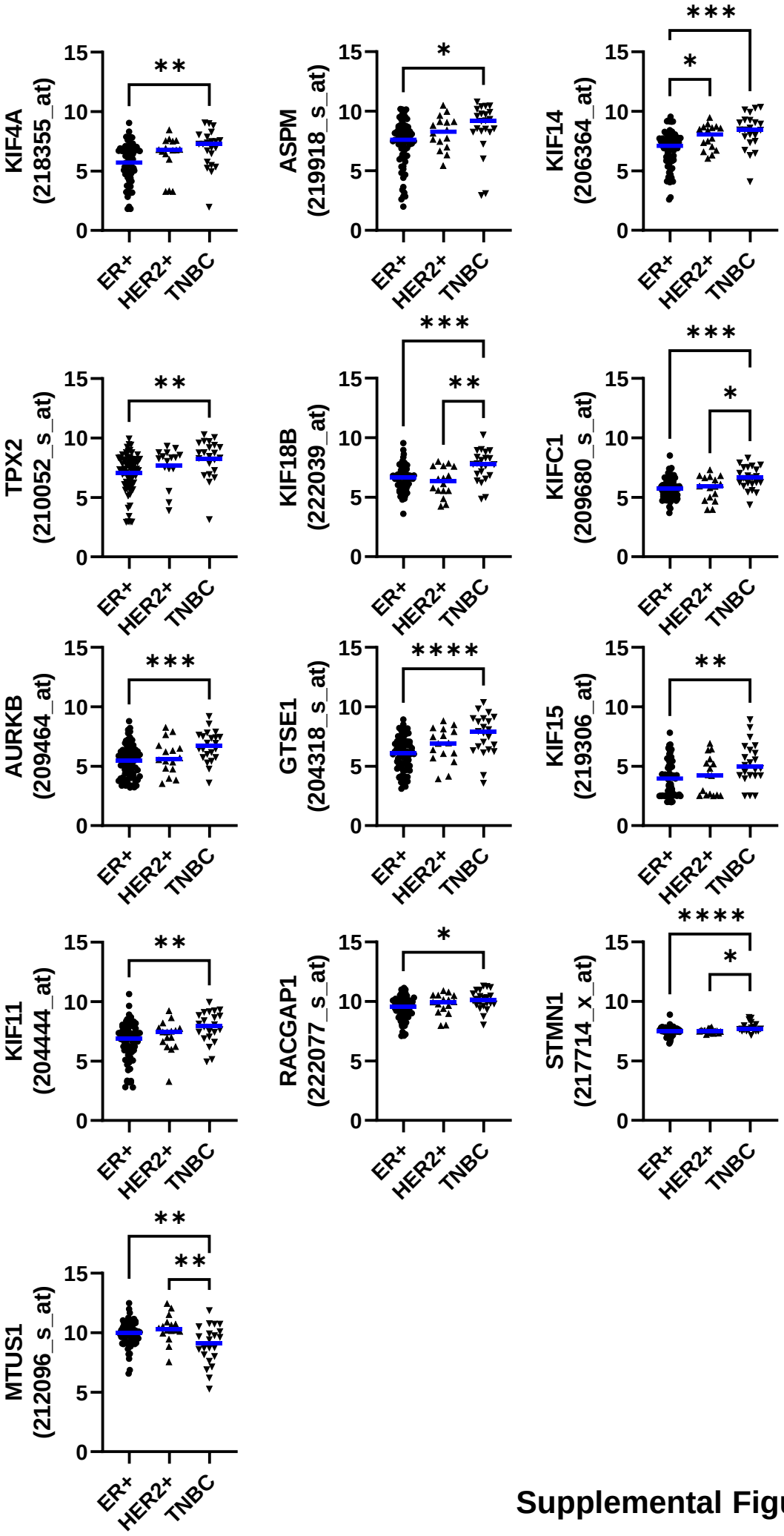

Supplemental Figure S2

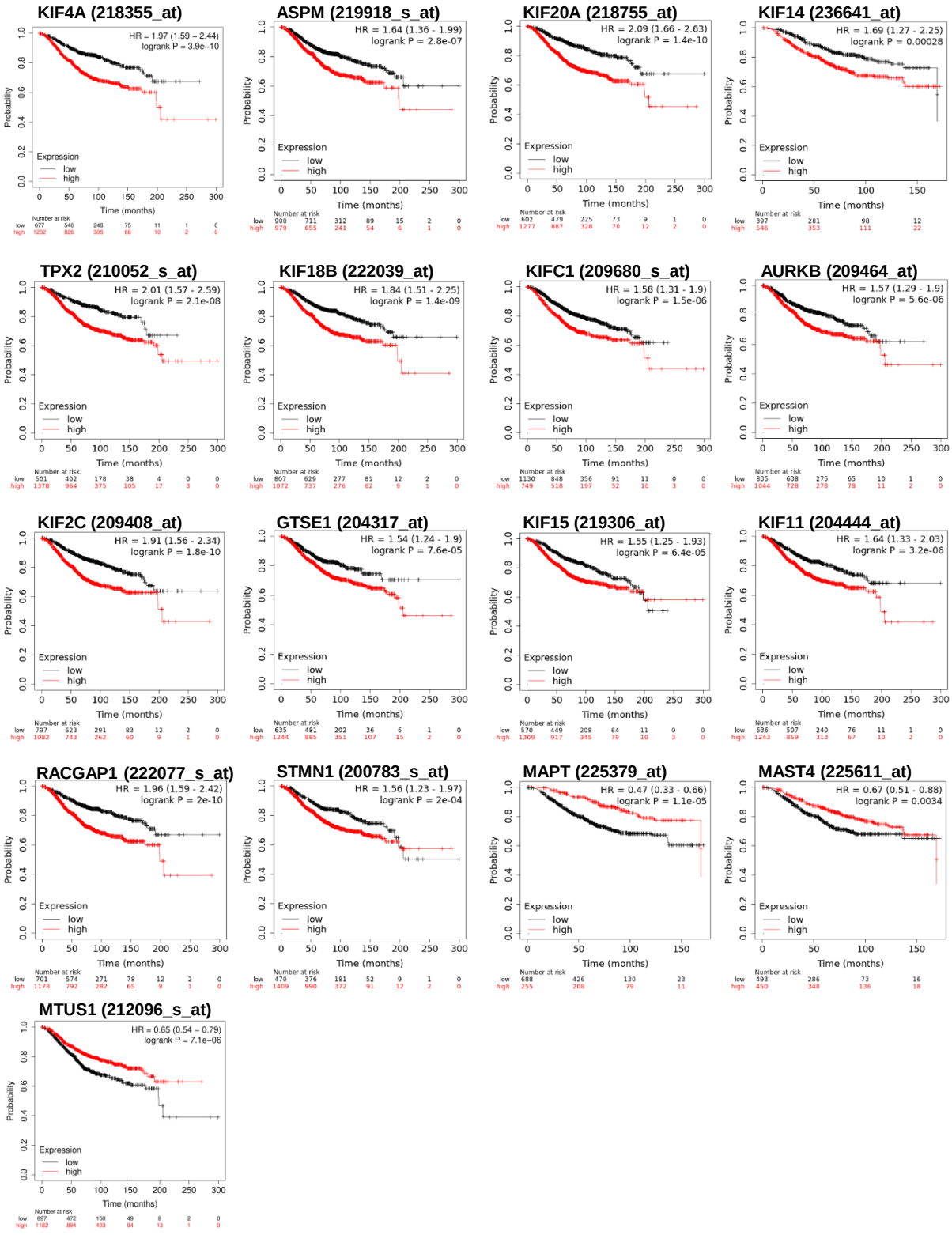

Supplemental Figure S3A

KIF4A (218355_at)

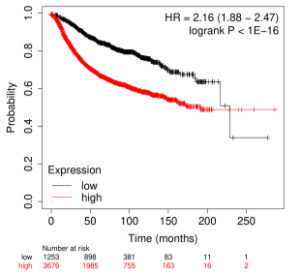

ASPM (219918_s_at)

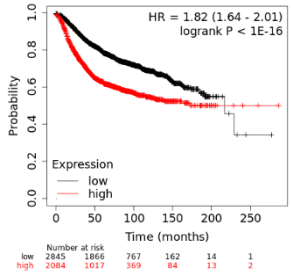

KIF20A (218755_at)

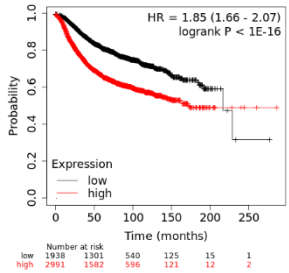

KIF14 (236641_at)

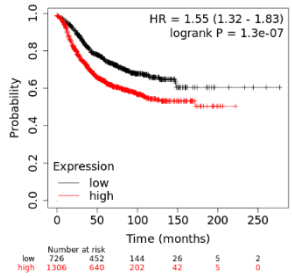

TPX2 (210052_s_at)

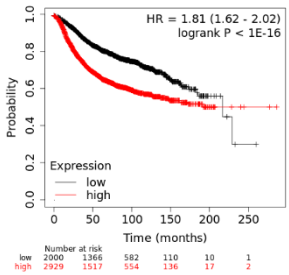

KIF18B (222039_at)

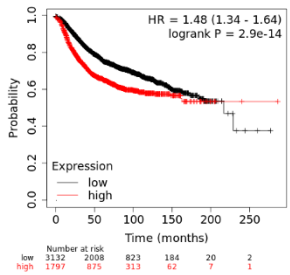

KIFC1 (209680_s_at)

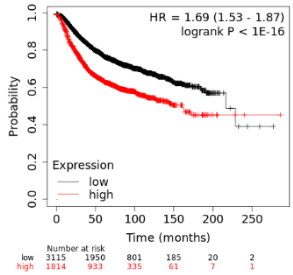

AURKB (209464_at)

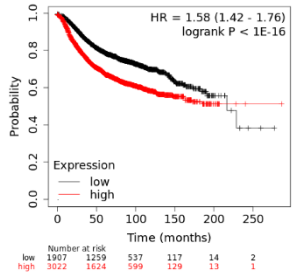

KIF2C (209408_at)

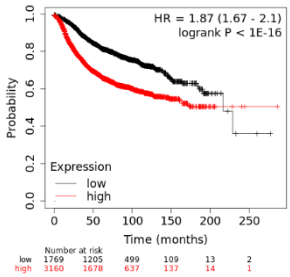

GTSE1 (204317_at)

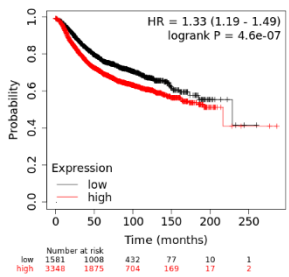

KIF15 (219306_at)

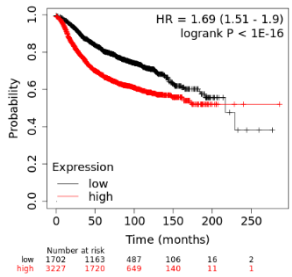

KIF11 (204444_at)

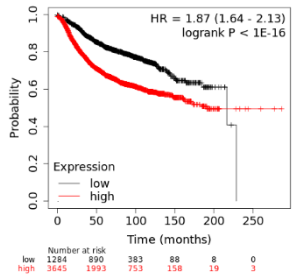

RACGAP1 (222077_s_at)

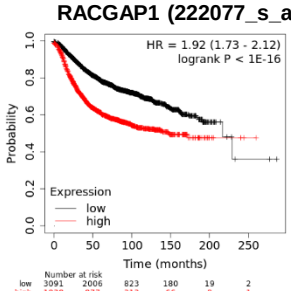

STMN1 (200783_s_at)

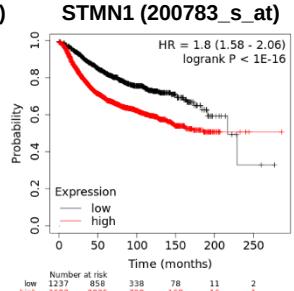

MAPT (225379_at)

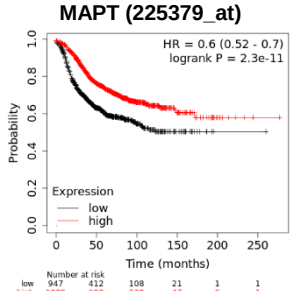

MAST4 (225611_at)

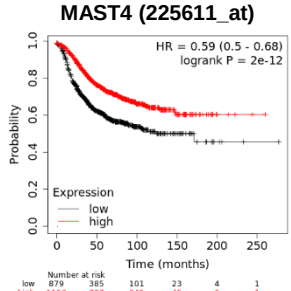

MTUS1 (212096_s_at)

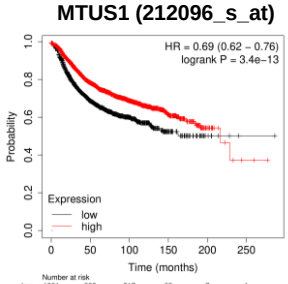

Supplemental Figure S3B

Gene	Fold change (Median)	Mann-Whitney p-value
KIF4A	17,79	$8{,}57.10^{-20}$
ASPM	14,66	$9{,}67.10^{-20}$
KIF20A	13,01	$3{,}59.10^{-19}$
KIF14	12,27	$4{,}05.10^{-19}$
TPX2	11,72	$4{,}38.10^{-20}$
KIF18B	11,45	$5{,}36.10^{-20}$
KIFC1	8,19	$6{,}22.10^{-20}$
AURKB	8,05	$5{,}98.10^{-19}$
KIF2C	7,89	$4{,}88.10^{-20}$
GTSE1	7,16	$1{,}81.10^{-19}$
KIF15	5,45	$7{,}97.10^{-19}$
KIF11	5,18	$3{,}23.10^{-19}$
RACGAP1	3,61	$2{,}12.10^{-19}$
STMN1	2,52	$3{,}39.10^{-17}$
MAPT	1,44	$8{,}46.10^{-4}$
MAST4	0,68	$1{,}39.10^{-4}$
MTUS1	0,66	$1{,}39.10^{-6}$

Supplemental Table S1: Differential expression of 17 MT-Rel genes in breast tumor samples relative to adjacent normal tissues.

(A) Pearson (r)	KIF4A	ASPM	KIF20A	KIF14	TPX2	KIF18B	KIFC1	AURKB	KIF2C	GTSE1	KIF15	KIF11	RACGAP1	STMN1	MAPT	MAST4	MTUS1
KIF4A	1	0,819	0,890	0,854	0,795	0,938	0,745	0,715	0,762	0,817	0,880	0,696	0,707	0,377	0,175	- 0,177	- 0,115
ASPM		1	0,795	0,842	0,865	0,809	0,718	0,780	0,748	0,764	0,834	0,743	0,679	0,381	0,114	- 0,230	- 0,066
KIF20A			1	0,780	0,796	0,922	0,764	0,753	0,731	0,848	0,878	0,699	0,694	0,366	0,143	- 0,203	- 0,104
KIF14				1	0,748	0,800	0,653	0,610	0,630	0,696	0,814	0,655	0,720	0,446	0,147	- 0,131	- 0,086
TPX2					1	0,814	0,726	0,743	0,808	0,790	0,798	0,712	0,660	0,338	0,159	- 0,263	- 0,148
KIF18B						1	0,776	0,797	0,752	0,883	0,911	0,720	0,677	0,359	0,150	- 0,211	- 0,115
KIFC1							1	0,736	0,739	0,758	0,751	0,702	0,595	0,477	0,240	- 0,199	- 0,070
AURKB								1	0,748	0,819	0,799	0,780	0,492	0,479	0,073	- 0,309	- 0,110
KIF2C									1	0,752	0,713	0,672	0,614	0,362	0,205	- 0,234	- 0,118
GTSE1										1	0,845	0,709	0,572	0,366	0,096	- 0,191	- 0,149
KIF15											1	0,793	0,646	0,377	0,118	- 0,143	- 0,060
KIF11												1	0,548	0,318	0,192	- 0,211	0,015
RACGAP1													1	0,246	0,233	- 0,101	- 0,027
STMN1														1	- 0,012	- 0,109	- 0,100
MAPT															1	- 0,077	0,119
MAST4																1	0,027
MTUS1																	1

(B) p values	KIF4A	ASPM	KIF20A	KIF14	TPX2	KIF18B	KIFC1	AURKB	KIF2C	GTSE1	KIF15	KIF11	RACGAP1	STMN1	MAPT	MAST4	MTUS1
KIF4A		2,76E-28	2,18E-39	5,54E-33	1,13E-25	2,13E-52	4,66E-21	7,86E-19	1,81E-22	4,16E-28	2,27E-37	1,59E-17	2,85E-18	4,19E-05	0,06	0,06	0,23
ASPM			1,18E-25	2,76E-31	1,00E-34	4,10E-27	4,87E-19	4,27E-24	2,44E-21	1,09E-22	3,31E-30	7,15E-21	1,99E-16	3,32E-05	0,23	0,01	0,49
KIF20A				4,29E-24	1,06E-25	4,64E-47	1,20E-22	9,95E-22	5,43E-20	3,59E-32	4,71E-37	9,94E-18	2,21E-17	7,31E-05	0,13	0,03	0,28
KIF14					2,43E-21	3,63E-26	6,06E-15	9,24E-13	9,88E-14	1,52E-17	9,10E-28	4,80E-15	3,71E-19	8,45E-07	0,12	0,17	0,37
TPX2						1,17E-27	1,28E-19	6,36E-21	4,65E-27	4,17E-25	5,87E-26	1,38E-18	2,63E-15	2,69E-04	0,09	0,01	0,12
KIF18B							8,52E-24	7,57E-26	1,26E-21	5,09E-38	3,45E-44	3,92E-19	2,46E-16	1,04E-04	0,11	0,03	0,23
KIFC1								2,32E-20	1,42E-20	4,22E-22	1,60E-21	6,43E-18	4,66E-12	1,08E-07	0,01	0,04	0,46
AURKB									2,83E-21	2,84E-28	4,47E-26	4,15E-24	3,54E-08	9,26E-08	0,44	9,09E-04	0,25
KIF2C										1,22E-21	1,15E-18	5,08E-16	5,83E-13	8,69E-05	0,03	0,01	0,22
GTSE1											1,01E-31	2,19E-18	4,59E-11	7,07E-05	0,31	0,04	0,12
KIF15												1,86E-25	1,42E-14	4,25E-05	0,22	0,13	0,53
KIF11													3,94E-10	6,31E-04	0,04	0,03	0,88
RACGAP1														8,94E-03	0,01	0,29	0,78
STMN1															0,90	0,25	0,29
MAPT																0,42	0,21
MAST4																	0,78
MTUS1																	

Supplemental Table S2: Pearson's correlation (r) values (**A**) and associated p-values (**B**) in normal breast tissues.

(A) Pearson (r)	KIF4A	ASPM	KIF20A	KIF14	TPX2	KIF18B	KIFC1	AURKB	KIF2C	GTSE1	KIF15	KIF11	RACGAP1	STMN1	MAPT	MAST4	MTUS1
KIF4A	1	0,558	0,602	0,412	0,627	0,641	0,600	0,628	0,722	0,538	0,649	0,647	0,555	0,575	-0,143	-0,101	-0,225
ASPM		1	0,558	0,531	0,428	0,504	0,500	0,441	0,607	0,548	0,533	0,568	0,347	0,532	-0,177	-0,038	-0,187
KIF20A			1	0,449	0,553	0,612	0,545	0,596	0,665	0,463	0,610	0,515	0,470	0,667	-0,162	-0,113	-0,284
KIF14				1	0,459	0,416	0,437	0,460	0,459	0,593	0,487	0,576	0,472	0,389	-0,076	-0,057	-0,116
TPX2					1	0,683	0,632	0,794	0,716	0,447	0,644	0,639	0,520	0,590	-0,190	-0,159	-0,222
KIF18B						1	0,714	0,671	0,703	0,468	0,781	0,566	0,536	0,538	-0,057	0,009	-0,236
KIFC1							1	0,626	0,598	0,581	0,673	0,557	0,524	0,482	-0,145	-0,068	-0,240
AURKB								1	0,725	0,464	0,640	0,619	0,547	0,644	-0,268	-0,280	-0,298
KIF2C									1	0,563	0,697	0,588	0,494	0,785	-0,119	-0,230	-0,289
GTSE1										1	0,501	0,497	0,389	0,441	-0,123	-0,143	-0,134
KIF15											1	0,675	0,632	0,591	-0,029	0,020	-0,165
KIF11												1	0,665	0,491	-0,132	0,074	-0,203
RACGAP1													1	0,468	-0,044	-0,070	-0,180
STMN1														1	-0,154	-0,157	-0,286
MAPT															1	0,372	0,082
MAST4																1	0,029
MTUS1																	1

(B) p values	KIF4A	ASPM	KIF20A	KIF14	TPX2	KIF18B	KIFC1	AURKB	KIF2C	GTSE1	KIF15	KIF11	RACGAP1	STMN1	MAPT	MAST4	MTUS1
KIF4A		1,65E-10	2,13E-12	6,42E-06	1,33E-13	2,58E-14	2,70E-12	1,22E-13	2,69E-19	9,30E-10	1,02E-14	1,26E-14	2,11E-10	3,51E-11	0,133	0,289	0,017
ASPM			1,68E-10	1,78E-09	2,50E-06	1,50E-08	1,96E-08	1,12E-06	1,31E-12	3,89E-10	1,50E-09	6,62E-11	1,82E-04	1,58E-09	0,061	0,691	0,048
KIF20A				7,04E-07	2,57E-10	7,82E-13	5,38E-10	4,24E-12	1,21E-15	2,81E-07	9,74E-13	6,17E-09	1,74E-07	9,98E-16	0,088	0,236	0,002
KIF14					3,63E-07	5,01E-06	1,50E-06	3,35E-07	3,67E-07	5,60E-12	5,11E-08	3,11E-11	1,49E-07	2,24E-05	0,428	0,552	0,223
TPX2						1,11E-16	7,50E-14	1,51E-25	7,68E-19	7,88E-07	1,96E-14	3,42E-14	4,16E-09	7,87E-12	0,045	0,093	0,019
KIF18B							9,14E-19	5,96E-16	5,74E-18	1,93E-07	3,04E-24	7,89E-11	1,11E-09	9,22E-10	0,549	0,925	0,012
KIFC1								1,65E-13	3,39E-12	1,92E-11	4,12E-16	1,84E-10	3,10E-09	7,50E-08	0,127	0,475	0,011
AURKB									1,48E-19	2,50E-07	3,12E-14	3,38E-13	4,19E-10	1,94E-14	0,004	0,003	0,001
KIF2C										1,07E-10	1,42E-17	9,23E-12	3,15E-08	1,16E-24	0,211	0,015	0,002
GTSE1											1,89E-08	2,41E-08	2,19E-05	1,11E-06	0,197	0,133	0,158
KIF15												3,20E-16	7,47E-14	6,96E-12	0,759	0,835	0,081
KIF11													1,21E-15	3,97E-08	0,166	0,436	0,032
RACGAP1														1,92E-07	0,648	0,466	0,057
STMN1															0,104	0,097	0,002
MAPT																0,000	0,393
MAST4																	0,759
MTUS1																	

Supplemental Table S3: Pearson's correlation (r) values (**A**) and associated p-values (**B**) in breast tumors.

		OS				RFS				Bad Prognosis
Gene	**Affy ID**	**HR**	**CI**	**P value**	**n**	**HR**	**CI**	**P value**	**n**	**Expression level**
KIF4A	218355_at	1,97	1,59-2,44	3.9e-10	1879	2,16	1,88-2,47	<1e-16	4929	High
ASPM	219918_s_at	1,64	1,36-1,99	2.8e-7	1879	1,82	1,64-2,01	<1e-16	4929	High
KIF20A	218755_at	2,09	1,66-2,63	1.4e-10	1879	1,85	1,66-2,07	<1e-16	4929	High
KIF14	236641_at	1,69	1,27-2,25	2.8e-4	943	1,55	1,32-1,83	1.3e-7	2032	High
TPX2	210052_s_at	2,01	1,57-2,59	2.1e-8	1879	1,81	1,62-2,02	<1e-16	4929	High
KIF18B	222039_at	1,84	1,51-2,25	1.4e-9	1879	1,48	1,34-1,64	2.9e-14	4929	High
KIFC1	209680_s_at	1,58	1,31-1,9	1.5e-6	1879	1,69	1,53-1,87	<1e-16	4929	High
AURKB	209464_at	1,57	1,29-1,9	5.6e-6	1879	1,58	1,42-1,76	<1e-16	4929	High
KIF2C	209408_at	1,91	1,56-2,34	1.8e-10	1879	1,87	1,67-2,1	<1e-16	4929	High
GTSE1	204317_at	1,54	1,24-1,9	7.6e-5	1879	1,33	1,19-1,49	4.6e-7	4929	High
KIF15	219306_at	1,55	1,25-1,93	6.4e-5	1879	1,69	1,51-1,9	<1e-16	4929	High
KIF11	204444_at	1,64	1,33-2,03	3.2e-6	1879	1,87	1,64-2,13	<1e-16	4929	High
RACGAP1	222077_s_at	1,96	1,59-2,42	2.0e-10	1879	1,92	1,73-2,12	<1e-16	4929	High
STMN1	200783_s_at	1,56	1,23-1,97	2.0e-4	1879	1,8	1,58-2,06	<1e-16	4929	High
MAPT	225379_at	0,47	0,33-0,66	1.1e-5	943	0,6	0,52-0,7	2.3e-11	2032	Low
MAST4	225611_at	0,67	0,51-0,88	0.0034	943	0,59	0,5-0,68	2.0e-12	2032	Low
MTUS1	212096_s_at	0,65	0,54-0,79	7.1e-6	1879	0,69	0,62-0,76	3.4e-13	4929	Low

Supplemental Table S4: Overall survival (OS) and Relapse-free survival (RFS) analysis in breast cancer patients.

	MDA-MB-231			MDA-MB-468		
	mean	sem	pvalue	mean	sem	pvalue
KIF4A	1,042	0,049	0,9995	1,017	0,094	0,9999
ASPM	0,768	0,042	0,4024	**0,472**	**0,020**	**0,0338**
KIF20A	0,977	0,103	0,9997	0,889	0,220	0,999
KIF14	0,930	0,093	0,9991	0,856	0,158	0,9892
TPX2	**0,395**	**0,026**	**0,0001**	**0,247**	**0,022**	**0,0008**
KIF18B	0,803	0,088	0,5984	1,080	0,252	0,9993
KIFC1	**0,410**	**0,086**	**0,0002**	**0,253**	**0,097**	**0,0009**
AURKB	**0,430**	**0,097**	**0,0003**	**0,298**	**0,069**	**0,002**
KIF2C	0,807	0,055	0,6272	0,545	0,073	0,0942
GTSE1	0,849	0,114	0,8637	0,536	0,074	0,0832
KIF15	0,868	0,132	0,9366	**0,373**	**0,094**	**0,0071**
KIF11	**0,312**	**0,100**	**<0,0001**	**0,018**	**0,006**	**<0,0001**
RACGAP1	**0,621**	**0,111**	**0,0317**	0,852	0,183	0,9876
STMN1	0,715	0,081	0,1841	0,561	0,072	0,1151

Supplemental Table S5: Functional consequences of MT-Rel silencing on breast cancer cell viability.

Breast cancer cell line	DepMap_ID	ASPM	AURKB	GTSE1	KIF2C	KIF4A	KIF11	KIF14	KIF15	KIF18B	KIF20A	KIFC1	RACGAP1	STMN1	TPX2
21NT	ACH-002399	-0,43	-2,10	-0,21	-0,49	-0,77	-2,97	-0,34	-0,24	-0,48	-0,49	-0,48	-1,81	0,09	-1,91
AU565	ACH-000248	-0,12	-2,65	-0,02	-0,35	-0,73	-2,48	-0,44	-0,10	-0,31	-0,35	-0,06	-1,33	0,15	-2,06
BT549	ACH-000288	-0,06	-2,90	-0,13	-0,50	-0,55	-2,70	-0,39	-0,26	-0,95	-0,75	-0,90	-1,72	0,03	-1,07
CAL120	ACH-000212	-0,85	-2,63	-0,04	-0,47	-0,47	-3,17	-0,14	-0,08	-0,42	-0,74	-0,25	-1,51	0,08	-1,75
CAL51	ACH-000856	-0,32	-2,15	-0,24	-0,32	-0,50	-2,50	-0,58	-0,21	-0,84	-0,68	-0,13	-1,40	-0,03	-1,16
CAMA1	ACH-000783	0,02	-2,52	-0,25	-0,14	-0,60	-3,47	-0,77	-0,15	-0,59	-0,79	-0,10	-1,27	0,06	-1,89
DU4475	ACH-000258	0,00	-1,49	-0,06	-0,90	-0,34	-2,59	-0,27	-0,10	-1,01	-0,62	-0,34	-1,72	-0,01	-1,86
EFM19	ACH-000330	-0,08	-1,62	-0,68	-0,18	-0,33	-3,17	-0,36	-0,26	-0,13	-0,45	-0,33	-1,34	0,08	-1,17
EVSAT	ACH-001065	-0,33	-2,58	-0,48	-1,28	-0,51	-2,84	-0,29	-0,09	-1,11	-0,72	0,02	-2,40	0,01	-0,75
HCC1143	ACH-000374	-0,30	-1,93	-0,35	-0,51	-0,09	-3,27	-0,57	-0,42	-0,77	-0,49	-0,29	-1,31	-0,13	-1,23
HCC1187	ACH-000111	-0,09	-2,91	-0,26	-0,40	-0,36	-2,32	-0,43	0,40	-0,05	-0,78	0,13	-1,82	0,25	-1,15
HCC1395	ACH-000699	-0,52	-1,98	-0,40	-0,48	-0,80	-3,81	-0,14	-0,40	-0,43	-0,94	-0,21	-1,61	-0,10	-1,93
HCC1419	ACH-000277	-0,16	-2,03	-0,10	-0,34	-0,83	-2,54	-1,17	-0,14	-0,25	-0,60	-0,30	-1,29	0,29	-1,00
HCC1428	ACH-000352	-0,50	-2,22	-0,12	-0,16	-0,50	-3,07	-0,30	0,01	-0,21	-0,40	-0,09	-1,42	-0,24	-1,46
HCC1806	ACH-000624	-0,29	-2,99	-0,11	-0,15	-0,36	-3,35	-0,62	-0,20	-0,25	-0,81	-0,06	-1,61	0,00	-1,15
HCC1937	ACH-000223	-0,30	-2,09	-0,18	-0,53	-0,53	-2,75	-0,61	-0,20	-0,49	-0,94	-0,17	-1,33	-0,01	-0,99
HCC1954	ACH-000859	-0,23	-2,05	-0,33	-0,17	-0,76	-3,25	-0,51	-0,21	-0,24	-0,51	-0,54	-1,52	0,13	-1,54
HCC202	ACH-000725	-0,34	-2,18	-0,39	-0,07	-1,04	-3,59	-0,25	-0,29	-0,40	-0,52	-0,17	-1,48	-0,04	-2,38
HCC38	ACH-000276	-0,26	-3,04	-0,79	-0,32	-0,74	-3,28	-1,11	-0,55	-0,47	-0,80	-0,08	-1,78	0,13	-1,90
HCC70	ACH-000668	-0,79	-3,10	-0,21	-0,55	-0,46	-3,08	-0,68	-0,12	-0,56	-1,00	-0,24	-2,01	-0,18	-1,47
HMC18	ACH-000721	-0,46	-2,59	-0,09	-0,35	-0,56	-2,65	-0,65	-0,06	-0,33	-0,56	-0,29	-1,43	0,10	-1,00
HS578T	ACH-000148	-0,26	-2,35	-0,24	-0,51	-0,50	-3,15	-0,29	-0,21	-0,45	-0,36	-0,18	-1,48	0,05	-1,09
JIMT1	ACH-000711	-0,45	-2,54	-0,32	-0,25	-0,24	-2,45	-0,40	-0,24	-0,20	-0,46	-0,41	-1,52	0,05	-0,87
KPL1	ACH-000028	-0,63	-2,15	-0,04	-0,32	-0,80	-1,83	-0,48	-0,08	-0,45	-0,35	-0,22	-1,52	0,00	-1,70
MCF7	ACH-000019	-0,41	-1,91	0,01	-0,21	-0,55	-2,84	-0,77	-0,16	-0,73	-0,65	-0,06	-1,49	-0,05	-1,69
MDAMB157	ACH-000621	-0,54	-2,74	-0,20	-0,37	-1,51	-3,03	-0,46	-0,02	-0,18	-0,76	-0,88	-1,66	0,01	-1,72
MDAMB231	ACH-000768	-0,36	-2,15	-0,01	-0,18	-0,31	-2,27	-0,30	-0,06	-0,32	-0,82	-0,25	-1,38	0,06	-0,87
MDAMB361	ACH-000934	-0,45	-2,31	-0,11	-0,37	-0,54	-2,98	-0,27	0,05	-0,37	-0,55	-0,03	-0,90	0,09	-3,29
MDAMB415	ACH-000876	0,00	-2,32	-0,19	-0,01	-0,51	-3,70	-0,35	0,01	-0,40	-0,20	-0,11	-1,78	0,11	-2,25
MDAMB436	ACH-000573	-0,13	-1,80	-0,35	-0,46	-0,43	-3,11	-0,42	-0,16	-0,62	-0,17	-0,23	-1,71	0,08	-1,13
MDAMB453	ACH-000910	-0,05	-2,31	-0,34	-0,38	-1,07	-3,70	-0,46	-0,08	-0,63	-0,41	-0,19	-1,36	-0,01	-2,14
MDAMB468	ACH-000849	-0,13	-2,92	-0,13	-0,27	0,03	-3,46	-0,90	-0,16	-0,12	-0,78	-0,20	-1,68	-0,35	-1,25
MFM223	ACH-001819	-0,94	-2,60	-0,50	-0,24	-0,43	-3,30	-0,89	-0,35	-0,22	-0,52	-0,02	-1,67	-0,02	-1,47
OCUBM	ACH-002179	-1,33	-2,56	0,14	-0,60	-0,98	-2,75	-1,18	0,09	-0,19	-0,88	0,09	-2,31	0,05	-2,02
SKBR3	ACH-000017	-0,58	-2,21	-0,17	-0,02	-0,46	-3,00	-0,47	-0,10	-0,22	-0,87	-0,19	-1,47	0,05	-1,03
SUM102PT	ACH-001388	-0,04	-2,16	-0,07	-0,48	-0,89	-3,25	-0,44	-0,15	-0,57	-0,53	-0,14	-1,28	-0,04	-1,43
SUM1315MO2	ACH-001389	-0,08	-3,20	-0,01	-0,29	-0,38	-2,84	-0,22	-0,38	-0,17	-0,67	-0,09	-1,35	-0,10	-1,28
SUM149PT	ACH-001390	-0,19	-1,82	0,06	-0,53	-0,47	-2,68	-0,41	0,03	-0,51	-0,64	-0,59	-0,91	-0,10	-0,77
SUM159PT	ACH-001391	-0,42	-2,38	-0,06	-0,09	-0,42	-3,02	-0,55	-0,15	-0,38	-1,29	-0,43	-1,63	-0,16	-1,60
SUM185PE	ACH-001392	-0,33	-2,30	-0,13	0,02	-0,38	-2,56	-0,66	-0,14	-0,26	-0,97	-0,11	-1,26	0,04	-1,57
SUM190PT	ACH-001393	-0,12	-1,74	-0,15	-0,27	-0,63	-3,64	-0,39	-0,12	-0,19	-0,46	-0,04	-1,23	0,11	-1,43
SUM229PE	ACH-001394	-0,16	-3,07	-0,60	-0,34	-0,47	-2,24	-0,47	-0,25	-0,47	-0,71	-0,03	-1,94	-0,18	-0,81
SUM52PE	ACH-001396	-0,34	-1,51	-0,18	-0,53	-0,53	-3,14	-0,52	-0,12	-0,75	-0,55	-0,23	-0,73	-0,07	-2,20
T47D	ACH-000147	0,11	-2,05	-0,14	-0,08	-0,29	-2,79	-0,38	-0,16	-0,26	-0,32	-0,06	-1,35	0,11	-1,44
UACC893	ACH-000554	-0,40	-0,84	-0,12	-0,22	-1,28	-3,87	-0,53	-0,07	-0,21	-0,46	-0,02	-0,55	0,22	-2,59
VP229	ACH-001419	-0,25	-1,93	-0,30	-0,44	-0,41	-2,94	-0,13	-0,29	-0,32	-0,72	-0,32	-1,42	0,05	-1,40
ZR751	ACH-000097	-0,22	-2,37	-0,21	-0,64	-0,71	-3,18	-0,43	-0,18	-0,68	-0,54	-0,08	-1,37	-0,25	-1,96

Supplemental Table S6: DepMap analysis of MT-Rel gene depletion on viability of 47 breast cancer cell lines.

REVIEW 3 – ORGANOTYPIC MODELING OF THE TUMOR LANDSCAPE

We wrote this review in collaboration with Dr. Océane Martin from the lab in which I did my M2 internship. The purpose if this review was to describe the recent advances in organotypic modeling of tumors and the tumor microenvironment during the different steps of carcinogenesis. In this review, we discuss the advantages of using 3D culture models, from the simple multicellular spheroids to the more sophisticated organ-on-chips, to model cancer progression and response to therapy.

This review was published on the 24th of November 2020.

frontiers in Cell and Developmental Biology

REVIEW
published: 24 November 2020
doi: 10.3389/fcell.2020.606039

Organotypic Modeling of the Tumor Landscape

*Maria M. Haykal[1], Clara Nahmias[1], Christine Varon[2] and Océane C. B. Martin[2]**

[1] Université Paris-Saclay, Institut Gustave Roussy, Inserm U981, Biomarqueurs Prédictifs et Nouvelles Stratégies Thérapeutiques en Oncologie, Villejuif, France, [2] Univ. Bordeaux, INSERM, BaRITOn, U1053, Bordeaux, France

Cancer is a complex disease and it is now clear that not only epithelial tumor cells play a role in carcinogenesis. The tumor microenvironment is composed of non-stromal cells, including endothelial cells, adipocytes, immune and nerve cells, and a stromal compartment composed of extracellular matrix, cancer-associated fibroblasts and mesenchymal cells. Tumorigenesis is a dynamic process with constant interactions occurring between the tumor cells and their surroundings. Even though all connections have not yet been discovered, it is now known that crosstalk between actors of the microenvironment drives cancer progression. Taking into account this complexity, it is important to develop relevant models to study carcinogenesis. Conventional 2D culture models fail to represent the entire tumor microenvironment properly and the use of animal models should be decreased with respect to the 3Rs rule. To this aim, *in vitro* organotypic models have been significantly developed these past few years. These models have different levels of complexity and allow the study of tumor cells alone or in interaction with the microenvironment actors during the multiple stages of carcinogenesis. This review depicts recent insights into organotypic modeling of the tumor and its microenvironment all throughout cancer progression. It offers an overview of the crosstalk between epithelial cancer cells and their microenvironment during the different phases of carcinogenesis, from the early cell autonomous events to the late metastatic stages. The advantages of 3D over classical 2D or *in vivo* models are presented as well as the most promising organotypic models. A particular focus is made on organotypic models used for studying cancer progression, from the less complex spheroids to the more sophisticated body-on-a-chip. Last but not least, we address the potential benefits of these models in personalized medicine which is undoubtedly a domain paving the path to new hopes in terms of cancer care and cure.

Keywords: tumor microenvironment, cancer, 3D model, therapies, metastasis, tumor dissemination

OPEN ACCESS

Edited by:
Hasan Korkaya,
Augusta University, United States

Reviewed by:
David Barbie,
Dana–Farber Cancer Institute, United States
Jianyu Rao,
University of California, Los Angeles, United States

***Correspondence:**
Océane C. B. Martin
oceane.martin@u-bordeaux.fr

Specialty section:
This article was submitted to Molecular Medicine, a section of the journal Frontiers in Cell and Developmental Biology

Received: *14 September 2020*
Accepted: *03 November 2020*
Published: *24 November 2020*

Citation:
Haykal MM, Nahmias C, Varon C and Martin OCB (2020) Organotypic Modeling of the Tumor Landscape. Front. Cell Dev. Biol. 8:606039. doi: 10.3389/fcell.2020.606039

INTRODUCTION

Carcinogenesis is a complex multistep process, often described as somatic evolution. Typically, cancer progression involves the accumulation of genetic and/or epigenetic somatic modifications and exposition to environmental factors. Indeed, the development of many tumors is tightly linked with genotoxicity, chronic infections, dietary habits, or autoimmunity; which are all

underlined by inflammation. Early on, Fearon and Vogelstein (1990) described a sequence of defined genetic events driving the formation of colorectal cancers. Afterward, the seminal works of Hanahan and Weinberg (2000, 2011) contributed to shift cancer research from a reductionist point of view with a sole focus on the cancer cell itself to a more comprehensive view involving cues from the neighboring niche. Therefore, carcinogenesis is the fruit of the interplay between multiple cell autonomous and non-autonomous processes, defined as "Hallmarks of cancer," that include genomic instability, proliferative abnormality, stromal reprogramming, angiogenesis, immune suppression and tumor sustaining inflammation. In the following sections, we first define the tumor microenvironment (TME) and briefly depict its different components. We also summarize the recently described interactions between the TME actors and the tumor cells in the cancer progression cascade. In depth understanding of such interactions renders necessary the study of tumor cells within their microenvironment, as this is crucial for cancer progression. In this line of thought, we describe the most promising organotypic models used for modeling cancer progression stages from the initial tumor and its microenvironment to dissemination and metastasis.

PART I—ROLE OF THE MICROENVIRONMENT IN TUMORAL PROGRESSION

The importance of the tumor microenvironment is embodied in the concept that cancer cells do not cause the disease alone, but rather corrupt recruited and neighboring normal cell types to serve as accessories to the crime (Hanahan and Coussens, 2012). In particular, interactions between cancer cells and their microenvironment represent a powerful relationship that influences disease initiation and progression and patient prognosis. For decades, the focus of cancer research has been almost exclusively on epithelial tumor cells. However, in the past few years, there has been a major shift toward the study of the TME, elucidating that tumor progression is dependent on an intricate network of interactions among cancer cells and their surroundings (McAllister and Weinberg, 2014; Taniguchi and Karin, 2018; Hinshaw and Shevde, 2019).

Tumors are unquestionably heterogenous entities, composed of phenotypically distinct cellular populations with different functions. This is illustrated by the clonal evolution theory (Nowell, 1976), TME heterogeneity (Junttila and de Sauvage, 2013) and hierarchal organization of cancer cell subpopulations that includes cancer stem cells (CSCs) and their progenies. Some studies have shown that CSCs are the driving force of tumor formation as they exhibit self-renewal and tumor−initiating capacities and phenotypic plasticity. Plasticity offers cancer cells the ability to switch from a differentiated state to an undifferentiated CSC-like state, responsible for long term tumor growth and drug resistance. Recently, observations of anatomically distinct niches of CSCs within tumors have emerged (reviewed in Plaks et al., 2015; Batlle and Clevers, 2017). These niches could have a role in preserving the plastic phenotype of CSCs and their protection from the immune system. Nonetheless, the heterogeneous tumor is a part of a larger society comprising many other actors that define the tumor microenvironment.

Defining the Tumor Microenvironment

The tumor microenvironment, a diversified compartment of differentiated and progenitor cells, comprises all the non-malignant host cellular and non-cellular components of the tumor niche including, but not restricted to, endothelial cells, adipocytes, cells of the immune and nervous systems, and the stroma.

Non-stromal Components

Endothelial Cells

The most well-known extrinsic modulator of cancer cell growth is neovascularization (Folkman, 1985). Early studies using mouse models show that the angiogenic switch increases the proliferation rate of cancer cells (Folkman et al., 1989). Angiogenesis is crucial to the ability of tumors to thrive and the vascular endothelium is an active participant in the formation of a growth-permissive tumor microenvironment. Vascularization is driven by the hypoxic center of the tumor where hyperproliferation results in increased oxygen demand. Consequently, low oxygen induces the expression of angiogenic proteins like vascular endothelial growth factor (VEGF) and basic fibroblast growth factor (bFGF) (Papetti and Herman, 2002) that activate endothelial cells and attract them toward the tumor to form new vessels, allowing the delivery of nutrients and oxygen. Without angiogenesis, tumors are condemned to quiescence and cell death. Tumor vascularization requires the cooperation of different TME cells, mainly vascular endothelial cells that provide structural integrity to the newly formed vessels and pericytes that ensure their coverage and maturity (Weis and Cheresh, 2011). Endothelial cells also constitute routes to metastatic dissemination via angiogenesis and contribute to resistance to chemotherapies through an overexpression of drug efflux pumps thereby decreasing the tumor's access to the drug (Hida et al., 2013).

Adipocytes

Cancer-associated adipocytes (CAAs) support cancer growth mainly through secretion of adipokines like adipsin (Goto et al., 2019), chemerin (Lu et al., 2019) as well as proinflammatory cytokines (Dirat et al., 2011) and growth factors. CAAs also supply lipids for cancer cell membranes and organelles, induce metabolic reprogramming in cancer cells and provide proteases for cancer cell invasion (reviewed in Deng et al., 2016). Moreover, through the production of tumor-promoting cytokines and factors, they have been shown to confer resistance to hormone therapies, chemotherapies, radiotherapies and targeted therapies in breast cancer (Choi et al., 2018), and to contribute to tumor progression across a variety of obesity-associated cancers (Park et al., 2014) such as esophagus, gastric, liver, kidney, colorectal, pancreatic, breast, ovarian, prostate, and thyroid cancers. Adipocytes from white adipose tissue are recruited to tumors, can differentiate into pericytes and incorporate

into vessel walls contributing to angiogenesis and to tumor proliferation (Zhang et al., 2012).

Infiltrating Immune Cells

Variations in immune profiles are linked to prognosis and therapeutic responses (Gentles et al., 2015). All adult solid tumors contain infiltrates of diverse immune cell subsets that influence pro-tumorigenic and antitumor phenotypes. Of all infiltrating myeloid immune subsets, tumor-associated macrophages (TAMs) best represent this paradigm. TAMs are abundant in all stages of tumor progression and can be polarized into inflammatory M1 or immuno-suppressive M2 macrophages, depending on microenvironment stimuli (Ruffell and Coussens Lisa, 2015). While a subset of TAMs has antitumoral effects, others stimulate cancer cell proliferation by secreting growth factors, produce proteolytic enzymes that digest the ECM to facilitate tumor cell dissemination, and provide a supportive niche for metastatic tumor cells (Mantovani and Allavena, 2015). Eosinophils, primitive actors of innate immunity, have been shown to infiltrate tumors and influence tumor progression. Activated eosinophils secrete IL-10 and IL-12, to inhibit cancer cells growth, or can mediate cell death by direct cytotoxicity (Gatault et al., 2015; Lucarini et al., 2017). However, they can also promote tumor growth by secreting growth factors such as epidermal growth factor (EGF) and transforming growth factor-β1 (TGF-β1) (Grisaru-Tal et al., 2020). As tumors grow, myeloid-derived suppressor cells (MDSCs) (Kumar et al., 2016), immunosuppressive precursors of macrophages and dendritic cells (DCs), promote tumor vascularization and disrupt major mechanisms of immunosurveillance, including tumoral antigen presentation, T cell activation and cytotoxicity (Lindau et al., 2013).

The other major subset of tumor infiltrating immune cells is of lymphoid origin and includes T lymphocytes and natural killer (NK) cells. T lymphocytes can be grouped into 3 major subtypes: (i) T_H lymphocytes divided mainly in two lineages: pro-inflammatory T_{H1} and anti-inflammatory T_{H2}; (ii) Regulatory T cells (T_{reg}), primarily pro-tumorigenic *via* their immunosuppressive activity; and (iii) cytotoxic T cells (T_C) that destroy tumor cells through granzyme and perforin mediated apoptosis (Fridman et al., 2012; Lindau et al., 2013). A third lineage of effector T_H cells, characterized by IL-17 secretion, called T_{H17} cells, acts as double-edged sword in anti-tumor immunity and tumorigenesis (Alizadeh et al., 2013).

Nerve Cells

Peripheral nerves are a common feature of the TME and emerging regulators of cancer progression. Innervated tumors are aggressive, have high proliferative indices and an increased risk of recurrence and metastasis (Magnon et al., 2015). Cancer cells can grow around nerves and invade them in a process called perineural invasion, which represents yet another route for dissemination (reviewed in Jobling et al., 2015). Recently, Zahalka et al. (2017) have shown that adrenergic nerves promote angiogenesis by activating the angiogenic switch in endothelial cells. Moreover, many studies described the formation of new nerve endings within tumors, showing that they stimulate their own innervation, a process termed axonogenesis, by expressing neurotrophic factors (Wang et al., 2014; Huang et al., 2015) or releasing exosomes containing axonal guidance molecules (Madeo et al., 2018). In return, nerves provide the tumor with neurotransmitters that enhance cancer cell growth.

Stromal Components

In healthy tissues, the stroma constitutes the main barrier against tumorigenesis. However, transformed cancer cells can direct stromal reprogramming to support tumor growth and progression.

The stroma is composed of the extracellular matrix (ECM) and specialized connective tissue cells, including fibroblasts, and mesenchymal stem cells.

The Extracellular Matrix

The ECM constitutes the scaffold of tissues and organs, providing the essential signals to maintain tissue architecture and to regulate cell growth and apoptosis. It is a complex network of glycoproteins, proteoglycans, glycosaminoglycans and other macromolecules. About 300 different proteins have been classified as ECM proteins, in what is called the matrisome (Hynes and Naba, 2012). The ECM undergoes constant remodeling by different actors, mainly enzymes such as collagenases and matrix metalloproteases (MMPs) and by fibroblasts. ECM stiffening, induced by increased collagen deposition and crosslinking, disrupts tissue morphogenesis contributing to malignant progression, but also facilitates metastasis and infiltration of immune cells in tumor sites (Bonnans et al., 2014).

Cancer-Associated Fibroblasts

Fibroblasts are widely distributed in all tissues. They constitute a multifunctional cell type residing in the ECM, shaping it by secreting collagens and fibrous macromolecules but also degrading it by releasing proteolytic enzymes, like MMPs.

Fibroblasts are known to modulate immune response by recruiting leucocyte infiltration and regulating inflammation *via* the secretion of growth factors, cytokines and chemokines and to play an important role in maintaining tissue homeostasis (Buckley et al., 2001). During wound healing or fibrosis, another type of specialized fibroblasts called myofibroblasts is present in the tissue (Tomasek et al., 2002). Tumors, for long considered as wounds that do not heal, are associated with a stroma similar to that observed in wound healing called the activated stroma, where fibroblasts resemble myofibroblasts and are called cancer-associated fibroblasts (CAFs). The activated stroma supports cancer progression (Hanahan and Coussens, 2012). Importantly, as for cancer cells, it has been described that CAF population is highly heterogeneous with tumor-promoting or tumor-suppressing CAFs and personalized anticancer therapies targeting CAFs could be of great interest (reviewed in Liu et al., 2019; Mhaidly and Mechta-Grigoriou, 2020).

Mesenchymal Stem Cells

The definition and characteristics of mesenchymal stem cells (MSCs) have been a matter of debate for a long time, and their characterization is an active field of research

(Nombela-Arrieta et al., 2011). It is now established that MSCs are multipotent progenitor cells originating from the bone marrow that can migrate systemically through blood vessels and differentiate into osteoblasts, chondrocytes, or adipocytes. To date, the primary functions of MSCs within the TME are to regulate the immune response by the release of immunomodulatory cytokines and to promote tissue regeneration. Owing to their multipotent and cell fusion properties, they can also be at the origin of vascular cells, contributing to angiogenesis, of myofibroblasts and more rarely of cancer cells themselves.

Crosstalk Between Tumor Cells and Components of the TME in Cancer Progression

The tumor microenvironment plays a critical role in determining tumor fate, and stromal reprogramming has been recognized to be critical for carcinogenesis (Mantovani et al., 2008). Rudolf Virchow first proposed the possibility of a link between chronic inflammation and tumorigenesis in the nineteenth century after the observation of infiltrating leukocytes within tumors. This is now considered a hallmark of cancer. Cancer progression is associated with an ever-evolving tissue interface of direct epithelial–stromal interactions that regulate cancer cell metastasis and disease progression. This section describes the complex crosstalk between the actors of the TME and the cancer cells that take place during the different stages of cancer progression from the early cell autonomous events to the late metastatic stages (**Figure 1**).

Primary Tumor Progression

Cancer cells reprogram the tumor-infiltrating stromal and immune cells, which facilitates primary tumor growth and progression. Therefore, it is important to decipher the reciprocal crosstalk between cancer cells and their heterotypic microenvironment.

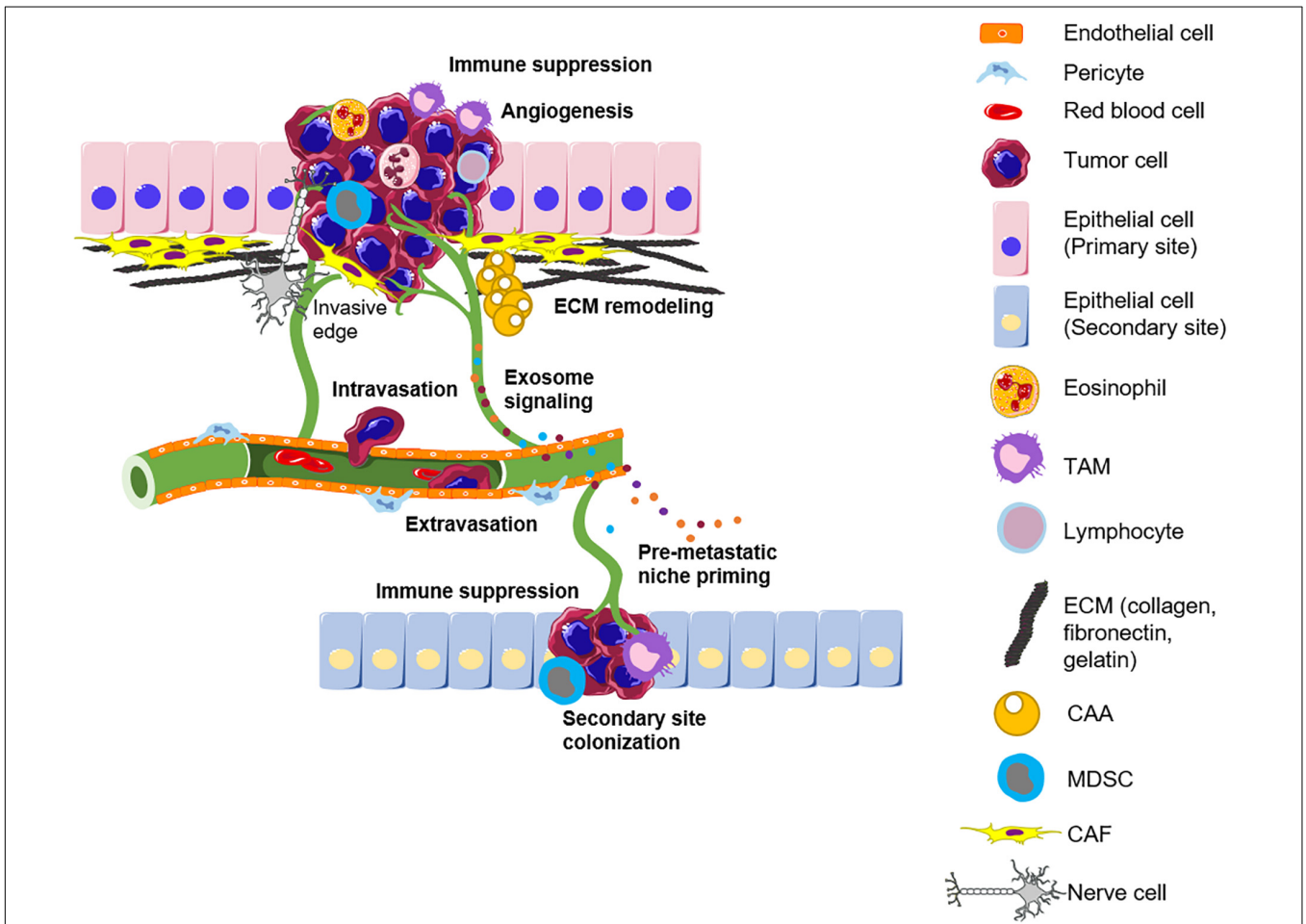

FIGURE 1 | The tumor microenvironment influences the different stages of cancer progression. The primary tumor is infiltrated by different immune subsets and surrounded by a remodeled matrix. Angiogenesis ensures tumor growth by supplying nutrients and also provides a route for metastasis. Intravasation of tumor cells into blood vessels allows their shuttling to a novel site. The secondary site is primed by exosomes secreted by tumor cells and the different actors of the TME to allow the successful seeding of incoming tumor cells. TAM, Tumor-associated macrophage; ECM, Extracellular matrix; CAA, Cancer-associated adipocytes; MDSC, Myeloid-derived suppressor cells; CAF, Cancer-associated fibroblast; TME, Tumor microenvironment.

Epithelial cancer progression is influenced by the cells' contact with immune cells and a carcinogen-exposed stroma (Barcellos-Hoff and Ravani, 2000), by an overexpression of metalloproteases (Fukuda et al., 2011) which create a suitable environment for invasion, or by the stimulation with altered stromal cells like CAFs. In the skin, epigenetic modifications of fibroblasts are induced by ultraviolet exposure, leading to the production of inflammatory cytokines and matrix-remodeling enzymes that together influence the formation of epithelial tumors (Hu et al., 2012). CAFs accumulate in the TME along with tumor growth (Kalluri, 2016) and are activated by cytokines and growth factors of the TME, such as TGF-β (Taniguchi et al., 2020) and Fibroblast Growth Factor (FGF). In their turn, CAFs provide growth factors like VEGF to enhance angiogenesis and vascular permeability (Fukumura et al., 1998). Furthermore, TAMs can support many aspects of tumoral progression. They can secrete mediators that enhance tumor cell survival and proliferation such as growth factors and cytokines [epidermal growth factor (EGF), interleukin 6 (IL-6), and tumor necrosis factor (TNF) (Noy and Pollard Jeffrey, 2014)].

Another crucial step for cancer progression is immune evasion. This is supported mainly by the action of MDSCs. These cells infiltrate the developing tumors and inhibit the mechanisms of immune editing of cytotoxic immune cells, all the while promoting tumor vascularization (Talmadge and Gabrilovich, 2013). TAMs can also promote cancer immune escape by displaying immunosuppressive functions (Noy and Pollard Jeffrey, 2014). Other myeloid cells including neutrophils, monocytes, and eosinophils infiltrate the tumor and promote tumor growth by inhibiting antitumor immunity. Neutrophils can even induce genotoxic damages (Wilson et al., 2015) or recruit tumor-promoting T_{H17} lymphocytes (Ortiz et al., 2015). Additionally, invasion of the basement membrane underlying the epithelium by the tumor cells is a basic step for the upcoming dissemination. For this, CAFs have a physical impact on tumors that results in increased ECM stiffness around tumor cells and consequent mechanical stress. TAMs are also capable of driving invasive phenotypes (Condeelis and Pollard, 2006). In breast cancer, they facilitate invasion of tumor cells by sustaining a signaling paracrine loop involving CSF-1 and EGF (Goswami et al., 2005), and by the secretion of proteases (Gocheva et al., 2010). Thus, once the tumor cells evade the host immune system and gain the ability to invade the surrounding tissue, metastatic dissemination of cancer cells can take place.

Metastatic Dissemination

Metastasis is the leading cause of mortality among cancer patients (Mehlen and Puisieux, 2006). In epithelial tumors, metastasis begins with the cellular invasion of the basement membrane and the subsequent migration of cancer cells into the blood stream. One of the initial steps for primary tumor invasion is epithelial-mesenchymal transition (EMT). Under the influence of various signals, mainly TGF-β, cells gradually lose their epithelial traits while gaining mesenchymal ones that confer migratory capacities (Mani et al., 2008). CAFs participate in a TGF-β and platelet-derived growth factor (PDGF) signaling crosstalk with tumor cells to support EMT and the acquisition of an invasive phenotype (van Zijl et al., 2009). EMT can also enable the acquisition of CSC traits (Mani et al., 2008), suggesting that not only it causes cancer cells to disseminate from the primary tumor but also can provide these cells with the self-renewal properties needed for their subsequent implantation at secondary sites. Although CSCs are not be the only cells responsible for metastasis, the CSC-generated hierarchy of stem-like and differentiated tumor cells is able to initiate metastatic growth (Merlos-Suárez et al., 2011). However, EMT is not the only mechanism used by epithelial cells for migration. Epithelial cancer cells can migrate as single cells, as loosely attached cords or as highly organized collective entities (reviewed in Friedl et al., 2012). During early stages of cancer migration, CAFs increase the production of collagen in the underlying stroma and the fibers become aligned, giving rise to a stiffer ECM hence allowing the migration of cancer cells away from the primary tumor (Conklin et al., 2011). This is largely mediated by CAFs secreted factors that stiffen the ECM, namely enzymes of the Lysyl Oxidase (LOX) family (Kalluri and Zeisberg, 2006).

During metastasis, cancer cells cross the endothelial barrier during a step called **intravasation** to enter the blood stream, and by **extravasation** to exit from circulation into distant tissues, processes that involve different receptors, a plethora of signaling pathways, and interactions with the actors of the surrounding microenvironment (Reymond et al., 2013). Intravasation seems to require the cooperative work of a triad consisting of macrophages that localize to blood vessels where they help tumor cells intravasate into the blood stream (Harney et al., 2015). However, despite the help of macrophages, only 0.01% of cells that intravasate form detectable metastases (Chambers et al., 2002). Cancer cells in the blood stream can be shielded by platelets from NK-mediated cytotoxicity (Palumbo et al., 2005), and platelet binding enhances cancer cell adhesion to vessel wall and subsequent extravasation (Zhang et al., 2011; Schumacher et al., 2013). Inflammation also modulates endothelial crossings through TNF-induced vascular permeabilization, cyclooxygenase 2 (COX2)-dependent prostaglandin production and MMP-mediated tissue remodeling.

Secondary Organ Colonization

Docking of cells in organs to form secondary tumors is not a random process. Organ tropism has been first described by Stephen Paget in 1886 as the "seed-and-soil" theory, in which he suggests that metastasis is not the fruit of hazard but tumors have clear organ preferences for secondary colonization. Paget's theory gave the basis for the description of the premetastatic niche: the primary tumor executes preparative events, preceding detectable metastasis, that render the secondary milieu less hostile for colonization by cancer cells. Studies of the premetastatic niche are still in their infancy but some traits and events are now clearer. Settlement of tumor cells at distant sites is dependent on tumor-secreted cytokines and extracellular vesicles, like exosomes, that enable the premetastatic microenvironment to support their colonization (Liu and Cao, 2016). These tumor-secreted factors communicate to both hematopoietic and mesenchymal stem cell compartments. It has been shown that bone marrow-derived VEGFR1+ cells are already present in premetastatic sites

before tumor cell arrival, suggesting the communication between primary and secondary sites (Kaplan et al., 2005). Seeding is also facilitated by the LOX-mediated fibronectin upregulation in resident fibroblasts and recruitment of myeloid cells (Erler et al., 2009). Neutrophils may also be involved in the priming of metastatic sites. Neutrophils accumulate in premetastatic livers of mice bearing colorectal tumors (Wang et al., 2017) and their accumulation has been shown to be required for pancreatic cancer metastasis (Steele et al., 2016). Recently, it was also shown that omentum resident macrophages are required for ovarian cancer metastasis (Etzerodt et al., 2020). Neutrophils also serve as an energy source to fuel metastatic tumor cells. In a breast cancer model, infiltrating neutrophils are induced to store lipids upon interaction with resident mesenchymal cells in the lung so that when disseminated tumor cells (DTCs) arrive, neutrophils transfer their stored lipids to DTCs for their survival and proliferation (Li et al., 2020).

Colonization of secondary tissues requires the same elements as growth of the primary tumor namely, sufficient nutrients and oxygenation. One important step for metastatic tumor cell survival is the reversal to an epithelial phenotype *via* mesenchymal–epithelial transition (MET) to regain the ability of proliferation and differentiation. Once tumor cells colonize the secondary site, genetic instability inherent in neoplastic cells continues to operate at each cell division, and these cells continue the remodeling of the site, just as described above.

Accordingly, the crosstalk between cancer cells and their microenvironment provides valuable insights into cancer formation, progression and spread. Hence, it is necessary to study cancer as a whole process by modeling the interactions between tumor cells and their microenvironment to improve development of new therapies against cancer progression and metastasis.

PART II—ORGANOTYPIC *IN VITRO* MODELS

Advantages of 3D Models Over 2D Models and Animal Experiments

Cancer research has long been based on two-dimensional (2D) cell culture, mainly in order to earn the right of passage to *in vivo* experiments. Conventional 2D cell cultures allowed the study of many mechanisms that drive tumor growth and the evaluation of optimal drug doses and toxicities. However, currently available cell lines fail to represent the genetic background across the range of human cancers (Huang A. et al., 2020) and may adapt to growth in culture, rather than mimic the behavior of the tumor in a complex microenvironment. Because they also lack all elements of the tumor stroma and surrounding tissue, they fail to mimic the complexity of the tumor microenvironment (Gillet et al., 2011). Owing to this, a large gap exists between the knowledge obtained in these models compared to *in vivo* cancer models because results of 2D experiments rarely predict therapeutic response in animals. This can be explained by the fact that cells cultured in 2D do not have the same architecture as cells *in vivo* that are arranged in three-dimensional (3D) structures unattached to planar surfaces. Furthermore, cultured monolayers lack the capacity to mimic *in vivo* tumoral hypoxia and exhibit a very different metabolism. Consequently, cells in monolayer cultures proliferate at unnaturally rapid rates (Langhans, 2018), differ in gene/protein expression compared to *in vivo* models, and alter their dynamic processes such as cell division and migration (Duval et al., 2017).

Even though *in vivo* experiments have the advantage of being physiologically relevant in contrast to cells cultured out of their bodily context, they have many flaws (Day et al., 2015). Aside from being long, expensive and ethically questionable, the use of human cancer cells in mouse models mostly requires the use of immunocompromised mice that lack, to varying extents, the immune components, thus limiting the advantages of these approaches in modeling tumoral progression and response to drugs. Indeed, the inflammatory immune cell component is lacking in immunocompromised mice. Although the engrafted tumors may exhibit a stromal response with the growth of endothelial cells and fibroblasts, these stromal cells originate from mice and therefore the implication of human TME could not be extrapolated. Moreover, it has recently been shown that patient-derived xenografts (PDXs) present genomic instability with continuously changing copy number alterations landscapes, and so their passaging causes a drift from the original tumor (Ben-David et al., 2017). As such, mouse co-clinical trials using PDXs have shown very little progress beyond proof of concept due to logistical issues (Clohessy and Pandolfi, 2015).

Even with strong supporting preclinical evidence, many targeted therapies produce modest clinical results, a fact now highlighted by the tremendous National Lung Matrix Trial that assessed personalized medicine in non–small cell lung cancer (NSCLC) (Middleton et al., 2020). The results have been fairly disappointing with a response rate of only 10% with some abandons due to lack of treatment efficacy. Genetically engineered mouse models of NSCLC, used for preclinical studies, have mutational burdens more than 100-fold lower than that of human disease (McFadden et al., 2016) arguing for the use of more appropriate preclinical models that integrate the immune and stromal landscapes beyond the genetic aberrations.

Another issue resides in the ability to translate results of immunotherapy from bench to clinic because of the high failure rate observed in human clinical trials after promising results obtained in mouse models. Even the durable clinical benefits observed with immune checkpoint blockers (ICBs) in some tumor types have been seen in a minority of patients (Cardin et al., 2014; Herbst et al., 2014; Hammel et al., 2016). Given the complexity of the tumor microenvironment, it is imperative to create models that include different immune cell types the administered compound may interact with.

Efforts have been made these last few years to "humanize" the mouse's immune system by grafting human hematopoietic stem cells in mice or by transgenic expression of Human Leucocyte Antigen (HLA) (reviewed in Shultz et al., 2012; De La Rochere et al., 2018). However, the high cost of recipient mice, scarcity of human bone marrow acquisitions, engraftment variability, and laborious technical demands represent high inconveniences in a preclinical setting. Hence, optimal mouse studies are very

cumbersome for simultaneous evaluation of numerous drugs and may be inefficient due to the different metabolic processing of drugs between humans and mice. Thus, high-throughput *in vitro* screening systems are essential precursors to *in vivo* evaluations. Developing 3D organotypic models that recapitulate physiological functions would allow further replacement and reduction of animal models as recommended by the 3Rs rule[1].

In vitro 3D cultures recapitulate much better the architecture of tissues and capture the complexity of solid tumors than 2D counterparts, all the while allowing the modeling of different stages of the carcinogenic process (Yamada and Cukierman, 2007; Tanner and Gottesman, 2015). The concentric arrangement of cells in 3D cultures resembles initial avascular stages of solid tumors *in vivo* and non-vascularized micro-metastatic foci. More sophisticated 3D cultures also include different elements of the TME; allowing their use to study cellular interactions within tumors and to model stages of cancer progression. Additionally, genome-wide screens performed on 3D cultures showed improved detection of cancer genes and pathways compared with those performed in 2D (Han et al., 2020). Thus, increased biologically relevant behavior and characteristics could be acquired from genetic editing in organoids, cocultures, and 3D growth models. Moreover, the coalition between biologists, bioengineers and physicians inspired many strategies to reproduce *ex vivo* the complexity of biological systems. These approaches mimic organ topography, mechanical forces of tumor cells, matrix stiffness, functionality, and complexity much better than 2D or even 3D culture systems (van Duinen et al., 2015).

In the following section, we will describe the existing *in vitro* organotypic models for cell culture (**Figure 2**).

Overview of *in vitro* Organotypic Cellular Models

Multicellular Spheroids

Multicellular spheroids (MCSs) or 3D cellular aggregates represent the bridge that fills the gap between 2D cultures and more elaborate 3D techniques. They are fairly representative of the *in vivo* situations because of their heterogeneity as they are composed of proliferating, non-proliferating, well-oxygenated, hypoxic and necrotic cells. Other features of MCSs like cell-cell signaling and interactions, the presence of different cellular layers, the genetic expression profiles, and drug resistance patterns are similar to characteristics of the natural cellular conditions. Currently, there exists many techniques for MCS production such as the forced floating methods in non-adherent plates, hanging drop method, the use of scaffolds and matrices, or even more sophisticated methods using microfluidic systems (reviewed in Ferreira et al., 2018).

MCS can be used for tumoral modeling by either forming homogenous cultures using solely cancer cells, or by more sophisticated cultures using cancer cells with components of the TME like fibroblasts, endothelial cells (Andrique et al., 2019) or immune cells, hence forming heterotypic spheroids. Encapsulating MCS in biomimetic hydrogel scaffolds offers biophysical and biochemical cues that simulate the behavior of extracellular matrix, essential for regulating cancer cell behavior (Li and Kumacheva, 2018).

Organoids

The term organoid, meaning resembling an organ, was first used in 1946 by Smith and Cochrane to describe a case of cystic teratoma. Ever since, it has been inaccurately used to describe some cell structures and aggregates, but the actual definition is now clearer: an organoid is a collection of organ-specific cell types that develops from stem cells, that possesses a minima of specific organ functions, and self-organizes to mimic the architecture of the organ itself (reviewed in Lancaster and Knoblich, 2014). Early pioneering works of Mina Bissell showed that primary epithelial cells derived from mouse mammary glands could self-organize into glandular structures and secrete milk proteins (Lee et al., 1984). These advances were followed by the works of Clevers' lab, that described the generation of intestinal crypt organoids from Lgr5+ stem cells (Sato et al., 2009).

Now, it is recognized that organoids can be generated using two types of stem cells: **pluripotent stem cells (PSCs)** which can be embryonic or induced pluripotent stem cells or **adult stem cells (ASCs)** that reside in adult tissues and are tissue-specific, cultured under specific growth factor cocktails that allow their long-term expansion by mimicking the organ stem cell niche. To date, organoids have been developed for many organs including intestine (Spence et al., 2011), kidney (Takasato et al., 2015), brain (Lancaster et al., 2017), liver (Camp et al., 2017), stomach (McCracken et al., 2014), pancreas (Hohwieler et al., 2017), ovary (Kessler et al., 2015), and lung (Dye et al., 2015) among others. These organoids have been used for multiple approaches such as high-throughput drug screening efficacy and toxicity, host-microbe interactions and infectious diseases (Bartfeld et al., 2015; Leslie et al., 2015; Garcez et al., 2016), and disease modeling (reviewed in Dutta et al., 2017) in particular tumor development, which will be later discussed in detail.

Epithelial organoids recapitulate many aspects of organ development and disease and represent many opportunities for cancer modeling and anticancer drug testing. However, it is important to note the existence of some drawbacks and limitations. Organoids lack the native organ microenvironment: the stromal compartment, immune cells and vascularization, and they are mostly cultured in poorly defined animal matrices. Although, novel synthetic analogous ECM may constitute a better alternative as they are controllable and permit fine tuning of matrix constituents (Gjorevski et al., 2016).

3D-Tissues

The recreation of simple tissues has been described in a cell sheet engineering method using cells grown to confluence on culture dishes grafted with a temperature-responsive polymer, poly-(N-isopropylacrylamide). This technique allows cell growth at 37°C and cell harvest at room temperature as intact cell sheets and subsequently the stacking of different sheets to generate heterotypic thin 3D tissue analogs. Using this technique vascularized tissues (Asakawa et al., 2010) and liver tissue-like structures (Kim et al., 2012) were obtained.

[1]https://www.nc3rs.org.uk/the-3rs

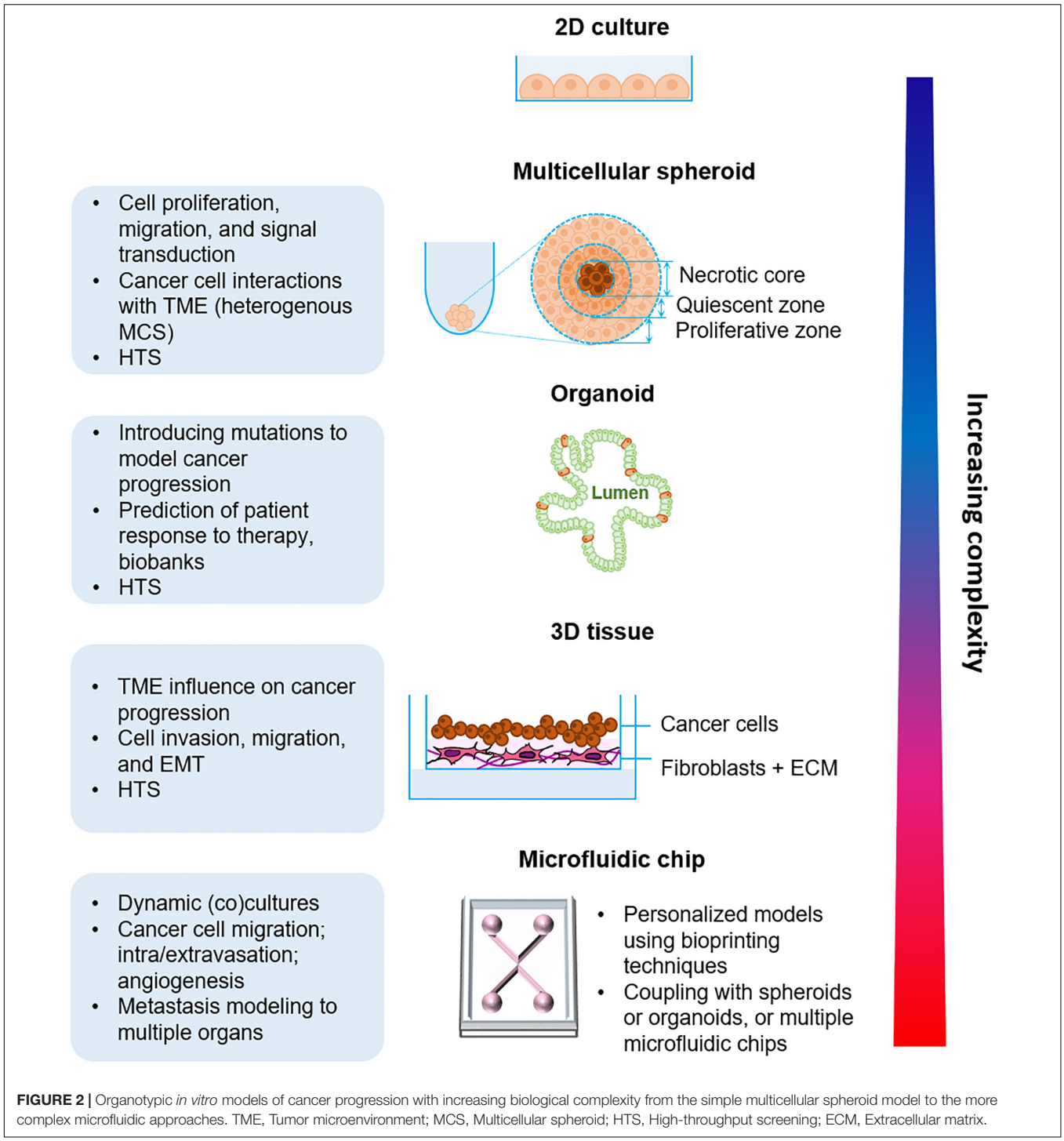

FIGURE 2 | Organotypic *in vitro* models of cancer progression with increasing biological complexity from the simple multicellular spheroid model to the more complex microfluidic approaches. TME, Tumor microenvironment; MCS, Multicellular spheroid; HTS, High-throughput screening; ECM, Extracellular matrix.

Organotypic epithelial raft cultures, originally developed to study keratinocytes (Fuchs, 1990), represent an interesting approach to study epithelial cancer cell behavior, notably cancer cell invasion. These cultures are mechanically supported by semipermeable inserts and are either submerged in medium or maintained at an air–liquid interface. Epithelial tissues can be constructed in stages by first embedding stromal cells, mainly fibroblasts, for several days followed by seeding of epithelial cells on top (Kalabis et al., 2012), or also embed immune cells within the layers to obtain an integral tissue (Huang et al., 2017). These cultures generate a stratified tissue resembling the epithelium seen *in vivo* with a proliferating basal layer and differentiating supra-basal layers. The use of 3D-tissue revealed some advantages compared to organoids when the access to the epithelial cells' apical surfaces is needed, for example to study host-pathogen interactions. To illustrate this using a colonic 3D-tissue, Martin and colleagues have shown that infection with genotoxin-producing *Salmonella* enterica synergises with the

loss of APC to promote genomic instability and carcinogenesis (Martin et al., 2019). Although it should be noted that an elegant recent study has described the possibility to revert organoid polarity allowing access to the apical surfaces of the cells (Co et al., 2019). Miniaturized 3D tissues can be used to facilitate high-throughput drug screening (Dutta et al., 2017).

Microfluidic Approaches

The static nature of nutrients and metabolites in 3D cultures isn't representative of the physiological conditions due to the lack of fluid shear stress and hydrostatic pressure that can greatly influence cell behavior (Polacheck et al., 2011). Microfluidic systems, based on the progress in synthetic biology, have enabled the development of *in vitro* assays that facilitate the study of cellular behavior under a spatiotemporally controlled microenvironment in which molecular, biophysical and cellular components can be tuned according to physiologically relevant parameters. These microfluidic cell culture systems, known under the term organ-on-a-chip, are usually made of continuously perfused hollow microchannels populated by living cells (reviewed in Bhatia and Ingber, 2014). To date, many organs have been successfully modeled in microfluidic devices. One of the first models was lung alveoli that responded to bacterial infection and inflammation (Huh et al., 2010), but also that reflected drug toxicity (Huh et al., 2012). Many studies followed that assessed nephrotoxicity in human kidney tubules-on-a-chip (Jang et al., 2013), liver function (Beckwitt et al., 2018), and more recently, a simulation of a body-on-a-chip multi-organ system (McAleer et al., 2019) to assess drug efficiency and toxicity.

PART III—ORGANOTYPIC MODELS OF CANCER PROGRESSION AND DRUG RESPONSE

Understanding the key aspects of tumoral progression is of utmost importance for the development of novel successful anticancer strategies. Organotypic modeling of these aspects alongside the interactions between the different actors of the TME would allow a better comprehension of the mechanisms that mediate tumoral progression and a first solid step toward preclinical drug screening in physiologically relevant situations. In this section, we describe how the previously mentioned organotypic models have been applied to study the different steps of tumor growth and metastasis (**Table 1**).

Cancer Modeling Using Organotypic Models

Tumor Growth *in situ*—Interactions of Cancer Cells With the TME Elements

Many *in vitro* organotypic models have been used to study tumor initiation and growth and to identify how parenchymal cells (endothelial, epithelial, immune, nerve and stromal cells) and components (ECM, secreted factors) of the TME influence the growth *in situ* of different cancer types.

Modeling cancer initiation using organoid is highly attractive owing to the relative ease of genetic manipulation of cells. Using CRISPR-Cas9 genome editing, tumor suppressors have been identified (Michels et al., 2020), as well as the consequences of mutations in the DNA repair deficiency genes (Drost et al., 2017) or mutations that drive cancer progression (Fumagalli et al., 2017) have been elucidated. Such approaches allow the introduction of defined mutations to transform normal organoids and induce tumor growth, upon xenotransplantation. Matano and colleagues model human colon adenocarcinoma by introducing canonical colorectal cancer (CRC) driver mutations into primary human colon organoid cultures (Matano et al., 2015), revealing that mutations in *APC*, *SMAD4*, *TP53*, and *KRAS* simultaneously are sufficient to model colonic adenomas but not tumorigenesis, perhaps due to the lack of TME components within the organoids. Similarly engineered CRC organoids with *APC* and *KRAS* mutations formed dysplasia and could invade submucosa (Takeda et al., 2019), and transformed mammary organoids formed tumors upon xenotransplantation (Dekkers et al., 2020). Thus, deconstructing carcinogenesis into single genetic elements by engineering cancer genes in untransformed human organoids is a powerful tool for investigating how individual genetic aberrations contribute to the acquisition of cancer phenotypes.

Nevertheless, the genetic alterations driving cancer initiation are supplemented by the interactions of cancer cells with their microenvironment to ensure successful cancer progression. A refined cancer 3D-tissue model using cancer-associated genetic modifications and a stromal department showed the neoplastic transformation of normal epithelia which became invasive (Ridky et al., 2010). Indeed, many tumors are characterized by a prominent stromal compartment that modulates tissue architecture, due to extensive ECM remodeling mainly mediated by CAFs. Adding stromal fibroblasts to prostate organoids facilitated their branching (Richards et al., 2019), while the addition of CAFs to lung squamous carcinoma spheroids recapitulated the pathological changes of tumorigenesis, from invasion and hyperplasia to dysplasia (Chen et al., 2018). Additionally, CAFs were shown to enhance invasion and migration of breast cancer cells in a 3D microfluidic device (Nguyen et al., 2018; Truong et al., 2019).

Furthermore, the coculture of pancreatic stellate cells, a resident mesenchymal cell population that differentiates into CAFs, with pancreatic cancer patient-derived organoids (PDOs) (Öhlund et al., 2017) or with spheroids (Ware et al., 2016) produced a highly desmoplastic stroma, typical of pancreatic carcinomas. Equally investigating the role of the TME in CRC initiation using organoids, Roulis and colleagues performed single-cell RNA sequencing of the murine intestinal mesenchymal niche and found a population of fibroblasts in intestinal crypts that orchestrate intestinal tumorigenesis by exerting paracrine control over tumor initiating stem cells (Roulis et al., 2020).

Other key elements of the TME which significantly affect cancer cell behavior are immune cells. Tumor-immune system interactions have been widely studied by culturing immune cells recovered from patients together with established cancer cell lines in conventional monolayer cultures. However, these approaches fail to account for critical aspects of the TME. Indeed,

TABLE 1 | Organotypic models used to study cancer progression stages and drug response.

	Primary tumor growth	TME-tumor cells interactions	Invasion and migration	Angiogenesis and intravasation	Extravasation and secondary organ colonization	Drug response
Multicellular spheroids	**Tumor growth** Ovarian cancer (Yin et al., 2016) Bladder cancer (Namekawa et al., 2020)	**CAF-mediated interactions** Lung cancer (Chen et al., 2018) Pancreatic cancer (Ware et al., 2016)	**Invasion** Breast cancer (Avgustinova et al., 2016) Colon cancer (Nam et al., 2018) Colorectal cancer (Libanje et al., 2019)	**Vessel sprouting and intravasation** Colon cancer (Ehsan et al., 2014)	**Niche activation and colonization** Breast cancer (del Pozo Martin et al., 2015)	**High-throughput toxicology assay** Breast cancer (Lee et al., 2008)
Organoids	**Introduction of carcinogenesis driver mutations** Colorectal cancer (Matano et al., 2015; Takeda et al., 2019) Breast cancer (Dekkers et al., 2020)	**Stromal interactions** Pancreatic cancer (Öhlund et al., 2017) Intestinal cancer (Roulis et al., 2020) **Immune cells-mediated interactions** Colorectal cancer (Dijkstra et al., 2018) Different tumor types and stages (Neal et al., 2018)	**EMT** Breast cancer (Jung et al., 2019) **Invasion and migration** Breast cancer (Zhang et al., 2019; Georgess et al., 2020)	**Angiogenesis** Breast cancer (Wörsdörfer et al., 2019)	**Extravasation** Breast cancer (Fernández-Periáñez et al., 2013) B Cell Lymphoma (Jia et al., 2020)	**Tumor genetic profiling and response to chemotherapy** Rectal cancer (Ganesh et al., 2019) Pancreatic cancer (Tiriac et al., 2018) Colorectal cancer (van de Wetering et al., 2015; Fujii et al., 2016; Ooft et al., 2019) Gastrointestinal cancers (Vlachogiannis et al., 2018) Renal cancer (Calandrini et al., 2020)
3D-tissues	**Neoplastic transformation** Multiple epithelia (Ridky et al., 2010) Colon cancer (Chen H. J. et al., 2016)	**ECM influence** Glioblastoma (Sood et al., 2019)	**Invasion** Multiple epithelia (Ridky et al., 2010) Glioblastoma (Koh et al., 2018)	**Angiogenic response** Breast cancer (Mazio et al., 2018)	**Colonization** Breast cancer (Xiong et al., 2015)	**High-throughput drug screening** Hepatocarcinoma (Chen et al., 2010) Breast cancer (Brancato et al., 2018)
Microfluidic approaches	**Tumor growth** Breast cancer (Nashimoto et al., 2020)	**CAF-mediated interactions** Breast cancer (Pelon et al., 2020; Truong et al., 2019) Melanoma (Jenkins et al., 2018)	**Invasion and migration** Breast cancer (Chen et al., 2018; Truong et al., 2019) **Migration** Lung cancer (Hsu et al., 2011) Breast cancer (Li et al., 2017)	**Angiogenesis** Microvessels formation and endothelial functions (Zheng et al., 2012) **Angiogenic growth and intravasation** Breast cancer (Zervantonakis et al., 2012; Tang et al., 2017; Sano et al., 2018; Shirure et al., 2018)	**Extravasation** Breast cancer (Jeon et al., 2015; Chen M. B. et al., 2016, 2017) **Metastasis** Breast cancer (Bersini et al., 2014)	**Response to chemotherapy** Lung cancer (Hassell et al., 2017) Breast cancer (Choi et al., 2015)

microfluidic devices customized with human tumor spheroids containing immune cells recapitulate some features of response or resistance to immune checkpoint blockade in melanoma (Jenkins et al., 2018), but without features of the stromal compartment. The recent promise of therapies manipulating tumor-infiltrating immune cells created a particular exigency for human cancer models that recapitulate this TME diversity. In an effort to integrate an immune competent microenvironment to organoid cultures, a platform to induce and analyze tumor-specific T-cell responses to epithelial cancers was established (Dijkstra et al., 2018). Enrichment of functional tumor-reactive T lymphocytes from CRC or non-small cell lung cancer (NSCLC) patients was successfully established by cocultures of peripheral blood lymphocytes with autologous tumor organoids. These tumor-reactive T cells efficiently recognize and kill autologous tumor organoids, while leaving healthy organoids unharmed. Moreover, a recent study presents organoid modeling that preserves primary tumor epithelium with its endogenous immune and non-immune stromal elements (Neal et al., 2018).

Cancer Progression: EMT, Cancer Cell Migration and Invasion

The metastatic cascade initiates with invasion and migration of tumor cells away from the primary tumor. Invasion through the basement membrane is considered a differentiating step between neoplasia and malignant tumors. Because cancer cell contractility and matrix stiffness are critical parameters for invasion, accurate invasion models should include tunable matrix parameters (Wisdom et al., 2018). This is possible using organotypic 3D tissues, where virtually any component can be readily modulated. The stromal compartment can be enriched not only with fibroblasts but with myofibroblasts, endothelial cells or inflammatory cells (reviewed in Coleman, 2014).

To study the basis of cancer invasion, significant efforts have been made to recapitulate tumor–stroma interactions. Multicellular spheroids combined with ECM containing fibroblasts showed enhanced invasion (Avgustinova et al., 2016). However, the tumor and its environment being highly dynamic, microfluidic approaches are more fitted to study tumor cell migration. Indeed, the use of such approaches unveiled the contributions of different cell types to tumor cell migration and invasiveness. A 3D microfluidic coculture system containing side-by-side tumor and stroma regions showed that CAFs enhanced the migration and invasiveness of cancer cells (Truong et al., 2019; Pelon et al., 2020). TGFβ secreted by cancer cells was shown to stimulate fibroblasts to transform into myofibroblasts, which then produced soluble factors that fed back to increase the migration speed of the cancer cells (Hsu et al., 2011). Likewise, the cytokines secreted by macrophages cocultured with cancer cells in a microfluidic device, increased cancer cell migration speed and persistence in a MMP-dependent fashion (Li et al., 2017).

Angiogenesis and Cancer Cell Intravasation

Over the last decade, biomimetic 3D vascular models have been developed, contributing to the understanding of angiogenic processes. Rings of tissue from human umbilical arteries embedded into a 3D matrix were able to sprout in response to tumor-derived proangiogenic factors (Seano et al., 2013). However, vascular organotypic models should not be static as shear forces and blood flow are important for the vascularization process. So, microfluidic approaches have been developed in which endothelial cells are seeded into a channel within ECM to form a primitive vasculature that can be stimulated by angiogenic factors (Zheng et al., 2012; Nguyen et al., 2018), or with an incorporated layer of human bone marrow stromal cells around the channels to recapitulate perivascular barrier function (Alimperti et al., 2017). These microfluidic chips can also be used to trigger vasculogenesis; in that case, instead of seeding endothelial cells beside the matrix, endothelial cells, fibroblasts (Jeon et al., 2014) and tumor cells (Chen M. B. et al., 2017) are loaded within the matrix. Moreover, the ability of organoid-on-a-chip to mimic perfusable blood vessels may address an important issue of organoid use: the lack of nutrient supply. To surmount this, a tumoroid-on-a-chip was developed. It was created in a microfluidic device consisting of three interconnected chambers that enable the self-assembly of endothelial cells into a 3D network of blood vessels and their angiogenic growth toward the organoid-like structures from breast cancer patients (Shirure et al., 2018). However, in such approaches, endothelial cells may not always be free to interact with tumor cells because of the artificial membranes used in the organ-on-a-chip devices. To address this issue, endothelial cells were modified to produce 'reset' vascular endothelial cells (R-VECs) that grew into 3D branching vessels capable of transporting human blood in microfluidic chambers and when transplanted into mice (Palikuqi et al., 2020). These R-VECs adapted their growth upon their coculture with either normal colon organoids or patient-derived colorectal organoids. They arborized normal colon organoids and helped sustain their proliferation while they erratically infiltrated tumor-derived organoids, thus providing a novel physiological platform to study vasculogenesis and angiogenesis.

Entry of tumor cells into the blood stream is a critical step in cancer metastasis. Using microfluidic devices, interactions between invasive cancer cells and endothelial cells have been studied. It was shown that treatment of the endothelium with TNF or coculture with macrophages resulted in rapid and increased numbers of tumor cell–endothelial cell attachment events (Zervantonakis et al., 2012). The secretion of cytokines and chemokines by cancer cells increases the permeability of the endothelial barrier, allowing tumor cells to intravasate and extravasate (Reymond et al., 2013). This feature was modeled using a perfused microfluidic platform containing a vascular compartment with breast cancer cells and their associated endothelial cells separated via a micropillar array interface that allows direct communication of tumor and endothelial cells. The permeability of the vessels was greatly increased in response to the presence of tumor cells or tumor cell-conditioned medium (Tang et al., 2017). Moreover, a tissue-engineered model containing a realistic microvessel in coculture with mammary tumor organoids allowed real-time monitoring of tumor cell-vessel interactions. Using this model, it was shown that tumor cells can reshape, destroy, or intravasate into blood vessels (Silvestri et al., 2020).

Extravasation and Secondary Site Colonization

Cancer cells within vessels must extravasate to colonize new sites. This process is different from intravasation, because the vasculature to be breached is healthier and cancer cells experience fluid shear stresses due to blood flow. After extravasation, cancer cells have one final task to complete: colonization of secondary sites. Extravasation of tumor cells has been shown to occur *via* endothelial apoptosis *in vitro* (Heyder et al., 2002) but *via* necroptosis *in vivo* (Strilic et al., 2016). Thus, accurate modeling of the extravasation and colonization steps requires tissue-specific cell types, microenvironmental cues, and vascularization. Breast cancer cells extravasated through a vascular network into a bone-mimicking microenvironment generated by culturing osteo-differentiated MSCs within a hydrogel, or within a microfluidic device (Jeon et al., 2015; Sano et al., 2018). It was shown that extravasation rates were much higher to the bone microenvironment than to stromal matrices alone. Another similar model showed that β1 integrin expression is required for cancer cells to be able to invade through the endothelial basement membrane (Chen M. B. et al., 2016). Increased complexity and clinical relevance can be incorporated into organ-on-a-chip models, as devices have been developed to mimic interactions between circulating tumor cells (CTCs), endothelium and bone microenvironments as a model of metastasis to bone (Bersini et al., 2014).

Therapeutic Applications of Organotypic Models

Although the demand for anticancer drugs is constantly increasing, their development is slow and fastidious. Monolayer cultured cells are the most widely used *in vitro* models

despite their inability to accurately reflect drug's metabolism and pharmacokinetics in the human body. For years, cell-based drug discovery was based on monolayer cultures of authenticated cell lines (Smith et al., 2010; Barretina et al., 2012), but in this blooming era of precision medicine (Prasad et al., 2016), organotypic models represent great promise for anticancer drug discovery.

In line with this, using an organ-on-a-chip approach, a human lung cancer chip has been developed to study tumor growth patterns and drug response (Hassell et al., 2017). When lung cancer cells were cultured within a physiological-like microenvironment composed of lung endothelial cells, normal lung alveolar epithelium and ECM, they presented rampant growth and resistance to tyrosine kinase inhibitors (TKI) similar to NSCLC patient's response, while they failed to do so in static conventional culture. Likewise, McAleer and colleagues designed a modulable five-chamber multi-organ system to monitor drug effects and simultaneously examine anticancer drug efficacy and off-target toxicity (McAleer et al., 2019). In two models incorporating an array of cancer and healthy human cell types, the system provided insight into the efficacy and toxicity of diclofenac, imatinib, and tamoxifen.

Beyond engineered organoids, organoids derived from patient biopsies or resected tumors, called patient-derived organoids (PDOs) have been successfully cultured with a high success rate and indefinite expansion. These contain tumor cells and stromal cells, thus providing a more realistic microenvironment and they seem to retain the tissue identity of the patient (Tiriac et al., 2018; Ganesh et al., 2019), indicating their great potential for personalized medicine approaches. Recent studies suggest that PDOs mirror clinical responses of individual patients to therapy within a clinically meaningful timeframe and even predict patient response to chemotherapy (Ooft et al., 2019; Pasch et al., 2019). Indeed, PDOs derived from glioblastoma samples were used to test responses to standard of care therapy as well as targeted treatments, like chimeric antigen receptor T (CAR-T) cell immunotherapy in a clinically relevant timescale (Jacob et al., 2020). These PDO properties laid the foundation of what is now known as organoid biobanks (van de Wetering et al., 2015; Calandrini et al., 2020) used for applications such as drug testing, cytological analyses, and xenografting.

With the significant need for biomarker identification of drug response, PDOs could also be considered as a tool for biomarker discovery by analyzing secreted factors such as extracellular vesicles (Huang L. et al., 2020) in contrast with PDX models, due to the presence of contaminating host factors. Although molecular diagnostic testing is now routinely used to determine the choice of targeted therapies for the treatment of cancer patients, patients in advanced stages who have exhausted standard clinical care approaches lack personalized therapeutics and will endure the arduous regimen of chemotherapy and see little or no benefit. Even if the use of functional testing in guiding personalized medicine in still in its infancy, the use of metastatic cancer site derived PDOs to evaluate drug response has proven its efficacy by recapitulating patient response (Weeber et al., 2015; Fujii et al., 2016; Pauli et al., 2017; Vlachogiannis et al., 2018). These evaluation platforms could be of great interest in orienting the treatment of advanced cancer patients.

Shortcomings and Future Directives of Organotypic Models in Translational and Preclinical Settings

The use of organotypic models for cancer modeling is a blooming area of research, however, there are still limitations to their use (Puca et al., 2018; Fujii and Sato, 2020). As an example, studying angiogenesis is rudimentary when it comes to organotypic models. Indeed, the use of vasculature is very basic and organotypic models with other surrounding tissue types are necessary to model more physiological situations. It would be of great interest to model angiogenesis and neovascularization within a transformed organoid. Additionally, complexifying organotypic models by engineering organoids surrounded by muscle, an immune system, and containing a neuronal network along with functional vasculature is something to look forward to in the near future.

When it comes to preclinical studies, organotypic models face many caveats. Spheroid-based 3D models must be used with caution when it comes to clinical relevance. Because they are generated from non-primary tumor cell lines (Friedrich et al., 2009), their use should be restricted to signaling pathways, mechanistic studies and first-line HTS drug screens. More sophisticated models like organoids could be used to validate drug candidates. Stem cell-derived organoids are important for modeling epithelial tumors. However, the lack of standardization and quality control of stem cell culture are an obstacle for their use in clinical studies. The use of pluripotent stem cells for organoid generation can be hampered by the presence of contaminating progenitors that can yield undesired cell types and a small population of undifferentiated PSCs can give rise to tumors that out-compete organ reconstitution *in vivo* (Fowler et al., 2020). Furthermore, due to different culture methods, organoids may present undesired phenotypic variabilities. Interestingly, the recent development of microwell arrays in a matrix-free solid manner allowed the high-throughput assessment of homogenous organoids in 3D culture (Brandenberg et al., 2020). The most exciting aspect for organoid use in clinics is the implementation of PDOs for personalized medicine but this requires that pure PDO cultures can be established, which is not always the case. For example, prostate cancer organoids can only be generated from metastases because normal prostate epithelial cells overgrow cancer cells (Gao et al., 2014). Additionally, the majority of organoids derived from intrapulmonary tumors were overgrown by normal airway organoids (Dijkstra et al., 2020), hampering their use for preclinical studies. Nonetheless, evidence of divergence from primary tumors emerged over time with a decreased abundance of populations from the TME coupled with lower expression of immune-related genes in PDOs (Jacob et al., 2020). Future studies are needed to improve this issue and to maintain the immune compartment, notably for relevant testing of immunotherapies in PDO biobanks.

Microfluidics require refined technical innovations to enable scaling up for HTS. Integration of organotypic models, spheroids, organoids or PDOs, with simulated physiology in microfluidic platforms could represent one of the most relevant *in vitro* models. Two very exciting studies recently reported a near complete body-on-a-chip system. One described an eight organ-chip model linked via vascular endothelial-lined compartments: gut, liver, heart, kidney, lung, heart, brain, blood-brain barrier, and skin (Novak et al., 2020). Using the same approach, intravenously administered cisplatin *via* an arteriovenous reservoir, provided clinically relevant results when compared to *in vivo* behavior (Herland et al., 2020). In this regard, the microfluidic field is still maturing, with a need for regulatory guidelines among the scientific community, specifically for the validation of organ-on-a-chip technology for pharmacological drug testing.

CONCLUDING REMARKS

Understanding tumors, now considered as heterogenous abnormal organs, is insufficient if the tumor cells are studied individually. Methods that are more inclusive are needed that integrate the cellular, genomic, microenvironmental and spatial features of cancers to be able to understand and overcome their numerous resistance mechanisms. Increasing the complexity of the used models lead to the development of many organotypic cancer models that are physiologically relevant and allow in-depth understanding of the interactions that take place within a tumor. Moreover, future studies are needed to standardize organoid culture methods across the scientific community, as this is very heterogenous at the moment. It is also needed to enhance such cultures by adding stromal and immune compartments to organoid culture to better mimic the tumor microenvironment. This is important because patient-derived organoids represent a very promising approach for personalized medicine, as they retain patient and tumor identity and mirror drug response, thus allowing the use of tailored medicine and avoiding the use of unnecessary treatments. Such organoids, cryo-preserved and collected to form biobanks, should they be available to the scientific community, may replace conventional drug screening assays because they fit the requirements of automated high-throughput screenings. More sophisticated organotypic models, fruits of the collaboration between biologists and engineers, could represent the future of cancer research. Multi-organoid systems also referred to as "body-on-a-chip" will enable the development of biologically complex systems, where organoids derived from different tissues are brought together and allowed to integrate, mimicking organ function and allowing disease modeling.

AUTHOR CONTRIBUTIONS

OM conceived the review outline. MH wrote the manuscript and made the figures with support from OM. CN and CV contributed to the final manuscript. All authors contributed to the article and approved the submitted version.

ACKNOWLEDGMENTS

We are grateful to Sylvie Rodrigues-Ferreira for the discussions and comments. We also thank the Foundation Janssen Horizon for supporting MH's Ph.D. thesis.

REFERENCES

Alimperti, S., Mirabella, T., Bajaj, V., Polacheck, W., Pirone, D. M., Duffield, J., et al. (2017). Three-dimensional biomimetic vascular model reveals a RhoA, Rac1, and N-cadherin balance in mural cell–endothelial cell-regulated barrier function. *Proc. Natl. Acad. Sci. U.S.A.* 114, 8758–8763. doi: 10.1073/pnas.1618333114

Alizadeh, D., Katsanis, E., and Larmonier, N. (2013). The Multifaceted Role of Th17 lymphocytes and their associated cytokines in cancer. *Clin. Dev. Immunol.* 2013, 1–11. doi: 10.1155/2013/957878

Andrique, L., Recher, G., Alessandri, K., Pujol, N., Feyeux, M., Bon, P., et al. (2019). A model of guided cell self-organization for rapid and spontaneous formation of functional vessels. *Sci. Adv.* 5:eaau6562. doi: 10.1126/sciadv.aau6562

Asakawa, N., Shimizu, T., Tsuda, Y., Sekiya, S., Sasagawa, T., Yamato, M., et al. (2010). Pre-vascularization of in vitro three-dimensional tissues created by cell sheet engineering. *Biomaterials* 31, 3903–3909. doi: 10.1016/j.biomaterials.2010.01.105

Avgustinova, A., Iravani, M., Robertson, D., Fearns, A., Gao, Q., Klingbeil, P., et al. (2016). Tumour cell-derived Wnt7a recruits and activates fibroblasts to promote tumour aggressiveness. *Nat. Commun.* 7:10305.

Barcellos-Hoff, M. H., and Ravani, S. A. (2000). Irradiated mammary gland stroma promotes the expression of tumorigenic potential by unirradiated epithelial cells. *Cancer Res.* 60, 1254–1260.

Barretina, J., Caponigro, G., Stransky, N., Venkatesan, K., Margolin, A. A., Kim, S., et al. (2012). The Cancer Cell Line Encyclopedia enables predictive modelling of anticancer drug sensitivity. *Nature* 483, 603–607.

Bartfeld, S., Bayram, T., van de Wetering, M., Huch, M., Begthel, H., Kujala, P., et al. (2015). In vitro expansion of human gastric epithelial stem cells and their responses to bacterial infection. *Gastroenterology* 148:126-36.e6.

Batlle, E., and Clevers, H. (2017). Cancer stem cells revisited. *Nat. Med.* 23, 1124–1134.

Beckwitt, C. H., Clark, A. M., Wheeler, S., Taylor, D. L., Stolz, D. B., Griffith, L., et al. (2018). Liver 'organ on a chip'. *Exp. Cell Res.* 363, 15–25.

Ben-David, U., Ha, G., Tseng, Y.-Y., Greenwald, N. F., Oh, C., Shih, J., et al. (2017). Patient-derived xenografts undergo mouse-specific tumor evolution. *Nat. Genet.* 49, 1567–1575. doi: 10.1038/ng.3967

Bersini, S., Jeon, J. S., Dubini, G., Arrigoni, C., Chung, S., Charest, J. L., et al. (2014). A microfluidic 3D in vitro model for specificity of breast cancer metastasis to bone. *Biomaterials* 35, 2454–2461. doi: 10.1016/j.biomaterials.2013.11.050

Bhatia, S. N., and Ingber, D. E. (2014). Microfluidic organs-on-chips. *Nat. Biotechnol.* 32, 760–772. doi: 10.1038/nbt.2989

Bonnans, C., Chou, J., and Werb, Z. (2014). Remodelling the extracellular matrix in development and disease. *Nat. Rev. Mol. Cell Biol.* 15, 786–801. doi: 10.1038/nrm3904

Brancato, V., Gioiella, F., Imparato, G., Guarnieri, D., Urciuolo, F., and Netti, P. A. (2018). 3D breast cancer microtissue reveals the role of tumor microenvironment on the transport and efficacy of free-doxorubicin in vitro. *Acta Biomaterialia* 75, 200–212. doi: 10.1016/j.actbio.2018.05.055

Brandenberg, N., Hoehnel, S., Kuttler, F., Homicsko, K., Ceroni, C., Ringel, T., et al. (2020). High-throughput automated organoid culture via stem-cell aggregation in microcavity arrays. *Nat. Biomed. Eng.* 4, 863–874. doi: 10.1038/s41551-020-0565-2

Buckley, C. D., Pilling, D., Lord, J. M., Akbar, A. N., Scheel-Toellner, D., and Salmon, M. (2001). Fibroblasts regulate the switch from acute resolving to chronic persistent inflammation. *Trends Immunol.* 22, 199–204. doi: 10.1016/s1471-4906(01)01863-4

Calandrini, C., Schutgens, F., Oka, R., Margaritis, T., Candelli, T., Mathijsen, L., et al. (2020). An organoid biobank for childhood kidney cancers that captures disease and tissue heterogeneity. *Nat. Commun.* 11:1310.

Camp, J. G., Sekine, K., Gerber, T., Loeffler-Wirth, H., Binder, H., Gac, M., et al. (2017). Multilineage communication regulates human liver bud development from pluripotency. *Nature* 546, 533–538. doi: 10.1038/nature 22796

Cardin, D. B., Goff, L., Li, C.-I., Shyr, Y., Winkler, C., DeVore, R., et al. (2014). Phase II trial of sorafenib and erlotinib in advanced pancreatic cancer. *Cancer Med.* 3, 572–579. doi: 10.1002/cam4.208

Chambers, A. F., Groom, A. C., and MacDonald, I. C. (2002). Dissemination, and growth of cancer cells in metastatic sites. *Nat. Rev. Cancer* 2, 563–572. doi: 10.1038/nrc865

Chen, A. A., Underhill, G. H., and Bhatia, S. N. (2010). Multiplexed, high-throughput analysis of 3D microtissue suspensions. *Integr. Biol.* 2, 517–527. doi: 10.1039/c0ib00054j

Chen, H. J., Wei, Z., Sun, J., Bhattacharya, A., Savage, D. J., Serda, R., et al. (2016). A recellularized human colon model identifies cancer driver genes. *Nat. Biotechnol.* 34, 845–851. doi: 10.1038/nbt.3586

Chen, M. B., Lamar, J. M., Li, R., Hynes, R. O., and Kamm, R. D. (2016). Elucidation of the roles of tumor integrin β1 in the extravasation stage of the metastasis cascade. *Cancer Res.* 76:2513. doi: 10.1158/0008-5472.can-15-1325

Chen, M. B., Whisler, J. A., Fröse, J., Yu, C., Shin, Y., and Kamm, R. D. (2017). On-chip human microvasculature assay for visualization and quantification of tumor cell extravasation dynamics. *Nat. Protoc.* 12, 865–880. doi: 10.1038/nprot.2017.018

Chen, S., Giannakou, A., Wyman, S., Gruzas, J., Golas, J., Zhong, W., et al. (2018). Cancer-associated fibroblasts suppress SOX2-induced dysplasia in a lung squamous cancer coculture. *Proc. Natl. Acad. Sci. U.S.A.* 115, E11671–E11680.

Choi, J., Cha, Y. J., and Koo, J. S. (2018). Adipocyte biology in breast cancer: from silent bystander to active facilitator. *Progr. Lipid Res.* 69, 11–20. doi: 10.1016/j.plipres.2017.11.002

Choi, Y., Hyun, E., Seo, J., Blundell, C., Kim, H. C., Lee, E., et al. (2015). A microengineered pathophysiological model of early-stage breast cancer. *Lab Chip.* 15, 3350–3357. doi: 10.1039/c5lc00514k

Clohessy, J. G., and Pandolfi, P. P. (2015). Mouse hospital and co-clinical trial project—from bench to bedside. *Nat. Rev. Clin. Oncol.* 12, 491–498. doi: 10.1038/nrclinonc.2015.62

Co, J. Y., Margalef-Català, M., Li, X., Mah, A. T., Kuo, C. J., Monack, D. M., et al. (2019). Controlling epithelial polarity: a human enteroid model for host-pathogen interactions. *Cell Rep.* 26, 2509–2520.e4. doi: 10.1016/j.celrep.2019.01.108

Coleman, S. J. (2014). Pancreatic cancer organotypics: high throughput, preclinical models for pharmacological agent evaluation. *World J. Gastroenterol.* 20, 8471–8481. doi: 10.3748/wjg.v20.i26.8471

Condeelis, J., and Pollard, J. W. (2006). Macrophages: obligate partners for tumor cell migration, invasion, and metastasis. *Cell* 124, 263–266. doi: 10.1016/j.cell.2006.01.007

Conklin, M. W., Eickhoff, J. C., Riching, K. M., Pehlke, C. A., Eliceiri, K. W., Provenzano, P. P., et al. (2011). Aligned collagen is a prognostic signature for survival in human breast carcinoma. *Am. J. Pathol.* 178, 1221–1232. doi: 10.1016/j.ajpath.2010.11.076

Day, C.-P., Merlino, G., and Van Dyke, T. (2015). Preclinical mouse cancer models: a maze of opportunities and challenges. *Cell* 163, 39–53. doi: 10.1016/j.cell.2015.08.068

De La Rochere, P., Guil-Luna, S., Decaudin, D., Azar, G., Sidhu, S. S., and Piaggio, E. (2018). Humanized mice for the study of immuno-oncology. *Trends Immunol.* 39, 748–763. doi: 10.1016/j.it.2018.07.001

Dekkers, J. F., Whittle, J. R., Vaillant, F., Chen, H.-R., Dawson, C., Liu, K., et al. (2020). Modeling Breast Cancer Using CRISPR-Cas9–mediated engineering of human breast organoids. *JNCI* 112, 540–544. doi: 10.1093/jnci/djz196

del Pozo Martin, Y., Park, D., Ramachandran, A., Ombrato, L., Calvo, F., Chakravarty, P., et al. (2015). Mesenchymal cancer cell-stroma crosstalk promotes niche activation, epithelial reversion, and metastatic colonization. *Cell Rep.* 13, 2456–2469. doi: 10.1016/j.celrep.2015.11.025

Deng, T., Lyon, C. J., Bergin, S., Caligiuri, M. A., and Hsueh, W. A. (2016). Obesity, inflammation, and cancer. *Ann. Rev. Pathol.* 11, 421–449.

Dijkstra, K. K., Cattaneo, C. M., Weeber, F., Chalabi, M., van de Haar, J., Fanchi, L. F., et al. (2018). Generation of tumor-reactive T cells by co-culture of peripheral blood lymphocytes and tumor organoids. *Cell* 174:1586-98.e12.

Dijkstra, K. K., Monkhorst, K., Schipper, L. J., Hartemink, K. J., Smit, E. F., Kaing, S., et al. (2020). Challenges in establishing pure lung cancer organoids limit their utility for personalized medicine. *Cell Rep.* 31:107588. doi: 10.1016/j.celrep.2020.107588

Dirat, B., Bochet, L., Dabek, M., Daviaud, D., Dauvillier, S., Majed, B., et al. (2011). Cancer-associated adipocytes exhibit an activated phenotype and contribute to breast cancer invasion. *Cancer Res.* 71, 2455–2465. doi: 10.1158/0008-5472.can-10-3323

Drost, J., van Boxtel, R., Blokzijl, F., Mizutani, T., Sasaki, N., Sasselli, V., et al. (2017). Use of CRISPR-modified human stem cell organoids to study the origin of mutational signatures in cancer. *Science* 358, 234–238. doi: 10.1126/science.aao3130

Dutta, D., Heo, I., and Clevers, H. (2017). Disease Modeling in Stem Cell-Derived 3D Organoid Systems. *Trends Mol. Med.* 23, 393–410. doi: 10.1016/j.molmed.2017.02.007

Duval, K., Grover, H., Han, L.-H., Mou, Y., Pegoraro, A. F., Fredberg, J., et al. (2017). Modeling physiological events in 2D vs. 3D cell culture. *Physiology* 32, 266–277. doi: 10.1152/physiol.00036.2016

Dye, B. R., Hill, D. R., Ferguson, M. A., Tsai, Y.-H., Nagy, M. S., Dyal, R., et al. (2015). In vitro generation of human pluripotent stem cell derived lung organoids. *eLife* 4:e05098.

Ehsan, S. M., Welch-Reardon, K. M., Waterman, M. L., Hughes, C. C. W., and George, S. C. (2014). A three-dimensional in vitro model of tumor cell intravasation. *Integr. Biol.* 6, 603–610. doi: 10.1039/c3ib40170g

Erler, J. T., Bennewith, K. L., Cox, T. R., Lang, G., Bird, D., Koong, A., et al. (2009). Hypoxia-induced lysyl oxidase is a critical mediator of bone marrow cell recruitment to form the premetastatic niche. *Cancer Cell* 15, 35–44. doi: 10.1016/j.ccr.2008.11.012

Etzerodt, A., Moulin, M., Doktor, T. K., Delfini, M., Mossadegh-Keller, N., Bajenoff, M., et al. (2020). Tissue-resident macrophages in omentum promote metastatic spread of ovarian cancer. *J. Exp. Med.* 217:e20191869.

Fearon, E. R., and Vogelstein, B. (1990). A genetic model for colorectal tumorigenesis. *Cell* 61, 759–767. doi: 10.1016/0092-8674(90)90186-i

Fernández-Periáñez, R., Molina-Privado, I., Rojo, F., Guijarro-Muñoz, I., Alonso-Camino, V., Zazo, S., et al. (2013). Basement membrane-rich organoids with functional human blood vessels are permissive niches for human breast cancer metastasis. *PLoS One* 8:e72957. doi: 10.1371/journal.pone.0072957

Ferreira, L. P., Gaspar, V. M., and Mano, J. F. (2018). Design of spherically structured 3D in vitro tumor models -Advances and prospects. *Acta Biomaterialia* 75, 11–34. doi: 10.1016/j.actbio.2018.05.034

Folkman, J. (1985). "Tumor Angiogenesis," in *Advances in Cancer Research*, eds G. Klein, and S. Weinhouse (Cambridge: Academic Press), 175–203.

Folkman, J., Watson, K., Ingber, D., and Hanahan, D. (1989). Induction of angiogenesis during the transition from hyperplasia to neoplasia. *Nature* 339, 58–61. doi: 10.1038/339058a0

Fowler, J. L., Ang, L. T., and Loh, K. M. (2020). A critical look: challenges in differentiating human pluripotent stem cells into desired cell types and organoids. *WIREs Dev. Biol.* 9:e368.

Fridman, W. H., Pagès, F., Sautès-Fridman, C., and Galon, J. (2012). The immune contexture in human tumours: impact on clinical outcome. *Nat. Rev. Cancer* 12, 298–306. doi: 10.1038/nrc3245

Friedl, P., Locker, J., Sahai, E., and Segall, J. E. (2012). Classifying collective cancer cell invasion. *Nat. Cell Biol.* 14, 777–783. doi: 10.1038/ncb2548

Friedrich, J., Seidel, C., Ebner, R., and Kunz-Schughart, L. A. (2009). Spheroid-based drug screen: considerations and practical approach. *Nat. Protoc.* 4, 309–324. doi: 10.1038/nprot.2008.226

Fuchs, E. (1990). Epidermal differentiation: the bare essentials. *J. Cell Biol.* 111, 2807–2814. doi: 10.1083/jcb.111.6.2807

Fujii, M., and Sato, T. (2020). Somatic cell-derived organoids as prototypes of human epithelial tissues and diseases. *Nat. Mater.* doi: 10.1038/s41563-020-0754-0 [Epub ahead of print].

Fujii, M., Shimokawa, M., Date, S., Takano, A., Matano, M., Nanki, K., et al. (2016). A colorectal tumor organoid library demonstrates progressive loss of niche factor requirements during tumorigenesis. *Cell Stem Cell* 18, 827–838. doi: 10.1016/j.stem.2016.04.003

Fukuda, A., Wang Sam, C., Morris John, P., Folias Alexandra, E., Liou, A., Kim Grace, E., et al. (2011). Stat3 and MMP7 contribute to pancreatic ductal adenocarcinoma initiation and progression. *Cancer Cell* 19, 441–455. doi: 10.1016/j.ccr.2011.03.002

Fukumura, D., Xavier, R., Sugiura, T., Chen, Y., Park, E.-C., Lu, N., et al. (1998). Tumor Induction of VEGF promoter activity in stromal cells. *Cell* 94, 715–725. doi: 10.1016/s0092-8674(00)81731-6

Fumagalli, A., Drost, J., Suijkerbuijk, S. J. E., van Boxtel, R., de Ligt, J., Offerhaus, G. J., et al. (2017). Genetic dissection of colorectal cancer progression by orthotopic transplantation of engineered cancer organoids. *Proc. Natl. Acad. Sci. U.S.A.* 114, E2357–E2364.

Ganesh, K., Wu, C., O'Rourke, K. P., Szeglin, B. C., Zheng, Y., Sauvé, C.-E. G., et al. (2019). A rectal cancer organoid platform to study individual responses to chemoradiation. *Nat. Med.* 25, 1607–1614.

Gao, D., Vela, I., Sboner, A., Iaquinta Phillip, J., Karthaus Wouter, R., Gopalan, A., et al. (2014). Organoid cultures derived from patients with advanced prostate cancer. *Cell* 159, 176–187.

Garcez, P. P., Loiola, E. C., Madeiro da Costa, R., Higa, L. M., Trindade, P., Delvecchio, R., et al. (2016). Zika virus impairs growth in human neurospheres and brain organoids. *Science* 352:40780.

Gatault, S., Delbeke, M., Driss, V., Sarazin, A., Dendooven, A., Kahn, J.-E., et al. (2015). IL-18 Is Involved in Eosinophil-Mediated Tumoricidal Activity against a Colon Carcinoma Cell Line by Upregulating LFA-1 and ICAM-1. *J. Immunol.* 195, 2483–2492. doi: 10.4049/jimmunol.1402914

Gentles, A. J., Newman, A. M., Liu, C. L., Bratman, S. V., Feng, W., Kim, D., et al. (2015). The prognostic landscape of genes and infiltrating immune cells across human cancers. *Nat. Med.* 21, 938–945. doi: 10.1038/nm.3909

Georgess, D., Padmanaban, V., Sirka, O. K., Coutinho, K., Choi, A., Frid, G., et al. (2020). Twist1-induced epithelial dissemination requires Prkd1 signaling. *Cancer Res.* 80, 204–218. doi: 10.1158/0008-5472.can-18-3241

Gillet, J.-P., Calcagno, A. M., Varma, S., Marino, M., Green, L. J., Vora, M. I., et al. (2011). Redefining the relevance of established cancer cell lines to the study of mechanisms of clinical anti-cancer drug resistance. *Proc. Natl. Acad. Sci. U.S.A.* 108, 18708–18713. doi: 10.1073/pnas.1111840108

Gjorevski, N., Sachs, N., Manfrin, A., Giger, S., Bragina, M. E., Ordóñez-Morán, P., et al. (2016). Designer matrices for intestinal stem cell and organoid culture. *Nature* 539, 560–564. doi: 10.1038/nature20168

Gocheva, V., Wang, H.-W., Gadea, B. B., Shree, T., Hunter, K. E., Garfall, A. L., et al. (2010). IL-4 induces cathepsin protease activity in tumor-associated macrophages to promote cancer growth and invasion. *Genes Dev.* 24, 241–255. doi: 10.1101/gad.1874010

Goswami, S., Sahai, E., Wyckoff, J. B., Cammer, M., Cox, D., Pixley, F. J., et al. (2005). Macrophages Promote the Invasion of Breast Carcinoma Cells via a Colony-Stimulating Factor-1/Epidermal Growth Factor Paracrine Loop. *Cancer Res.* 65, 5278–5283. doi: 10.1158/0008-5472.can-04-1853

Goto, H., Shimono, Y., Funakoshi, Y., Imamura, Y., Toyoda, M., Kiyota, N., et al. (2019). Adipose-derived stem cells enhance human breast cancer growth and cancer stem cell-like properties through adipsin. *Oncogene* 38, 767–779. doi: 10.1038/s41388-018-0477-8

Grisaru-Tal, S., Itan, M., Klion, A. D., and Munitz, A. (2020). A new dawn for eosinophils in the tumour microenvironment. *Nat. Rev. Cancer* 20, 594–607. doi: 10.1038/s41568-020-0283-9

Hammel, P., Huguet, F., van Laethem, J.-L., Goldstein, D., Glimelius, B., Artru, P., et al. (2016). Effect of Chemoradiotherapy vs Chemotherapy on Survival in Patients With Locally Advanced Pancreatic Cancer Controlled After 4 Months of Gemcitabine With or Without Erlotinib: the LAP07 Randomized Clinical Trial. *JAMA* 315, 1844–1853. doi: 10.1001/jama.2016.4324

Han, K., Pierce, S. E., Li, A., Spees, K., Anderson, G. R., Seoane, J. A., et al. (2020). CRISPR screens in cancer spheroids identify 3D growth-specific vulnerabilities. *Nature* 580, 136–141. doi: 10.1038/s41586-020-2099-x

Hanahan, D., and Coussens, L. M. (2012). Accessories to the crime: functions of cells recruited to the tumor microenvironment. *Cancer Cell* 21, 309–322. doi: 10.1016/j.ccr.2012.02.022

Hanahan, D., and Weinberg, R. A. (2000). The hallmarks of cancer. *Cell* 100, 57–70.

Hanahan, D., and Weinberg, R. A. (2011). Hallmarks of cancer: the next generation. *Cell* 144, 646–674. doi: 10.1016/j.cell.2011.02.013

Harney, A. S., Arwert, E. N., Entenberg, D., Wang, Y., Guo, P., Qian, B.-Z., et al. (2015). Real-time imaging reveals local, transient vascular permeability, and tumor cell intravasation stimulated by TIE2hi macrophage-derived VEGFA. *Cancer Discov.* 5, 932–943. doi: 10.1158/2159-8290.cd-15-0012

Hassell, B. A., Goyal, G., Lee, E., Sontheimer-Phelps, A., Levy, O., Chen, C. S., et al. (2017). Human organ chip models recapitulate orthotopic lung cancer growth. therapeutic responses, and tumor dormancy in vitro. *Cell Rep.* 21, 508–516. doi: 10.1016/j.celrep.2017.09.043

Herbst, R. S., Soria, J.-C., Kowanetz, M., Fine, G. D., Hamid, O., Gordon, M. S., et al. (2014). Predictive correlates of response to the anti-PD-L1 antibody MPDL3280A in cancer patients. *Nature* 515, 563–567.

Herland, A., Maoz, B. M., Das, D., Somayaji, M. R., Prantil-Baun, R., Novak, R., et al. (2020). Quantitative prediction of human pharmacokinetic responses to drugs via fluidically coupled vascularized organ chips. *Nat. Biomed. Eng.* 4, 421–436. doi: 10.1038/s41551-019-0498-9

Heyder, C., Gloria-Maercker, E., Entschladen, F., Hatzmann, W., Niggemann, B., Zänker, K., et al. (2002). Realtime visualization of tumor cell/endothelial cell interactions during transmigration across the endothelial barrier. *J. Cancer Res. Clin. Oncol.* 128, 533–538. doi: 10.1007/s00432-002-0377-7

Hida, K., Akiyama, K., Ohga, N., Maishi, N., and Hida, Y. (2013). Tumour endothelial cells acquire drug resistance in a tumour microenvironment. *J. Biochem.* 153, 243–249. doi: 10.1093/jb/mvs152

Hinshaw, D. C., and Shevde, L. A. (2019). The Tumor Microenvironment Innately Modulates Cancer Progression. *Cancer Res.* 79, 4557–4566. doi: 10.1158/0008-5472.can-18-3962

Hohwieler, M., Illing, A., Hermann, P. C., Mayer, T., Stockmann, M., Perkhofer, L., et al. (2017). Human pluripotent stem cell-derived acinar/ductal organoids generate human pancreas upon orthotopic transplantation and allow disease modelling. *Gut* 66, 473–486. doi: 10.1136/gutjnl-2016-312423

Hsu, T.-H., Xiao, J.-L., Tsao, Y.-W., Kao, Y.-L., Huang, S.-H., Liao, W.-Y., et al. (2011). Analysis of the paracrine loop between cancer cells and fibroblasts using a microfluidic chip. *Lab Chip.* 11, 1808–1814. doi: 10.1039/c1lc20090a

Hu, B., Castillo, E., Harewood, L., Ostano, P., Reymond, A., Dummer, R., et al. (2012). Multifocal epithelial tumors and field cancerization from loss of mesenchymal CSL signaling. *Cell* 149, 1207–1220. doi: 10.1016/j.cell.2012.03.048

Huang, A., Garraway, L. A., Ashworth, A., and Weber, B. (2020). Synthetic lethality as an engine for cancer drug. (target). discovery. *Nat. Rev. Drug Discov.* 19, 23–38. doi: 10.1038/s41573-019-0046-z

Huang, L., Bockorny, B., Paul, I., Akshinthala, D., Frappart, P.-O., Gandarilla, O., et al. (2020). PDX-derived organoids model in vivo drug response and secrete biomarkers. *JCI Insight* 5:e135544.

Huang, S., Boda, B., Vernaz, J., Ferreira, E., Wiszniewski, L., and Constant, S. (2017). Establishment and characterization of an in vitro human small airway model (SmallAir^{TM}). *Eur. J. Pharmaceut. Biopharmaceut.* 118, 68–72. doi: 10.1016/j.ejpb.2016.12.006

Huang, S.-M., Lin, C., Lin, H.-Y., Chiu, C.-M., Fang, C.-W., Liao, K.-F., et al. (2015). Brain-derived neurotrophic factor regulates cell motility in human colon cancer. *Endocrine Relat. Cancer* 22, 455–464. doi: 10.1530/erc-15-0007

Huh, D., Leslie, D. C., Matthews, B. D., Fraser, J. P., Jurek, S., Hamilton, G. A., et al. (2012). A human disease model of drug toxicity–induced pulmonary edema in a lung-on-a-chip microdevice. *Sci. Transl. Med.* 4:159ra147. doi: 10.1126/scitranslmed.3004249

Huh, D., Matthews, B. D., Mammoto, A., Montoya-Zavala, M., Hsin, H. Y., and Ingber, D. E. (2010). Reconstituting organ-level lung functions on a chip. *Science* 328, 1662–1668. doi: 10.1126/science.1188302

Hynes, R. O., and Naba, A. (2012). Overview of the matrisome–an inventory of extracellular matrix constituents and functions. *Cold Spring Harb. Perspect. Biol.* 4:a004903. doi: 10.1101/cshperspect.a004903

Jacob, F., Salinas, R. D., Zhang, D. Y., Nguyen, P. T. T., Schnoll, J. G., Wong, S. Z. H., et al. (2020). A patient-derived glioblastoma organoid model and biobank recapitulates inter- and intra-tumoral heterogeneity. *Cell* 180, 188-204.e22.

Jang, K.-J., Mehr, A. P., Hamilton, G. A., McPartlin, L. A., Chung, S., Suh, K.-Y., et al. (2013). Human kidney proximal tubule-on-a-chip for drug transport and nephrotoxicity assessment. *Integr. Biol.* 5, 1119–1129. doi: 10.1039/c3ib40049b

Jenkins, R. W., Aref, A. R., Lizotte, P. H., Ivanova, E., Stinson, S., Zhou, C. W., et al. (2018). Ex Vivo Profiling of PD-1 blockade using organotypic tumor spheroids. *Cancer Discov.* 8, 196–215.

Jeon, J. S., Bersini, S., Gilardi, M., Dubini, G., Charest, J. L., Moretti, M., et al. (2015). Human 3D vascularized organotypic microfluidic assays to study breast cancer cell extravasation. *Proc. Natl. Acad. Sci. U.S.A.* 112, 214–219. doi: 10.1073/pnas.1417115112

Jeon, J. S., Bersini, S., Whisler, J. A., Chen, M. B., Dubini, G., Charest, J. L., et al. (2014). Generation of 3D functional microvascular networks with human mesenchymal stem cells in microfluidic systems. *Integr. Biol.* 6, 555–563. doi: 10.1039/c3ib40267c

Jia, X., Gábris, F., Jacobsen, Ó, Bedics, G., Botz, B., Helyes, Z., et al. (2020). Foliate Lymphoid Aggregates as Novel Forms of Serous Lymphocyte Entry Sites of Peritoneal B Cells and High-Grade B Cell Lymphomas. *J. Immunol.* 204, 23–36. doi: 10.4049/jimmunol.1900851

Jobling, P., Pundavela, J., Oliveira, S. M. R., Roselli, S., Walker, M. M., and Hondermarck, H. (2015). Nerve-cancer cell cross-talk: a novel promoter of tumor progression. *Cancer Res.* 75, 1777–1781. doi: 10.1158/0008-5472.can-14-3180

Jung, H.-Y., Fattet, L., Tsai, J. H., Kajimoto, T., Chang, Q., Newton, A. C., et al. (2019). Apical–basal polarity inhibits epithelial–mesenchymal transition and tumour metastasis by PAR-complex-mediated SNAI1 degradation. *Nat. Cell Biol.* 21, 359–371. doi: 10.1038/s41556-019-0291-8

Junttila, M. R., and de Sauvage, F. J. (2013). Influence of tumour microenvironment heterogeneity on therapeutic response. *Nature* 501, 346–354. doi: 10.1038/nature12626

Kalabis, J., Wong, G. S., Vega, M. E., Natsuizaka, M., Robertson, E. S., Herlyn, M., et al. (2012). Isolation and characterization of mouse and human esophageal epithelial cells in 3D organotypic culture. *Nat. Protoc.* 7, 235–246. doi: 10.1038/nprot.2011.437

Kalluri, R. (2016). The biology and function of fibroblasts in cancer. *Nat. Rev. Cancer* 16, 582–598. doi: 10.1038/nrc.2016.73

Kalluri, R., and Zeisberg, M. (2006). Fibroblasts in cancer. *Nat. Rev. Cancer* 6, 392–401.

Kaplan, R. N., Riba, R. D., Zacharoulis, S., Bramley, A. H., Vincent, L., Costa, C., et al. (2005). VEGFR1-positive haematopoietic bone marrow progenitors initiate the pre-metastatic niche. *Nature* 438, 820–827. doi: 10.1038/nature04186

Kessler, M., Hoffmann, K., Brinkmann, V., Thieck, O., Jackisch, S., Toelle, B., et al. (2015). The Notch and Wnt pathways regulate stemness and differentiation in human fallopian tube organoids. *Nat. Commun.* 6:8989.

Kim, K., Ohashi, K., Utoh, R., Kano, K., and Okano, T. (2012). Preserved liver-specific functions of hepatocytes in 3D co-culture with endothelial cell sheets. *Biomaterials* 33, 1406–1413. doi: 10.1016/j.biomaterials.2011.10.084

Koh, I., Cha, J., Park, J., Choi, J., Kang, S.-G., and Kim, P. (2018). The mode and dynamics of glioblastoma cell invasion into a decellularized tissue-derived extracellular matrix-based three-dimensional tumor model. *Sci. Rep.* 8:4608.

Kumar, V., Patel, S., Tcyganov, E., and Gabrilovich, D. I. (2016). The nature of myeloid-derived suppressor cells in the tumor microenvironment. *Trends Immunol.* 37, 208–220.

Lancaster, M. A., Corsini, N. S., Wolfinger, S., Gustafson, E. H., Phillips, A. W., Burkard, T. R., et al. (2017). Guided self-organization and cortical plate formation in human brain organoids. *Nat. Biotechnol.* 35, 659–666. doi: 10.1038/nbt.3906

Lancaster, M. A., and Knoblich, J. A. (2014). Organogenesis in a dish: modeling development and disease using organoid technologies. *Science* 345:1247125. doi: 10.1126/science.1247125

Langhans, S. A. (2018). Three-dimensional in vitro cell culture models in drug discovery and drug repositioning. *Front. Pharmacol.* 9:6. doi: 10.3389/fphar.2018.00006

Lee, E. Y., Parry, G., and Bissell, M. J. (1984). Modulation of secreted proteins of mouse mammary epithelial cells by the collagenous substrata. *J. Cell Biol.* 98, 146–155. doi: 10.1083/jcb.98.1.146

Lee, M.-Y., Kumar, R. A., Sukumaran, S. M., Hogg, M. G., Clark, D. S., and Dordick, J. S. (2008). Three-dimensional cellular microarray for high-throughput toxicology assays. *Proc. Natl. Acad. Sci. U.S.A.* 105, 59–63. doi: 10.1073/pnas.0708756105

Leslie, J. L., Huang, S., Opp, J. S., Nagy, M. S., Kobayashi, M., Young, V. B., et al. (2015). Persistence and toxin production by clostridium difficile within human intestinal organoids result in disruption of epithelial paracellular barrier function. *Infect. Immunity* 83, 138–145. doi: 10.1128/iai.02561-14

Li, P., Lu, M., Shi, J., Gong, Z., Hua, L., Li, Q., et al. (2020). Lung mesenchymal cells elicit lipid storage in neutrophils that fuel breast cancer lung metastasis. *Nat. Immunol.* 21, 1444–1455. doi: 10.1038/s41590-020-0783-5

Li, R., Hebert, J. D., Lee, T. A., Xing, H., Boussommier-Calleja, A., Hynes, R. O., et al. (2017). Macrophage-Secreted TNFα and TGFβ1 influence migration speed and persistence of cancer cells in 3D tissue culture via independent pathways. *Cancer Res.* 77, 279–290. doi: 10.1158/0008-5472.can-16-0442

Li, Y., and Kumacheva, E. (2018). Hydrogel microenvironments for cancer spheroid growth and drug screening. *Sci. Adv.* 4:eaas8998. doi: 10.1126/sciadv.aas8998

Libanje, F., Raingeaud, J., Luan, R., Thomas, Z., Zajac, O., Veiga, J., et al. (2019). ROCK2 inhibition triggers the collective invasion of colorectal adenocarcinomas. *EMBO J.* 38:e99299.

Lindau, D., Gielen, P., Kroesen, M., Wesseling, P., and Adema, G. J. (2013). The immunosuppressive tumour network: myeloid-derived suppressor cells, regulatory T cells and natural killer T cells. *Immunology* 138, 105–115. doi: 10.1111/imm.12036

Liu, T., Han, C., Wang, S., Fang, P., Ma, Z., Xu, L., et al. (2019). Cancer-associated fibroblasts: an emerging target of anti-cancer immunotherapy. *J. Hematol. Oncol.* 12:86.

Liu, Y., and Cao, X. (2016). Characteristics and significance of the pre-metastatic niche. *Cancer Cell* 30, 668–681. doi: 10.1016/j.ccell.2016.09.011

Lu, Z., Liang, J., He, Q., Wan, Q., Hou, J., Lian, K., et al. (2019). The serum biomarker chemerin promotes tumorigenesis and metastasis in oral squamous cell carcinoma. *Clin. Sci.* 133, 681–695. doi: 10.1042/cs20181023

Lucarini, V., Zicchedda, G., Macchia, I., La Sorsa, V., Peschiaroli, F., Buccione, C., et al. (2017). IL-33 restricts tumor growth and inhibits pulmonary metastasis in melanoma-bearing mice through eosinophils. *OncoImmunology* 6:e1317420. doi: 10.1080/2162402x.2017.1317420

Madeo, M., Colbert, P. L., Vermeer, D. W., Lucido, C. T., Cain, J. T., Vichaya, E. G., et al. (2018). Cancer exosomes induce tumor innervation. *Nat. Commun.* 9:4284.

Magnon, C., Hall, S. J., Lin, J., Xue, X., Gerber, L., Freedland, S. J., et al. (2015). Autonomic nerve development contributes to prostate cancer progression. *Science* 341:1236361. doi: 10.1126/science.1236361

Mani, S. A., Guo, W., Liao, M.-J., Eaton, E. N., Ayyanan, A., Zhou, A. Y., et al. (2008). The epithelial-mesenchymal transition generates cells with properties of stem cells. *Cell* 133, 704–715.

Mantovani, A., and Allavena, P. (2015). The interaction of anticancer therapies with tumor-associated macrophages. *J. Exp. Med.* 212, 435–445. doi: 10.1084/jem.20150295

Mantovani, A., Allavena, P., Sica, A., and Balkwill, F. (2008). Cancer-related inflammation. *Nature* 454, 436–444.

Martin, O. C. B., Bergonzini, A., D'Amico, F., Chen, P., Shay, J. W., Dupuy, J., et al. (2019). Infection with genotoxin-producing *Salmonella enterica* synergises with loss of the tumour suppressor *APC* in promoting genomic instability via the PI3K pathway in colonic epithelial cells. *Cell. Microbiol.* 21:e13099. doi: 10.1111/cmi.13099

Matano, M., Date, S., Shimokawa, M., Takano, A., Fujii, M., Ohta, Y., et al. (2015). Modeling colorectal cancer using CRISPR-Cas9–mediated engineering of human intestinal organoids. *Nat. Med.* 21, 256–262. doi: 10.1038/nm.3802

Mazio, C., Casale, C., Imparato, G., Urciuolo, F., and Netti, P. A. (2018). Recapitulating spatiotemporal tumor heterogeneity in vitro through engineered breast cancer microtissues. *Acta Biomaterialia* 73, 236–249. doi: 10.1016/j.actbio.2018.04.028

McAleer, C. W., Long, C. J., Elbrecht, D., Sasserath, T., Bridges, L. R., Rumsey, J. W., et al. (2019). Multi-organ system for the evaluation of efficacy and off-target toxicity of anticancer therapeutics. *Sci. Transl. Med.* 11:eaav1386. doi: 10.1126/scitranslmed.aav1386

McAllister, S. S., and Weinberg, R. A. (2014). The tumour-induced systemic environment as a critical regulator of cancer progression and metastasis. *Nat. Cell Biol.* 16, 717–727. doi: 10.1038/ncb3015

McCracken, K. W., Catá, E. M., Crawford, C. M., Sinagoga, K. L., Schumacher, M., Rockich, B. E., et al. (2014). Modelling human development and disease in pluripotent stem-cell-derived gastric organoids. *Nature* 516, 400–404.

McFadden, D. G., Politi, K., Bhutkar, A., Chen, F. K., Song, X., Pirun, M., et al. (2016). Mutational landscape of EGFR-, MYC-, and Kras-driven genetically

engineered mouse models of lung adenocarcinoma. *Proc. Natl. Acad. Sci. U.S.A.* 113:E6409.

Mehlen, P., and Puisieux, A. (2006). Metastasis: a question of life or death. *Nat. Rev. Cancer* 6, 449–458. doi: 10.1038/nrc1886

Merlos-Suárez, A., Barriga Francisco, M., Jung, P., Iglesias, M., Céspedes María, V., Rossell, D., et al. (2011). The intestinal stem cell signature identifies colorectal cancer stem cells and predicts disease relapse. *Cell Stem Cell* 8, 511–524. doi: 10.1016/j.stem.2011.02.020

Mhaidly, R., and Mechta-Grigoriou, F. (2020). Fibroblast heterogeneity in tumor micro-environment: role in immunosuppression and new therapies. *Semin. Immunol.* [Online ahead of print] doi: 10.1016/j.smim.2020.101417

Michels, B. E., Mosa, M. H., Streibl, B. I., Zhan, T., Menche, C., Abou-El-Ardat, K., et al. (2020). Pooled In Vitro and In Vivo CRISPR-Cas9 screening identifies tumor suppressors in human colon organoids. *Cell Stem Cell* 26, 782-92.e7.

Middleton, G., Fletcher, P., Popat, S., Savage, J., Summers, Y., Greystoke, A., et al. (2020). The National Lung Matrix Trial of personalized therapy in lung cancer. *Nature* 583, 807–812.

Nam, S. H., Kim, D., Lee, D., Lee, H.-M., Song, D.-G., Jung, J. W., et al. (2018). Lysyl-tRNA synthetase–expressing colon spheroids induce M2 macrophage polarization to promote metastasis. *J. Clin. Invest.* 128, 5034–5055. doi: 10.1172/jci99806

Namekawa, T., Ikeda, K., Horie-Inoue, K., Suzuki, T., Okamoto, K., Ichikawa, T., et al. (2020). ALDH1A1 in patient-derived bladder cancer spheroids activates retinoic acid signaling leading to TUBB3 overexpression and tumor progression. *Int. J. Cancer* 146, 1099–1113. doi: 10.1002/ijc.32505

Nashimoto, Y., Okada, R., Hanada, S., Arima, Y., Nishiyama, K., Miura, T., et al. (2020). Vascularized cancer on a chip: the effect of perfusion on growth and drug delivery of tumor spheroid. *Biomaterials* 229:119547. doi: 10.1016/j.biomaterials.2019.119547

Neal, J. T., Li, X., Zhu, J., Giangarra, V., Grzeskowiak, C. L., Ju, J., et al. (2018). Organoid modeling of the tumor immune microenvironment. *Cell* 175, 1972-88.e16.

Nguyen, M., De Ninno, A., Mencattini, A., Mermet-Meillon, F., Fornabaio, G., Evans, S. S., et al. (2018). Dissecting effects of anti-cancer drugs and cancer-associated fibroblasts by on-chip reconstitution of immunocompetent tumor microenvironments. *Cell Rep.* 25, 3884-93.e3.

Nombela-Arrieta, C., Ritz, J., and Silberstein, L. E. (2011). The elusive nature and function of mesenchymal stem cells. *Nat. Rev. Mol. Cell Biol.* 12, 126–131. doi: 10.1038/nrm3049

Novak, R., Ingram, M., Marquez, S., Das, D., Delahanty, A., Herland, A., et al. (2020). Robotic fluidic coupling and interrogation of multiple vascularized organ chips. *Nat. Biomed. Eng.* 4, 407–420. doi: 10.1038/s41551-019-0497-x

Nowell, P. (1976). The clonal evolution of tumor cell populations. *Science* 194, 23–28. doi: 10.1126/science.959840

Noy, R., and Pollard Jeffrey, W. (2014). Tumor-associated macrophages: from mechanisms to therapy. *Immunity* 41, 49–61. doi: 10.1016/j.immuni.2014.06.010

Öhlund, D., Handly-Santana, A., Biffi, G., Elyada, E., Almeida, A. S., Ponz-Sarvise, M., et al. (2017). Distinct populations of inflammatory fibroblasts and myofibroblasts in pancreatic cancer. *J. Exp. Med.* 214, 579–596. doi: 10.1084/jem.20162024

Ooft, S. N., Weeber, F., Dijkstra, K. K., McLean, C. M., Kaing, S., van Werkhoven, E., et al. (2019). Patient-derived organoids can predict response to chemotherapy in metastatic colorectal cancer patients. *Sci. Transl. Med.* 11:eaay2574.

Ortiz, M. L., Kumar, V., Martner, A., Mony, S., Donthireddy, L., Condamine, T., et al. (2015). Immature myeloid cells directly contribute to skin tumor development by recruiting IL-17–producing CD4+ T cells. *J. Exp. Med.* 212, 351–367. doi: 10.1084/jem.20140835

Palikuqi, B., Nguyen, D.-H. T., Li, G., Schreiner, R., Pellegata, A. F., Liu, Y., et al. (2020). Adaptable haemodynamic endothelial cells for organogenesis and tumorigenesis. *Nature* 585, 426–432. doi: 10.1038/s41586-020-2712-z

Palumbo, J. S., Talmage, K. E., Massari, J. V., La Jeunesse, C. M., Flick, M. J., Kombrinck, K. W., et al. (2005). Platelets and fibrin(ogen) increase metastatic potential by impeding natural killer cell–mediated elimination of tumor cells. *Blood* 105, 178–185. doi: 10.1182/blood-2004-06-2272

Papetti, M., and Herman, I. M. (2002). Mechanisms of normal and tumor-derived angiogenesis. *Am. J. Physiol. Cell Physiol.* 282, C947–C970.

Park, J., Morley, T. S., Kim, M., Clegg, D. J., and Scherer, P. E. (2014). Obesity and cancer—mechanisms underlying tumour progression and recurrence. *Nat. Rev. Endocrinol.* 10, 455–465. doi: 10.1038/nrendo.2014.94

Pasch, C. A., Favreau, P. F., Yueh, A. E., Babiarz, C. P., Gillette, A. A., Sharick, J. T., et al. (2019). Patient-derived cancer organoid cultures to predict sensitivity to chemotherapy and radiation. *Clin. Cancer Res.* 25, 5376–5387. doi: 10.1158/1078-0432.ccr-18-3590

Pauli, C., Hopkins, B. D., Prandi, D., Shaw, R., Fedrizzi, T., Sboner, A., et al. (2017). Personalized in vitro and in vivo cancer models to guide precision medicine. *Cancer Discov.* 7, 462–477.

Pelon, F., Bourachot, B., Kieffer, Y., Magagna, I., Mermet-Meillon, F., Bonnet, I., et al. (2020). Cancer-associated fibroblast heterogeneity in axillary lymph nodes drives metastases in breast cancer through complementary mechanisms. *Nat. Commun.* 11:404.

Plaks, V., Kong, N., and Werb, Z. (2015). The cancer stem cell niche: how essential is the niche in regulating stemness of tumor cells? *Cell Stem Cell* 16, 225–238. doi: 10.1016/j.stem.2015.02.015

Polacheck, W. J., Charest, J. L., and Kamm, R. D. (2011). Interstitial flow influences direction of tumor cell migration through competing mechanisms. *Proc. Natl. Acad. Sci. U.S.A.* 108, 11115–11120. doi: 10.1073/pnas.1103581108

Prasad, V., Fojo, T., and Brada, M. (2016). Precision oncology: origins, optimism, and potential. *Lancet Oncol.* 17, e81–e86.

Puca, L., Bareja, R., Prandi, D., Shaw, R., Benelli, M., Karthaus, W. R., et al. (2018). Patient derived organoids to model rare prostate cancer phenotypes. *Nat. Commun.* 9:2404.

Reymond, N., d'Água, B. B., and Ridley, A. J. (2013). Crossing the endothelial barrier during metastasis. *Nat. Rev. Cancer* 13, 858–870. doi: 10.1038/nrc3628

Richards, Z., McCray, T., Marsili, J., Zenner, M. L., Manlucu, J. T., Garcia, J., et al. (2019). Prostate stroma increases the viability and maintains the branching phenotype of human prostate organoids. *iScience* 12, 304–317. doi: 10.1016/j.isci.2019.01.028

Ridky, T. W., Chow, J. M., Wong, D. J., and Khavari, P. A. (2010). Invasive three-dimensional organotypic neoplasia from multiple normal human epithelia. *Nat. Med.* 16, 1450–1455. doi: 10.1038/nm.2265

Roulis, M., Kaklamanos, A., Schernthanner, M., Bielecki, P., Zhao, J., Kaffe, E., et al. (2020). Paracrine orchestration of intestinal tumorigenesis by a mesenchymal niche. *Nature* 580, 524–529. doi: 10.1038/s41586-020-2166-3

Ruffell, B., and Coussens Lisa, M. (2015). Macrophages and therapeutic resistance in cancer. *Cancer Cell* 27, 462–472. doi: 10.1016/j.ccell.2015.02.015

Sano, E., Mori, C., Nashimoto, Y., Yokokawa, R., Kotera, H., and Torisawa Y-s. (2018). Engineering of vascularized 3D cell constructs to model cellular interactions through a vascular network. *Biomicrofluidics* 12:042204. doi: 10.1063/1.5027183

Sato, T., Vries, R. G., Snippert, H. J., van de Wetering, M., Barker, N., Stange, D. E., et al. (2009). Single Lgr5 stem cells build crypt-villus structures in vitro without a mesenchymal niche. *Nature* 459, 262–265. doi: 10.1038/nature07935

Schumacher, D., Strilic, B., Sivaraj Kishor, K., Wettschureck, N., and Offermanns, S. (2013). Platelet-derived nucleotides promote tumor-cell transendothelial migration and metastasis via P2Y2 receptor. *Cancer Cell* 24, 130–137. doi: 10.1016/j.ccr.2013.05.008

Seano, G., Chiaverina, G., Gagliardi, P. A., di Blasio, L., Sessa, R., Bussolino, F., et al. (2013). Modeling human tumor angiogenesis in a three-dimensional culture system. *Blood* 121, e129–e137.

Shirure, V. S., Bi, Y., Curtis, M. B., Lezia, A., Goedegebuure, M. M., Goedegebuure, S. P., et al. (2018). Tumor-on-a-chip platform to investigate progression and drug sensitivity in cell lines and patient-derived organoids. *Lab Chip.* 18, 3687–3702. doi: 10.1039/c8lc00596f

Shultz, L. D., Brehm, M. A., Garcia-Martinez, J. V., and Greiner, D. L. (2012). Humanized mice for immune system investigation: progress, promise and challenges. *Nat. Rev. Immunol.* 12, 786–798. doi: 10.1038/nri3311

Silvestri, V. L., Henriet, E., Linville, R. M., Wong, A. D., Searson, P. C., and Ewald, A. J. (2020). A tissue-engineered 3D microvessel model reveals the dynamics of mosaic vessel formation in breast cancer. *Cancer Res.* 80, 4288–4301. doi: 10.1158/0008-5472.can-19-1564

Smith, S. C., Baras, A. S., Lee, J. K., and Theodorescu, D. (2010). The COXEN Principle: translating signatures of in vitro chemosensitivity into tools for

clinical outcome prediction and drug discovery in cancer. *Cancer Res.* 70, 1753–1758. doi: 10.1158/0008-5472.can-09-3562

Sood, D., Tang-Schomer, M., Pouli, D., Mizzoni, C., Raia, N., Tai, A., et al. (2019). 3D extracellular matrix microenvironment in bioengineered tissue models of primary pediatric and adult brain tumors. *Nat. Commun.* 10:4529.

Spence, J. R., Mayhew, C. N., Rankin, S. A., Kuhar, M. F., Vallance, J. E., Tolle, K., et al. (2011). Directed differentiation of human pluripotent stem cells into intestinal tissue in vitro. *Nature* 470, 105–109.

Steele, C. W., Karim, S. A., Leach, J. D. G., Bailey, P., Upstill-Goddard, R., Rishi, L., et al. (2016). CXCR2 inhibition profoundly suppresses metastases and augments immunotherapy in pancreatic ductal adenocarcinoma. *Cancer Cell* 29, 832–845. doi: 10.1016/j.ccell.2016.04.014

Strilic, B., Yang, L., Albarrán-Juárez, J., Wachsmuth, L., Han, K., Müller, U. C., et al. (2016). Tumour-cell-induced endothelial cell necroptosis via death receptor 6 promotes metastasis. *Nature* 536, 215–218. doi: 10.1038/nature19076

Takasato, M., Er, P. X., Chiu, H. S., Maier, B., Baillie, G. J., Ferguson, C., et al. (2015). Kidney organoids from human iPS cells contain multiple lineages and model human nephrogenesis. *Nature* 526, 564–568. doi: 10.1038/nature15695

Takeda, H., Kataoka, S., Nakayama, M., Ali, M. A. E., Oshima, H., Yamamoto, D., et al. (2019). CRISPR-Cas9–mediated gene knockout in intestinal tumor organoids provides functional validation for colorectal cancer driver genes. *Proc. Natl. Acad. Sci. U.S.A.* 116, 15635–15644. doi: 10.1073/pnas.1904714116

Talmadge, J. E., and Gabrilovich, D. I. (2013). History of myeloid-derived suppressor cells. *Nat. Rev. Cancer* 13, 739–752.

Tang, Y., Soroush, F., Sheffield, J. B., Wang, B., Prabhakarpandian, B., and Kiani, M. F. (2017). A biomimetic microfluidic tumor microenvironment platform mimicking the EPR effect for rapid screening of drug delivery systems. *Sci. Rep.* 7:9359.

Taniguchi, K., and Karin, M. (2018). NF-κB, inflammation, immunity and cancer: coming of age. *Nat. Rev. Immunol.* 18, 309–324. doi: 10.1038/nri.2017.142

Taniguchi, S., Elhance, A., Duzer, A. V., Kumar, S., Leitenberger, J. J., and Oshimori, N. (2020). Tumor-initiating cells establish an IL-33–TGF-b niche signaling loop to promote cancer progression. *Science* 369:eaay1813.

Tanner, K., and Gottesman, M. M. (2015). Beyond 3D culture models of cancer. *Sci. Transl. Med.* 7:283s9.

Tiriac, H., Belleau, P., Engle, D. D., Plenker, D., Deschênes, A., Somerville, T. D. D., et al. (2018). Organoid profiling identifies common responders to chemotherapy in pancreatic cancer. *Cancer Discov.* 8, 1112–1129.

Tomasek, J. J., Gabbiani, G., Hinz, B., Chaponnier, C., and Brown, R. A. (2002). Myofibroblasts and mechano-regulation of connective tissue remodelling. *Nat. Rev. Mol. Cell Biol.* 3, 349–363. doi: 10.1038/nrm809

Truong, D. D., Kratz, A., Park, J. G., Barrientos, E. S., Saini, H., Nguyen, T., et al. (2019). A Human organotypic microfluidic tumor model permits investigation of the interplay between patient-derived fibroblasts and breast cancer cells. *Cancer Res.* 79, 3139–3151. doi: 10.1158/0008-5472.can-18-2293

van de Wetering, M., Francies Hayley, E., Francis Joshua, M., Bounova, G., Iorio, F., Pronk, A., et al. (2015). Prospective derivation of a living organoid biobank of colorectal cancer patients. *Cell* 161, 933–945. doi: 10.1016/j.cell.2015.03.053

van Duinen, V., Trietsch, S. J., Joore, J., Vulto, P., and Hankemeier, T. (2015). Microfluidic 3D cell culture: from tools to tissue models. *Curr. Opin. Biotechnol.* 35, 118–126. doi: 10.1016/j.copbio.2015.05.002

van Zijl, F., Mair, M., Csiszar, A., Schneller, D., Zulehner, G., Huber, H., et al. (2009). Hepatic tumor–stroma crosstalk guides epithelial to mesenchymal transition at the tumor edge. *Oncogene* 28, 4022–4033. doi: 10.1038/onc.2009.253

Vlachogiannis, G., Hedayat, S., Vatsiou, A., Jamin, Y., Fernández-Mateos, J., Khan, K., et al. (2018). Patient-derived organoids model treatment response of metastatic gastrointestinal cancers. *Science* 359, 920–926.

Wang, D., Sun, H., Wei, J., Cen, B., and DuBois, R. N. (2017). CXCL1 is critical for premetastatic niche formation and metastasis in colorectal cancer. *Cancer Res.* 77, 3655–3665. doi: 10.1158/0008-5472.can-16-3199

Wang, K., Demir, I. E., D'Haese, J. G., Tieftrunk, E., Kujundzic, K., Schorn, S., et al. (2014). The neurotrophic factor neurturin contributes toward an aggressive cancer cell phenotype, neuropathic pain and neuronal plasticity in pancreatic cancer. *Carcinogenesis* 35, 103–113. doi: 10.1093/carcin/bgt312

Ware, M. J., Keshishian, V., Law, J. J., Ho, J. C., Favela, C. A., Rees, P., et al. (2016). Generation of an in vitro 3D PDAC stroma rich spheroid model. *Biomaterials* 108, 129–142. doi: 10.1016/j.biomaterials.2016.08.041

Weeber, F., van de Wetering, M., Hoogstraat, M., Dijkstra, K. K., Krijgsman, O., Kuilman, T., et al. (2015). Preserved genetic diversity in organoids cultured from biopsies of human colorectal cancer metastases. *Proc. Natl. Acad. Sci. U.S.A.* 112, 13308–13311. doi: 10.1073/pnas.1516689112

Weis, S. M., and Cheresh, D. A. (2011). Tumor angiogenesis: molecular pathways and therapeutic targets. *Nat. Med.* 17, 1359–1370. doi: 10.1038/nm.2537

Wilson, C. L., Jurk, D., Fullard, N., Banks, P., Page, A., Luli, S., et al. (2015). NFκB1 is a suppressor of neutrophil-driven hepatocellular carcinoma. *Nat. Commun.* 6:6818.

Wisdom, K. M., Adebowale, K., Chang, J., Lee, J. Y., Nam, S., Desai, R., et al. (2018). Matrix mechanical plasticity regulates cancer cell migration through confining microenvironments. *Nat. Commun.* 9:4144.

Wörsdörfer, P., Dalda, N., Kern, A., Krüger, S., Wagner, N., Kwok, C. K., et al. (2019). Generation of complex human organoid models including vascular networks by incorporation of mesodermal progenitor cells. *Sci. Rep.* 9:15663.

Xiong, G., Flynn, T. J., Chen, J., Trinkle, C., and Xu, R. (2015). Development of an ex vivo breast cancer lung colonization model utilizing a decellularized lung matrix. *Integr. Biol.* 7, 1518–1525. doi: 10.1039/c5ib00157a

Yamada, K. M., and Cukierman, E. (2007). Modeling tissue morphogenesis and cancer in 3D. *Cell* 130, 601–610. doi: 10.1016/j.cell.2007.08.006

Yin, M., Li, X., Tan, S., Zhou, H. J., Ji, W., Bellone, S., et al. (2016). Tumor-associated macrophages drive spheroid formation during early transcoelomic metastasis of ovarian cancer. *J. Clin. Invest.* 126, 4157–4173. doi: 10.1172/jci87252

Zahalka, A. H., Arnal-Estapé, A., Maryanovich, M., Nakahara, F., Cruz, C. D., Finley, L. W. S., et al. (2017). Adrenergic nerves activate an angio-metabolic switch in prostate cancer. *Science* 358, 321–326. doi: 10.1126/science.aah5072

Zervantonakis, I. K., Hughes-Alford, S. K., Charest, J. L., Condeelis, J. S., Gertler, F. B., and Kamm, R. D. (2012). Three-dimensional microfluidic model for tumor cell intravasation and endothelial barrier function. *Proc. Natl. Acad. Sci. U.S.A.* 109, 13515–13520. doi: 10.1073/pnas.1210182109

Zhang, J., Goliwas, K. F., Wang, W., Taufalele, P. V., Bordeleau, F., and Reinhart-King, C. A. (2019). Energetic regulation of coordinated leader–follower dynamics during collective invasion of breast cancer cells. *Proc. Natl. Acad. Sci. U.S.A.* 116, 7867–7872. doi: 10.1073/pnas.1809964116

Zhang, N., Zhang, W.-J., Cai, H.-Q., Liu, H.-L., Peng, L., Li, C.-H., et al. (2011). Platelet adhesion and fusion to endothelial cell facilitate the metastasis of tumor cell in hypoxia-reoxygenation condition. *Clin. Exp. Metastasis* 28, 1–12. doi: 10.1007/s10585-010-9353-9

Zhang, Y., Daquinag, A. C., Amaya-Manzanares, F., Sirin, O., Tseng, C., and Kolonin, M. G. (2012). Stromal progenitor cells from endogenous adipose tissue contribute to pericytes and adipocytes that populate the tumor microenvironment. *Cancer Res.* 72, 5198–5208. doi: 10.1158/0008-5472.can-12-0294

Zheng, Y., Chen, J., Craven, M., Choi, N. W., Totorica, S., Diaz-Santana, A., et al. (2012). In vitro microvessels for the study of angiogenesis and thrombosis. *Proc. Natl. Acad. Sci. U.S.A.* 109, 9342–9347. doi: 10.1073/pnas.1201240109

Conflict of Interest: The authors declare that the research was conducted in the absence of any commercial or financial relationships that could be construed as a potential conflict of interest.

VIII. SYNTHÈSE

Introduction

Le cancer du sein, en tant que pathologie complexe, reste au cœur des préoccupations médicales en raison de sa diversité et de ses formes agressives, nécessitant des approches thérapeutiques spécifiques. Dans cette perspective, les sous-types de cancers du sein déficients en ATIP3 se démarquent par leur agressivité et un taux d'aneuploïdie élevé couplé à une signature d'instabilité chromosomique. La présente thèse s'inscrit dans cette quête cruciale de solutions novatrices, visant à identifier des cibles thérapeutiques adaptées et à comprendre les mécanismes moléculaires sous-jacents.

Contexte

Le cancer du sein demeure la pathologie la plus fréquemment diagnostiquée chez les femmes, avec une incidence mondiale élevée. Face à la diversité génomique et phénotypique de cette maladie, il devient impératif de développer des stratégies thérapeutiques personnalisées, particulièrement pour les sous-types les plus agressifs. Les cancers du sein déficients en ATIP3, caractérisés par des profils aneuploïdes marqués, se distinguent par leur progression rapide, justifiant ainsi l'exploration de cibles thérapeutiques alternatives.

Objectif de la thèse

L'objectif fondamental de cette thèse était de répondre au besoin pressant de cibler spécifiquement les cancers du sein déficients en ATIP3, en identifiant une cible thérapeutique pertinente. L'étude se concentre sur la kinase WEE1, régulatrice du cycle cellulaire, dans l'espoir de tirer profit de la vulnérabilité particulière des cellules aneuploïdes pour élaborer des stratégies thérapeutiques plus efficaces.

Résultats et avancées scientifiques

Les résultats de cette étude révèlent une sensibilité accrue des cellules aneuploïdes, spécifiquement déficientes en ATIP3, à l'inhibition de WEE1. L'aneuploïdie, caractéristique inévitable de ces cancers, engendre une instabilité génomique et un stress de réplication, des phénomènes exacerbés en cas de carence en ATIP3. Ces anomalies conduisent à des défauts mitotiques sévères et à une pulvérisation chromosomique, émergeant comme des mécanismes clés dans la réponse cellulaire à l'inhibition de WEE1.

Dans le contexte spécifique des cancers du sein, les cellules tumorales exprimant faiblement ATIP3 présentent une vulnérabilité marquée l'inhibition de WEE1. Cette observation suggère la possibilité d'une fenêtre thérapeutique spécifique pour cette sous-population de patients, ouvrant ainsi des perspectives prometteuses pour des interventions plus ciblées et personnalisées. Les études *in vivo* sur des xénogreffes de cancer du sein montrent que l'administration d'un inhibiteur de WEE1 prévient la croissance tumorale, avec un effet plus marqué sur les tumeurs déficientes en ATIP3. Ces observations confirment l'efficacité potentielle de l'inhibition de WEE1 dans le contexte clinique des cancers du sein déficients en ATIP3.

Exploration des Mécanismes Moléculaires :

Pour élucider les mécanismes sous-jacents, des analyses approfondies ont été menées. En particulier, les cellules déficientes en ATIP3, exposées à l'inhibition de WEE1, présentent des niveaux accrus de stress réplicatif et de dommages à l'ADN. L'inhibition de WEE1 induit un phénotype mitotique atypique, caractérisé par le détachement des protéines centromériques de l'ADN, conduisant à une pulvérisation chromosomique spectaculaire. Ce phénomène est exacerbé dans les cellules déficientes en ATIP3, soulignant la contribution significative de cette protéine à la régulation des processus mitotiques et à la préservation de l'intégrité chromosomique. En explorant les acteurs moléculaires impliqués, l'implication

cruciale de l'hélicase/nucléase DNA2 a été mise en évidence. La suppression de DNA2 a atténué les phénotypes mitotiques anormaux et a prévenu la pulvérisation chromosomique dans les cellules déficientes en ATIP3 exposées à l'inhibition de WEE1. Ces résultats soulignent le rôle central de DNA2 dans la régulation des conséquences mitotiques suite à une inhibition de WEE1 dans le contexte aneuploïde.

Implications Thérapeutiques et Perspectives Futures

Au-delà de la compréhension moléculaire, cette étude apporte des implications concrètes pour le développement de thérapies novatrices contre les cancers du sein déficients en ATIP3. En exploitant la vulnérabilité des cellules aneuploïdes à l'inhibition de WEE1, cette approche offre une alternative prometteuse aux traitements conventionnels, visant à surmonter la résistance tumorale et à améliorer les résultats cliniques. Ces résultats ouvrent ainsi la voie à des essais cliniques ciblés et à des avancées significatives dans la prise en charge des formes les plus agressives de cancer du sein.

université PARIS-SACLAY | ÉCOLE DOCTORALE Cancérologie : biologie - médecine - santé (CBMS)

Titre : Cibler le cycle cellulaire : une nouvelle stratégie thérapeutique contre les cancers du sein déficients en protéine ATIP3

Mots clés : cancer du sein, aneuploïdie, WEE1, dommages à l'ADN, biomarqueur

Résumé : Le cancer du sein est la première cause de décès par cancer chez la femme. Il est nécessaire de trouver des biomarqueurs permettant l'accès à des thérapies personnalisées, notamment pour les cancers du sein triple-négatifs (TNBC). ATIP3 est une protéine associée aux microtubules identifiée pour la première fois au sein de notre équipe. Une déficience en ATIP3 est retrouvée dans 65-80% des cancers TNBC et est associée à un mauvais pronostic clinique.Dans le but d'adresser le besoin d'une médecine personnalisée, mon projet de thèse a pour objectif l'identification de nouvelles approches thérapeutiques pour le traitement des cancers du sein déficients en ATIP3. En partant du fait que les cancers déficients en ATIP3 présentent un taux élevé d'aneuploïdie, nous avons émis l'hypothèse que l'augmentation de l'instabilité chromosomique avec des inhibiteurs de kinases du cycle cellulaire pourrait induire plus de mort cellulaire, rendant ainsi les tumeurs déficientes en ATIP3 plus vulnérables à une thérapie ciblée dirigée contre une kinase du cycle. J'ai mis en évidence que les cellules déficientes en ATIP3 sont plus sensibles à l'inhibition de la kinase WEE1, régulatrice de l'entre en mitose. Cette sensibilité accrue des cellules déficientes en ATIP3 à l'inhibition de WEE1 est due à une combinaison de effets : une induction d'un stress réplicatif et de dommages à l'ADN de manière excessive pendant la phase S du cycle, combinée à une entrée prématurée en mitose induisant une mortalité plus élevée. J'ai montré qu'en réponse à l'inhibition de WEE1 les cellules déficientes en ATIP3 présentent des mitoses aberrantes avec un détachement des protéines centromériques de l'ADN, qui lui-même est exclu du fuseau mitotique, empêchant ainsi la division et entrainant la mort cellulaire. J'ai également montré que ce phénotype aberrant est dû à l'activité dérégulée de l'hélicase/nucléase DNA2, qui fragmente l'ADN d'une manière excessive en réponse à l'inhibition de WEE1. Ainsi, l'ensemble de mes travaux propose la kinase WEE1 comme une nouvelle cible personnalisée contre les cancers du sein déficients en ATIP3, et décrit les effets de l'inhibition de WEE1 ainsi que les mécanismes par lesquels les cellules déficientes en ATIP3 sont plus sensibles à cette inhibition.

Title : Targeting the cell cycle: a novel therapeutic strategy against ATIP3-deficient breast cancers

Keywords : breast cancer, aneuploidy, WEE1, DNA damage, biomarker

Abstract : Breast cancer is the leading cause of cancer-related deaths in women. The need to identify biomarkers for personalized therapies is imperative, especially for triple-negative breast cancers (TNBC). ATIP3 is a microtubule-associated protein identified by our team, and its deficiency is found in 65-80% of TNBC cases, associated with poor clinical prognosis. ATIP3-deficient tumors are of higher grade and exhibit a strong metastatic potential. My thesis project aims to identify novel therapeutic approaches for ATIP3-deficient breast cancer, driven by the urgent need for personalized medicine. Given that ATIP3-deficient cancers exhibit high levels of aneuploidy and chromosomal instability, we hypothesized that increasing genomic instability with cell cycle kinase inhibitors could induce more cell death, rendering ATIP3-deficient tumors more vulnerable to targeted kinase therapy. I have demonstrated that ATIP3-deficient cells are more sensitive to the inhibition of the WEE1 kinase, a regulator of mitotic entry. This heightened sensitivity results from a combination of effects, including induction of replicative stress and excessive DNA damage during the S phase of the cell cycle, in concert with premature mitotic entry and higher mortality. Furthermore, I have shown that in response to WEE1 inhibition, ATIP3-deficient cells exhibit aberrant mitoses with detachment of centromere proteins from DNA, preventing proper division and causing cell death. This abnormal phenotype is attributed to the dysregulated activity of the DNA2 helicase/nuclease, which excessively fragments DNA in response to WEE1 inhibition. In summary, my research highlights WEE1 kinase as a potential personalized target for ATIP3-deficient breast cancers and elucidates the effects of WEE1 inhibition and the mechanisms by which ATIP3-deficient cells become more susceptible to this inhibition.